VOLUME 22 (1961) No. 1

NUCLEAR PHYSICS

JOURNAL DEVOTED TO THE EXPERIMENTAL AND THEORETICAL STUDY OF THE FUNDAMENTAL CONSTITUENTS OF MATTER AND THEIR INTERACTIONS

EDITOR: L. ROSENFELD - COPENHAGEN

G. E. BROWN, L. CASTILLEJO and J. A. EVANS, The dipole state in nuclei . . . 1
W. BRENIG, Long range correlations and photo effect in nuclei 14
D. ROBSON, Polarization in (d, p) reactions 34
D. ROBSON, Spin-orbit effects in the stripping reaction involving polarized particles 47
K. S. TOTH and O. B. NIELSEN, Dy^{155} and Dy^{157} decay schemes 57
V. S. BARASHENKOV, Inelastic interactions of π-mesons with nucleons at 6.8 GeV 71
D. J. THOULESS, Vibrational states of nuclei in the random phase approximation 78
N. CINDRO, I. ŠLAUS, P. TOMAŠ and B. EMAN, The $O^{16}(n, \alpha)C^{13}$ reaction by the thin crystal method 96
A. KOMAR, "Minimal property" of electromagnetic interaction for spin $\frac{1}{2}$ particles 101
D. H. RESTER, M. S. MOORE, F. E. DURHAM and C. M. CLASS, Internal conversion electrons from Coulomb excitation of heavy elements 104
B. G. PETTERSSON, J. H. HAMILTON and J. E. THUN, Higher-order effects in an allowed positon decay in Co^{56} 131
P. E. HODGSON, J. AGUILAR, A. GARCÍA, and J. B. A. ENGLAND, The elastic scattering of 19.5 MeV deuterons by krypton 138
E. BODENSTEDT, H. J. KÖRNER, C. GÜNTHER and J. RADELOFF, The gyromagnetic ratio of the 80 keV rotational state of Erbium 166 145
ELIZABETH BARANGER and CHONG WAN LEE, Spurious states arising from the centre-of-mass motion of a nucleus 157
T. T. CROW and W. G. HOLLADAY, A contribution to the anomalous magnetic moments of the baryons 164
H. PILKUHN, Isospin for $N+\bar{N} \to K+\bar{K}+k\pi$ and similar reactions 168

January 1961

NORTH-HOLLAND PUBLISHING COMPANY - AMSTERDAM

NUCLEAR PHYSICS, VOLUME 22, No. 1, pp. 1—176

EDITORIAL BOARD

AUSTRALIA & NEW ZEALAND:	H. Messel (Sydney), M. L. Oliphant (Canberra)
AUSTRIA:	B. Karlik (Vienna), H. Thirring (Vienna)
BELGIUM:	M. de Hemptinne (Louvain), J. Verhaeghe (Ghent)
CANADA:	G. Volkoff (Vancouver)
DENMARK:	C. Møller (Copenhagen), S. Rozental (Copenhagen), G. E. Brown (Copenhagen)
FINLAND:	L. Simons (Helsinki)
FRANCE:	A. Berthelot (Saclay), S. Gorodetzky (Strasbourg)
GERMANY (DEM. REP.):	G. Hertz (Leipzig)
GERMANY (FED. REP.):	W. Gentner (Freiburg i. B.), J. H. D. Jensen (Heidelberg)
GREAT BRITAIN:	W. E. Burcham (Birmingham), T. H. R. Skyrme (Harwell)
HUNGARY:	L. Janossy (Budapest)
INDIA:	H. Bhabha (Bombay), R. Ramanna (Trombay)
IRISH REPUBLIC:	J. McConnell (Maynooth)
ISRAEL:	G. Racah (Jerusalem)
ITALY:	E. Amaldi (Rome)
JAPAN:	S. Kikuchi (Tokai), S. Tomonaga (Tokyo)
MEXICO:	M. Moshinsky (Mexico)
NETHERLANDS:	H. Brinkman (Groningen), S. R. de Groot (Leiden)
NORWAY:	E. Hylleraas (Oslo), A. Lundby (Oslo), H. Wergeland (Trondheim)
POLAND:	L. Infeld (Warsaw), J. Werle (Warsaw)
PORTUGAL:	J. M. Araújo (Porto), J. R. de Almeida Santos (Coimbra)
SOUTH AMERICA:	G. Beck (Saõ Paulo), J. Leite Lopes (Rio de Janeiro)
SPAIN:	J. M. Otero (Madrid), C. Sanchez del Rio (Madrid)
SWEDEN:	O. Klein (Stockholm), K. Siegbahn (Uppsala), I. Waller (Uppsala)
SWITZERLAND:	P. Huber (Basel), P. Scherrer (Zürich)
U.A.R. & ARAB COUNTRIES:	F. El Bedewi (Cairo), M. G. Nooh (Cairo)
U.S.A.:	H. H. Barschall (Madison, Wisconsin), S. Devons (New York), V. F. Weisskopf (Cambridge, Mass.)
U.S.S.R.:	M. A. Markov (Moscow), I. S. Shapiro (Moscow), D. V. Skobeltzyn (Moscow)
YUGOSLAVIA:	I. Supek (Zagreb)

CONTRIBUTIONS may be sent to the Editor, Professor L. Rosenfeld, NORDITA, Blegdamsvej 17, Copenhagen Ø, either directly, or preferably through the intermediary of one of the members of the Editorial Board of the country or region in which the author is working. They may be written in English, French or German.

NUCLEAR PHYSICS is published in fortnightly issues. The subscription price per volume of 700 pages is fl 57.00; 114s; $ 15.00. Post-free.

SUBSCRIPTIONS should be sent to the publishers, NORTH-HOLLAND PUBLISHING COMPANY, P.O. Box 103, Amsterdam or to any subscription-agent.

BOOKS FOR REVIEW should be sent to Professor Rosenfeld.

No part of this issue may be reproduced in any form, by print, photoprint, microfilm or any other means without permission from the publisher.

Printed in the Netherlands

1.D.1:
1.D.2

Nuclear Physics **22** (1961) 1—13; © *North-Holland Publishing Co., Amsterdam*
Not to be reproduced by photoprint or microfilm without written permission from the publisher

THE DIPOLE STATE IN NUCLEI

G. E. BROWN †, L. CASTILLEJO and J. A. EVANS
Mathematical Physics Department, University of Birmingham

Received 4 August 1960

Abstract: The mechanism of the particle-hole interaction in producing the "Dipole State", i.e., the giant dipole resonance, in nuclei is discussed in detail. Calculations in j—j coupling are carried out with zero-range forces for the nuclei O^{16} and Ca^{40}. Comparison with finite-range calculations in the case of O^{16} shows that the zero-range calculations reproduce well not only qualitative, but also most quantitative features. In all cases, the particle-hole interaction concentrates the dipole-strength in the uppermost states, the energies of which are also shifted upwards by the interaction.

1. Introduction

Most nuclei possess what we shall call a "Dipole State", that is, a state very strongly excited by γ-rays of the appropriate energy (14—20 MeV, depending on the nucleus) which is responsible for the familiar giant resonance for photon absorption. Recently [1]) a schematic model was proposed to show how the particle-hole interaction could combine single-particle excitations arising in the absorption of a dipole γ-ray so as to produce in nuclei a "dipole state" at a high excitation energy. The model neglected, however, many features of the actual nuclear problem. The purpose of the present note is to include some of these.

In particular, we shall show that the inclusion of spin, isobaric spin, and statistics does not change the conclusions of ref. [1]). In order to keep the treatment simple, we shall still employ zero-range forces and will neglect spin-orbit interactions in the early discussion. Later, results of calculations which include spin-orbit interactions will be given.

The treatment we undertake here is still somewhat simplified, and cannot be expected to produce quantitative results. Calculations with more realistic forces would be necessary for this. One such calculation [2]) has been carried out for O^{16}, and has been exceedingly successful in predicting experimental results [3, 4]). We believe it to be instructive to begin by repeating this calculation in zero range, because with this much simpler calculation one can understand the mechanism producing the dipole state more easily. It is also easier to vary the exchange mixture and to include effects left out by Elliott and Flowers. Furthermore, the zero-range calculations can be extended fairly easily to more complex cases, e.g., to nuclei with valence particles, whereas extension of the finite-range calculations would require an immense amount of labour, because of com-

† Now at Nordita, Nordisk Institut for Teoretisk Atomfysik, Copenhagen, Denmark.

plications with the angular momentum. The success of the calculations of Elliott and Flowers in predicting characteristics of states at excitation energies up to 24 MeV leads us to believe that the mechanism producing these levels must be insensitive to details of the forces and wave functions. The particular exchange mixture chosen by Elliott and Flowers is not given unambiguously by the lower-energy date fitted there and certain aspects of it — in particular, the interaction in odd states — are unreasonable. We will show that, within our simplifying assumptions, forces differing markedly in exchange mixture give similar results. Since we employ zero-range forces, there is no interaction in odd states; but just because the calculations of ref. [2]) were so successful, we believe that the odd-state interactions are not very important. Certainly the interaction in relative S-states is the most important one, as in most nuclear phenomena.

2. Formulation

It is convenient to formulate the problem using the techniques of 2nd quantization, as Bell [5]) has pointed out, since antisymmetrization is automatically carried out and the problem of determining relative signs of quantities is simplified. We begin by considering the γ-ray to be absorbed by a nucleus with closed neutron and proton shells, and assume complete symmetry between neutrons and protons. We denote the ground state of the nucleus by $|0\rangle$ and treat it as the physical vacuum, referring to absent particles as holes. The interaction of the dipole γ-ray with the nucleus is described by

$$\delta H = \sum_{\alpha,\beta} C \int \psi_\alpha^*(\mathbf{r}) \frac{e\tau_3 z}{2} \psi_\beta(\mathbf{r}) \mathrm{d}^3\mathbf{r} a_\alpha^\dagger(p) a_\beta(h), \tag{1}$$

where the ψ_α are a complete set of single particle wave functions enumerated by the index α. For the central forces only, which we shall consider in this section, it is convenient to choose a representation in which α stands for all the angular momentum, spin and isobaric spin labels, i.e., α is the set l, m, Σ, t_3, where l is the orbital angular momentum and m its projection, Σ is the spin projection and t_3 is that of the isobaric spin, equal to $+1$ for protons and -1 for neutrons. C is a constant and the operators $a_\alpha^\dagger$ and a_β are the creation operators for particles and holes respectively. Since the interaction $\tau_3 ez$ is independent of spin, we see that $\Sigma_\alpha = \Sigma_\beta$. Furthermore, only the third component of isobaric spin τ_3 is involved, so that $(t_3)_\alpha = (t_3)_\beta$.

The interaction δH acting on the vacuum $|0\rangle$ will produce states of unit angular momentum. Such normalized states are

$$|\mathrm{ph}\rangle = \tfrac{1}{2} \sum_{\substack{m_1, m_2 \\ \Sigma}} (-1)^{l_2 - m_2} (l_1 m_1 l_2 - m_2 | 10) \{a^\dagger_{l_2 m_2 \Sigma+1}(p) a_{l_1 m_1 \Sigma+1}(h) - a^\dagger_{l_2 m_2 \Sigma-1}(p) a_{l_1 m_1 \Sigma-1}(h)\}|0\rangle, \tag{2}$$

where the neutron excitation (with lower suffix -1) appears with sign opposite to that of the proton because of the τ_3 in the creation Hamiltonian. The above state is a ^{31}P state in spectroscopic language, triplet in isobaric spin and singlet in ordinary spin. The phase factor $(-1)^{l_2-m_2}$ and Clebsch-Gordan coefficient $(l_1, m_1, l_2-m_2|10)$ are necessary to combine the particle and hole into a P state. This phase factor arises because in the usual definitions of phases, $(Y_l^m)^*$ transforms under rotations like $(-1)^{l-m}Y_l^{-m}$.

The particle-hole interaction Hamiltonian is

$$H_{12} = \frac{1}{2!}\sum_{\alpha,\beta,\gamma,\delta}\int \psi_\alpha^*(2)\psi_\beta^*(1)V\psi_\gamma(1)\psi_\delta(2)\mathrm{d}^3\mathbf{r}_1\,\mathrm{d}^3\mathbf{r}_2 a_\alpha^\dagger a_\beta^\dagger a_\gamma a_\delta, \tag{3}$$

where the sign convention is such that V is the particle-particle interaction, and, therefore, negative. Matrix elements of the secular matrix will be given by

$$\langle \mathrm{p'h'}|H_{12}|\mathrm{ph}\rangle. \tag{4}$$

The interaction H_{12} conserves total spin and isobaric spin so that only the states (2) are coupled together. Factor pairing the annihilation and creation operators gives us two types of terms, illustrated in fig. 1, which are often referred to as

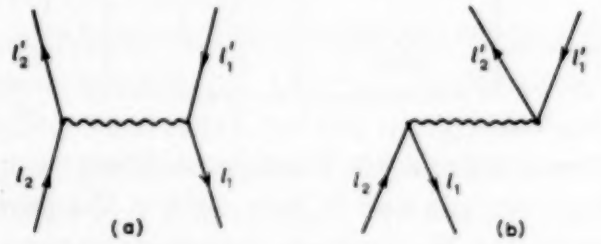

Fig. 1. Graphs illustrating (a) a direct process and (b) an exchange process.

direct and exchange terms. Aside from factors depending on isobaric spin, which we will handle separately, these two terms are

$$\begin{aligned} D = &-\sum_{m,\Sigma}(-1)^{l'_2-m'_2}(l'_1 m'_1 l'_2 - m'_2|10)(-1)^{l_2-m_2}(l_1 m_1 l_2 - m_2|10) \\ &\iint \psi^*_{l'_2 m'_2 \Sigma'}(2)\,\psi^*_{l_1 m_1 \Sigma}(1) V \psi_{l'_1 m'_1 \Sigma'}(1)\,\psi_{l_2 m_2 \Sigma}(2)\mathrm{d}^3\mathbf{r}_1\mathrm{d}^3\mathbf{r}_2, \\ E = &\sum_{m,\Sigma}(-1)^{l'_2-m'_2}(l'_1 m'_1 l'_2 - m'_2|10)(-1)^{l_2-m_2}(l_1 m_1 l_2 - m_2|10) \\ &\iint \psi^*_{l'_2 m'_2 \Sigma'}(1)\psi^*_{l_1 m_1 \Sigma}(2) V \psi_{l'_1 m'_1 \Sigma'}(1)\psi_{l_2 m_2 \Sigma}(2)\mathrm{d}^3\mathbf{r}_1\mathrm{d}^3\mathbf{r}_2, \end{aligned} \tag{5}$$

where D and E stand for the direct and exchange terms, respectively. To show how the spin and isobaric spin enter in, let us consider the case in which V does not depend on spin or isobaric spin, i.e., where V is a "Wigner Force". First of all, we see that if, in fig. 1, l_2 represents a proton, then l_1 represents the lack of a

proton. Therefore, in labelling the isobaric character of a given particle-hole state it is sufficient to say whether it is a proton or neutron excitation. Similarly, one need specify the spin projection of the particle only, the hole being the lack of that same spin (δH of eq. (1) contains no terms which can flip the spin). Hence, we can represent our particle-hole wave functions symbolically as †

$$|\mathrm{ph}\rangle = \tfrac{1}{2}(\mathrm{P}\uparrow + \mathrm{P}\downarrow - \mathrm{N}\uparrow - \mathrm{N}\downarrow), \tag{6}$$

where P denotes a proton excitation, N a neutron one and the arrows $\uparrow$ and $\downarrow$ represent particle spin up and down, repectively. Now, it is clear that if we consider a matrix element

$$\langle \mathrm{p'h'}|\mathrm{H}_{12}|\mathrm{ph}\rangle,$$

we need symmetrize only the initial state in the way given in eq. (6), the final state being taken simply as $\mathrm{P}\uparrow$, for example. We can now build up a table describing the isobaric and spin characteristics of the interactions:

$\mathrm{P}\uparrow \quad \mathrm{P}\uparrow$	$D \quad -E$
$\mathrm{P}\uparrow \quad \mathrm{P}\downarrow$	$\quad -E$
$\mathrm{P}\uparrow \quad \mathrm{N}\uparrow$	$\quad +E$
$\mathrm{P}\uparrow \quad \mathrm{N}\downarrow$	$\quad +E$
total	D

(7)

The direct term is zero for the lower three possibilities, since the interaction in fig. 1 can flip neither the spin nor isobaric spin of the particle, V depending only on spacial coordinates. The exchange terms are nonzero in all cases, however, since the particle can always drop into the hole from which it came. The signs of the exchange terms differ in the first two and last two cases because of the difference in signs in the wave function, eq. (6). We see that the nett particle-hole interaction is just D. This is the negative of the direct term in the particle-particle interaction. Consequently, introduction of spin, isobaric spin and statistics just leads one back to the picture of the schematic model of ref. [1]), where it was argued that since the particle-particle interaction is attractive, the particle-hole one must be repulsive. We note that this is true only in $T = 1$ states. In $T = 0$ states, the interaction would be $D - 4E$, and strongly attractive, since the signs in front of the last two terms in the wave function eq. (6), must be reversed.

Qualitative features of various exchange mixtures are easy to see if we make the zero-range approximation for V, i.e. set $V = -V_0\delta(\mathbf{r}_1 - \mathbf{r}_2)$. In this case, $D = E$ and for a Wigner force, the particle-hole interaction is $V_0\mathscr{S}$ in $T = 1$

† This corresponds to solution 1, eq. (5.25) of Glassgold, Heckrotte and Watson [6]), who work with nuclear matter.

states, and $-3V_0\mathcal{I}$ in $T = 0$ states, where $\mathcal{I}$ stands for the integral over $d^3\mathbf{r}_1$ and $d^3\mathbf{r}_2$ indicated in eq. (5). With a Rosenfeld mixture in zero range,

$$V = \boldsymbol{\tau}_1 \cdot \boldsymbol{\tau}_2 \frac{V_0}{3} (0.3+0.7\boldsymbol{\sigma}_1 \cdot \boldsymbol{\sigma}_2)\delta(\mathbf{r}_1-\mathbf{r}_2), \tag{8}$$

the results are easily found by similar arguments to be $1.2V_0\mathcal{I}$ and $-2.4V_0\mathcal{I}$ for $T = 1$ and $T = 0$ states, respectively. A Serber mixture clearly gives the same results as a Wigner force in zero-range. Consequently, it is seen that one can expect the particle-hole interaction to be mainly positive in $T = 1$ states and negative in $T = 0$ ones, irrespective of the exchange mixture. The latter must, of course, be chosen so as to give an attractive particle-particle interaction. Recently, Soper [7]) has analyzed data on Li^6, Li^7 and Li^8 to derive a different exchange mixture

$$V = (0.3+0.43P_M+0.27P_B)V(\mathbf{r}_1-\mathbf{r}_2), \tag{8.1}$$

where P_M and P_B are the Majorana and Bartlett exchange operators. Taking $V = -V_0\delta(\mathbf{r}_1-\mathbf{r}_2)$ we find contributions in $T = 1$ and $T = 0$ states to be $1.27V_0\mathcal{I}$ and $-2.19V_0\mathcal{I}$, respectively.

We should remark that the precise division of contributions to the $T = 0$ or $T = 1$ matrix elements between the direct and exchange terms depends on the exchange mixture. The final result for the matrix elements is, however, not very dependent upon exchange mixture, and we can say that in general the particle-hole interaction is attractive in $T = 0$ states and repulsive in $T = 1$ states. Since exchange mixtures [7]) currently used in p-shell nuclei are rather close to Serber forces, we have some reason to believe the division given in eq. (7) and following to be close to the actual one.

3. Stability of the Dipole State

Calculations have been carried out by Soper in $L-S$ coupling, with zero-range forces, to check the qualitative conclusions of Brown and Bolsterli [1]). These calculations which will be published elsewhere, were remarkably successful in reproducing the qualitative features of the Elliott-Flowers calculation. His results were quite insensitive to assumptions about the particle-shell and hole-shell interactions, which enter into the diagonal elements of the secular matrix. We shall now demonstrate that if the matrix elements have approximately the form given by Brown and Bolsterli [1]), then one would expect the dipole state to be quite stable against perturbations.

Take $\Phi_1, \Phi_2, \ldots \Phi_n$ to be the eigenfunctions of H_0, the idealized particle-hole

Hamiltonian of ref. [1]), given by

$$H_0 = \begin{vmatrix} \varepsilon-(l_1+1)G & \sqrt{(l_1+1)(l_2+1)}G \ldots \\ \sqrt{(l_1+1)(l_2+1)}G & \varepsilon-(l_2+1)G \quad \ldots \\ \ldots\ldots\ldots \text{ etc. } \ldots\ldots\ldots\ldots\ldots \end{vmatrix}. \tag{9}$$

In particular, Φ_n is the dipole state

$$\Phi_n = \frac{1}{\sqrt{\sum(l_i+1)}} \begin{pmatrix} \sqrt{l_1+1} \\ \sqrt{l_2+1} \\ \ldots\ldots \\ \sqrt{l_n+1} \end{pmatrix}. \tag{9.1}$$

Now consider how this dipole state will be spread among the eigenfunctions of the Hamiltonian

$$H = H_0+D,$$

where D is a diagonal matrix coming from particle-shell and hole-shell (pairing force) interactions. The eigenfunctions of H will be Ψ_i, with energies E_i. We expand

$$\Phi_n = \sum a_{ni}\Psi_i, \quad \Psi_i = \sum a_{ni}\Phi_n, \tag{9.2}$$

and easily find

$$\begin{aligned} \Phi_n D\ \Phi_n &= \sum_i a_{ni}^2(E_i-E_n^{(0)}), \\ \Phi_n D^2\Phi_n &= \sum_i a_{ni}^2(E_i-E_n^{(0)})^2. \end{aligned} \tag{9.3}$$

where $E_n^{(0)}$ is the energy of Φ_n. Naturally, we choose ε so that the first moment is zero. If D has elements D_i, then the r.m.s. moment is

$$\sqrt{\frac{\sum(l_i+1)D_i^2}{\sum(l_i+1)}}, \quad \text{or} \quad \sqrt{\overline{D_i^2}}. \tag{9.4}$$

Thus, if the diagonal elements aside from the particle-hole ones, are the order of 1 MeV or so, they will spread the dipole state this much among the perturbed eigenfunctions. If the dipole state is well-separated from the other Φ_i, introduction of D will have but little effect.

The same argument suggests that contributions from valence nucleons, etc., will not upset things much, as long as their contribution to the dipole transition amplitude is small. In this case, one would introduce a perturbing matrix possessing off-diagonal elements.

4. Formulation in *j*—*j* Coupling

We discuss now the formulation in *j*—*j* coupling, which gives a more correct description, and will see from results of simple calculations that the qualitative

results reached in the foregoing simple discussion in L—S coupling are still realized in the main. The discussion of isobaric spin goes through just as in L—S coupling, so we will not indicate dependence on isobaric spin.

The basic particle-hole states are

$$|\mathrm{ph}\rangle = \sum_{m_1, m_2} (-1)^{j_2-m_2}(j_1 m_1 j_2 - m_2|10) a^\dagger_{j_2 m_2}(p) a_{j_1 m_1}(h)|0\rangle \qquad (10)$$

and the graphology of interaction is the same as in fig. 1 with l_i replaced by j_i. The direct and exchange terms are obtained from eq. (5) by the same replacements, and suppression of all Σ's, which are now included in the j's.

The dipole transition amplitude, obtained from δH of eq. (1), is defined as

$$D = \langle \mathrm{pH}|\delta H|0\rangle \qquad (11)$$

and is easily found to be

$$D = \tfrac{1}{6} Ce\sqrt{(2j_1+1)(2j_2+1)}(-1)^{j_1-\frac{1}{2}}(j_1 \tfrac{1}{2} j_2 - \tfrac{1}{2}|10)\int R_{j_1} R_{j_2} r^3 \mathrm{d}r, \qquad (12)$$

with the selection rule $l_1 = l_2 \pm 1$. Here, R_{j_1} and R_{j_2} are the radial functions of the hole and particle, respectively. It is often convenient to choose the phase of the particle-hole state $|\mathrm{ph}\rangle$ so that D is positive.

The formulation in terms of j—j coupling makes it possible to take account of spin-orbit effects easily. This is discussed fully in the next section.

5. Detailed Calculations

5.1. O^{16}

In this nucleus, the 1p levels are just filled and the dipole excitations can be obtained by raising one nucleon into the 1d, or 2s shells. The configurations which can contribute to a dipole state are the first five listed in table 1, which

TABLE 1

Energies of single-particle and single-hole excitations in O^{16}

configuration	Dipole moment (%)	j, π	$\Delta_1(j, \pi)$ (MeV)	j', π'	$\Delta_2(j', \pi')$ (MeV)	$\Delta_1 - \Delta_2$ (MeV)
$p^{-1}_{\frac{1}{2}} s_{\frac{1}{2}}$	11	$\frac{1}{2}+$	−3.28	$\frac{3}{2}-$	−21.74	18.46
$p^{-1}_{\frac{1}{2}} d_{\frac{5}{2}}$	50	$\frac{5}{2}+$ (g.s.)	−4.15	$\frac{3}{2}-$	−21.74	17.59
$p^{-1}_{\frac{1}{2}} d_{\frac{3}{2}}$	28	$\frac{3}{2}+$	+0.93	$\frac{1}{2}-$ (g.s.)	−15.60	16.53
$p^{-1}_{\frac{1}{2}} s_{\frac{1}{2}}$	5.5	$\frac{1}{2}+$	−3.28	$\frac{1}{2}-$ (g.s.)	−15.60	12.32
$p^{-1}_{\frac{1}{2}} d_{\frac{3}{2}}$	5.5	$\frac{3}{2}+$	+0.93	$\frac{3}{2}-$	−21.74	22.67
$p^{-1}_{\frac{1}{2}} d_{\frac{5}{2}}$	0	$\frac{5}{2}+$ (g.s.)	−4.15	$\frac{1}{2}-$ (g.s.)	−15.60	11.45

also indicates the percentage of the dipole sum which each carries. The 5×5 secular matrix consists of two parts, the first of which is the particle-hole interaction and is nondiagonal. The other is diagonal and corresponds to the sum of particle-shell, and hole-shell interactions. These elements differ according

to the value of j, that is, they include what are usually called spin-orbit forces. We will obtain them from empirical data.

It is necessary, when computing the empirical transition energies to observe a strict sign convention. We will always, speak in terms of particle-particle interactions, which are attractive. The "hole-shell" interactions are to be interpreted as the interaction a particle would have with the rest of the nucleus if it occupied the "hole-state". We are interested in the energy difference between a one-particle, one-hole configuration and the ground state of the nucleus. This difference is clearly equal to

$$\Delta_1 - \Delta_2 = \text{(particle-hole interaction with shell)},$$

where

$$\Delta_1 = \sum \text{(particle-shell interactions)},$$
$$\Delta_2 = \sum \text{(hole-shell interactions)},$$

the summation in Δ_1 going over all the core particles, and in Δ_2 over the core minus one. To obtain Δ_1 we consider the ground and low-lying excited states of O^{17}. We could use F^{17}, but it is within the spirit of this work to assume complete charge independence of nuclear interactions. Let the binding energy of an Oxygen nucleus of mass A, in state $J\pi$ be $E(A, J, \pi)$. Then,

$$E(17, J, \pi) = E(16, 0+) + \Delta_1(J, \pi),$$

from which the particle-shell interaction is found. The value naturally depends on J and π and hence on the corresponding single-particle level in the mass 17 nucleus. The quantity $E(17, J, \pi)$ is computed by simply adding the ground state binding energy [8]) (negative) to the excitation energy [9]) of the state J, π. In a similar way, we have

$$E(15, J', \pi') = E(16, 0+) - \Delta_2(J', \pi').$$

The results of this calculation are presented in table 1, the last column giving the empirical diagonal elements used in the secular matrix for O^{16}.

Assuming a spin-orbit force of the form $(\boldsymbol{\sigma} \cdot \mathbf{l})$, one can locate the mean position of the split p and d levels, and from this determine the oscillator constant $\hbar\omega$. It turns out to be about 17 MeV.

The matrix elements of the particle-hole interaction were calculated using a zero-range force between nucleons, together with harmonic-oscillator wave functions. Calculations were carried out for both an ordinary force, and for the Soper mixture mentioned earlier. Comparison between the two is interesting, but the latter may be expected to give more meaningful results. Finally, the matrices were diagonalized with the aid of a computer.

From the eigenvectors, the dipole matrix element M of each eigenstate was calculated. The γ-ray width of a state is proportional to $E^3|M|^2$, where E is the

energy eigenvalue. The distribution of this quantity among the various states appears in table 2, together with those of ref. [2]) for comparison. The agreement,

TABLE 2

Calculated energies and dipole strengths of levels in O^{16}

Ordinary force		Super mixture		Elliott and Flowers	
E(MeV)	% dipole str.	E(MeV)	% dipole str.	E(MeV)	% dipole str.
25.6	15	25.0	29	25.2	32
21.5	81	22.2	68	22.6	67
19.9	1	20.0	1	20.4	0
17.7	2	17.6	1	17.3	1
13.9	1	13.7	1	13.1	0

especially with the Soper mixture is strikingly good. Our interaction strength was adjusted so that the sum of our eigenvalues is the same as that of Elliott and Flowers. While their potential was

$$V(r) = \frac{V_c\, e^{-r/a}}{r/a}, \quad \text{with} \quad V_c = 43 \text{ MeV},$$

our interaction strength is given by

$$\frac{V_0}{4\pi b^3} = 8.50 \text{ MeV} \times 10^{39} \text{ cm}^{-3},$$

where b is the usual range parameter in the wave functions. It is easily shown that our force has the same volume integral as a Yukawa force of the range employed by Elliott and Flowers, but with a strength $V_c = 14.6$ MeV. This indicates that for Oxygen the zero range force is more effective than a finite range one.

It has been suggested to the authors that $3\hbar\omega$ transitions might have some effect on the dipole state. They carry no dipole moment themselves, but by mixing with the $1\hbar\omega$ configurations they can transfer dipole strength to a high-energy state. This effect has been estimated in O^{16}, by including the configuration $p^{-1}3s$ and $p^{-1}2d$. A small dipole state is produced at about 60 MeV excitation, but it carries only a few percent of the dipole sum. This result may be modified, however, if one employs a non-harmonic well, since the wave functions of the higher states are quite different for more realistic wells.

5.2. Ca^{40}

Here the $1d$ and $2s$ levels are just filled, and eight dipole states can be obtained from the configurations $d^{-1}f$, $d^{-1}2p$ and $2s^{-1}2p$. For this case, it is not so easy to evaluate the empirical diagonal elements. Although the ground state

energies of Ca^{41} and Ca^{39} are known [8]), there is a shortage of information about the excitation energies of states in Ca^{41} describable as single particle states, and the relevant hole states in Ca^{39}. Most of this information was found in the work of Sliv and Volchok [10]). Apart from these difficulties, the problem was solved exactly as in the previous case of O^{16}. At first the same value of V_0 was used, although b^3 was decreased in the ratio of the atomic weights, 16/40. This value of V_0 gave the giant resonance at too low an energy, so that V_0 was finally multiplied by 1.70. The need to change V_0 probably arises from the fact that a zero range force is a poor approximation in O^{16}, and a small value must be chosen to compensate for this. In Ca^{40} the approximation is not so bad, so that a stronger zero range force must be used. With this force, reasonable agreement was obtained with the experimental [12]) energy of the giant resonance in Ca^{40}.

TABLE 3

Calculated energies and dipole strengths of levels in Ca^{40}

Ordinary force		Soper mixture	
E(MeV)	% dipole str.	E(MeV)	% dipole str.
21.5	9	20.6	44
18.5	80	19.2	55
17.6	99	17.8	0
16.6	1	16.8	1
15.3	0	15.4	0
13.6	1	13.4	0
13.0	0	12.9	0
10.2	0	10.2	0

From the results in table 3 it is seen that the distribution of dipole strength is strongly influenced by the exchange mixture. In particular, the high spin-flip state at 21.5 MeV is not given sufficient dipole strength by the ordinary force. This feature was equally obvious in O^{16}. The eigenvectors for both nuclei are listed in the Appendix.

6. Discussion

In sect. 3 in making the argument about the stability of the dipole state, we essentially made also the argument that valence particles will not change the results derived for closed-shell nuclei very much, in that they would simply add one or two more columns and rows to the secular matrix, and, if these do not carry a very large dipole transition probability, then they will not alter the dipole state much. At first sight, one might think this to be in contradiction with the well known fact that the dipole state is much narrower at closed-shell nuclei than it is well away from them, thus indicating that the valence particles have a strong effect on the width of the state, although not on its energy. We

would offer the following tentative explanation of this fact. In closed-shell nuclei, all the unperturbed transitions lead to states which are still bound, i.e. at negative energy, or very nearly bound. Therefore, within the approximation in which we have been working, the dipole state would possess no natural width, since the elementary excitations of which it is a superposition have wavefunctions dropping off exponentially away from the edge of the nucleus. Some width is, of course, introduced in transitions of unperturbed energy $3\hbar\omega$, which we have not included in our truncated Hamiltonian, but one would not expect this to be large. In fact, very small widths are observed experimentally in oxygen [3]), supporting this hypothesis.

Now the valence particles, which are introduced as one moves away from closed-shell nuclei, are of course, bound in their intitial state, but not in their final state. Since, within our approximation, one gets no width for natural decay of the state in closed-shell nuclei, the width added by the valence particles is very appreciable, even though their number is small. Thus, we would say that the dipole state is not essentially changed, but that its width is increased by the valence particles.

The development presented in the preceding sections is essentially standard shell-model methodology in a new language. It is well known [12]) that these methods must be modified when the shift in energy of the state one is calculating becomes comparable with the energies of the elementary excitations. When this is so, correlations in the ground state of the nucleus become important. These cannot, however, be adequately dealt with in zero-range, and we feel that the qualitative features of our calculations of Oxygen and Calcium are probably valid, because the energy shift in these light nuclei is not yet comparable with the energy of the elementary excitations. The inclusion of these ground-state correlations will be discussed in a future publication dealing with vibrational states, where they are even more important than here.

We should mention the relation of this work to work done for the case of the infinite nucleus. If we used a $\boldsymbol{\tau}_1 \cdot \boldsymbol{\tau}_2$ force and kept only the exchange terms in fig. 1. (and took account of ground-state correlations), we should have the theory of Ferentz, Gell-Mann and Pines [13]), but for a finite nucleus. One can easily see that in these graphs, only the $\tau_{1z}\tau_{2z}$ part of the force is operative. But this commutes with the dipole operator, and therefore, such theories must just reproduce the classical sum rule $\sum f_{n0} = A$, where f_{n0} is the oscillator strength of the n^{th} level. But it is well known [14]) that this sum is enhanced by a factor of about $1+0.8x$, where x is the proportion of exchange force, and this enhancement must come from the direct terms in fig. 1. It is, therefore, clear that they must be included.

It has been suggested [15]) that there is a giant dipole spin-flip state ($T = 1$, $S = 1$) as well as the non spin-flip state described in sect. 2. Such a state is also predicted by Glassgold *et al.* [6]) (their solution No. 2). This is indeed related to

the distributions of the dipole strength between two states in Oxygen, the $S = 0$ and $S = 1$ states being mixed by the spin-orbit force, as suggested in ref. [15]). The calculations in $j-j$ coupling automatically take this into account.

We believe that the foregoing discussion and results help to clarify the mechanism of the dipole state. More quantitative calculations are now being carried out using forces of finite range and taking ground-state correlations into account.

We are happy to acknowledge many illuminating and helpful communications from B. Bayman. We are also grateful to D. J. Thouless and Professor R. E. Peierls for much useful criticism and many helpful suggestions. We would also like to acknowledge useful discussions with Aage Bohr, J. P. Elliott, H. J. Lipkin and J. M. Soper. We should like to thank W. Brenig for sending a preprint, discussing the relationship between various models (see following paper).

Appendix

The states are listed in the same order as in tables 2 and 3, that is in order of decreasing energy. However, corresponding pairs of states calculated with ordinary and Soper forces are placed together to facilitate comparison. In each pair, the ordinary force eigenvector is on top. The choice of phases is such that the dipole amplitudes are positive.

O^{16}

Energy	$p^{-1}_{\frac{1}{2}}s_{\frac{1}{2}}$	$p^{-1}_{\frac{3}{2}}d_{\frac{3}{2}}$	$p^{-1}_{\frac{1}{2}}d_{\frac{3}{2}}$	$p^{-1}_{\frac{3}{2}}s_{\frac{1}{2}}$	$p^{-1}_{\frac{1}{2}}d_{\frac{5}{2}}$
25.6	0.08	−0.12	0.23	0.02	0.98
25.0	0.10	0.09	0.27	−0.01	0.95
21.5	0.23	0.92	0.34	0.00	0.02
22.2	0.20	0.90	0.35	0.04	−0.20
19.9	0.97	−0.24	0.01	0.00	−0.12
20.0	0.96	−0.24	−0.02	0.06	−0.08
17.7	−0.11	−0.29	0.92	−0.02	−0.25
17.6	−0.09	−0.38	0.90	0.01	−0.21
13.9	0.00	0.00	0.01	1.00	−0.03
13.7	−0.06	−0.02	−0.02	1.00	0.02

Ca^{40}

Energy	$d^{-1}_{\frac{3}{2}} f_{\frac{7}{2}}$	$d^{-1}_{\frac{3}{2}} f_{\frac{5}{2}}$	$d^{-1}_{\frac{5}{2}} f_{\frac{7}{2}}$	$d^{-1}_{\frac{3}{2}} p_{\frac{3}{2}}$	$d^{-1}_{\frac{5}{2}} p_{\frac{3}{2}}$	$d^{-1}_{\frac{5}{2}} p_{\frac{1}{2}}$	$s^{-1}_{\frac{1}{2}} p_{\frac{3}{2}}$	$s^{-1}_{\frac{1}{2}} p_{\frac{1}{2}}$
21.5	−0.18	0.87	0.32	0.09	−0.05	−0.02	−0.07	0.30
20.6	0.18	0.77	0.42	0.14	−0.01	0.03	0.13	0.35
18.5	0.67	−0.13	0.34	0.12	0.03	0.07	0.38	0.46
19.2	0.75	−0.42	0.30	0.14	0.04	0.09	0.38	−0.03
17.6	0.31	0.25	0.19	0.36	−0.05	0.05	0.20	−0.78
17.8	0.15	0.30	0.05	0.32	0.00	0.08	−0.21	−0.86
16.6	−0.16	−0.21	−0.06	0.89	−0.13	0.07	−0.27	0.22
16.8	−0.17	−0.19	−0.04	0.88	0.00	0.18	−0.21	0.30
15.3	−0.41	0.03	−0.23	0.14	−0.10	−0.11	0.85	0.08
15.4	−0.31	0.12	−0.26	0.23	−0.05	−0.05	0.86	−0.16
13.6	−0.41	−0.36	0.81	−0.08	−0.09	−0.18	0.03	−0.11
13.4	−0.47	−0.27	0.79	0.00	−0.12	−0.22	0.06	−0.16
13.0	0.21	0.03	−0.11	0.02	−0.37	−0.90	−0.09	0.02
12.9	0.21	0.03	−0.15	0.18	−0.33	−0.89	0.08	0.04
10.2	0.04	−0.01	−0.02	−0.17	−0.91	0.39	−0.01	0.01
10.2	0.03	−0.01	−0.02	−0.07	−0.94	0.34	−0.01	0.00

References

1) G. E. Brown and M. Bolsterli, Phys. Rev. Letters **3** (1959) 472
2) J. P. Elliott and B. H. Flowers, Proc. Roy. Soc. A **242** (1957) 57
3) S. G. Cohen, P. S. Fisher and E. K. Warburton, Phys. Rev. Letters **3** (1959) 433
4) N. W. Tanner, G. C. Thomas and W. E. Meyerhof, Nuovo Cim. **14** (1959) 1
5) J. S. Bell, Nuclear Physics **12** (1959) 117
6) A. E. Glassgold, W. Heckrotte and K. M. Watson, Annals of Physics **6** (1959) 1
7) J. M. Soper (to be published)
8) A. H. Wapstra, Physica **21** (1955) 367
9) F. Azyenberg-Selove and T. Lauritsen, Nuclear Physics **11** (1959) 1
10) L. A. Sliv and B. A. Volchok JETP **361** (1959) 539
11) R. G. Summers-Gill, R. N. Haslam and L. Katz, Canadian J. Phys. **31** (1953) 70
12) R. A. Ferrell, Phys. Rev. **107** (1957) 1631
13) M. Ferentz, M. Gell-Mann and D. Pines, Phys. Rev. **92** (1953) 836
14) J. S. Levinger and H. A. Bethe, Phys. Rev. **78** (1950) 115
15) M. K. Pal and Y. C. Lee, Bull. Am. Phys. Soc. **4** (1959) 406

2.I

Nuclear Physics **22** (1961) 14—33; © *North-Holland Publishing Co., Amsterdam*

Not to be reproduced by photoprint or microfilm without written permission from the publisher

LONG RANGE CORRELATIONS AND PHOTO EFFECT IN NUCLEI

W. BRENIG †

Department of Physics and Laboratory for Nuclear Science, Massachusetts Institute of Technology, Cambridge 39, *Massachusetts* ††

Received 6 July 1960

Abstract: A detailed quantum mechanical treatment of the collective model for the giant dipole resonance in the low energy nuclear photo effect is presented. A relation $\omega_D = ck_D$ for the resonance energy ω_D is derived from sum rule considerations, where k_D is related to the nuclear radius by $k_D \approx \pi/2R$ and c to the structure factor $s(k)$ of nuclear matter at small momenta k by $s(k) = k/2mc$. The velocity c is calculated and the semiclassical expression for c in terms of the symmetry energy K ($c = (2K/m)^{\frac{1}{2}}$) is found to be valid only for extremely strong interactions. For weaker forces one obtains a larger value of c than indicated by this relation and a value of ω_D in better agreement with the results of shell model configuration mixing calculations.

1. Introduction

In the collective model [1]) for the giant resonance in the low energy nuclear photo effect the resonance state is assumed to be connected with a collective oscillation of the proton fluid against the neutron fluid. For vanishing two particle interactions this description has been shown to be identical with the single-particle model [2]).

The single-particle model, however, seems to give a value of the resonance energy which is only half of the observed value. In the past the introduction of an effective mass $m^* \approx \frac{1}{2}m$ has been suggested [3]) to remove this discrepancy. This however is in disagreement with experimental results in direct reactions [4]) and with the current fashion in the theory of nuclear matter, which assumes a smaller momentum dependence of the effective two particle forces in nuclear matter and consequently an effective mass $m^* \approx m$ †††.

The effect of two particle interactions has been included approximately in the collective model in a semiclassical treatment [7]) which allowed to relate the resonance energy directly to the symmetry energy of nuclear matter. However, it has been pointed out [8]) that in slightly non-ideal Fermi gases such as nuclear

† On leave of absence from Max Planck Institut für Physik, München, Germany.

†† This work is supported in part through AEC Contract AT(30-1)-2098 by Funds provided by the U. S. Atomic Energy Commission, the Office of Naval Research and the Air Force Office of Scientific Research.

††† The equilibrium condition which seemed to suggest the introduction of a small effective mass [5]) is now supposed to be fulfilled by means of a strong density dependence of the forces leading to rearrangement terms [6]).

matter the semiclassical treatment is not valid. The collective eigenstates resulting from a more rigorous quantum mechanical calculation agree with the classical solutions only in the limiting case of very strong interactions, whereas the actual nuclear forces effects the energy of the quantum mechanical solutions only by a few percent [9]). This is in apparent contradiction to the results of shell model configuration mixing [10]) calculations which indicate a strong influence of two particle interactions on the resonance energy. These discrepancies may be considered as a motivation for a reinvestigation of the collective model.

2. Dipole Strength and Two-Particle Correlation

The scattering of γ-rays is determined by the index of refraction which for low energies where the wavelength of the light is small compared to the size of the nucleus is proportional to the dipole strength function

$$n(\omega)=d\,(\omega)-i\pi a(\omega)=\sum_n \frac{|\langle 0|D|n\rangle|^2}{\omega_n-\omega+i\gamma}+(\omega\to-\omega). \tag{1}$$

The real part $d(\omega)$ is proportional to the elastic scattering cross-section, whereas the imaginary part determines the total absorption cross-section $\sigma(\omega)\approx\omega a(\omega)$. The width γ occurring in (1) is in general different for different levels, but as far as one is not interested in the fine structure of $\sigma(\omega)$ one can replace it by an average value γ. The dipole operator D in (1) is given by

$$D=\frac{1}{Z}\sum_{\text{prot.}} x_i-\frac{1}{N}\sum_{\text{neutr.}} x_i. \tag{2}$$

It is the distance between the centre of mass of the protons and the neutrons. $|0\rangle$ is the ground state and $|n\rangle$ are the excited states of the system, $\omega_n=E_n-E_0$ the excitation energies. Experimentally one finds a resonance in the total absorption cross-section, i.e. a rather well defined peak at an energy of about $\omega_D\approx 80/A^{\frac{1}{3}}$ MeV (A is the mass number of the nucleus).

In the shell model the only possible excitations contributing to (1) are single-particle excitations. For an oscillator well, for instance, only the matrix elements between neighboring shells are different from zero, which would give a value

$$\omega_D=\omega_{osc}\approx\frac{1.24}{A^{\frac{1}{3}}}\frac{k_F^2}{2m}=0.94\frac{k_F}{mR}\approx\frac{40\text{ MeV}}{A^{\frac{1}{3}}} \tag{3}$$

for the resonance energy, following from the requirement that the mean square radius $\int r^2\rho(r)\mathrm{d}^3r$ of the nucleus be equal to $\frac{3}{5}r_0^2A^{\frac{1}{3}}$. This is only half as large as the experimental value for ω_D. Now there are, in general, many degenerate single-particle excitations contributing to (1) and one has to solve a secular equation among them to get the eigenstates after taking the interaction into

account. This has been done in a schematic model by Brown and Bolsterli and for O^{16} by Elliot and Flowers both calculations [10]) indicating that the dipole strength is pushed up to higher energies.

Let us consider a qualitative argument for this effect which is independent of configuration mixing calculations and which can be used for a quantitative estimate later on. Consider, for instance, as a measure for the location of the dipole strength the average value

$$\omega_D = \frac{\int \omega a(\omega) d\omega}{\int a(\omega) d\omega}, \tag{4}$$

then, using (1), summing over the intermediate states and introducing the dipole state $|D\rangle = D|0\rangle$, one obtains for it

$$\omega_D = \frac{\langle D|H|D\rangle}{\langle D|D\rangle} - E_0. \tag{5}$$

There are a few cases in which the dipole state is an eigenstate of the Hamiltonian; for instance, in the shell model with an oscillator well (as pointed out by Brink [2])). The same is true in the schematic Brown-Bolsterli model [10]) and in the semiclassical collective model [7]) to be discussed below. In general, however, this is not the case and in large nuclei the dipole state is far from being an eigenstate. Nevertheless the expectation value of its energy is a useful quantity because of its close connection [5]) with the measurable quantity (4).

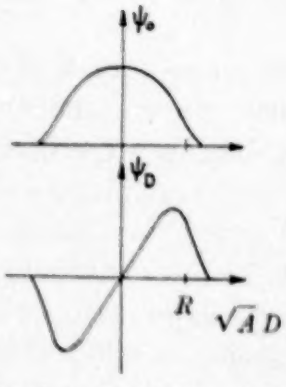

Fig. 1. Probability amplitudes for D in the ground state and dipole state (schematic).

To see the influence of interactions on (5) one may compare the average probability or probability amplitude for the centre of mass distance D between protons and neutrons in the ground state and the dipole state. They are plotted schematically in fig. 1 which shows that in the dipole state the protons are pushed away from the neutrons, which for attractive interactions between the particles pushes the energy of the dipole state up. Roughly speaking $|D\rangle$ may be considered as the first excited state of a collective oscillation of protons

against neutrons. It has been pointed out by Migdal, Jensen and Steinwedel [7]), that in these oscillations the nucleons have to do work against the symmetry energy. Since this is known to be about twice as large experimentally as the theoretical value for a free Fermi gas one can expect the interactions to have a large effect on ω_D.

Let us now consider the collective proton-neutron vibrations more in detail. As long as surface contributions are unimportant the properties of these excitations can be obtained from the properties of (infinitely extended) nuclear matter as is done in the semiclassical collective model. The excitations in this case are plain waves, corresponding to a periodical fluctuation in the neutron excess ($|0\rangle$ is now the ground state of nuclear matter),

$$\rho_k|0\rangle = |k\rangle, \tag{6}$$

ρ_k being the Fourier transform of the neutron excess density

$$\rho_k = \frac{1}{Z}\sum_{\text{prot.}} e^{ikx_i} - \frac{1}{N}\sum_{\text{neutr.}} e^{ikx_i}. \tag{7}$$

The finite size of the nucleus then is only important in determining the effective wavelength which has to be used in (6). Comparing the collective state (6) with fig. 1 one expects k to be of the order of $k \approx \pi/2R$. Jensen and Steinwedel, who gave a detailed semiclassical analysis of the collective modes (6), determine k by the condition that there is no flow of protons against neutrons across the boundary of the nucleus yielding

$$k = 2.08/R. \tag{8}$$

Another determination of the k to be used in (6) may be obtained directly from (5). If one uses the Thomas-Kuhn-Reiche sum rule to evaluate the numerator in (5), one obtains

$$\omega_D = \frac{1}{2m\langle D^2\rangle}, \tag{9}$$

where the average value of D^2 in the ground state involves only the two particle correlation function $\rho(r, r') = \langle 0|\rho_r\rho_{r'}|0\rangle$,

$$\langle D^2\rangle = \int xx'\rho(r, r')\mathrm{d}^3r\mathrm{d}^3r',$$

with

$$\rho_r = \frac{1}{Z}\sum_{\text{prot.}} \delta(r-r_i) - \frac{1}{N}\sum_{\text{neutr.}} \delta(r-r_i). \tag{10}$$

The TKR dipole sum rule is only valid in the absence of exchange forces.

Bethe and Levinger[11]) have shown that exchange forces modify (9) into

$$\omega_D = \frac{1+\alpha}{2m\langle D^2\rangle}, \tag{9a}$$

with α being of the order of 0.3 to 0.4 thus giving a higher value for ω_D. Approximately the same result was obtained by Gell-Mann, Goldberger and Thirring[12]) using dispersion relation techniques. The physical reason behind this result is, that the dipole state has more pairs in relative p-states than the ground state. Since the exchange forces are repulsive in p-states they tend to push up the energy of the dipole state. To evaluate (10) we use the approximation

$$\rho(r, r') = \rho(r)\rho(r')\sigma(r-r'), \tag{11}$$

where $\rho(r)$ is the particle density normalized to 1 and $\sigma(r)$ the two-particle correlation function of nuclear matter. Introducing the Fourier transformation (ρ_0 the density of nuclear matter)

$$\rho_0\sigma(r) = \int s(k)e^{ik\cdot r}d^3k \tag{12}$$

of $\sigma(r)$ one obtains

$$\langle D^2\rangle = \frac{1}{\rho_0}\int\left|\int x\rho(r)e^{ik\cdot r}d^3r\right|^2 s(k)d^3k. \tag{13}$$

For large nuclei the main contribution of this integral comes from small values of k ($k \approx 1/R$) for which as we shall see $s(k)$ is proportional to k; $s(k) = k/2mc$. Therefore (13) may be approximated by

$$\langle D^2\rangle = \frac{1}{2mck_D} = \frac{s(k_D)}{k_D^2}, \tag{14}$$

where k_D is independent of the form of the two particle correlation (consequently independent of the interaction) and only determined by the size of the nucleus. Using (9) and (14) one obtains

$$\omega_D = \frac{k_D^2(1+\alpha)}{2ms(k_D)} = ck_D. \tag{15}$$

This result now may be compared with the assumption of the collective model, namely that the energy of the dipole state is given by the energy of a collective mode (6) of nuclear matter. Indeed one finds (neglecting exchange forces) exactly [13])

$$\frac{\langle k_D|H|k_D\rangle}{\langle k_D|k_D\rangle} - E_0 = \frac{k_D^2}{2ms(k_D)}. \tag{16}$$

The value of k_D now can be determined by comparing (16) in the non-interacting case with the result (3). Straightforward evaluation of the left hand of

(16) for an ideal Fermi gas gives

$$\omega_D = \tfrac{2}{3}\frac{k_F}{m} k_D. \tag{17}$$

Therefore one obtains using (3)

$$k_D = 1.57/R \approx \pi/2R. \tag{18}$$

We should mention that (17) is in disagreement with both the Jensen-Steinwedel result and the value recently given by Brueckner and Thieberger [14]). Jensen and Steinwedel assume the relation

$$c = \sqrt{\frac{2K}{m}}, \tag{19}$$

where K is the symmetry energy parameter in the Bethe-Weizsäcker formula. Since for an ideal Fermi gas $K = k_F^2/6m$ one obtains

$$c = \frac{1}{\sqrt{3}}\frac{k_F}{m}, \tag{19a}$$

whereas Brueckner and Thieberger obtain

$$c = \frac{k_F}{m}. \tag{19a}$$

Jensen and Steinwedels result is smaller than (17), however, they use a value (8) of k_D which is larger than (15). We therefore, conclude that as in the collective models the energy of the dipole state can be determined from the energy of the corresponding collective mode (6) in nuclear matter. However, one obtains only rough estimates of their energy by using semiclassical pictures.

In fact, it has been observed by Landau [9]) that a weakly non-ideal Fermi gas can sustain collective excitations but of a nature rather different from ordinary classical type, and we shall see later on that these excitations contribute only part of the long range behaviour of a Fermi gas.

These observations are in agreement with the success of the shell model and the optical model, which indicates a mean free path of nucleons large compared to the size of the nucleus, whereas for a stable classical density fluctuation one would expect a mean free path small compared to the wavelength $1/k$.

3. Long Range Correlations of a Fermi gas

In the last few years several methods have been developed to treat the long range and collective behaviour of Fermi gases. They may be classified into three apparently different but essentially equivalent groups:

a) The most elementary method consists of the "time dependent self-consistent field" equation for the excited states. The theory of Landau [8]) mentioned above is based on a Thomas-Fermi field but can be generalized to the Hartree Fock method [15]).

b) The "random phase approximation" which originally was invented for the treatment of long range correlations in dense electron gases [16]), but later on has been applied also to nuclear matter [9]).

c) The "summation of selected diagrams" in perturbation theory which also has been applied to the dense electron gas [17, 18]).

The various interrelations between these methods may be most elegantly studied using the method of Greens functions [19]). We do not want to give a new derivation of the results obtained in all these methods but restrict ourselves to a brief discussion of what is necessary for our purpose.

Let us base our discussion again on the "strength function" which in the nuclear matter case in analogy to (1) may be defined as

$$n(k,\omega) = d(k,\omega) - i\pi a(k,\omega) = \sum_n \frac{|\langle 0|\rho_k|n\rangle|^2}{\omega_n - \omega + i\gamma} + (\omega \to -\omega) \tag{20}$$

and which is connected with the index of refraction of nuclear matter [20]). The Fourier transform of the two-particle correlation $s(k)$ can be obtained from the imaginary part of $n(k,\omega)$ by integration over ω:

$$s(k) = \int_0^\infty a(k,\omega)\mathrm{d}\omega. \tag{21}$$

Let us first calculate $n(k,\omega)$ in zeroth order. This has been done already by Hubbard [17]) but we need his results only in the limiting case of small k values which can be obtained more easily by direct calculation. In zeroth order $\rho_k|0\rangle$ has only non-vanishing matrix elements to states with one particle above and one hole inside the Fermi sea having the total momentum $\mathbf{k}$, spin zero and isospin 1:

$$|n\rangle = \Big(\sum_{\text{prot.}} - \sum_{\text{neutr.}}\Big) a^\dagger(\mathbf{q}+\tfrac{1}{2}\mathbf{k}) a(\mathbf{q}-\tfrac{1}{2}\mathbf{k})|0\rangle = |\mathbf{k},\mathbf{q}\rangle, \tag{22}$$

where $a^\dagger$ and a are the creation and destruction operators of nucleons and the sum is to be taken over the two spin possibilities. The energies ω_n of these states are

$$\omega_{k,q} = \frac{1}{2m}[(\mathbf{q}+\tfrac{1}{2}\mathbf{k})^2 - (\mathbf{q}-\tfrac{1}{2}\mathbf{k})^2] = \frac{\mathbf{k}\cdot\mathbf{q}}{m}. \tag{23}$$

Therefore after introduction of the momentum distribution n_k of the ideal Fermi gas

$$n_k = \begin{cases} 1 & (|\mathbf{k}| \leqq k_F), \\ 0 & (|\mathbf{k}| > k_F), \end{cases} \tag{24}$$

eq. (20) takes the form (assuming equal numbers of protons and neutrons)

$$n_0(k,\omega) = \frac{4}{A}\sum_q \frac{(1-n_{q+\frac{1}{2}k})n_{q-\frac{1}{2}k}}{\frac{\mathbf{k}\cdot\mathbf{q}}{m}-\omega+i\gamma} + (\omega \to -\omega)$$
$$= \frac{3}{4\pi k_F{}^3}\int \frac{(1-n_{q+\frac{1}{2}k})n_{q-\frac{1}{2}k}}{\frac{\mathbf{k}\cdot\mathbf{q}}{m}-\omega+i\gamma}\,\mathrm{d}^3q + (\omega \to -\omega). \tag{25}$$

Fig. 2 shows the region of integration in q-space. For small values of k one can

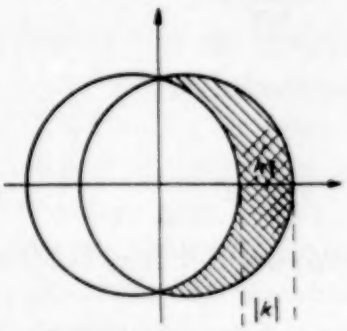

Fig. 2. Region of integration in q-space.

use the approximation

$$(1-n_{q+\frac{1}{2}k})n_{q-\frac{1}{2}k} = \frac{\mathbf{k}\cdot\mathbf{q}}{|\mathbf{q}|}\delta(|\mathbf{q}|-k_f) \tag{26}$$

and after introducing the quantity

$$\omega_k = \frac{k_F}{m}k, \tag{27}$$

which is the maximum possible excitation energy for a given momentum k, one obtains for the dispersive and absorbtive parts of $n_0(k,\omega)$

$$a_0(k,\omega) = \begin{cases} \frac{3}{2}\dfrac{k|\omega|}{k_F\omega_k{}^2} & (|\omega| \leqq \omega_k), \\ 0 & (|\omega| > \omega_k), \end{cases} \tag{28a}$$

$$d_0(k,\omega) = \tfrac{3}{2}\frac{m}{k_F{}^2}\left(2+\frac{\omega}{\omega_k}\ln\left|\frac{\omega-\omega_k}{\omega+\omega_k}\right|\right). \tag{28b}$$

Fig. 3 shows $d_0(k,\omega)$ for positive values of ω. From (28a) it follows immediately

$$s_0(k) = \int_0^{\omega_k} a_0(k_1\omega)\mathrm{d}\omega = \tfrac{3}{4}\frac{k}{k_F}, \tag{29}$$

which agrees with (16) and (17).

Let us now take the interaction into account to first order. A graphical representation of the first order terms is given in fig. 4, in which the wavy line

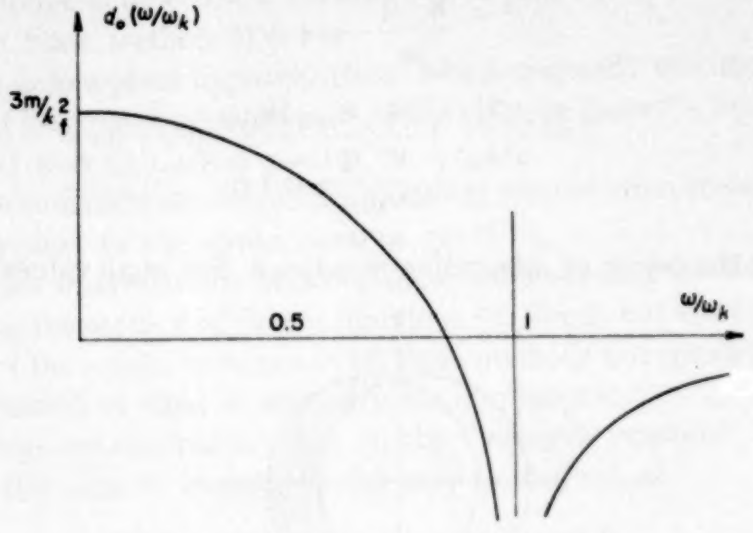

Fig. 3. Dispersive part of n_0 as function of ω.

represents the light quantum (corresponding to the operator ρ_k). In zeroth order this light quantum creates a particle hole pair, whose propagation functions are indicated by the solid lines. The interaction indicated by the dotted line then produces a scattering (or an annihilation and recreation) of

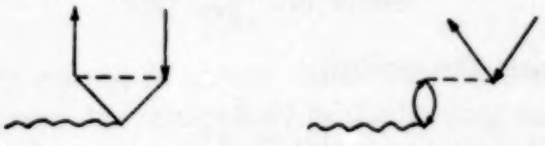

Fig. 4. Diagrams for the particle-hole interaction.

the particle hole pair. In our case, where the pair creation by the γ ray is connected with an isospin flip the annihilation diagram is absent and the scattering diagram gives the contribution

$$n_1(k,\omega) = \frac{4}{A}\sum_{qq'} \frac{n_{q+\frac{1}{2}k} - n_{q-\frac{1}{2}k}}{\dfrac{\mathbf{k}\cdot\mathbf{q}}{m} - \omega + i\gamma}\, v(q'-q)\, \frac{n_{q'+\frac{1}{2}k} - n_{q'+\frac{1}{2}k}}{\dfrac{\mathbf{k}\cdot\mathbf{q}'}{m} - \omega + i\gamma}, \tag{30}$$

where

$$v(q) = \int \mathrm{e}^{i\mathbf{q}\cdot\mathbf{r}} v(r)\,\mathrm{d}^3r \tag{31}$$

is the matrix element of the interaction. Since most of the integral (30) comes from the doubly shaded region in fig. 3, the matrix element for small values of k may be approximately replaced by an average value v_0 close to $v(0)$.

This gives finally

$$n(k, \omega) = n_0(k, \omega) + \tfrac{1}{4}\rho_0 v_0 n_0^2(k, \omega). \tag{32}$$

This result shows that even for arbitrarily small values of v_0 the first order term is large compared to the zeroth order term if n_0 becomes large. This breakdown of straight forward perturbation theory is of course to be expected because of the degeneracies involved in the zeroth order result. A finite answer can be obtained after summing the ladder diagrams of the particle hole scattering, yielding

$$n(k, \omega) = \frac{n_0(k, \omega)}{1 - \tfrac{1}{4}\rho_0 v_0 n_0(k, \omega)}. \tag{33}$$

This is indeed the result following from the theories mentioned above. If there is a hard core, in addition to the ladders introduced above, one has to sum the diagrams for particle-particle scattering, to remove the infinities of the matrix element v_0. This will be discussed in the next section. Furthermore, there are the terms responsible for the energy gap. We will neglect these with the argument that the energy gap is of the order of 1 MeV and is therefore expected to effect the final result for ω_D ($\approx$ 20 MeV for intermediate nuclei) not very much, even if it should require a drastic change in the formalism to include those terms. Eq. (33) now provides us with the desired information about the correlation function $s(k)$ and in addition about the perturbed eigenvalues, which are given by the poles of $d(k, \omega)$. Since the poles of n, according to (33), are given by the zeros of the denominator, one has the eigenvalue equation

$$d_0(k, \omega_n) = \frac{4}{\rho_0 v_0}. \tag{34}$$

Let us compare this condition with the common secular equation method. In this method one assumes the eigenstates to be linear combinations of the states (22),

$$|n\rangle = \sum_q c_{k,q} |\mathbf{k}, \mathbf{q}\rangle, \tag{35}$$

the coefficients $c_{k,q}$ being determined by the secular equation (V is the volume)

$$\omega_n c_{k,q} = \frac{\mathbf{k} \cdot \mathbf{q}}{m} c_{k,q} - \frac{1}{V} \sum_{q'} v(q' - q) c_{k,q'}. \tag{36}$$

If one uses the same average value of the matrix element as in (32), one obtains from (36)

$$\frac{4}{A} \sum \frac{(1 - n_{q+\frac{1}{2}k}) n_{q-\frac{1}{2}k}}{\dfrac{\mathbf{k} \cdot \mathbf{q}}{m} - \omega_n} = \frac{4}{\rho_0 v_0}, \tag{37}$$

which is the same as (35) except for the term ($\omega_n \to -\omega_n$) which is contained in (34) because of (25) but missing in (37).

These terms arise in method a) quoted above from the self consistency requirement, in method b) from an approximate treatment of ground state correlations in the secular equation. In fact the missing terms in (37) correspond to contributions of particles inside and holes outside the Fermi sea which can not occur in the absence of correlations in the ground state, in method c) since all graphs are even functions of ω ("crossing symmetry".)

Let us consider the simple example of Brown and Bolsterli to see if the difference between (34) and (37) is quantitatively relevant. The simple secular equation corresponding to (37) gives

$$\sum_l \frac{l+1}{\omega-\omega_l} = \frac{\sum(l+1)}{\Delta}, \tag{38}$$

where Δ is a measure of the interaction strength and supopsed to be of the order of $\Delta \approx \langle \omega_l \rangle \approx \omega_{\text{osc}}$.

The equation corresponding to (34) is obtained from (38) by adding the term $(\omega \to -\omega)$ yielding

$$\sum_l \frac{2(l+1)\omega_l}{\omega^2-\omega_l^2} = \frac{\sum(l+1)}{\Delta}. \tag{39}$$

After replacing ω_l by its average $\approx \omega_{\text{osc}}$ one obtains the two solutions

$$\omega_{\text{D}} = \omega_{\text{osc}}+\Delta, \tag{40a}$$

$$\omega_{\text{D}} = \sqrt{\omega_{\text{osc}}^2+2\Delta\omega_{\text{osc}}}. \tag{40b}$$

If one assumes $\Delta = \omega_{\text{osc}}$ then (40a) gives $\omega_{\text{D}} = 2\omega_{\text{osc}}$ whereas (40b) gives only $\omega_{\text{D}} = \sqrt{3}\omega_{\text{osc}}$. This seems to indicate, that the difference between both methods is not very large although not entirely negligible †. It seems to be desirable to have a clearer picture of the physical origin of the additional terms in (34) apart from their half formal occurrence in the three methods quoted above.

Let us now consider the imaginary part of n. According to (33) one obtains

$$a = \frac{a_0}{(1-\frac{1}{4}\rho_0 v_0 d_0)^2+(\frac{1}{4}\pi\rho_0 v_0 a_0)^2}. \tag{41}$$

Let us introduce the dimensionless measure $\lambda = 3m\rho_0 v_0/4k_{\text{F}}^2$ of the interaction strength. In the next chapter a relation $\lambda = K/K_0-1$ will be derived, where K_0 is the symmetry energy of the free Fermi gas. Experimentally λ is close to one. In fig. 5, a is plotted as a function of ω for fixed k, and for $\lambda = 1$. For small values of ω/k one finds a value $a \approx a_0(1+\lambda)^{-2}$. If ω/k increases this value is exceeded because of a zero of $1-\frac{1}{4}\rho_0 v_0 d_0$ occurring close to ω_k.

† Compare, however, the discussion after eq. (45a).

There is another zero ω_c of $1-\frac{1}{4}\rho_0 v_0 d_0$ for $\omega_c > \omega_k$. This zero corresponds to an isolated discrete eigenvalue above the zero order continuum of particle-hole states and therefore to a kind of bound state of the particle-hole pair. This state has been discussed in great detail in the papers on collective states in Fermi gases quoted above. Since a_0 is zero for $\omega > \omega_k$ the value of a is not defined at ω_c. But taking the limiting value of $a_0 \to 0$ one obtains

$$a(k, \omega) = \frac{4}{\rho_0 v_0} \delta(1-\tfrac{1}{4}\rho_0 v_0 d_0(k_1 \omega). \tag{42}$$

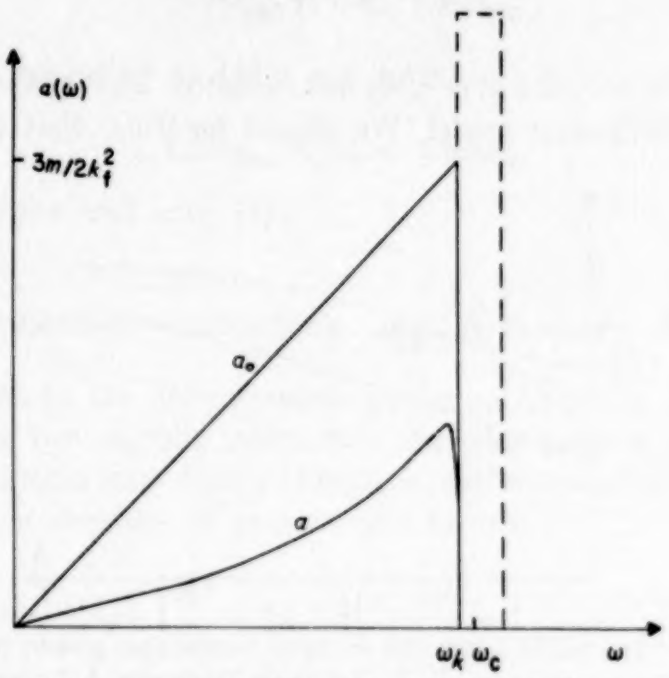

Fig. 5. Absorptive part of n as compared with a_0. The dotted line indicates the area of the δ-function at ω_c.

Using the approximation

$$d_0 = \frac{3m}{2k_F^2}\left\{2-\ln 2+\ln\left|\frac{\omega}{\omega_k}-1\right|\right\} \quad (\omega \approx \omega_k), \tag{43}$$

one finds

$$a = \frac{12}{\lambda^2}\frac{k}{k_F} e^{-(2+2/\lambda)} \delta(\omega-\omega_c) \quad (\omega > \omega_k), \tag{44}$$

$$\omega_c = \omega_k(1+2e^{-(2+2/\lambda)}), \tag{45}$$

which for $\lambda = 1$ gives $a = s_0(k) \cdot 0.27 \cdot \delta(\omega-\omega_c)$, where $s_0(k) = \frac{3}{4}k/k_F$. The integral $\int_0^{\omega_k} a(k, \omega)\, d\omega$ has been evaluated numerically and found to be $0.31\, s_0(k)$. Therefore together with (44) one obtains a value of

$$s(k) = 0.58\, s_0(k), \quad \omega_D = 1.73(1+\alpha)\omega_{osc}, \tag{46}$$

which shows the importance of long range correlations in pushing up the dipole strength to higher energies.

The approximations (43), (44) and (45) are only valid if λ is sufficiently small, so that $\omega_c \approx \omega_k$. In the other extreme of $\lambda \gg 1$ one obtains

$$d_0 = \frac{m}{k_F^2}\left(\frac{\omega_k}{\omega}\right)^2, \tag{43a}$$

$$a = \frac{k}{2mc}\delta(\omega - \omega_c), \tag{44a}$$

$$\omega_c = ck = \sqrt{\frac{2K}{m}}\, k. \tag{45a}$$

Furthermore, the part of a at $\omega < \omega_k$ has vanished. This is exactly the assumption of the semiclassical model. We should mention, that the result (45a)

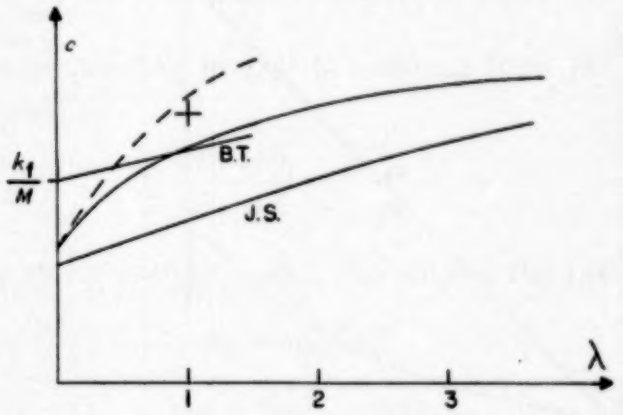

Fig. 6. Velocity c as function of interaction strength. Dotted line: present theory including exchange; solid line: without exchange. B. T.: Brueckner-Thieberger. J. S.: semiclassical model of Jensen-Steinwedel. +: Experiment.

would not follow from the secular eq. method since the difference between (37) and (34) becomes larger with increasing interaction strength. The same can be seen from (40). Whereas (40b) gives a dependence of $\omega_D \approx \sqrt{v_0}$ in accordance with (45a) the simple secular equation method would give a linear dependence of ω_D on v_0. In fig. 6 the results of various theories for c as a function of λ are plotted.

Let us now estimate the value of Δ in (38) to compare our result with (40b). According to Brown and Bolsterli [10]) we have

$$\Delta = \sum (l+1)G, \quad G = \frac{v_0}{4\pi} < \int_0^\infty R_l R_{l+1} R_{l'} R_{l'+1} r^2 \mathrm{d}r. \tag{47}$$

G is some average value of the matrix element between two particle-hole states. One can get an upper limit for G by taking the radial wave function to be constant,

$$R_l \approx \sqrt{3/r_0^3 A},$$

yielding

$$\sigma \approx 3v_0/(4\pi r_0^3 A).$$

In general one will get a smaller value because of destructive interference and concentration of the integrand in (47) at smaller r-values. Let us assume the lower limit to be about half of the upper limit. If one furthermore approximates $\sum(l+1)$ by $\frac{1}{2}(\frac{3}{2}A)^{\frac{4}{3}}$ following from the number of states in the highest oscillator shell then using (3) one obtains finally

$$0.7\lambda\omega_{\text{osc}} \lesssim \Delta \leqq 1.4\lambda\omega_{\text{osc}}$$

and for $\lambda \approx 1$ according to (40b) one finds

$$1.55\omega_{\text{osc}} \lesssim \omega_{\text{D}} < 1.95\omega_{\text{osc}} \tag{48}$$

which agrees quite well with (46).

4. Collective Excitations and Symmetry Energy

We now come to the determination of the parameter v_0 representing the strength of the two particle interaction. For this purpose we consider the Hartree-Fock ground state energy of nuclear matter including small deviations from equilibrium densities of protons and neutrons

$$\varepsilon = \frac{3}{5}\frac{k_{\text{F}}^2}{3m} + \frac{3}{8}\rho_0 v_0 + \left(\frac{k_{\text{F}}^2}{3m} + \tfrac{3}{4}\rho_0 v_0\right)\left(\frac{\rho-\rho_0}{\rho}\right)^2 + \left(\frac{k_{\text{F}}^2}{6m} - \frac{\rho_0 v_0}{8}\right)\left(\frac{N-Z}{A}\right)^2. \tag{49}$$

The first term is the average binding energy

$$\varepsilon_{\text{b}} = -16\ \text{MeV}, \tag{50}$$

the second one contains the reciprocal compressibility

$$\frac{1}{\kappa} = 11 \text{ to } 17\ \text{MeV}, \tag{51}$$

and the third one the symmetry energy

$$K \approx 24\ \text{MeV}. \tag{52}$$

Using these three different experimental values and in addition the single-particle energy at the Fermi surface

$$\frac{k_{\text{F}}^2}{2m} + \tfrac{3}{4}\rho_0 v_0 = -16\ \text{MeV}, \tag{53}$$

which because of the saturation condition is equal to ε_{b}, one obtains with

$k_F^2/2m = 38$ MeV four different values for $\rho_0 v_0$,

$$-\rho_0 v_0 \begin{cases} =104 \\ = 72 \\ \approx 15 \\ \approx 90 \end{cases} \text{MeV}; \quad \text{from} \begin{cases} \text{binding energy,} \\ \text{single-part. energy,} \\ \text{compressibility,} \\ \text{symmetry energy.} \end{cases} \tag{54}$$

The considerable variation of these values reflects the well-known failure of the weak zero range force model to produce the right saturation properties of nuclear matter. If one wants to take into account the hard core to get saturation one has to replace the potential v in (30) by the appropriate pseudopotential w which we have to determine now.

It is well-known that the pseudopotential appropriate for the ground state energy is the Brueckner K-matrix. Glassgold, Heckrotte and Watson [12]) therefore replace v in (30) by K. We shall see, however, that this is a poor approximation being not valid even in second order perturbation theory.

The pseudopotential depends on the states the properties of which it is used to describe. In particular, it depends on the density and the neutron excess. Indeed (54) indidates that there is a strong density dependence and less strong dependence on the neutron excess. As we shall show the appropriate pseudopotential for the collective excitations responsible for the dipole resonance should be determined from the symmetry energy according to

$$-\frac{\rho_0 v_0}{8} = K - \frac{k_F^2}{6m}. \tag{55}$$

Since the experimental value of K is close to twice the theoretical value of an ideal Fermi gas we arrive at the relation

$$-\rho_0 v_0 \approx \frac{4}{3}\frac{k_F^2}{m}, \tag{56}$$

which was used in the calculations above. In doing this we still have neglected the spin-, isospin- and momentum-dependence of the force. We hope that this approximation does not introduce large errors, since all these effects enter in a similar way in the dipole state and the symmetry energy and are therefore taken into account partly by using the experimental value of the symmetry energy.

Similarly the effective potential for the regular density fluctuations (sound waves, resp. Landau's [8]) zeroth sound) is connected with the compressibility. Because of the strong density dependence of the pseudopotential pointed out above this is quantitatively very different from what one would obtain using the binding energy. It is therefore important in the discussion of the imaginary roots of the eigenvalue eq. (34) considered by Glassgold, Heckrotte and Watson [9]). In the case of density fluctuations the states (22) have to be replaced by

$$|k, q\rangle = \tfrac{1}{2}\Big(\sum_{\text{prot.}} + \sum_{\text{neutr.}}\Big) a^\dagger_{q q+\frac{1}{2}k} a_{q-\frac{1}{2}k}|0\rangle.$$

and the eigenvalue eq. (34) takes the form:

$$\frac{4}{A}\sum_{q}\frac{(1-n_{q+\frac{1}{2}k})n_{q-\frac{1}{2}k}}{\omega-\dfrac{\mathbf{k}\cdot\mathbf{q}}{m}}+(\omega\to-\omega)=\frac{4}{3\rho_0\bar{v}_0}.$$

The change in sign of the right-hand side compared to (34) is a consequence of the annihilation diagram of fig. 4 which contributes in the case of spin (and isospin) zero states like sound waves. Introducing again the approximation (26) and $3m\rho_0\bar{v}_0/4k_F^2=-\tilde{\lambda}$, one obtains

$$\int_{-1}^{1}\frac{\eta\mathrm{d}\eta}{\omega/\omega_k-\eta}=-\frac{2}{3\tilde{\lambda}},$$

which for negative $\tilde{\lambda}$ has no real solutions but may have imaginary roots, i.e. solutions of

$$\frac{1}{2}\int_{-1}^{1}\frac{\eta^2\mathrm{d}\eta}{(i\omega/\omega_k)^2+\eta^2}=2/3\tilde{\lambda},$$

with $i\omega$ real. Since the left-hand side of this equation is always smaller than one, these imaginary roots can only occur if $\tilde{\lambda}>\frac{2}{3}$, i.e. for sufficiently strong forces, a case which could not be excluded using the ground state K-matrix as the effective particle hole interaction matrix, yielding $\tilde{\lambda}\approx 1$ whereas the $\tilde{\lambda}$ determined from the compressibility is smaller by a factor of about seven. This seems to indicate, that in the case of nuclear matter the unstable solutions of Glassgold, Heckrotte and Watson are not likely to occur, although they cannot be excluded in general for a many body system.

To justify our use of the symmetry energy above, let us first determine the pseudopotential in second order. This can be done in the most elementary way using the time independent (Rayleigh-Schrödinger) perturbation theory. In this method the excited states in zeroth order are linear combinations of the particle hole excitations (spin and isospin omitted in the following considerations):

$$\varphi_{k,l}=a_k^{\dagger}a_l|0\rangle, \tag{57}$$

$$\psi=\sum_{k,l}c_{k,l}\varphi_{k,l}. \tag{58}$$

The higher order terms then may be obtained in general from

$$\psi=\sum c_{k,l}\varphi_{k,l}-\frac{P}{H_0-E}v\psi, \tag{59}$$

where H_0 is the kinetic energy, v the interaction potential, E the energy of ψ and P the projection operator

$$P=1-\sum_{k,l}|\varphi_{k,l}\rangle\langle\varphi_{k,l}|. \tag{60}$$

The solution of (59) can be written as

$$\psi=\sum_{k,l}c_{k,l}\psi_{k,l}, \tag{61}$$

where $\psi_{k,l}$ is the solution of

$$\psi_{k,l} = \varphi_{k,l} - \frac{P}{H_0 - \mathscr{E}_{k,l}} (v - E + \mathscr{E}_{k,l}) \psi_{k,l}. \tag{62}$$

$\mathscr{E}_{k,l} = \mathscr{E}_0 + \varepsilon_k - \varepsilon_l$ is the zeroth order energy of the single particle energy. The Schroedinger equation then finally gives a secular equation for $c_{k,l}$:

$$E c_{k,l} = (\mathscr{E}_{k,l} + \langle \varphi_{k,l} | v | \psi_{k,l} \rangle) c_{k,l} + \sum_{k', l' \neq k, l} \langle \varphi_{k',l} | v | \psi_{k.l} \rangle c_{k',l'}, \tag{62}$$

which in first order $\psi_{k,l} = \varphi_{k,l}$ is equivalent to (36). In second order

$$\psi_{k,l} = \varphi_{k,l} - \frac{P}{H_0 - \mathscr{E}_{k,l}} v \varphi_{k,l} \tag{63}$$

one obtains for the effective non-diagonal matrix element

$\langle \varphi_{k,l} | v | \psi_{k',l'} \rangle$

$$\begin{aligned} &= v_{kl',lk'} + \sum_{p,q} \frac{v_{kl',pq} v_{pq,lk'}}{\varepsilon_k + \varepsilon_l - \varepsilon_p - \varepsilon_q} (1 - n_p)(1 - n_q) - \sum_{p,q} \frac{v_{kl',pq} v_{pq,lk'}}{\varepsilon_k + \varepsilon_{l'} - \varepsilon_p - \varepsilon_q} n_p n_q \\ &+ 2 \sum_{p',p} \frac{v_{kp,k'p'} v_{l'p',lp}}{\varepsilon_{l'} + \varepsilon_{p'} - \varepsilon_l - \varepsilon_p} (1 - n_{p'}) n_p + 2 \sum_{p',p} \frac{v_{l'p',lp} v_{kp,k'p'}}{\varepsilon_k + \varepsilon_p - \varepsilon_{k'} - \varepsilon_{p'}} n_{p'} (1 - n_p). \end{aligned} \tag{64}$$

The first of the four second order terms is just the second order term in the expansion of the Brueckner K-matrix

$$K_{kl',lk'} = v_{kl',lk'} - \sum_{p,q} \frac{v_{kl',pq} v_{pq,lk'}}{\varepsilon_p + \varepsilon_q - \varepsilon_l - \varepsilon_{k'}} (1 - n_p)(1 - n_q). \tag{65}$$

The other three terms therefore are missing in the effective particle-hole force, if one takes it to be just $K_{kl',lk'}$.

More elegantly these terms are obtained in the method c) quoted above. I this case the effective particle-hole force consists of all diagrams which canno. be written as ladders with one particle and one hole line (fig. 7). Therefore in second order one has essentially the three graphs of fig. 7(b). The first one corresponds to an intermediate particle-particle scattering and to the second order term of the K-matrix expansion of fig. 7(c) and the second and third graphs of fig. 7(b) may be identified with the intermediate hole-hole and hole-particle scattering terms of (64).

One can now find a connection between the pseudopotential and the symmetry energy in comparing (64) with Landau's ansatz for the effective particle-hole force. He considers the energy E of excited states as a function (resp. functional in infinite nuclear matter) of the momentum distribution n_k)† and

† In second order for the pseudopotential we may use the zeroth order n_k since there is no first order change in n_k.

postulates

$$w_{kk',\,kk'} = \langle \varphi_{kk'} | v | \psi_{kk'} \rangle = \frac{\partial^2 E}{\partial n_k \, \partial n_{k'}}, \tag{66}$$

the derivatives being taken at the ground state values of the n_k's.

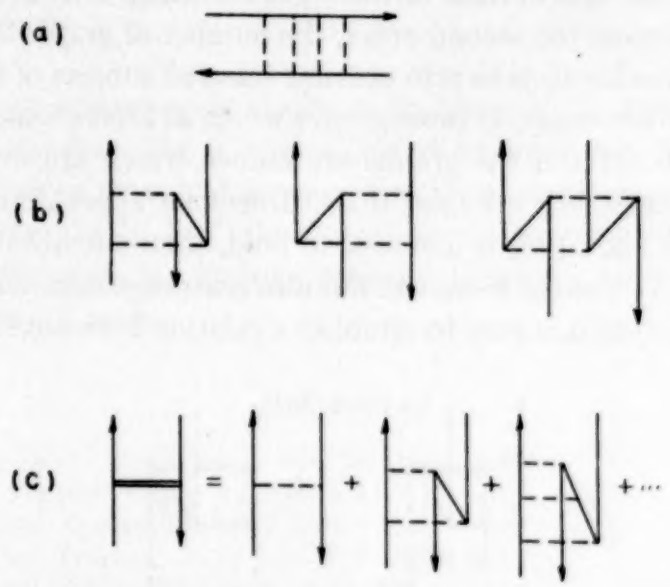

Fig. 7. (a) Particle-hole ladder, (b) second order graphs for the pseudopotential, and (c) K-matrix expansion.

Now taking the second order expression for E,

$$E = \sum \frac{p^2}{2m} n_p + \tfrac{1}{2} \sum v_{pp',\,pp'} n_p n_{p'} - \tfrac{1}{2} \sum \frac{|v_{pq,\,p'q}|^2}{\varepsilon_{p'} + \varepsilon_{q'} - \varepsilon_p - \varepsilon_q} (1 - n_{p'})(1 - n_{q'}) n_p n_q, \tag{67}$$

one obtains

$$w_{kk',\,kk'} = v_{kk',\,kk'} - \sum_{p,\,q} \frac{|v_{kk',\,pq}|^2}{\varepsilon_p + \varepsilon_q - \varepsilon_k - \varepsilon_{k'}} [(1 - n_p)(1 - n_q) - n_p n_q] + 4 \sum_{p,\,p'} \frac{|v_{kp,\,k'p'}|^2}{\varepsilon_{k'} + \varepsilon_{p'} - \varepsilon_k - \varepsilon_p} (1 - n_{p'}) n_p. \tag{68}$$

These terms are easily identified with the corresponding ones in (64) in the limiting case $l \to k$, $l' \to k'$ i.e. long wavelengths of the collective modes. Only in this case the Landau theory can be expected to be valid. This indicates another interpretation of the higher order corrections: If one writes E as

$$E = \sum \frac{p^2}{2m} n_p + \tfrac{1}{2} \sum K_{pp',\,pp'} n_p n_{p'}, \tag{69}$$

with $K_{pp',\,pp'}$ given by (65), the second and third graphs in fig. 7(b) correspond

to derivatives of the K-matrix, i.e. rearrangement terms following from the dependence of the propagator

$$\frac{(1-n_p)(1-n_q)}{\varepsilon_p+\varepsilon_q-\varepsilon}$$

on the momentum distribution of the state for which it is used.

If one goes beyond the second order, the number of graphs increases rapidly and it is only possible to take into account selected subsets of the whole series. The Landau method suggests those graphs which at least should be summed for the particle hole force if the graphs are known which are important for the ground state energy. For instance, if the Brueckner approximation is valid for the ground state, and (66) is assumed to hold, then one obtains not only the diagrams of fig. 7(c) of the K-matrix but also rearrangement terms like those in fig. 8. Assuming (66) it is easy to establish a relation between the pseudopoten-

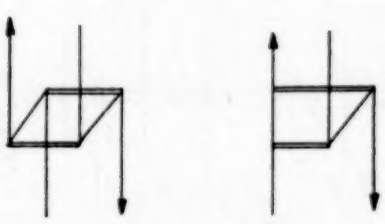

Fig. 8. Rearrangement terms in the particle-hole force.

tial and the symmetry energy, resp. the compressibility. For this purpose consider the change in energy by replacing a certain amount $\delta N = \sum_{\text{neutr.}} \delta n_k$ of neutrons by $\delta Z = \sum_{\text{prot.}} \delta n_k = -\delta N$ protons with δn_k distributed uniformly over the Fermi surface. Then on the one hand one obtains, using (66),

$$\delta E = \tfrac{1}{2} \sum w_{kk',\,kk'} \delta n_k \delta n_{k'} + \frac{k_F^2}{6m} \left(\frac{\delta N - \delta Z}{A} \right)^2, \tag{70}$$

the last term coming from the change in the Fermi momenta for the neutrons and protons. On the other hand the definition of the symmetry energy gives

$$\delta E = K \left(\frac{\delta N - \delta Z}{A} \right)^2. \tag{71}$$

Therefore, instead of the simple relation (55) one obtains

$$-\tfrac{1}{8}\rho_0 \int w(\Omega) \mathrm{d}\Omega / 4\pi = K - \frac{k_F^2}{6m}, \tag{72}$$

where the angle integration should be understood to run over the angle between $\mathbf{k}$ and $\mathbf{k}'$ the absolute magnitude of them being equal to $|\mathbf{k}| = |\mathbf{k}'| = k_F$.

A similar consideration for the density fluctuations gives a relation between the effective force $\tilde{w}$ and the compressibility namely

$$\tfrac{3}{4}\rho_0 \int \tilde{w}(\Omega)\mathrm{d}\Omega/4\pi = \frac{1}{\kappa} - \frac{{k_\mathrm{F}}^2}{3m}.$$

This result differs from Landau's formula [8]) by a factor $\frac{3}{2}$, only because of the inclusion of isospin.

The author takes pleasure in thanking Professor V. F. Weisskopf for many stimulating discussions. He is also indebted to Professor K. Gottfried and Professor A. Kerman for valuable comments. He wishes to express his gratitude to the members of the M. I. T. theoretical physics group for their hospitality. The Bundesministerium für Atomkernenergie, Germany, supported his visit to U.S.A. by a travel grant.

References

1) M. Goldhaber and E. Teller, Phys. Rev. **74** (1948) 1046
2) D. M. Brink, Nuclear Physics **4** (1957) 215
3) D. H. Wilkinson, Physica **12** (1956) 1039
4) Schiffer, Lee and Zeidman, Phys. Rev. **115** (1959) 427
5) V. F. Weisskopf, Nuclear Physics **3** (1957) 423
6) K. A. Brueckner, Phys. Rev. **110** (1958) 597
7) A. Migdal, J. Phys. USSR **8** (1944) 337;
H. Steinwedel and J. H. D. Jensen, Z. Naturf. **5a** (1950) 413
8) L. D. Landau, Sovj. Phys. JETP **3** (1957) 920
9) A. E. Glassgold, W. Heckrotte and K. M. Watson, Ann. Phys. **6** (1959) 1
10) J. P. Elliot and B. H. Flowers, Proc. Roy. Soc. A **242** (1957) 57;
G. E. Brown and M. Bolsterli, Phys. Rev. Letters **3** (1960) 472
11) J. S. Levinger and H. A. Bethe, Phys. Rev. **78** (1950) 115
12) M. Gell-Mann, M. L. Goldberger and W. Thirring, Phys. Rev. **95** (1954) 1612
13) R. P. Feynman, Phys. Rev. **94** (1954) 262
14) K. M. Brueckner and R. Thieberger, Phys. Rev. Letters **4** (1960) 466
15) Ferrel, Phys. Rev. **107** (1957) 1631;
F. Goldstone and K. Gottfried, Nuovo Cim. **13** (1959) 849
16) D. Bohm and D. Pines, Phys. Rev. **92** (1953) 609
17) F. Hubbard, Proc. Roy. Soc. A **423** (1957) 336
18) M. Gell-Mann and K. A. Brueckner, Phys. Rev. **106** (1957) 364
19) V. M. Galitskii and A. Migdal, Sovj. Phys. JETP **7** (1958) 96
20) F. Lindhardt, Mat. Fys. Medd. Dan. Vid. Selsk. **28**, No. 8 (1954)

2.G

Nuclear Physics **22** (1961) 34—46; © *North-Holland Publishing Co., Amsterdam*

Not to be reproduced by photoprint or microfilm without written permission from the publisher

POLARIZATION IN (d, p) REACTIONS

D. ROBSON

Physics Department, University of Melbourne

Received 12 August 1960

Abstract: Previous treatments of the distorted wave theory in stripping are extended to include the effects of spin-orbit forces in both incident and final channels. Numerical calculations of the C^{12}(d, p)C^{13} ground state reaction at 8.9 MeV incident energy using rounded optical model potentials yield the correct sign for the polarization of the emergent protons. The inclusion of spin-orbit forces in both channels relieves the 33⅓ % restriction on the size of the polarization. Polarizations as large as 70 % are predicted in this way and provide a likely explanation of the large experimental polarizations. The distorted wave functions used to describe the stripping reaction are also used to predict elastic scattering angular distributions and polarizations. Good agreement is found with experiment in cases where data are available.

1. Introduction

Several investigations have been carried out to improve on the simple stripping theories [1]) by using distorted waves for the incident and emergent particles [2, 3]). The simple theories although quite useful for the purposes of nuclear spectroscopy are based essentially on the 'plane-wave' Born approximation and consequently predict zero polarization for the emergent particles. Huby *et al.* [4]) in the case of spin independent distorting potentials, have shown that the polarization is limited to a maximum of $33\frac{1}{3}$ %. However, experimental measurements of the polarization in the C^{12}(d, p)C^{13} ground state reaction at 4 MeV by Hillman [5]) and at 9 MeV by Bokhari *et al.* [6]) show that the polarization reaches 60 % at certain angles.

The $33\frac{1}{3}$ % theoretical restriction is relaxed if spin-dependent forces are included in the distortion. Newns and Refai [7]) have shown that the restriction is only slightly removed if a small spin-orbit force is introduced into the proton-nucleus interaction. In this case the interaction of the deuteron with the nucleus was represented by a hard sphere and the proton-nucleus interaction by a complex central potential plus a spin-orbit potential. Newns and Refai were unable to predict the correct sign for the polarization in the C^{12}(d, p)C^{13} reaction for 3.3 MeV deuterons.

Recently Tobocman [3]) has improved on the Newns and Refai calculations by using rounded optical model potentials, (but neglecting spin-orbit effects), for both the deuteron and proton interactions and also by allowing the process to take place throughout the nucleus. In this way the correct sign for the polarization in the B^{10}(d, p)B^{11} reaction was obtained. In order to obtain the

correct sign for the polarization at angles corresponding to the stripping peak, it has been shown [7]) that the effects of the deuteron distortion must predominate over the proton distortion. Apparently the use of a hard sphere for the deuteron-nucleus interaction is too crude an approximation where polarization is concerned.

It will be seen that the correct sign for the polarization in the C^{12}(d, p)C^{13} reaction for 9 MeV deuterons is obtained by using rounded optical model potentials for both the deuteron and proton interactions. In order to explain the large experimental values for the polarization, calculations have been carried out including spin-orbit interactions in both the deuteron-nucleus interaction and the proton-nucleus interaction. Predicted magnitudes for the polarization reach 70 % at some angles and the polarization produced when spin orbit forces are included is much larger than was previously found [7]). The sizes of the spin-orbit potentials are larger than that used by Newns and Refai. In the case of the proton-nucleus interaction the size of the spin-orbit interaction used here is shown to be consistent with elastic scattering by comparing the theoretical prediction for the polarization in the elastic scattering of protons on carbon with experiment. The deuteron elastic scattering angular distribution and polarization are also calculated and the angular distribution compared with available data.

2. Theory

In this section the general expression for the transition matrix for the reaction A(d, p)B including spin-orbit interactions in both initial and final channels is obtained. Previous derivations of the transition matrix, (e.g. Cheston [8]), subsequently corrected by Sawicki [9])), have included a spin-orbit interaction in the final channel only. A similar notation to Cheston and Sawicki is used here.

The amplitude for the reaction A(d, p)B using distorted waves is given [4]) by

$$I_{M_B M_A} = \int \psi_p(\mathbf{k}_p, \mathbf{r}'_p s_p)^* \chi_{I_B M_B}(\xi \mathbf{r}_n s_n)^* V_{np}(|\mathbf{r}_n - \mathbf{r}_p|) \phi_d(\mathbf{r}_n - \mathbf{r}_p) \times \psi_d(\mathbf{k}_d, \mathbf{r}_n \mathbf{r}_p s_n s_p) \chi_{I_A M_A}(\xi) d\tau \tag{2.1}$$

Here $\chi_{I_A M_A}$ and $\chi_{I_B M_B}$ are the wave functions of the target nucleus A and final nucleus B respectively. ψ_p and ψ_d are the spatial-spin wave functions of the proton and deuteron relative to the target nucleus, as distorted by some suitable spin-dependent potentials due to the nucleus. V_{np} is a triplet state potential and ϕ_d the orbital internal wave function of the deuteron. The tensor effects arising from the small D-state part of the deuteron wave function, and the tensor component of the interaction V_{np} have been shown to be small [10]) and are neglected in the present discussion. The co-ordinates are as defined in ref. [4]).

The integration over ξ may be carried out in the usual way [4]),

$$\int \chi_{I_B M_B}(\xi \mathbf{r}_n s_n)\chi_{I_A M_A}(\xi)\mathrm{d}\xi$$
$$= \sum_{j\mu_j l m_{\mu_n}} C(I_A j I_B, M_A \mu_j M_B) C(l\tfrac{1}{2} j, m\mu_n \mu_j)\theta^*_{jl} u_l(r_n)^* i^{-l} Y_l^m(\theta_n, \phi_n)^* \chi_{\mu_n}(s_n). \quad (2.2)$$

Here j and l are the total and orbital angular momenta with which the stripped neutron enters the nucleus. The coefficient θ_{jl} is a "reduced width amplitude". χ_{μ_n} is a neutron spin wave function and u_l is a normalised orbital wave function. The Clebsch-Gordan coefficients are as defined by Rose [11]).

The distorting potential is assumed to be a Woods-Saxon optical potential plus a Thomas-Fermi type spin-orbit potential,

$$V(\mathbf{r}, \boldsymbol{\sigma}\cdot\mathbf{L}) = -(V+iW)g(r)+V_s\left(\frac{\hbar}{m_\pi c}\right)^2 r^{-1}\frac{\mathrm{d}g}{\mathrm{d}r}\boldsymbol{\sigma}\cdot\mathbf{L}. \quad (2.3)$$

The potential parameters V and W are positive real functions so that the central force is attractive and absorptive, and V_s is a positive real quantity corresponding to the sign of the spin-orbit force in the shell model. $(\hbar/m_\pi c)$ is the Compton pion wavelength and $g(r)$ is the Woods-Saxon form factor,

$$g(r) = \{1+\exp[(r-R)/a]\}^{-1}, \quad (2.4)$$

where a is the diffuseness parameter. In the case of the deuteron $\boldsymbol{\sigma}\cdot\mathbf{L}$ may take three values depending on whether $J_d = L_d \pm 1, L_d$; i.e.

$$\boldsymbol{\sigma}\cdot\mathbf{L}_d = \begin{cases} 2L_d & , \ J_d = L_d+1, \\ -2 & , \ J_d = L_d, \\ -2(L_d+1), & J_d = L_d-1. \end{cases} \quad (2.5)$$

The use of such potentials for nucleons is well established [12]) and the extension to deuterons has been shown by Watanabe [13]).

For a particle moving in such a potential the constants of motion are J^2, L^2, S^2 and J_z and hence the appropriate partial wave expansions are [14])

$$\psi(\mathbf{krs}) = \sum_{LM}\sum_{JM_J} \mathscr{A}^*(LM)C(LsJ, M\mu M_J)\psi(JLM_J), \quad (2.6)$$

in which J, L and s have their usual meanings and $\mathscr{A}(LM)$ is defined such that $\psi(\mathbf{krs})$ is normalised to unit amplitude at infinity, i.e.

$$\mathscr{A}^*(LM) = 4\pi i^L Y_L^M(\theta_k, \phi_k)^*, \quad (2.7)$$

and

$$\psi(JLM_J) = \sum_{\bar{M}\bar{\mu}} C(LsJ, \bar{M}\bar{\mu}M_J)\psi(JL\bar{M})\chi_{\bar{\mu}}(s). \quad (2.8)$$

The integral is easily evaluated if a zero range force is taken for V_{np}, e.g.

$$V_{np}(|\mathbf{r}_n-\mathbf{r}_p|)\phi_d(\mathbf{r}_n-\mathbf{r}_p) = \frac{-\hbar^2\sqrt{8\pi\alpha}}{2M_{np}}\delta(\mathbf{r}_n-\mathbf{r}_p) = K\delta(\mathbf{r}_n-\mathbf{r}_p), \quad (2.9)$$

where M_{np} is the reduced mass of the neutron in the deuteron and α is the wave number required to give the binding energy of the deuteron.

Following a similar argument to ref. [8, 9]) the transition matrix may now be written

$$\begin{aligned} I_{\mu_p M_B, \mu_d M_A} &= K(4\pi)^{-\frac{1}{2}} \sum_{l_j L_p L_d J_p J_d} C(I_A j I_B, M_A \mu_j M_B) C(L_d l L_p, 000) \frac{\hat{L}_d \hat{l}}{\hat{L}_p} \\ &\times \theta^*_{jl} i^{-l} R_{L_p L_d J_p J_d l_j} \sum_{M_p M_d} \mathscr{A}(L_p M_p) \mathscr{A}^*(L_d M_d) C(L_p \tfrac{1}{2} J_p, M_p \mu_p M_p+\mu_p) \\ &\times C(L_d 1 J_d, M_d \mu_d M_d+\mu_d) \sum_{\mu_j \bar{\mu}_d \bar{\mu}_p} C(L_p \tfrac{1}{2} J_p, M_p+\mu_p-\bar{\mu}_p \bar{\mu}_p M_p+\mu_p) \\ &\times C(L_d 1 J_d, M_d+\mu_d-\bar{\mu}_d \bar{\mu}_d, M_d+\mu_d) C(l \tfrac{1}{2} j, \mu_j-\bar{\mu}_d+\bar{\mu}_p, \bar{\mu}_d-\bar{\mu}_p, \mu_j) \\ &\times C(\tfrac{1}{2}\tfrac{1}{2}1, \bar{\mu}_d-\bar{\mu}_p \bar{\mu}_p \bar{\mu}_d) C(L_d l L_p, M_d+\mu_d-\bar{\mu}_d \bar{\mu}_d-\bar{\mu}_p-\mu_j M_p+\mu_p-\bar{\mu}_p), \end{aligned} \quad (2.10)$$

in which the subscripts p and d indicate proton and deuteron respectively and

$$R_{L_p L_d J_p J_d l_j} = \int f_{J_p L_p}(k_p r) u_l(r)^* f_{J_d L_d}(k_d r) r^2 \mathrm{d}r, \quad (2.11)$$

where the functions $f_{J_p L_p}(k_p r)$ and $f_{J_d L_d}(k_d r)$ are radial wave functions for the proton and deuteron respectively. The notation $\hat{j} = (2j+1)^{\frac{1}{2}}$ is used for brevity. If the spin-orbit interaction in the incident channel is neglected, (2.10) reduces to the form of eq. (2) of ref. [9]).

The sum over $\bar{\mu}_d$ and $\bar{\mu}_p$ in (2.10) is performed using Racah algebra and the resultant expression for the amplitude is

$$\begin{aligned} I_{\mu_p M_B, \mu_d M_A} &= K(4\pi)^{\frac{1}{2}} \sum_{l_j L_p L_d J_p J_d} C(I_A j I_B, M_A \mu_j M_B) C(L_d l L_p, 000) \\ &\times (-1)^{L_d+L_p+J_p+J_d} i^{L_d-l-L_p} \sqrt{3} \hat{l} \hat{j} \hat{L}_d \hat{J}_d \theta^*_{jl} R_{L_p L_d J_p J_d l_j} \\ &\times X(L_p \tfrac{1}{2} J_p, l \tfrac{1}{2} j, L_d 1 J_d) \sum_{M_p \mu_j} (-1)^{\mu_j} C(L_p \tfrac{1}{2} J_p, M_p \mu_p M_p+\mu_p) \\ &\times C(L_d 1 J_d, M_p+\mu_j+\mu_p-\mu_d \mu_d M_p+\mu_j+\mu_p) \\ &\times C(J_d j J_p, M_p+\mu_j+\mu_p, -\mu_j M_p+\mu_p) Y^{M_p}_{L_p}(\theta_{k_p}, \phi_{k_p}) Y^{M_p+\mu_j+\mu_p-\mu_d}_{L_d}(\theta_{k_d}, \phi_{k_d})^*. \end{aligned} \quad (2.12)$$

This final form for the transition amplitude is probably the best form for numerical calculations. Tables of the X-coefficient occurring in (2.12) are available in both decimal [15]) and algebraic [16]) form.

The cross section and polarization are related to the amplitude by

$$\sigma(\theta) = \frac{m_p^* m_d^* k_p}{(2\pi\hbar^2)^2 k_d 3(2I_A+1)} \sum_{\mu_p M_B \mu_d M_A} |I_{\mu_p M_B, \mu_d M_A}|^2, \tag{2.13}$$

and

$$P(\theta) = P_z = \frac{\sum_{\mu_d M_A M_B} |I(\mu_p = +\frac{1}{2})|^2 - \sum_{\mu_d M_A M_B} |I(\mu_p = -\frac{1}{2})|^2}{\sum_{\mu_d M_A M_B} |I(\mu_p = +\frac{1}{2})|^2 + \sum_{\mu_d M_A M_B} |I(\mu_p = -\frac{1}{2})|^2}, \tag{2.14}$$

where the axis of quantisation is chosen parallel to the vector $\mathbf{k}_d \times \mathbf{k}_p$, i.e. perpendicular to the plane of the reaction.

In the case of the spin-orbit interaction being neglected (2.13) and (2.14) are much simpler and are given [4]) by

$$\sigma_0(\theta) = \frac{m_p^* m_d^* k_p (2I_B+1)}{(2\pi\hbar^2)^2 k_d 2(2I_A+1)} \sum_{jl} \theta_{jl}^2 \Big(\sum_m |B_l^m|^2 \Big), \tag{2.15}$$

and

$$P_0(\theta) = \frac{\sum_{jl} (-1)^{j-l-\frac{1}{2}} \theta_{jl}^2 (j+\frac{1}{2})^{-1}}{3 \sum_{jl} \theta_{jl}^2} \left\{ \frac{\sum_m m |B_l^m|^2}{\sum_m |B_l^m|^2} \right\}, \tag{2.16}$$

where B_l^m are amplitudes for the absorption of the neutron with quantum numbers (l, m) as defined in ref. [6]). Numerical calculations for C^{12}(d, p)C^{13} at 8.9 MeV deuteron energy are discussed in section 4.

3. Elastic Scattering of Protons and Deuterons by Carbon

As a test of the optical model wave functions used to describe the stripping reaction, the elastic scattering cross sections and polarizations are calculated using the same optical model parameters. For 8.9 MeV deuterons, the emerging protons from the C^{12}(d, p)C^{13} ground state reaction have an energy of 11.6 MeV. The cross section and polarization for elastic scattering of nucleons using the complex spin-dependent potential of eq. (2.3) are given [17]) by

$$\sigma(\theta) = A^* A + B^* B, \tag{3.1}$$

and

$$\mathbf{P}(\theta) = P(\theta)\mathbf{n} = [(A^* B + B^* A)/(A^* A + B^* B)]\mathbf{n}, \tag{3.2}$$

where $A(\theta)$ and $B(\theta)$ are the amplitudes for spin-independent and spin-dependent scattering respectively [17]). For the 11.6 MeV protons on C^{13} Coulomb effects were neglected. Fig. 1 shows the theoretical cross section for the elastic scattering of 11.6 MeV nucleons by C^{13} using the optical parameters, $V_p = 45$ MeV, $W_p = 10$ MeV, $V_{s_p} = 8$ MeV, $a_p = 0.5 \times 10^{-13}$ cm and $R_p = 1.2 \times 10^{-13} A^{\frac{1}{3}}$ cm.

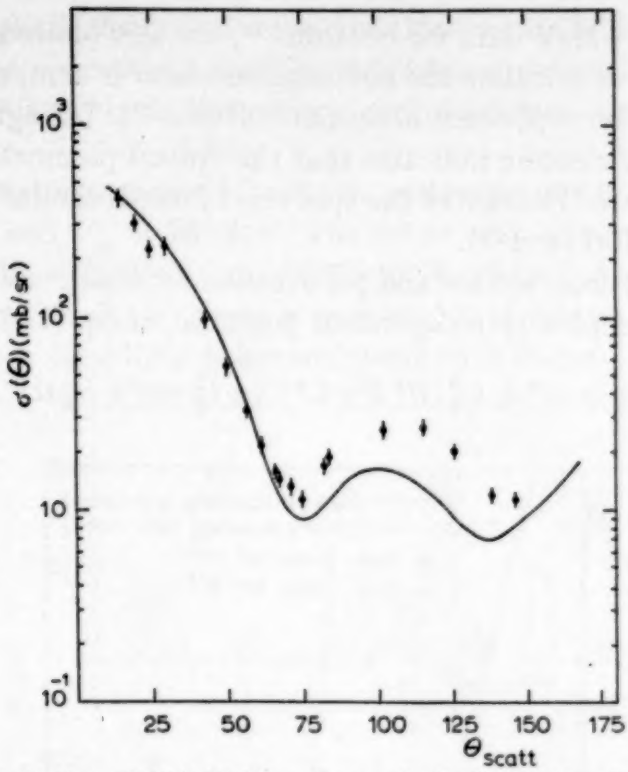

Fig. 1. Angular distribution of 11.6 MeV nucleons, elastically scattered from C^{13}. The optical model parameters used are: $V_p = 45$ MeV, $W_p = 10$ MeV, $V_{s_p} = 8$ MeV, $a_p = 0.5\times10^{-13}$ cm and $R_p = 1.2\times10^{-13}A^{\frac{1}{3}}$ cm. The experimental points [18]) are for 14 MeV neutrons on C^{12}.

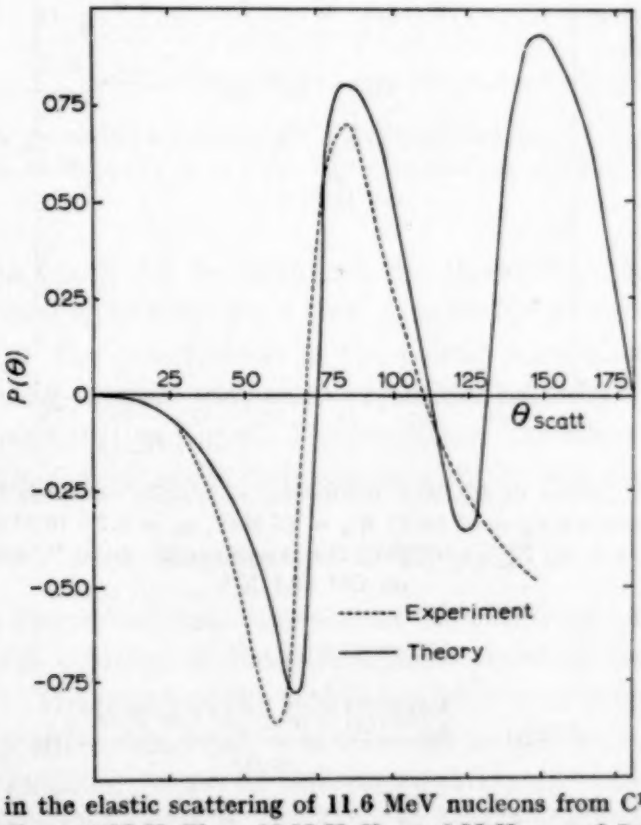

Fig. 2. Polarization in the elastic scattering of 11.6 MeV nucleons from C^{13}. The optical model parameters used are $V_p = 45$ MeV, $W_p = 10$ MeV, $V_{s_p} = 8$ MeV, $a_p = 0.5\times10^{-13}$ cm and $R_p = 1.2\times10^{-13}A^{\frac{1}{3}}$ cm. The experimental curve [19]) is for 11.5 MeV protons on C^{12}.

For comparison 14 MeV data for neutrons [18]) are also plotted. The same parameters were used to calculate the polarization which is compared in fig. 2 with the 11.5 MeV proton experimental results of Rosen [19]). The agreement obtained for the elastic polarization indicates that the optical parameters used here are reasonably accurate. The size of the spin orbit force is similar to those used by Fernbach and Bjorklund [12]).

The differential cross section and polarization for elastic scattering of deuterons using the complex spin-dependent potential of eq. (2.3) are given [20]) by

$$\sigma(\theta) = A^*A + \tfrac{2}{3}(B^*B + C^*C) + (\tfrac{1}{2}\cos^2\theta + \tfrac{1}{6})D^*D, \tag{3.3}$$

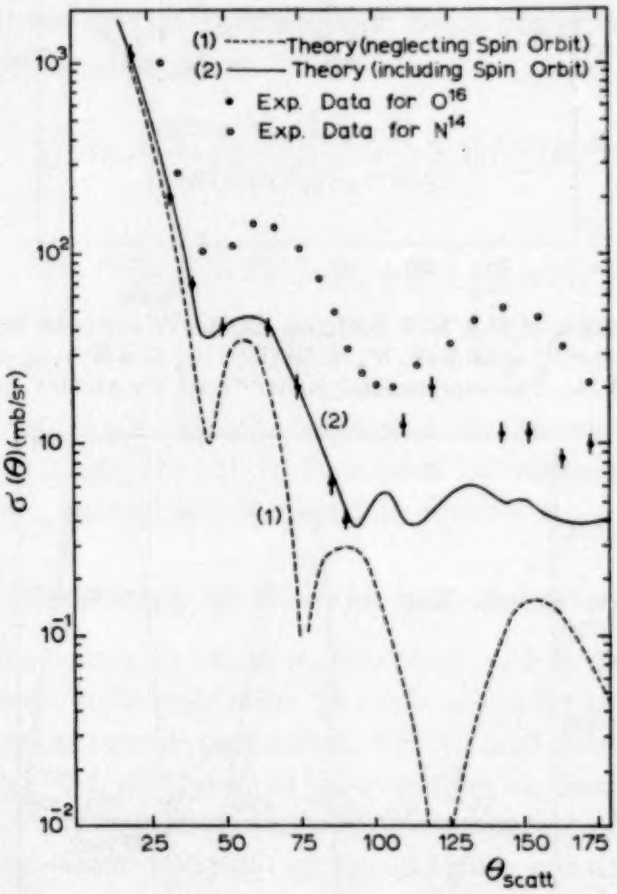

Fig. 3. Angular distribution of 8.9 MeV deuterons, elastically scattered from C^{12}. The optical model parameters used are $V_d = 55$ MeV, $W_d = 15$ MeV, $a_d = 0.7\times10^{-13}$ cm, $R_d = 1.59\times10^{-13}$ $A^{\frac{1}{3}}$ cm and (1) $V_{s_d} = 0$, (2) $V_{s_d} = 10$ MeV. The experimental points [21]) are for 8 MeV deuterons on O^{16} and N^{14}.

and

$$P(\theta)\mathbf{n} = \frac{\frac{4}{3}\,\mathrm{Re}[(A + C + \frac{1}{2}D\cos\theta)B^*]}{\sigma(\theta)}\mathbf{n}, \tag{3.4}$$

in which, except for a factor of $\sqrt{4\pi}$, A, B, C and D are given in ref. [20]).

The complex phase shifts and wave functions were obtained by numerical integration of the appropriate complex Schrödinger equation using the digital computer CSIRAC for both the protons and deuterons, neglecting Coulomb effects.

Fig. 3 shows the cross sections for elastic scattering of 8.9 MeV deuterons by C^{12} for $V_{s_d} = 0$ and $V_{s_d} = 10$ MeV. The other optical parameters used are $V_d = 55$ MeV, $W_d = 15$ MeV, $a_d = 0.7 \times 10^{-13}$ cm and $R_d = 1.59 \times 10^{-13} A^{\frac{1}{3}}$ cm. Similar parameters V, W, a and R were used by Tobocman [3]) but V_{s_d} is just a reasonable guess since little is known about such forces.

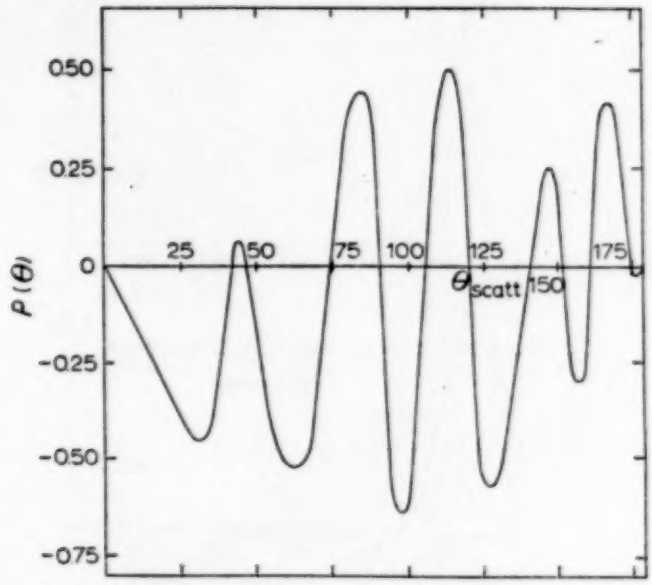

Fig. 4. Polarization in the elastic scattering of 8.9 MeV deuterons by C^{12}. The optical model parameters used are $V_d = 55$ MeV, $W_d = 15$ MeV, $V_{s_d} = 10$ MeV, $a_d = 0.7 \times 10^{-13}$ and $R_d = 1.59 \times \times 10^{-13} A^{\frac{1}{3}}$ cm.

As carbon data could not be obtained the theoretical predictions for the cross section are compared with the 8 MeV data for N^{14} and O^{16} [21]). The theoretical prediction for the polarization in the elastic scattering of deuterons at 8.9 MeV is shown for interest only since experimental data is not available for deuteron elastic polarization (fig. 4). The oscillatory character is typical of spin-orbit forces and the magnitude is comparable with nucleon elastic polarization.

4. Results for C^{12}(d, p)C^{13}

For simplicity the radial wave function of the captured neutron is taken to be the square well solution of the Schrödinger equation for orbital angular momentum $l = 1$. The depth of the well is adjusted so that the value and derivative of the 1p wave function is continuous at the boundary. The wave function in the external region is the spherical Hankel function $h_l^{(1)}(ik_n r_n)$, where k_n is given by $\hbar k_n^2/2M_n^* = Q + 2.226$ MeV, M_n^* being the reduced mass

of the neutron. Q is the Q value for the reaction. The neutron is assumed to be captured with $j = \frac{1}{2}$ and $l = 1$, in accordance with shell model assignment and $Q = 2.719$ MeV for this reaction.

In the present work Coulomb effects are neglected since the incident energy of 8.9 MeV is well above the Coulomb barrier. The Butler prediction for the cross section (fig. 5(a)) is sufficient to show that an $l = 1$ assignment is correct. There is considerable discrepancy at angles close to zero. The experimental

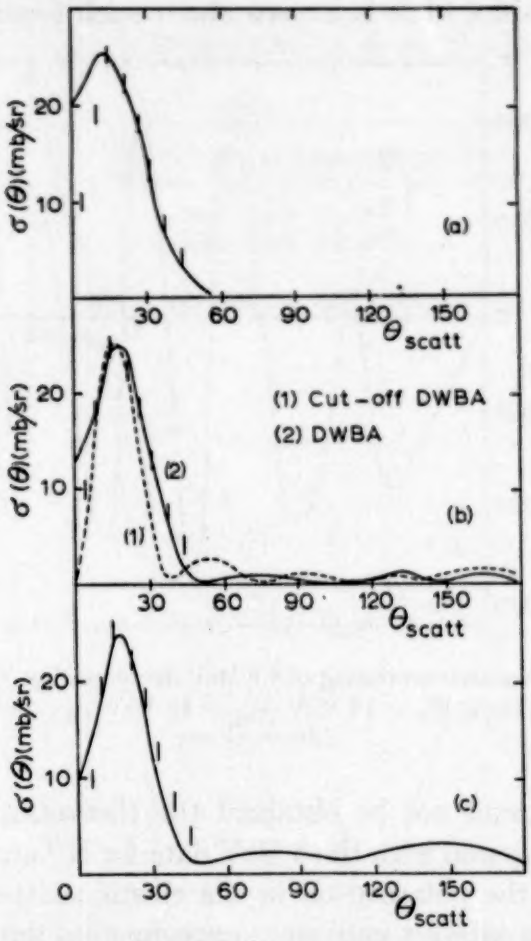

Fig. 5. Angular distribution in the stripping reaction C^{12}(d, p)C^{13}, $Q = 2.72$ MeV for 8.9 MeV deuterons. (a) is the Butler prediction for $R = 4.2\times10^{-13}$ cm and $l = 1$. (b) are the theoretical predictions for the optical model parameters $V_d = 55$ MeV, $W_d = 15$ MeV, $a_d = 0.7\times10^{-13}$ cm and $R_d = 1.59\times10^{-13}\,A^{\frac{1}{3}}$ cm, and $V_p = 45$ MeV, $W_p = 10$ MeV, $a_p = 0.5\times10^{-13}$ cm and $R_p = 1.2\times10^{-13}\,A^{\frac{1}{3}}$ cm. Curve (1) is for the cut-off DWBA at $R = 6.5\times10^{-13}$ cm and curve (2) is the DWBA without any cut-off. (c) is the theoretical prediction for the DWBA when the spin orbit potentials $V_{s_d} = 10$ MeV and $V_{s_p} = 8$ MeV are included, also using the same optical parameters as (b). The experimental points are due to Green and Middleton [22]).

points are due to Middleton and Green [22]). The stripping radius used in the Butler prediction is $R = 4.2\times10^{-13}$ cm and the reduced width [22]) $2MR\gamma/3\hbar^2 = 0.05$.

If any distortion is included in the deuteron-nucleus interaction or the proton-nucleus interaction then polarization results. Eq. (2.16) indicates that if spin-orbit effects are small then the polarization takes a different sign depending whether $j = l \pm \frac{1}{2}$. In the case of C^{12} the sign of the polarization round the stripping peak is experimentally found to be negative [6]). The previous calculation of Newns and Refai for distortion in both channels indicated a positive polarization and the calculations of Weidenmuller [10]) at a higher energy gave a very

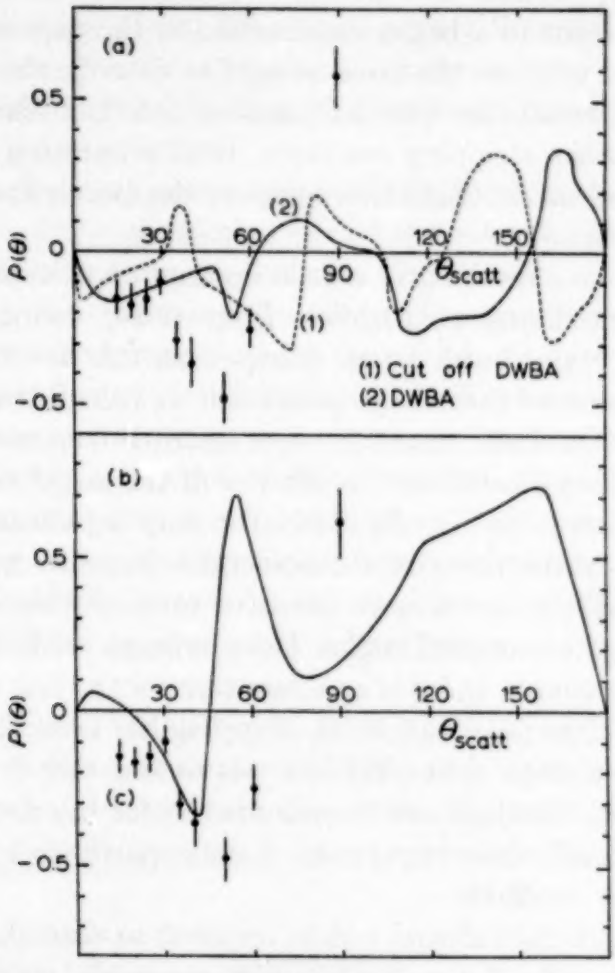

Fig. 6. Polarization in the stripping reaction C^{12}(d, p)C^{13}, $Q = 2.72$ MeV for 8.9 MeV deuterons. (a) are the theoretical predictions for the optical model parameters $V_d = 55$ MeV, $W_d = 15$ MeV, $a_d = 0.7 \times 10^{-13}$ cm and $R_d = 1.59 \times 10^{-13}\, A^{\frac{1}{3}}$ cm, and $V_p = 45$ MeV, $W_p = 10$ MeV, $\alpha_p = 0.5 \times$ $\times 10^{-13}$ cm and $R_p = 1.2 \times 10^{-13}\, A^{\frac{1}{3}}$ cm. Curve (1) is the cut-off DWBA at $R = 6.5 \times 10^{-13}$ cm and curve (2) is the DWBA without any cut-off. (c) is the theoretical prediction for the DWBA when the spin orbit potentials $V_{s_d} = 10$ MeV and $V_{s_p} = 8$ MeV are included, also using the same optical parameters as (b). The experimental points are due to Bokhari *et al.* [6]).

small negative polarization. In both these calculations a hard sphere of radius 6.5×10^{-13} cm was used for the deuteron-nucleus interaction. If a rounded optical model potential is used in place of the hard sphere, both the sign and the size of the polarization at the stripping peak are predicted. The results

using eq. (2.16) are shown in fig. 6(a) for two cases. In the first case the interaction is only allowed to take place outside a radius of $R = 6.5 \times 10^{-13}$ cm and corresponds to the cut-off distorted wave Born approximation as described by Tobocman [3]). In the second case the interaction is allowed to take place throughout the interior region. In both these cases spin-orbit forces were neglected.

Comparison of the two cases for the polarization in (fig. 6(a)) and the cross section (fig. 5(b)), indiates that the contribution from the nuclear interior is considerable and leads to a better explanation of the experimental data. The optical parameters used are the same as used to describe the elastic scattering data. Very similar results for spin-independent distortions have been found by Tobocman [3]) in other stripping reactions. It is interesting to note that the inclusion of optical model distortion removes the discrepancy at small angles for the cross section.

Although the above results give a good description of events near the stripping peak, the predicted polarization from (2.16) cannot exceed $33\frac{1}{3}\%$, whereas experimentally much larger values than this are found. In order to understand the cause of these large polarizations, calculations including spin-orbit interactions in both channels were carried out and the interaction allowed to take place throughout the interior of the target nucleus. The effect on the cross section is seen in fig. 5(c): the only significant changes are at backward angles where there is a considerable increase in magnitude. The polarization fig. 6(b) is much more sensitive to spin-orbit effects but is still predominantly negative at small angles. The maximum predicted values are now comparable to experiment and it is apparent that for the first time a qualitative understanding of large polarizations in stripping has been obtained. The time taken to calculate a single spin-orbit case was so long that it was not practical to vary parameters. Furthermore the parameters for the deuteron interaction could only be guessed, since experimental data, particularly elastic deuteron polarization is not available.

In connection with the reduced widths required to normalize the theoretical cross sections given in fig. 5 it was necessary to use much larger values than that used for the Butler prediction. In the spin-orbit calculation the value found for $2MR\gamma/3\hbar^2$ was 0.33 which is six or seven times greater than the Butler reduced width prediction. The value required for the no spin-orbit calculation was similar i.e. $2MR\gamma/3\hbar^2 = 0.50$. This is typical of distorted wave calculations and has been mentioned previously [23]) by Tobocman.

5. Discussion

The size of the predicted polarization when spin-orbit effects are included may seem surprisingly large when one considers that the Newns and Refai

calculations predicted very small effects. However, the difference between the two calculations is considerable.

Firstly the spin orbit potential included in the deuteron nucleus interaction is effective up to $L_d = 5$ or so, whereas the proton-nucleus spin orbit effect is very small above $L_p = 2$ or 3. Consequently since the majority of the contribution comes from transitions involving values of L_p and L_d between two and six it is not unexpected that the combined deuteron and proton spin-orbit effects are larger than the proton spin-orbit effect. Secondly the size of the spin-orbit potentials used are about three times greater than those used by Newns and Refai or Cheston. Finally the inclusion of the interior of the nucleus enhances the contribution from the lower angular momenta and therefore is likely to increase the spin-orbit effects.

We have shown that the spin-independent DWBA gives a considerably better explanation of the stripping reaction in carbon than the "plane-wave cut-off" Butler theory. However, if large values are to be predicted for polarization in stripping reactions it is necessary to modify the spin-independent DWBA by including spin-orbit interactions in both the initial and final channels. The use of spin-orbit potentials in the DWBA treatment follows as a natural consequence of using the elastic scattering wave functions in the evaluation of the stripping matrix, since the explanation of elastic scattering requires the inclusion of a spin-orbit interaction. Further tests of the DWBA are necessary and to accomplish this more data and more calculations to compare with the data are required. Extension of the theory to include polarized incident beams is being carried out and will be reported on in a later paper.

The author wishes to thank Dr. F. Hirst and his computer staff for their willing assistance in the operation of CSIRAC, and Associate Professor C. B. O. Mohr for his continued interest in this work.. He would also like to thank Mr. B. A. Robson for programming the complex Schrödinger equation.

References

1) S. T. Butler, Proc. Roy. Soc. A **208** (1951) 559;
A. B. Bhatia, K. Huang, R. Huby and H. C. Newns, Phil. Mag. **43** (1952) 485
2) J. Horowitz and A. M. L. Messiah, Journ. de Phys. et Rad. **14** (1953) 695;
W. Tobocman and M. H. Kalos, Phys. Rev. **97** (1955) 132
3) W. Tobocman, Phys. Rev. **115** (1959) 98
4) R. Huby, M. Y. Refai and G. R. Satchler, Nuclear Physics **9** (1958/59) 94
5) P. Hillman, Phys. Rev. **104** (1956) 176
6) M. S. Bokhari, J. A. Cookson, B. Hird and B. Weesakul, Proc. Phys. Soc. A **72** (1958) 90
7) H. C. Newns and M. Y. Refai, Proc. Phys. Soc. A **71** (1958) 627
8) W. B. Cheston, Phys. Rev. **96** (1954) 1590
9) J. Sawicki, Phys. Rev. **106** (1957) 172
10) H. A. Weidenmuller, Z. f. Physik **150** (1958) 389
11) M. E. Rose, Elementary theory of angular momentum (Wiley, New York 1957)

12) S. Fernbach and F. Bjorklund, Phys. Rev. **109** (1958) 1298
13) S. Watanabe, Nuclear Physics **8** (1958) 484
14) J. Sawicki, Nuovo Cimento **2** (1955) 1322
15) K. Smith and J. W. Stevenson, Tables of Wigner 9*j* coefficients, Argonne National Lab. ANL-5776
16) H. Matsunobe and H. Takebe, Prog. Theor. Phys. **14** (1955) 589
17) J. V. Lepore, Phys. Rev. **79** (1950) 137
18) J. D. Anderson, C. C. Gardiner, J. W. McClure, M. P. Nakada and C. Wong, Phys. Rev. **111** (1958) 572
19) L. Rosen, Proc. Int. Conf. on the Nuclear Optical Model, Florida State University, Tallahassee (1959)
20) O. D. Cheishvili, JETP (USSR) **3** (1956) 974
21) E. J. Burge, H. B. Burrows, W. M. Gibson and J. Rotblat, Proc. Roy. Soc. A **210** (1951/52) 534
22) T. S. Green and R. Middleton, Proc. Phys. Soc. A **69** (1956) 28
23) W. Tobocman, Brookhaven Conference, Statistical Aspects of the Nucleus (1955)

2.G

Nuclear Physics **22** (1961) 47—56; © *North-Holland Publishing Co., Amsterdam*

Not to be reproduced by photoprint or microfilm without written permission from the publisher

SPIN-ORBIT EFFECTS IN THE STRIPPING REACTION INVOLVING POLARIZED PARTICLES

D. ROBSON

Physics Department, University of Melbourne

Received 12 August 1960

Abstract: The theory of the stripping reaction involving polarized particles is considered. The angular distribution and polarization of the product of the stripping reaction induced by polarized particles in unpolarized nuclei are determined by the distorted wave method including spin-orbit coupling. An attempt is made to investigate the validity of stripping formulae in which spin-orbit effects are neglected.

1. Introduction

In a preceding paper [1]) we obtained expressions for the angular distribution and polarization of emergent protons in the (d, p) stripping reaction when spin-orbit effects are included in both initial and final channels. These expressions are, however, not in a suitable form for a discussion of the stripping reaction in which polarized incident particles are involved.

In the present paper general expressions, including spin-orbit effects in both initial and final channels, are obtained for the angular distribution and polarization of the emerging protons from the (d, p) reaction involving the interaction of polarized deuterons with unpolarized nuclei. The angular distribution of protons produced in the stripping reaction using polarized deuterons has an azimuthal asymmetry. Previous treatments [2, 3]) of the stripping reaction involving polarized deuterons have neglected spin-orbit effects and have given the following simple relation between the angular distribution using polarized deuterons and the angular distribution using unpolarized deuterons:

$$[\sigma(\theta)]_{\mathrm{pol}} = (1+3\mathbf{P}_{\mathrm{p}} \cdot \mathbf{P}_{\mathrm{d}})[\sigma(\theta)]_{\mathrm{unpol}}, \tag{1.1}$$

where $\mathbf{P}_{\mathrm{p}}$ and $\mathbf{P}_{\mathrm{d}}$ are the polarization vectors for proton and deuteron respectively. The positive directions of the polarization vectors are taken to be along the vector $\mathbf{k}_{\mathrm{d}} \times \mathbf{k}_{\mathrm{p}}$.

If the spin-orbit effects are small, then the above relation is a good approximation and a study of the azimuthal asymmetry of the emergent protons from the stripping reaction using polarized deuterons would lead to the same information about the structure of the nucleus as the polarization of the protons. However, we have shown [1, 4]) that there no longer remains any justification for

assuming that spin-orbit effects are small in a direct interaction process.

In the present paper a comparable expression to eq. (1.1) is obtained for the (d, p) reaction in which spin-orbit effects are included. The result is more complicated and shows that the differential cross section for polarized deuterons depends on the higher spin moments of the deuterons as well as on the vector polarization of the deuterons.

Calculations are carried out for the C^{12}(d, p)C^{13} ground state reaction for completely polarized incident beams to test the validity of using the simple relation (1.1) as an alternative procedure to measuring the polarization directly. Calculations are also carried out to investigate the importance of 'spin-flip' transitions in stripping polarization.

2. Theory

Polarization phenomena in the (d, p) reaction may be described by the density matrix for the reaction, the elements of which completely determine the spin state of the particles taking part in the reaction. The density matrix of the total system in the initial state is simply the direct product of the density matrix $\rho^{\mathrm{d}} = \rho_{\mu_{\mathrm{d}}\mu'_{\mathrm{d}}}$ for the spin space of the deuteron and the density matrix $\rho^{\mathrm{A}} = \rho_{M_{\mathrm{A}}M'_{\mathrm{A}}}$ for the spin space of the initial nucleus. μ_{d}, μ'_{d}, M_{A} and M'_{A} are possible values of the spin projections of the deuteron and initial nucleus respectively.

The polarization of particles with spin s is conveniently described by certain spin tensors $\langle T^{kq}\rangle$ with $k = 0, 1, 2 \ldots 2k$. These are the expectation values of the irreducible set of tensor operators T^{kq} which are covariant combinations of the components of the spin operator s. Here we define the spin tensors $\langle T^{kq}\rangle$ in terms of the density matrix by

$$\langle T^{kq}\rangle = \sum_{\mu\mu'} \rho_{\mu\mu'}(s) T^{kq}_{\mu\mu'}(s). \tag{2.1}$$

The tensor T^{kq} is only dependent on s, μ, μ', k and q and has matrix elements expressed in terms of Clebsch-Gordan coefficients:

$$T^{kq}_{\mu\mu'} = (-1)^{s+\mu'} C(ssk, \mu, -\mu' q). \tag{2.2}$$

In the case of the deuteron, $s = 1$ and the possible values for k are 0, 1, and 2, which are directly related to the differential cross section, vector polarization and tensor polarization respectively.

For the sake of simplicity the initial nucleus is assumed to be unpolarized. The density matrix for an unpolarized nucleus with spin I is given from (2.1) and (2.2) by putting $k = 0$, $q = 0$ and $s = I$ as

$$\rho_{M_{\mathrm{A}}M'_{\mathrm{A}}} = \frac{\delta_{M_{\mathrm{A}}M'_{\mathrm{A}}}}{(2I_{\mathrm{A}}+1)}. \tag{2.3}$$

Using the orthogonality property of Clebsch-Gordan coefficients the deuteron density matrix expanded in terms of the spin tensors $\langle T^{IM}\rangle$ is given by

$$\rho_{\mu_d\mu'_d} = \sum_{IM} \langle T^{IM}\rangle T^{IM}_{\mu_d\mu'_d}. \tag{2.4}$$

The density matrix in the initial state ρ is given by the direct product of $\rho_{M_A M'_A}$ and $\rho_{\mu_d\mu'_d}$ and is normalized to unity: $\mathrm{Tr}\,\rho = 1$. The dynamics of the process are described by the change in the density matrix from the initial value ρ to the final value ρ' given by

$$\rho' = I_\rho I^\dagger, \tag{2.5}$$

where I is the reaction matrix and $\mathrm{Tr}\,\rho' = (v_d/v_p)\sigma(\theta)$.

It has been shown [1]) that the general form for the reaction matrix including spin-orbit effects is given by

$$\begin{aligned} I_{\mu_p M_B;\,\mu_d M_A} = &\sum_{L_p L_d J_p J_d l_j} C(I_A j I_B, M_A \mu_j M_B) A(L_p L_d J_p J_d l j) \\ &\times \sum_{M_p \mu_j} (-1)^{\mu_j} \mathscr{A}(L_p M_p) \mathscr{A}^*(L_d M_p + \mu_j + \mu_p - \mu_d) \\ &\times C(L_p \tfrac{1}{2} J_p, M_p \mu_p M_p + \mu_p) C(L_d 1 J_d, M_p + \mu_j + \mu_p - \mu_d \mu_d M_p + \mu_j + \mu_p) \\ &\times C(J_d j J, M_p + \mu_j + \mu_p, -\mu_j M_p + \mu_p), \end{aligned} \tag{2.6}$$

where

$$\begin{aligned} A(L_p L_d J_p J_d l j) = (-1)^{L_p + L_d + J_p + J_d} \theta^*_{jl} K i^{-l} \sqrt{3} \hat{l} \hat{j} \hat{L}_d \hat{J}_d R_{L_p L_d J_p J_d l_j} \\ \times C(L_d l L_p, 000) X(L_p \tfrac{1}{2} J_p, l \tfrac{1}{2} j, L_d 1 J_d), \end{aligned}$$

and $\hat{j}$ denotes $(2j+1)^{\frac{1}{2}}$.

Using the expansions (2.3) and (2.4) in (2.5), we write the density matrix of the final state in the form

$$\rho_{\mu_p M_B,\,\mu'_p M'_B} = \sum_{IM} \langle T^{IM}\rangle \sum_{\mu_d \mu'_d} I_{\mu_p M_B;\,\mu_d M_A} T^{IM}_{\mu_d \mu'_d} I^*_{\mu'_d M_A;\,\mu'_p M'_B}. \tag{2.7}$$

The density matrix for the emergent protons in the stripping reaction is given from (2.7) by summing incoherently over the spin projections M_B of the final nucleus, i.e.

$$\rho_{\mu_p \mu'_p} = \sum_{M_B} \rho_{\mu_p M_B,\,\mu'_p M_B}.$$

The spin polarization of the emergent protons may also be expressed in terms of spin tensors, viz.

$$\langle T^{RT}\rangle \mathrm{Tr}\,\rho' = \sum_{\mu_p \mu'_p} \rho_{\mu_p \mu'_p} T^{RT}_{\mu_p \mu'_p} \tag{2.8}$$

of rank $R = 0$ and 1. The term $\mathrm{Tr}\,\rho'$ occurs in (2.8) so as to normalize the final density matrix ρ' to unity.

Inserting (2.6) and (2.7) in (2.8) and summing over M_A and M_B we obtain the spin tensors $\langle T^{RT}\rangle$ in the form

$$\begin{aligned}
\langle T^{RT}\rangle \operatorname{Tr}\rho' = {} & \frac{(2I_B+1)}{(2I_A+1)} \sum_{IM} \langle T^{IM}\rangle \sum_{\alpha\alpha' lj} \frac{1}{(2j+1)} A(\alpha, lj) A(\alpha', lj) \\
& \times \sum_{pq} B(pq) \sum_{\mu_d \mu_j \mu_p M_p M'_p} (-1)^{M-T+\mu_j+M_p-M'_p-\frac{1}{2}} C(11I, \mu_d M-\mu_d M) \\
& \times C(\tfrac{1}{2}\tfrac{1}{2}R, \mu_p T-\mu_p T) C(L_p \tfrac{1}{2} J_p, M_p \mu_p M_p+\mu_p) \\
& \times C(L_d 1 J_d, M_p+\mu_j+\mu_p-\mu_d \mu_d M_p+\mu_j+\mu_p) C(J_d j J_p, M_p+\mu_j+\mu_p, -\mu_j M_p+\mu_p) \\
& \times C(L_p L'_p p, M_p, -M'_p \mu) \qquad (2.9) \\
& \times C(L_d L'_d q, \mu_d-M_p-\mu_j-\mu_p M'_p+\mu_j+\mu_p+M-T-\mu_d M-T-\mu) \\
& \times C(L'_p \tfrac{1}{2} J'_p, M'_p \mu_p-T M'_p+\mu_p-T) \\
& \times C(J'_d j J'_p, M'_p+\mu_j+\mu_p-T, -\mu_j M'_p+\mu_p-T) \\
& \times C(L'_d 1 J'_d, M'_p+\mu_j+\mu_p-T-\mu_d+M\mu_d-M M'_p+\mu_j+\mu_p-T) \\
& \times Y_p^{\mu}(\theta_{k_p}, \phi_{k_p}) Y_q^{-(\mu+T-M)}(\theta_{k_d}, \phi_{k_d}),
\end{aligned}$$

where

$$B(pq) = 4\pi\, i^{L_d-L_p+L'_p-L'_d} \frac{\hat{L}_p \hat{L}'_p \hat{L}_d \hat{L}'_d}{\hat{p}\hat{q}} C(L_d L'_d q, 000) C(L_p L'_p p, 000),$$

and where we have used the coupling rule for spherical harmonics

$$Y_L^M(\theta, \phi) Y_{L'}^{M'}(\theta, \phi) = \sum_p \frac{\hat{L}\hat{L}'}{\sqrt{4\pi}\,\hat{p}} C(LL'p, MM'\mu) C(LL'p, 000) Y_p^{\mu}(\theta, \phi).$$

In connection with (2.9) it should be noted that only a single sum over l occurs due to parity considerations. α and α' denote collectively the projectile quantum numbers.

With the help of known sum rules [5]) we carry out the summations over spin projections μ_d, μ_p and μ_j, and also over the projections M_p and $M_{p'}$. We find

$$\begin{aligned}
\langle T^{RT}\rangle \operatorname{Tr}\rho' = {} & \frac{(2I_B+1)}{(2I_A+1)} \sum_{IM} \langle T^{IM}\rangle \sum_{\alpha\alpha' ljpq} \frac{1}{(2j+1)} A(\alpha, lj) A(\alpha', lj) B(pq) \\
& \times \sum_{rt} (-1)^{L'_p+L_d+p+t} \hat{p}\hat{q}\hat{R}\hat{I}\hat{J}_d\hat{J}'_d (2t+1)(2J_p+1)(2J'_p+1) \\
& \times W(J'_p j t J_d; J'_d J_p) W(pRqI; tr) X(L_d L'_d q, 11I, J_d J'_d t) \qquad (2.10) \\
& \times X(L_p L'_p p, \tfrac{1}{2}\tfrac{1}{2}R, J_p J'_p t) C(RIr, T, -MT-M) \\
& \times \sum_{\mu} (-1)^T C(pqr, \mu, -\mu+M-T, M-T) Y_p^{\mu}(\theta_{k_p}, \phi_{k_p}) Y_q^{-\mu+M-T}(\theta_{k_d}, \phi_{k_d}).
\end{aligned}$$

For $R = 1$ this formula determines the polarization of the protons. The

components of the polarization vector are related to the spin tensors $\langle T^{RT}\rangle$ by

$$P_x = \langle T^{11}\rangle - \langle T^{1,-1}\rangle, \quad P_y = i(\langle T^{11}\rangle + \langle T^{1,-1}\rangle) \quad \text{and} \quad P_z = -\sqrt{2}\langle T^{10}\rangle,$$

and the spin tensors are normalized by the condition $\langle T^{00}\rangle = -1/\sqrt{2}$.

For $R = 0$ and $T = 0$, we find from (2.10) that the angular distribution of the protons is given by

$$\begin{aligned}\operatorname{Tr}\rho' = {} & \frac{(2I_B+1)}{(2I_A+1)} \sum_{IM} \langle T^{IM}\rangle \sum_{\alpha\alpha' ljpq} \frac{1}{(2j+1)} A(\alpha, lj) A(\alpha', lj) B(pq) \\ & \times (-1)^{L_d+p-J_p-\frac{1}{2}} \hat{p}\hat{q}\hat{J}_d\hat{J}'_d(2J_p+1)(2J'_p+1) W(J'_p jpJ_d; J'_d J_p) \\ & \times X(L_d L'_d q, 11I, J_d J'_d p) W(L'_p L_p J'_p J_p; p\tfrac{1}{2}) \\ & \times \sum_{\mu} C(pqI, \mu, -\mu+MM) Y_p^{\mu}(\theta_{k_p}, \phi_{k_p}) Y_q^{-\mu+M}(\theta_{k_d}, \phi_{k_d}).\end{aligned} \tag{2.11}$$

Formulae (2.10) and (2.11) are the most general cases for the polarization and angular distribution of the protons emergent from a stripping reaction involving arbitrarily polarized deuterons. In the particular case when the deuterons are unpolarized, we find, putting $\langle T^{IM}\rangle = 1/\sqrt{3}\delta_{I0}\delta_{M0}$; the cross section for unpolarized deuterons

$$\begin{aligned}\{\operatorname{Tr}\rho'\}_0 = {} & \frac{(2I_A+1)}{(2I_B+1)} \sum_{\alpha\alpha' ljp} \frac{1}{(2j+1)} A(\alpha, lj) A(\alpha', lj) B(pp) (-1)^{J'_d+J_d+L'_d-J_p-\frac{1}{2}} \\ & \times \tfrac{1}{3}\hat{J}_d\hat{J}'_d(2J_p+1)(2J'_p+1) W(pL'_d J_d 1; L_d J'_d) W(J'_p jpJ_d; J'_d J_p) \\ & \times W(L'_p L_p J'_p J_p; p\tfrac{1}{2}) \sum_{\mu} (-1)^{\mu} Y_p^{\mu}(\theta_{k_p}, \phi_{k_p}) Y_p^{-\mu}(\theta_{k_d}, \phi_{k_d}),\end{aligned} \tag{2.12}$$

and the polarization for unpolarized deuterons

$$\begin{aligned}\langle T^{RT}\rangle_0\{\operatorname{Tr}\rho'\}_0 = {} & \frac{(2I_A+1)}{(2I_B+1)} \sum_{\alpha\alpha' ljp} \frac{1}{(2j+1)} A(\alpha, lj) A(\alpha', lj) B(pp) \\ & \times (-1)^{J'_d+J_d+L'_d+L'_p} \tfrac{1}{3}(2p+1)\hat{J}_d J'_d(2J_p+1)(2J_p'+1) \\ & \times W(pL'_d J_d 1; L_d J'_d) W(J'_p jpJ_d, J'_d J_p) X(L_p L'_p p, \tfrac{1}{2}\tfrac{1}{2}R, J_p J'_p p) \\ & \times \sum_{\mu} (-1)^T C(ppR, \mu, -\mu-T\ -T) Y_p^{\mu}(\theta_{k_p}, \phi_{k_p}) Y_p^{-\mu-T}(\theta_{k_d}, \phi_{k_d}).\end{aligned} \tag{2.13}$$

From (2.11), (2.12) and (2.13) we can write $\operatorname{Tr}\rho'$ in the form

$$\begin{aligned}\operatorname{Tr}\rho' = \{\operatorname{Tr}\rho'\}_0 \Bigg\{ 1 - {} & \frac{\sum_{\alpha\alpha' ljp} \sqrt{6} H(\alpha\alpha' ljp) G(p, 1) F(p, 0)}{\sum_{\alpha\alpha' ljp} H(\alpha\alpha' ljp) G(p, 0) F(p, 1)} \langle T_d^{10}\rangle \langle T_p^{10}\rangle \\ & + \frac{\sum_{\alpha\alpha' ljpq} \sqrt{3} H(\alpha\alpha' ljp) G(q, 2) F(p, 0) \sum_M \rho_{2M} \langle T_d^{2M}\rangle}{\sum_{\alpha\alpha' ljp} H(\alpha\alpha' ljp) G(p, 0) F(p, 0) \rho_{00}} \Bigg\},\end{aligned} \tag{2.14}$$

in which

$$H(\alpha\alpha' ljp) = \frac{(2I_B+1)}{(2I_A+1)(2j+1)} A(\alpha, lj)A(\alpha', lj)B(pq)\hat{q}(-1)^{L_d-J_p-\frac{1}{2}} \times \hat{J}_d\hat{J}'_d(2J_p+1)(2J'_p+1)W(J'_p jpJ_d, J'_d J_p),$$

$$G(q, I) = \hat{p}X(L_d L'_d q, 11I, J_d J'_d p),$$

$$F(p, R) = (-1)^{J_p+\frac{1}{2}+L'_p-q}\hat{p}X(L_p L'_p p, \tfrac{1}{2}\tfrac{1}{2}R, J_p J'_p q),$$

and

$$\rho_{IM} = \sum_{\mu} (-1)^p C(pqI, \mu, -\mu+M, M)Y_p{}^{\mu}(\theta_{k_p}, \phi_{k_p})Y_q{}^{-\mu+M}(\theta_{k_d}, \phi_{k_d}).$$

From (2.14) we see that the angular distribution for a polarized incident beam in which spin-orbit effects are incuded, is of the general form

$$[\sigma(\theta)]_{\text{pol}} = [\sigma(\theta)]_{\text{unpol}}\{1+f(\alpha\alpha' ljp)\mathbf{P}_p \cdot \mathbf{P}_d+g(\alpha\alpha' ljpq)\sum_M \rho_{2M}\langle T^{2M}\rangle\}, \quad (2.15)$$

and hence $[\sigma(\theta)]_{\text{pol}}$ depends on the tensor polarization components $\langle T^{2M}\rangle$ of the deuteron. The factors f and g depend on the phenomenological transition probabilities $R_{L_p L_d J_p J_d lj}$ and therefore will vary from one reaction to another.

The corresponding relations for the particular case where spin-orbit interactions are neglected are found from the general expressions above by summing over J_p, J'_p, J_d and J'_d. The summation is possible because in this approximation the phenomenological radial integrals are independent of spin. The expressions obtained are

$$\langle T^{RT}\rangle \operatorname{Tr}\rho' = \frac{3(2I_B+1)}{(2I_A+1)}\sum_{IM}\langle T^{IM}\rangle\sum_{jlt}\theta^2_{jl}(-1)^{R-T+\frac{1}{2}+j+t} \times \hat{I}\hat{R}W(\tfrac{1}{2}\tfrac{1}{2}lt; tj)X(\tfrac{1}{2}R\tfrac{1}{2}, \tfrac{1}{2}t\tfrac{1}{2}, 1I1) \times C(RIt, -TMM-T)\sum_m (-1)^m C(llt, -mm+M-TM-T) \times F_l{}^m F_l{}^{m+M-T*}, \quad (2.16)$$

$$\operatorname{Tr}\rho' = \frac{3(2I_B+1)}{(2I_A+1)}\sum_{IM}\langle T^{IM}\rangle\sum_{jl}\theta^2_{jl}(-1)^{j+\frac{1}{2}} \times W(\tfrac{1}{2}\tfrac{1}{2}ll; Ij)W(11\tfrac{1}{2}\tfrac{1}{2}; I\tfrac{1}{2}) \times \sum_m (-1)^m C(llI, -mm+MM)F_l{}^m F_l{}^{m+M*}, \quad (2.17)$$

$$\langle T^{RT}\rangle_0\{\operatorname{Tr}\rho'\}_0 = \frac{(2I_B+1)}{(2I_A+1)}\sum_{jl}\theta^2_{jl}(-1)^{R-T+\frac{1}{2}+j}W(\tfrac{1}{2}\tfrac{1}{2}ll; Rj) \times W(\tfrac{1}{2}\tfrac{1}{2}\tfrac{1}{2}\tfrac{1}{2}; R1)\sum_m (-1)^m C(llR, -mm-T, -T) \times F_l{}^m F_l{}^{m-T*}, \quad (2.18)$$

and

$$\{\mathrm{Tr}\,\rho'\}_0 = \sum_{jl} \frac{(2I_B+1)}{2(2I_A+1)} \frac{\theta_{jl}^2}{(2l+1)} |F_l^m|^2, \tag{2.19}$$

where

$$F_l^m = \sqrt{\frac{\alpha m_p^*}{\pi m_{np}}} \int \psi_p(\mathbf{k}_p\mathbf{r}) u_l(r) i^{-l} Y_l^m(\theta_n, \phi_n)^* \psi_d(\mathbf{k}_d\mathbf{r}) \mathrm{d}\mathbf{r} \tag{2.20}$$

contains the phenomenological part of the mechanism.

These relations are slightly simpler than the corresponding ones derived in ref. [2]) in which the channel spin formalism was employed. We have used j—j coupling throughout. Putting $R = 1$ and $T = 0$ in (2.18) yields the polarization of the protons for an unpolarized deuteron beam

$$\mathbf{P}_p = P_{z_p} = \tfrac{2}{3} \sum_{jl} \frac{(-1)^{j-l-\frac{1}{2}} \theta_{jl}^2 (2j+1)^{-1} (2l+1)^{-1} \sum_m m |F_l^m|^2}{\sum_{jl} \theta_{jl}^2 (2l+1)^{-1} \sum_m |F_l^m|^2}, \tag{2.21}$$

in agreement with Huby *et al.* [6]).

The analogous expression to (2.15) is obtained from (2.17), (2.18) and (2.19) as

$$[\sigma(\theta)]_{\mathrm{pol}} = (1+3\mathbf{P}_p \cdot \mathbf{P}_d)[\sigma(\theta)]_{\mathrm{unpol}}. \tag{2.22}$$

Comparing (2.15) and (2.22), we see that (2.22) is a special case of (2.15) where the coefficient g is zero and the coefficient f is a pure number. If (2.22) is valid one can conclude that this relation yields an alternative procedure for determining the polarization of the emergent protons in a stripping reaction. The validity of (2.22) is investigated in the next section for the C^{12}(d, p)C^{13} reaction.

3. Results for C^{12}(d, p)C^{13} using 9 MeV Deuterons

We may express (2.22) in two alternative forms which are more amenable to discussion, viz.

$$\mathbf{P}_p = P_{z_p} = (\sigma^+ - \sigma^-)/6\sigma_0|\mathbf{P}_d|, \tag{3.1}$$

and

$$S \equiv \frac{\sigma^+ + \sigma^-}{2\sigma_0} = 1, \tag{3.2}$$

in which σ^+ and σ^- are the cross sections for deuterons polarized along and against the direction $\mathbf{k}_d \times \mathbf{k}_p$ respectively, and σ_0 is the cross section for unpolarized deuterons. Here for simplicity of calculation we assume completely polarized deuterons: $|\mathbf{P}_d| = 1$.

σ^+, σ^- and σ_0 are calculated including spin-orbit effects and $\mathbf{P}_p$ then predicted from (3.1). This prediction is compared in fig. 1 with the polarization calculated exactly. The parameters used for these distorted wave calculations are the

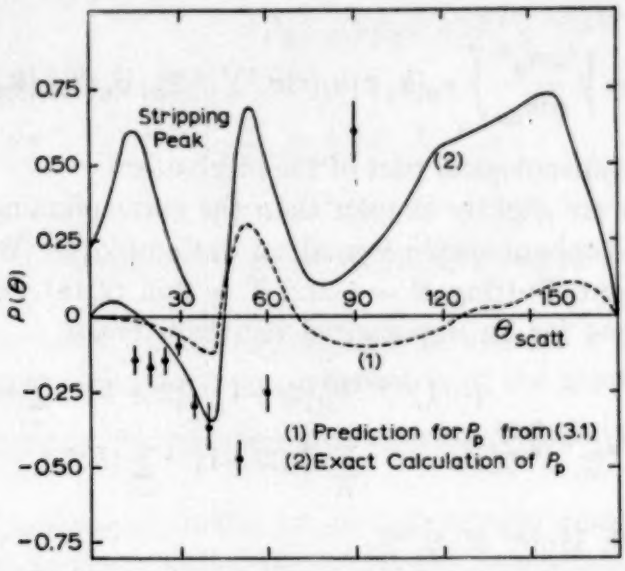

Fig. 1. Polarization in the stripping reaction C^{13}(d, p)C^{13}, $Q = 2.72$ MeV for 8.9 MeV deuterons. (1) is the predicted curve for P_p using (3.1) and (2) is the predicted curve for P_p calculated directly. The optical parameters used are shown in table 1.

same as in the preceding article [1]) and are shown in table 1 using the same notation.

TABLE 1

Parameters used to calculate σ^+, σ^-, σ_0 and $\mathbf{P}_p$

Protons	$V_p =$ 45 MeV	$W_p =$ 10 MeV	$V_{s_p} =$ 8 MeV	$a_p =$ 0.5×10^{-13} cm	$R_p =$ $1.2\times10^{-13}\,A^{\frac{1}{3}}$cm
Deuterons	$V_d =$ 55 MeV	$W_d =$ 15 MeV	$V_{s_d} =$ 10 MeV	$a_d =$ 0.7×10^{-13} cm	$R_d =$ $1.59\times10^{-13}\,A^{\frac{1}{3}}$cm

The polarization predicted from (3.1) when spin-orbit effects are included has the correct sign at the stripping peak but is reduced in magnitude. At large angles (3.1) is obviously inadequate.

The calculated values of σ^+, σ^- and σ_0 are also inserted in (3.2). The result is shown in fig. 2 and indicates that at the stripping peak there is at least an error of 10—20 % if spin-orbit effects are included, and at backward angles (3.2) is also invalid. Since the polarizations around the stripping peak are usually only 10—20 % we must conclude that the use of (2.22), or the alternative forms (3.1) and (3.2), could easily lead to erroneous spin assignments in nuclear spectroscopy. If the polarization of the product of a stripping reaction

are to be measured correctly, it must be determined directly using a second scatterer.

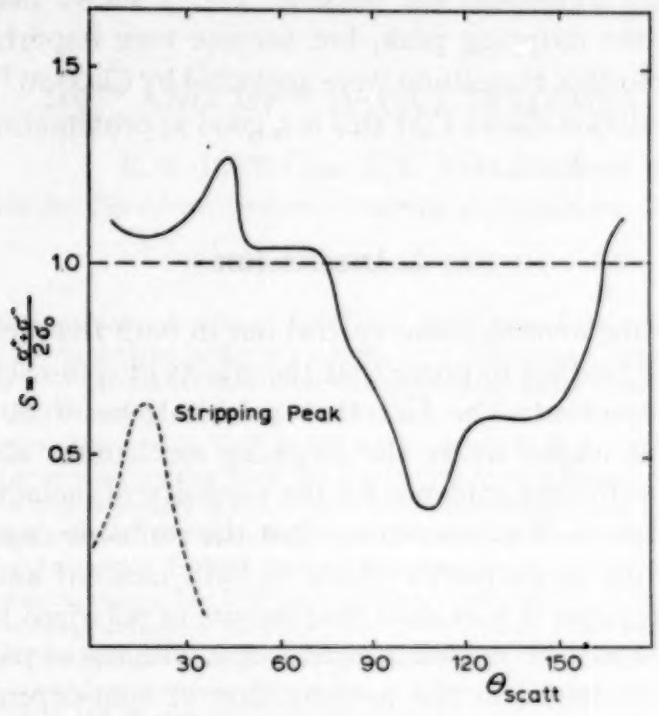

Fig. 2. Predicted curves for the quantity $S = \sigma^+ + \sigma^-/2\sigma_0$ in the stripping reaction C^{13}(d, p) C^{13}, $Q = 2.72$ MeV for 8.9 MeV deuterons. The straight line at $S = 1$ is for (3.2) and the curve is the theoretical prediction for S calculated directly. The optical parameters used are shown in table 1.

The use of polarized beams would be very useful for determining the importance of spin-dependent distortion such as spin-orbit coupling. An example of this is shown in fig. 3 where we show the theoretical prediction for the polarization of protons, for completely polarized deuterons, in which spin-orbit effects

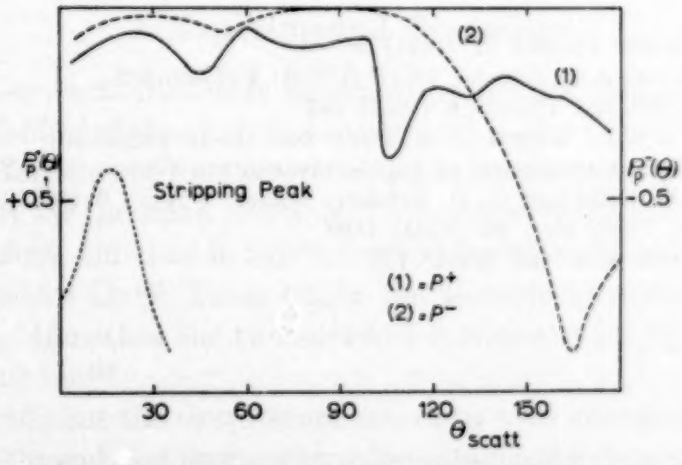

Fig. 3. Polarization in the stripping reaction C^{13}(d, p)C^{13}, $Q = 2.72$ MeV for completely polarized deuterons at 8.9 MeV. The two curves, (1) and (2), are the theoretical predictions for $P_d = +1$ and -1 respectively. The optical parameters used are shown in table 1.

are included. If spin-orbit effects are neglected and completely polarized deuterons used, then the protons emerge fully polarized. If spin-orbit effects are included, spin-flip transitions are possible. Fig. 3 shows that 'spin-flips' are unimportant at the stripping peak, but become very important at backward angles. These 'spin-flip' transitions were neglected by Cheston [7]) but fortunately the present calculation shows that this is a good approximation at angles close to the stripping peak.

4. Discussion

The results of the investigations carried out in both the present paper and a preceding paper [1]) suffice to prove that the effects of spin-orbit interactions in stripping are important. The fact that polarizations of 50 % are found [8]) experimentally at angles where the stripping mechanism almost completely predominates is sufficient evidence for the necessity of including some form of spin-dependent forces. We have shown that the probable explanation of large polarizations is due to spin-orbit effects in both incident and final channels. From the present paper it is evident that the use of polarized beams is unlikely to be reliable as a tool for nuclear spectroscopy. The use of polarized beams in stripping could be useful in the investigation of spin-dependent forces and possibly higher spin moments of the incident particles.

The author wishes to thank Dr. F. Hirst and his computer staff for their help in the operation of CSIRAC, and Associate Professor C. B. O. Mohr for his continued interest in this work. He would also like to thank Mr. B. A. Robson for programming the complex Schrödinger equation.

References

1) D. Robson, Nuclear Physics **22** (1961) 34
2) G. L. Vysotskii and A. G. Sitenko, JETP (USSR) **4** (1959) 812
3) G. R. Satchler, Nuclear Physics **6** (1958) 543
4) B. A. Robson and D. Robson, Proc. Phys. Soc. (to be published)
5) M. E. Rose, Elementary theory of angular momentum (Wiley, New York, 1957)
6) R. Huby, M. Y. Refai and G. R. Satchler, Nuclear Physics **9** (1958/59) 94
7) W. B. Cheston, Phys. Rev. **96** (1954) 1590
8) P. Hillman, Phys. Rev. **104** (1956) 176

3A.:3.B

Nuclear Physics **22** (1961) 57—70; © *North-Holland Publishing Co., Amsterdam*

Not to be reproduced by photoprint or microfilm without written permission from the publisher

Dy^{155} AND Dy^{157} DECAY SCHEMES

K. S. TOTH † and O. B. NIELSEN

Institute for Theoretical Physics, University of Copenhagen, Denmark

Received 19 August 1960

Abstract: The disintegration schemes of Dy^{155} and Dy^{157} have been studied. In addition to obtaining conversion-electron and γ-ray spectra, $e-\gamma$ coincidence measurements have been performed. The Dy^{157} results are conclusive and support the decay scheme proposed by Michelich, Harmatz and Handley on the basis of differences and sums of accurately determined transition energies. The level in Tb^{157} at 327-keV is shown to be $\frac{3}{2}-$. The relative intensities of the three E1 γ-rays proceeding from this level to the three members of a ground rotational band based on a spin of $\frac{3}{2}+$ are found to agree with the corresponding branching ratios found for the analogous case in Tb^{159} involving a $\frac{3}{2}-$ 364-keV level and a ground rotational band again with a $\frac{3}{2}+$ base state. In both instances the experimental intensities disagree with the theoretical branching ratios. The Dy^{155} coincidence results are inconclusive due chiefly to the presence of interfering activities. However, our Dy^{155} data do corroborate some features of a disintegration scheme proposed by Toth and Rasmussen for this isotope and based on accurately measured transition energies. Also a new level in Tb^{155} at approximately 880 keV has been established in the course of this investigation.

1. Introduction

Levels in Tb^{155} and Tb^{157} populated following the decay of Dy^{155} and Dy^{157}, respectively, have been investigated prior to this time [1, 2]). The present work was undertaken to confirm these earlier results and to obtain new information concerning the Dy^{155} and Dy^{157} decay schemes.

2. Experimental Procedure

The dysprosium activities were produced by bombarding gadolinium oxide powder with 20-MeV alpha particles accelerated in the Copenhagen cyclotron. At the bombarding energy the two predominant reactions are (α, n) and (α, 2n). The former is by far the more probable. Two varieties of gadolinium oxide were irradiated, the first, enriched in Gd^{154}, to yield Dy^{157}, and, the second, enriched in Gd^{152}, to produce Dy^{155}. Table 1 lists the isotopic abundances of the two forms of Gd_2O_3. Hereafter the two enriched varieties of Gd_2O_3 will be referred to as Gd^{152} and Gd^{154}.

After bombardment the dysprosium activities were chemically purified and separated from the gadolinium mass by using a standard ion-exchange method [3]). The beta-ray spectrometer source preparation has been described previously [4]).

† Present address: Oak Ridge National Laboratory, Oak Ridge, Tennessee.

TABLE 1

Isotopic abundances of target gadolinium oxides

	152	154	155	156	157	158	160
Enriched Gd^{152}	14.96	9.75	27.26	19.32	10.08	11.67	6.97
Enriched Gd^{154}	0.32	33.17	38.57	15.92	5.49	4.50	2.05

Gamma-ray spectra were obtained using a 100-channel pulse-height analyzer. A six-gap beta-ray spectrometer [5]) was employed to obtain conversion-electron spectra, and, in conjunction with the 100-channel analyzer, to perform e—γ measurements.

Let us bear in mind the isotopic abundances in table 1 and the fact that (α, n) and (α, 2n) are the only reactions, energetically possible, yielding dysprosium activities. Then, immediately after chemical separation, the dysprosium fractions produced in Gd^{154} bombardments must have contained only Dy^{157}. Dy^{159}, though present, would have an extremely low specific activity due to its long half-life of 134 days. Dy^{155} would also have a low specific activity being produced by an (α, n) reaction on Gd^{152}, an isotope constituting just 0.3 % of the bombarded material. In fact, the prominent 227-keV γ-ray of Dy^{155} decay reported previously [1]) was not seen in Gd^{154} bombardments. Finally, the terbium daughter of Dy^{157} has a half-life presumably either very long or very short and has never been observed. No radiations that might be assigned to Tb^{157} decay were noticed during our investigations.

The chemically purified dysprosium fractions produced in Gd^{152} bombardment would, on the other hand, be expected to contain not only Dy^{155}, but also Dy^{157} and with the passage of time an increasing amount of Tb^{155} (5 days) growing in from its Dy^{155} parent. All three activities were indeed observed in our Gd^{152} bombardments.

3. Dy^{157} Results

The results of the Gd^{154} bombardments will now be discussed assuming, according to the arguments above, that Dy^{157} was the only activity present in any amount in the purified dysprosium fractions.

The Dy^{157} conversion-electron spectrum is shown in fig. 1. In agreement with the data of Michelich *et al.* [2]) a total of six transitions are identified, though not all of the conversion lines observed by them are seen due to our poorer resolution. The energies have been determined using the most intense conversion line as a standard. The energy of this line was taken to be 275 keV from the more precise measurements of Michelich *et al.* [2]). The K/L ratios of the 327- and 182-keV transitions (see table 3) agree with the theoretical ratios for dipole transitions. The peak at approximately the energy of the L line of the 61-keV

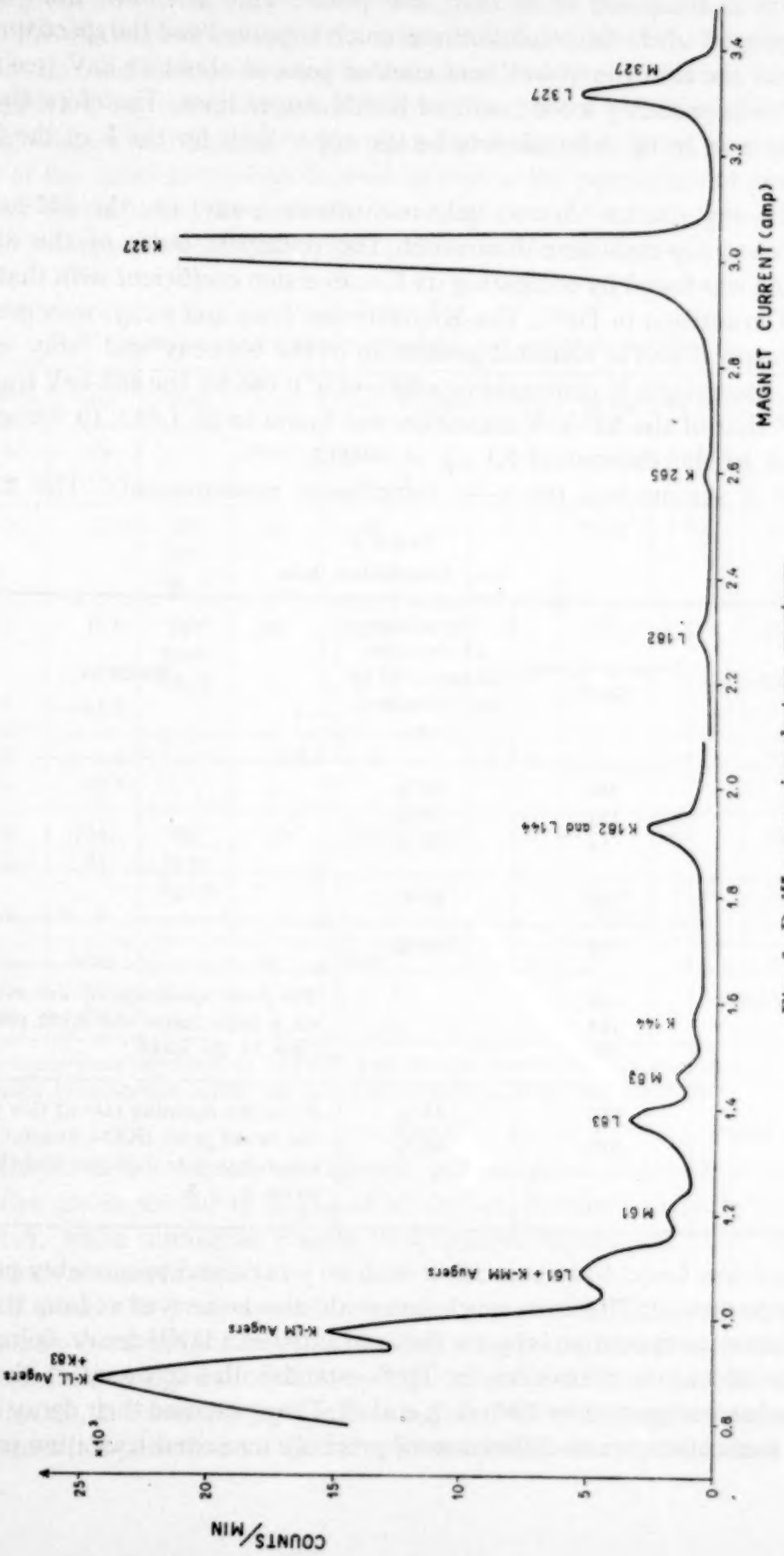

Fig. 1. Dy^{157} conversion-electron spectrum.

transition is composed of at least two peaks. This is known from a Gd^{152} bombardment where the resolution was much improved and the spectrum clearly showed the L of the 61-keV and another peak at about 49 keV (see fig. 4). The latter is probably a composite of K-MM Auger lines. Therefore the peak intensity seen in fig. 1 is taken to be the upper limit for the L of the 61-keV transition.

Total γ-ray spectra showed only one intense γ-ray, i.e. the 327-keV. No higher energy γ-rays were discovered. The multipole order of the 327-keV transition was found by comparing its K-conversion coefficient with that of the 662-keV transition in Ba^{137}. The K-conversion lines and γ-rays were measured for both transitions in identical geometries in the beta-ray and γ-ray spectrometers. Assuming a K-conversion coefficient of 0.095 for the 662-keV transition in Ba^{137} that of the 327-keV transition was found to be 1.04×10^{-2} essentially identical to the theoretical E1 α_K of 0.0115.

Table 2 summarizes the e—γ coincidence measurements. The 327-keV

TABLE 2

e—γ Coincidence data

Gating Electron	Coincident γ-ray (keV)	Percentage of electrons accompanied by the coincident γ-ray	Remarks
L61	265 182 83	15 % 70 % 25 %	
L83	182	90 %	
K144	182	100 %	
K182+L144	83 144 182		The β-ray spectrometer was evidently set a little above the K182 peak and close to the L144.
K83+Augers	$\frac{182}{327}$	$\approx \frac{15\ \%}{85\ \%}$	From the counting rate at this part of the broad peak (K83+Augers) it was concluded that K/L for 83-keV transition is > 3

transition was found to be coincident with no γ-rays, and presumably proceeds directly to ground. The same conclusion could also be arrived at from its intensity because the transition is by far the most intense in Dy^{157} decay. Coincidence relations of the six transitions in Tb^{157} establish the accuracy of the Dy^{157} decay scheme suggested by Michelich *et al.* [2]). They proposed their decay scheme on the basis of sums and differences of precisely measured transition energies.

Knowing the γ-ray efficiencies of the NaI(Tl) crystal used in the coincidence circuit, the relative intensities of the transitions represented by the conversion line and the coincident γ-rays can be estimated. A complete discussion of such quantitative γ-ray intensity measurements has been published by Gregers Hansen, Nielsen and Sheline [6]). For each conversion line listed in table 2 the energy of the coincident γ-rays is given as well as the percentage of conversion electrons accompanied by a particular γ-ray.

Table 3 summarizes conversion line and γ-ray intensities as well as calculated

TABLE 3

Dy^{157} intensities, conversion coefficients, and multipole assignments

E_γ	Shell	I_{line}	$I_{\gamma\,exp}$	$I_{\gamma\,calc}$	I_{trans}	K/L_{exp}	K/L_{theo}	$\alpha_{K\,exp}$	$\alpha_{K\,theo}$	Assignment
327	K L	113 16		9800	9930	7	7.3		0.011[illegible]	E1
265	K	0.8	"40" from fig. 2	40	40		7.2	"0.02"	0.02	E1
182	K L	10.0 ≈1.2	"190" from fig. 2	180	190	≈8	7.1	"0.052"	0.055	E1
144	K L	1.5 (0.8)		3.5	6		1.8		0.42	E2
83	K L M	(164) 21 7	"68" from fig. 2	50	240	>3	7.8	 $\alpha_L \approx$ "0.32"	3.3 $\alpha_L \approx$ 0.42	M1+(E2)
61	K L M	(210) (30) 10		30	280		≈7.0		7.6	M1+(E2)

Note: Intensities are expressed in 1/10 000 of all decays. Numbers in parentheses are computed, while results in quotation marks are based on e–γ coincidence measurements.

and theoretical conversion coefficients and assigned multipole orders. All intensities are expressed in $\frac{1}{10000}$ of all decays. Numbers in parentheses are computed, while numerical results in quotation marks are based on e—γ coincidence measurements.

Fig. 2 shows the γ-ray spectrum in coincidence with the L-conversion line of the 61-keV transition. Included in this diagram is a singles spectrum for comparison. From fig. 2 the relative γ-ray strengths of three transitions can be found, i.e. 83, 182 and 265 keV. Assuming the 182-keV transition to be of E1 order, the multipolarities of the other two transitions may be found. Let us

justify this assumption. The K/L ratio indicates the 182-keV transition to be dipole in character. The 327-keV transition, by means of an independent measurement, has been shown to be an E1 transition. It proceeds to the ground state of Tb^{157}. The first two excited levels in Tb^{157} apparently are members of a rotational band based on the ground state spin of $\frac{3}{2}$ [2]). Then the spin of the 327-keV level must be either $\frac{1}{2}$ or $\frac{3}{2}$ or $\frac{5}{2}$ and its parity opposite that of the rotational band members. The first 2 spin choices may be eliminated because the 182-keV

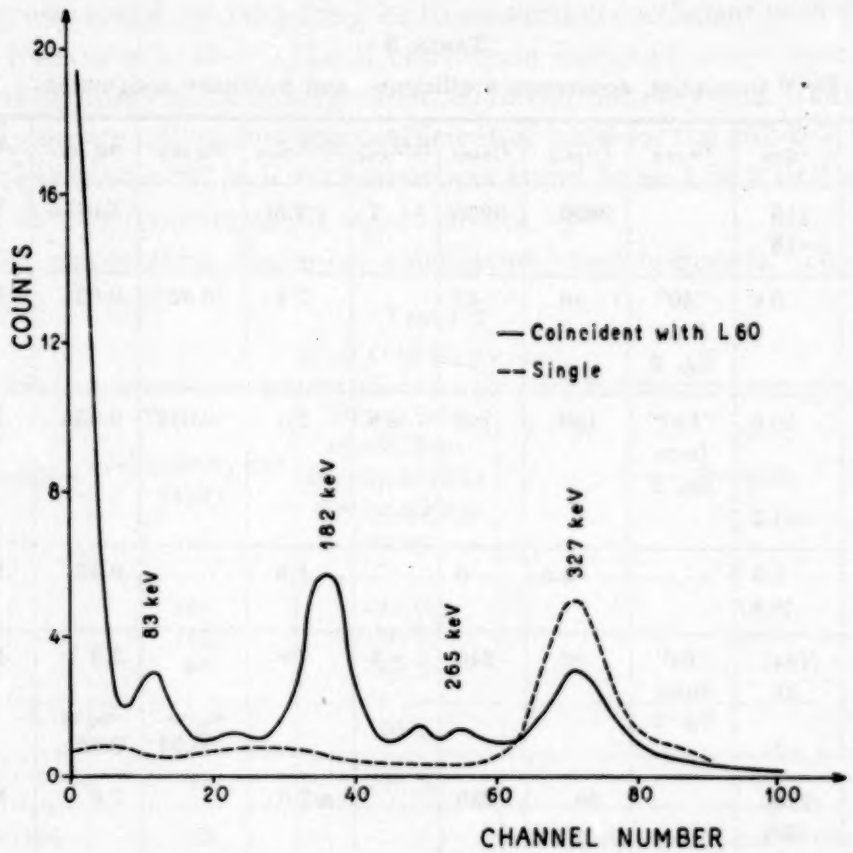

Fig. 2. γ-ray spectrum in coincidence with L of 61-keV. A singles spectrum is included for comparison.

transition to the $\frac{7}{2}$ rotational band member must be dipole in nature. This leaves the 327-keV level spin to be $\frac{5}{2}$ and makes the 182-keV an E1 transition. The calculated 265-keV α_K and the 83-keV α_L show that the 265-keV transition is an E1 while the 83-keV transition is an M1. These multipole assignments agree with the above considerations of level spins and parities.

Similar conclusions may be arrived at if the 83-keV transition is assumed to be M1. Its K/L ratio is known from table 2 to be > 3 and this indicates that the transition is mainly of dipole character. An intense γ-ray in the singles spectrum would be expected if the transition were an E1. The absence of such an intense γ-ray strongly suggests the transition to be an M1. Then using the relative γ-ray

intensities from fig. 2 the calulated 182- and 265-keV K conversion coefficients show these 2 transitions to be of E1 multipole order.

The 61-keV multipole order, to preserve consistency with the remainder of the decay scheme, should be mainly M1 with some E2 admixture possible. The multipole order is confirmed by the L subshell intensities reported by Michelich *et al.* [2]): $L_I/L_{II}/L_{III} = 180/20/20$. The upper limit (from fig. 1) of the 61-keV L conversion line intensity makes it imperative for the transition to be mostly M1, because the E2 K/L ratio at this energy is small, ≈ 0.3. The total transition intensity (using the L line upper limit) is: (a) < 509, assuming M1 multipole order, and (b) < 83, assuming E2 order. The intensity must be at least equal to the sum of the 83- and 265-keV intensities, i.e. 280, thus making M1 the probable choice for the 61-keV transition. The total intensity may be estimated from its M conversion line intensity, using the empirical fact that L/M ratios are consistently equal to 3, the theoretical M1 K/L ratio, and, either the M1 theoretical K or L conversion coefficient.

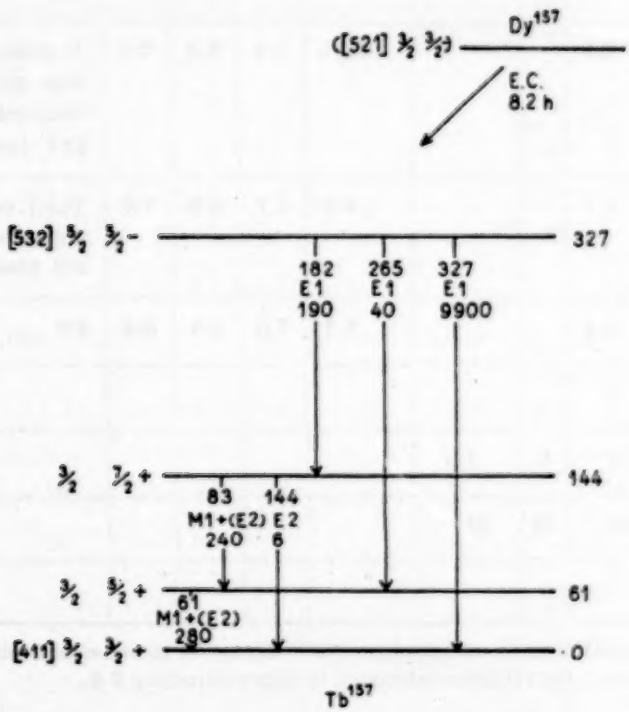

Fig. 3. Dy^{157} decay scheme. Intensities are expressed in 1/10 000 of all decays.

The 144-keV transition has to be an E2 and the assignment is confirmed by the conversion line intensities reported by Michelich *et al.* [2]): $K/L_{II}/L_{III} = 20/5/5$.

The Dy^{157} decay scheme is shown in fig. 3.

4. Dy^{155} Results

Fig. 4 shows the conversion spectrum obtained in a Gd^{152} bombardment. The beta-ray source in this particular experiment was quite thin and the spectrometer was operated with only 2 of the 6 gaps open in order to improve the resolution. The improvement is evident on comparing figs. 1 and 4. Lines assigned to Dy^{155} decay and their intensities are summarized in table 4. Assign-

TABLE 4

Dy^{155} conversion-electron intensities

Transition energy (keV)	Relative intensities				K/L (exp)	Theoretical K/L ratios			Multipole assignment and remarks
	K	L	M	N		E1	E2	M1	
227	316	<50	7	2	>6.3	7.1	3.1	7.0	E1 from an independent measurement. Low K/L ratio due to K of 271-keV present under L of 227-keV.
271	≈6	2.8			≈2.1	7.1	3.8	7.0	Possibly E2. The K line intensity was estimated by assuming the theoretical K/L ratio for the 227-keV transition.
206	<13.3	2.1			<6.3	7.1	2.9	7.0	The L of 161-keV and the L lines of a group of three Gd^{155} transitions are present under the K_{206} peak.
156	9.6	4.4			2.2	7.0	2.0	6.9	E2
161	19.1								
91		58	8	1.9					
65		385	73	23					
184	21								

An electron line of about 66 keV is also assigned to Dy^{155} decay. It is uncertain whether the line represents a K or an L conversion electron. Its relative intensity is approximately 7.5.

ments were made by (1) eliminating the already known Dy^{157} conversion lines, and, (2) assuming only the more prominent Tb^{155} conversion-electron lines would be visible at the time the spectrum was taken. The Tb^{155} lines are known from the work of Michelich *et al.* [2]). Also we determined the Tb^{155} spectrum using the same Dy^{155} source after Dy^{157} and Dy^{155} had decayed. Though the source was weak we were able to identify the more intense Tb^{155} lines reported by Michelich *et al.* [2]). Energies in table 4 are based on the most intense line

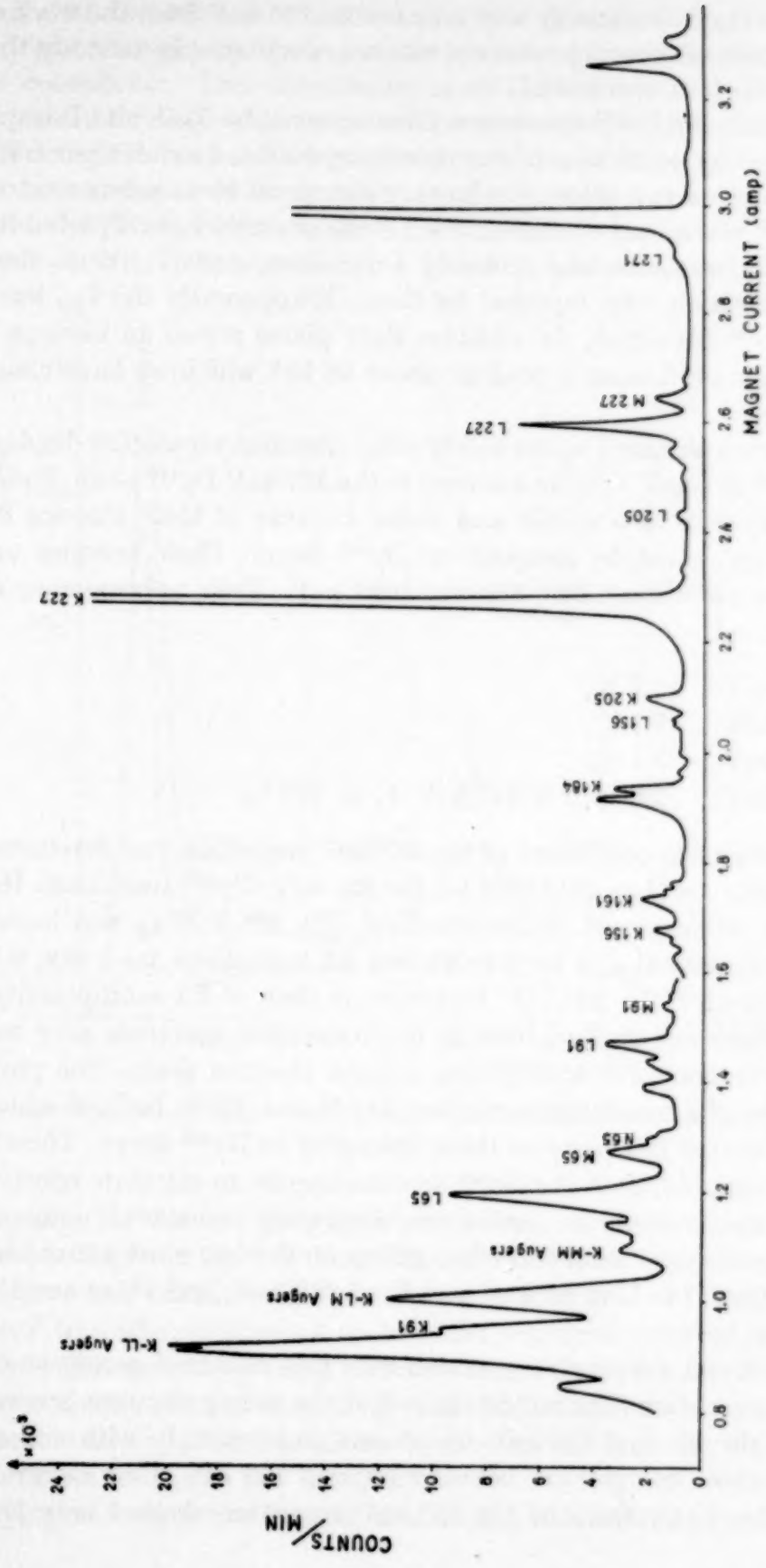

Fig. 4. Conversion-electron spectrum obtained in a Gd^{155} bombardment. Only those electron lines assigned to Dy^{155} decay are labelled.

belonging to Dy^{155}. Its energy was taken to be 175 keV from the work of Toth and Rasmussen who used permanent magnet spectrographs to study the Dy^{155} conversion-electron spectrum [1]).

While not all the Dy^{155} conversion lines reported by Toth and Rasmussen [1]) were observed by us because of our poorer resolution, most of their transitions < 300 keV in energy were. We have re-examined their permanent magnet spectrograph plates and conclude that (1) the electron lines reported by them for a 43.1-keV transition are probably Auger lines, and (2) the L_I line of an 88.0-keV transition, also reported by them, is apparently the L_{III} line of the 86.7-keV Tb^{155} transition. In addition their plates reveal an electron line of 66.3 keV, thus confirming a peak at about 66 keV which we have assigned to Dy^{155} decay.

γ-ray spectra obtained immediately after chemical separation displayed the intense Dy^{155} 227-keV γ-ray in addition to the 327-keV Dy^{157} γ-ray. Four higher energy peaks were also visible and these, because of their absence in Gd^{154} bombardments, must be assigned to Dy^{155} decay. Their energies are: 510 (annihilation radiation), 660, 880 and 1090 keV. Their approximate relative intensities are

a) 510 keV: 12.7 %,
b) 660 keV: 7.3 %,
c) 880 keV: 3.1 %,
d) 1090 keV: 3.8 %, if 227-keV I_γ is 100 %.

The K-conversion coefficient of the 227-keV transition was determined in a manner similar to that described for the 327-keV Dy^{157} transition. Here the 327-keV transition served as the standard. The 227-keV α_K was found to be 0.022. The theoretical α_K's for E1, M1 and E2 transitions are 0.029, 0.18, and 0.11, respectively. The 227-keV transition is thus of E1 multipolarity.

Due to numerous electron lines in the conversion spectrum e—γ measurements were inconclusive when gating on weak electron peaks. The problem is intensified by the interfering activities, Dy^{157} and Tb^{155}, both of which have many lines similar in energy to those belonging to Dy^{155} decay. Therefore we have not attempted, as in the Gd^{154} bombardments, to calculate relative γ-ray intensities and conversion coefficients employing coincident γ-ray spectra. However, results were obtained when gating on the two most prominent Dy^{155} conversion lines, i.e. L of 65 keV and K of 227 keV, and these are discussed qualitatively below.

Fig. 5 contrasts the singles spectrum with that obtained gating on the L of the 65-keV transition. The indication is that the gating electrons are in coincidence with the 91- and 184-keV transitions and probably with one or more transitions whose energies are between 100 and 180 keV. Low energy spectra gating on the K electrons of the 227-keV transition showed only K x-rays

indicating that the 227-keV transition proceeds directly to ground. Spectra taken at higher energies and gating on the same line showed the 660-keV γ-ray to be in coincidence. This coincidence result added to the presence of an 880-keV peak in the singles spectrum indicates an excited level at about 880 keV.

A Dy^{155} decay scheme has been proposed by Toth and Rasmussen [1]) based on (1) differences and sums of accurately measured transition energies and (2) the assumption that Tb^{155}, as its neighbors Tb^{157} and Tb^{159}, exhibits a ground rotational band with a spin sequence of $\frac{3}{2}$ (0 keV), $\frac{5}{2}$(65 keV) and $\frac{7}{2}$(156 keV).

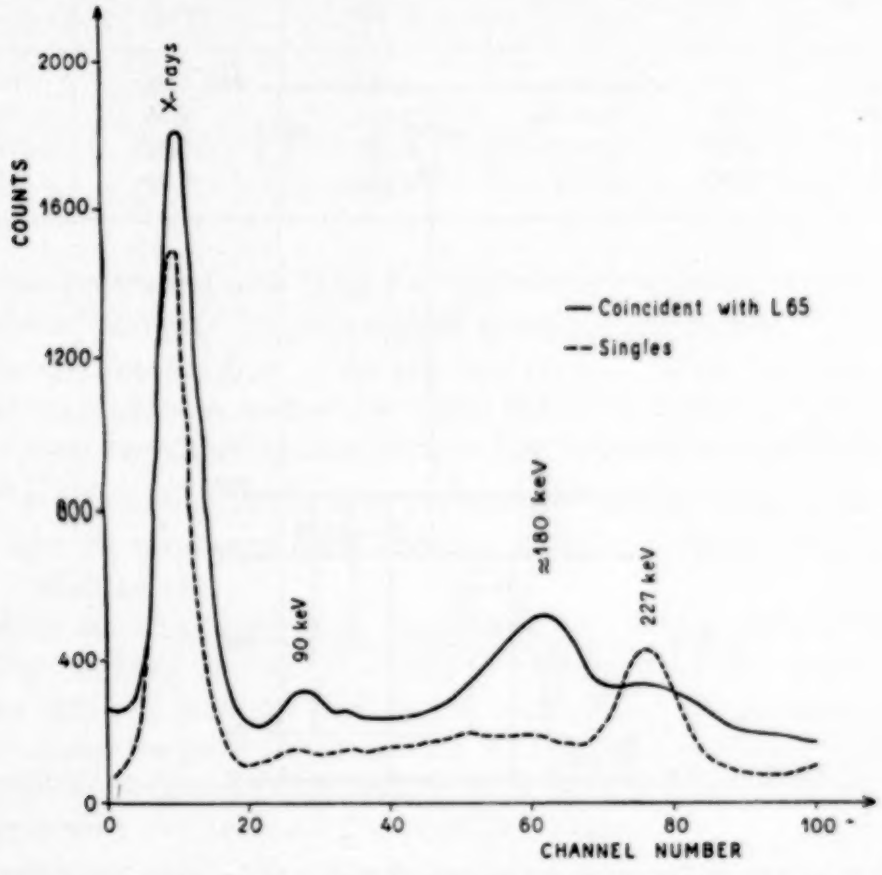

Fig. 5. γ-ray spectrum in coincidence with L of 65-keV. A singles spectrum is included for comparison.

Their proposed Tb^{155} level structure, together with our newly discovered level at 880 keV, is shown in fig. 6. Present data support their decay scheme. Thus, the 65- and 91-keV transitions do seem to be in coincidence. The K/L ratio of the 156-keV transition indicates it to be of E2 multipole order as expected for the cross-over between the $\frac{7}{2}$ and $\frac{3}{2}$ members of a rotational band. The 227-keV transition evidently does proceed to ground. No coincidence data concerning the 271-keV state are available. However, it is certain that the 271- and 206-keV transitions do follow the decay of Dy^{155}.

Employing conversion line intensities and theoretical conversion coefficients,

total relative intensities have been calculated for the 227, 161, 156, 91 and 65 keV transitions, assuming that they have the following multipole orders: E1, E1, E2, M1 and M1, respectively. The intensities are included in fig. 6, together with the 660 and 880 γ-ray intensities.

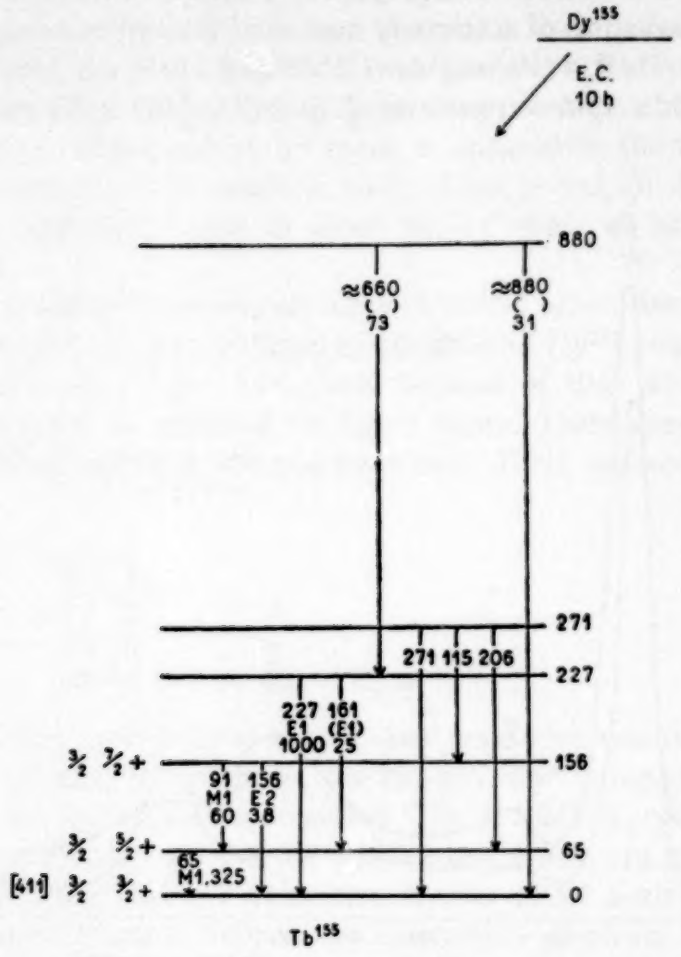

Fig. 6. Dy^{155} decay scheme. Intensities are normalized relative to I_{227} which has arbitrarily been made equal to 1000. The intensities given for the 660- and 880-keV transitions are γ-ray intensities and not total intensities. The multipole orders of the two transitions are unknown.

5. Discussion

The four isotopes, Tb^{155}, Tb^{157}, Tb^{159} and Tb^{161}, differ from one another only by pairs of neutrons. It is not surprising that their level structures exhibit strong similarities. One striking feature is that all four of the nuclei have ground state rotational bands based on a spin of $\frac{3}{2}+$. This ground state, according to the classification of Mottelson and Nilsson, is a [411] $\frac{3}{2}$ orbital which is the expected lowest configuration for $Z = 65$ [7]). Table 5 summarizes the rotational energies for the four isotopes together with the corresponding constants B and

$3\hbar^2/\mathcal{I}$, where B is the correction term for the simple rotational energy relationship and $3\hbar^2/\mathcal{I}$ is the inertial parameter. The rotational formula used for the calculations was $E_I = E_0 + (\hbar^2/2\mathcal{I})[I(I+1)] + B[I(I+1)]^2$, where the decoupling term was omitted since it is non-zero only when $K = \frac{1}{2}$. The inertial parameters are contrasted with those for neighboring even-even nucleides one unit less in mass, following the procedure of Mottelson and Nilsson [7]). The contrast indicates the contribution of the last odd nucleon to the moment of inertia. The odd mass isotopes, as has been noted before [7]), display a larger moment of inertia than the neighboring even isotopes. The contribution due to the odd particle in Tb^{155} is obscured since the even nucleus Gd^{154} is just barely in the deformed region and its rotational band energies deviate markedly from the simple $I(I+1)$ relationship.

TABLE 5

Constants for ground rotational bands based on a [411] $\frac{3}{2}+$ orbital

Isotope	Energy of $\frac{3}{2}+$ state (keV)	Energy of $\frac{7}{2}+$ state (keV)	B (keV)	$3\hbar^2/\mathcal{I}$ (keV)	$3\hbar^2/\mathcal{I}_{e-e}$ (keV)	Ref.
Tb^{155}	65.4	155.8	−0.0138	78.9	123	[1])
Tb^{157}	60.8	143.9	−0.0240	73.7	89	[2])
Tb^{159}	58.0	137.5	−0.0202	70.2	79	[8])
Tb^{161}	56.6	134.2	−0.0191	68.5	76	[9])

Previous investigations have established an intrinsic state at 364 keV in Tb^{159} that has been classified [7]) as [532] $\frac{5}{2}-$. Our present data indicate strongly that the 327-keV level in Tb^{157} is the same odd-parity intrinsic state. The reduced transition probabilities for the 3 E1 γ-rays from this $\frac{5}{2}-$ state to the 3 members of the ground rotational band for both isotopes are listed below and compared with the theoretically predicted values:

$$Tb^{157}\ \gamma_{327}/\gamma_{265}/\gamma_{183} = 1/0.0075/0.105,$$

$$Tb^{159}\ \gamma_{364}/\gamma_{305}/\gamma_{225} = 1/0.016\ /0.11 \quad (\text{ref. } [10])),$$

$$\text{Theoretical:} \qquad 1/0.43\ /0.07.$$

The experimental values for both cases agree quite well with one another, but deviate from the theoretical predictions. The deviations in Tb^{159} have been ascribed to the expected slowness of the transitions due to the fact that they are strongly hindered by the asymptotic selection rules [7, 10]). The same explanation should apply to the 3 Tb^{157} E1 transitions.

The Dy^{157} ground level has been suggested to be [521] $\frac{3}{2}$-state [7]), that is, the same assignment as for the Gd^{155} ground state because the 2 nuclei have the same last odd neutron. Present data support the assignment since the 327-keV

[532] $\frac{5}{2}-$ level is strongly populated in direct electron capture decay (no high energy γ-rays were observed), while the two remaining excited states, with spins of $\frac{5}{2}+$ and $\frac{7}{2}+$, are essentially not fed by direct electron capture decay.

The 227-keV state in Tb^{155} apparently has odd parity and it is tempting to classify that level as the same [532] $\frac{5}{2}-$ state discussed above. The data are not clear and not sufficient enough to eliminate $\frac{1}{2}-$ or $\frac{3}{2}-$ as possible spin assignments for this level. Even assuming that the 161-keV transition is an E1 and does proceed from the 227-keV level to the $\frac{5}{2}+$ 65-keV state, the $\frac{5}{2}-$ to $\frac{7}{2}+$ 71-keV transition has not been observed. According to the branching ratios given above the 71-keV transition should be more intense than the 161-keV transition. The photographic plates of Toth and Rasmussen reveal no lines that may be due to L electrons of the 71-keV transition, though it is possible that these might be obscured by the more intense M and N lines of the 65-keV transition. The absence of the 71-keV transition would tend to support $\frac{3}{2}-$ or $\frac{1}{2}-$ for the spin of the 227-keV level.

If the K/L ratio of the 271-keV transition is correct, then the Tb^{155} level at that energy should have even parity. There are a number of even parity low-lying excited states expected in this region [7]) and it is not possible to say which of these is represented by the 271-keV level.

The 880-keV Tb^{155} level may be the [411] $\frac{1}{2}+$ excited state observed in $Eu^{153}(Z = 63)$, $Ho^{163}(Z = 67)$ which also appears [7]) as the ground state in Tm^{167}, Tm^{169} and $Tm^{171}(Z = 69)$.

The Dy^{155} ground state may be expected to be the same orbital as the ground level [7]) in Gd^{153}, i.e., [651] $\frac{3}{2}+$. The data obtained here are insufficient and the Dy^{155} decay scheme is far too incomplete to say just how much each of the Tb^{155} excited states is populated in direct electron capture decay.

We would like to thank Professor Niels Bohr for the excellent working conditions at his Institute. We are very grateful to Miss E. Johanssen who assisted in all of the chemical separations. One of us (KST) would like to thank the Fulbright Foundation for making it possible for him to spend an instructive year at the Institute for Theoretical Physics.

References

1) K. S. Toth and J. O. Rasmussen, Phys. Rev. **115** (1959) 150
2) Michelich, Harmatz and Handley, Phys. Rev. **108** (1957) 989
3) Thompson, Harvey, Choppin and Seaborg, J. Am. Chem. Soc. **76** (1954) 6229
4) K. S. Toth and O. B. Nielsen, Phys. Rev. **115** (1959) 1004
5) O. B. Nielsen and O. Kofoed-Hansen, Mat. Fys. Medd. Dan. Vid. Selsk. **29**, No. 6 (1955)
6) Gregers Hansen, Nielsen and Sheline, Nuclear Physics **12** (1959) 389
7) B. R. Mottelson and S. G. Nilsson, Mat. Fys. Skr. Dan. Vid. Selsk. **1** (1959) 8
8) Chupp, DuMond, Gordon, Jopson and Mark, Phys. Rev. **112** (1958) 518
9) Schmid, Burson and Cork, Phys. Rev. **115** (1959) 174
10) K. O. Nielsen, O. B. Nielsen and O. Skilbreid, Nuclear Physics **7** (1958) 561

8.B

Nuclear Physics **22** (1961) 71—77; © *North-Holland Publishing Co., Amsterdam*

Not to be reproduced by photoprint or microfilm without written permission from the publisher

INELASTIC INTERACTIONS OF π-MESONS WITH NUCLEONS AT 6.8 GeV

V. S. BARASHENKOV

Laboratory of Theoretical Physics, Joint Institute for Nuclear Research, Dubna, USSR

Received 10 June 1960

Abstract: The results of experiments with π-mesons are compared with the calculations by the statistical theory. Good agreement is observed in the distribution of stars with number of prongs and with momentum of the particles produced.

Peripheral collisions are taken into account to explain angular distributions. Experimental data can be brought into agreement with the theory under the assumption that the cross-section of peripheral collisions accounts for more than a half of the total cross section of all inelastic processes.

The resonant interaction of π-mesons is discussed.

1. Introduction

A model of central and peripheral ($\pi\pi$)- and (πN)-interactions was suggested in ref. [1]) to explain the experimental data on inelastic interaction of fast π-mesons by nucleons. For the cross section of inelastic peripheral interactions the following lower estimate was obtained

$$\sigma_{\mathrm{p}} > (0.2 \div 0.3)\sigma_{\mathrm{in}},$$

where $\sigma_{\mathrm{in}} \simeq 20 \times 10^{-27}$ cm^2 is the total cross section of all inelastic (πN)-interactions. Non-single-valuedness in σ_{p} was largely due to the fact that in ref. [2]) a portion of positively charged particles was not identified as protons or π^+-mesons. Therefore, the experimental values of angular asymmetry of charged π-mesons and protons could vary within a braod range †

$$A_\pi \equiv \vec{n}_\pi/\overleftarrow{n}_\pi = (1.1 \div 1.9), \quad A_{\mathrm{p}} \equiv \vec{n}_{\mathrm{p}}/\overleftarrow{n}_{\mathrm{p}} = (0 \div 0.5).$$

Certain experiments on the interaction of π-mesons with photo-emulsion nuclei at 6.8 GeV have recently been completed in Dubna. On the basis of strict selection criteria, 530 cases of interaction between π-mesons and nucleons were isolated and analyzed. The values of angular asymmetry $A = \vec{n}/\overleftarrow{n}$ for

† In the following we shall use the same notation as in ref. [1]). Thus, $\vec{n}_{\mathrm{p}}$ and $\overleftarrow{n}_{\mathrm{p}}$ are the numbers of protons emitted in the centre-of-mass of the colliding π-meson and nucleon into the front and rear hemispheres, respectively (with respect to the velocity vector of the primary π-meson); $\vec{n}_\pi$ and $\overleftarrow{n}_\pi$ are the same for charged π-mesons. The centre-of-mass system of the colliding primary π-meson and proton will be designated for brevity as "system (πp)".

protons and charged π-mesons were measured with greater accuracy than in ref. [2]).

In the sections below we shall consider the results obtained in ref. [3]) in detail.

2. Comparison with the Statistical Theory of Multiple Production

Fig. 1 represents the ratio of the average number of experimentally observed stars with different number of prongs to the theoretically calculated one: $N(\mathrm{n})_{\mathrm{exper}}/N(\mathrm{n})_{\mathrm{theor}}$. It is clear that experiment and theory are in better agreement than in the case of (NN)-collisions (cf. ref. [4])).

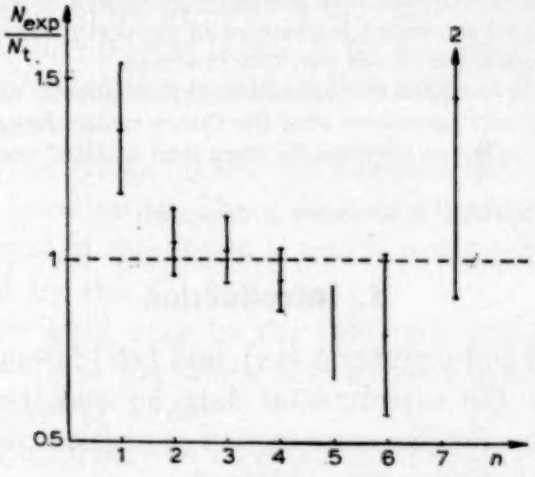

Fig. 1. Ratio of the experimentally observed number of stars with n prongs to that calculated by the statistical theory. Odd number of prongs: $(\pi^-\mathrm{p})$-collision; even number of prongs: $(\pi^-\mathrm{n})$-collision. Errors of experimental data are given.

The experimental values of the average number of charged particles produced in one event of $(\pi^-\mathrm{p})$- and $(\pi^-\mathrm{n})$-collisions at 6.8 GeV,

$$\bar{n}(\pi^-\mathrm{p}) = 2.98 \pm 0.02, \quad \bar{n}(\pi^-\mathrm{n}) = 2.98 \pm 0.02,$$

are in good agreement with the theoretical values †

$$\bar{n}(\pi^-\mathrm{p}) \approx \bar{n}(\pi^-\mathrm{n}) = 3.$$

For the average number of charged π-mesons produced in one act of (π^-N)-interaction at 6.8 GeV in a bubble propane chamber the value $\bar{n}_\pi = 2.5$ is obtained [6]) which is in good agreement with that calculated by the statistical theory.

Figs. 2 and 3 represent the momentum spectra of charged π-mesons and protons produced in $(\pi^-\mathrm{p})$-collisions. Both the experimental and theoretical

† This value $\bar{n}(\pi^-\mathrm{p})$ is approximately 2 % higher than that indicated in the graph of ref. [5]) due to the fact that in ref. [5]) only $(\pi^-\mathrm{p})$-events with two and four prongs are taken into account.

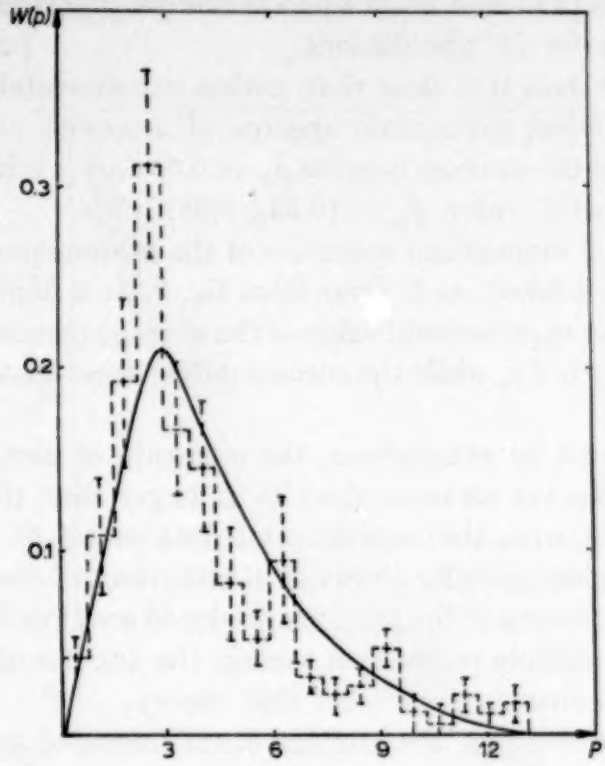

Fig. 2. The momentum spectrum of π-mesons in the centre-of-mass system of the colliding π^--meson and proton. The dashed line is an experimental histogram for π-mesons. The momenta p are represented in the units μc, where μ is the mass of π-meson.

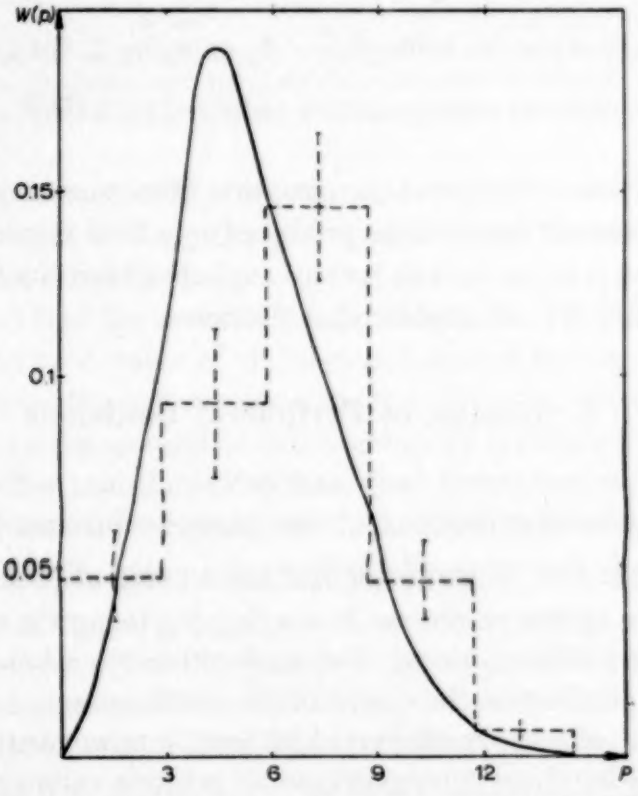

Fig. 3. The momentum spectrum of protons in the centre-of-mass system of the colliding π^--meson and proton. The dashed line is an experimental histogram for protons. The momenta p are given in units of μc, where μ is the mass of π-meson.

spectra of particles produced in (π^-n)-collisions are practically the same as the respective spectra for (π^-p)-collisions.

From the above data it is clear that, within experimental error, the experimental and theoretical momentum spectra of π-mesons are very close. The theoretical value of the average impulse $\bar{p}_\pi = 0.55$ GeV/c is in good agreement with the experimetal value $\bar{p}_\pi = (0.53 \pm 0.03)$GeV/$c$.

The experimental momentum spectrum of the protons produced in inelastic (π^-N)-collisions is peaked, as is clear from fig. 3, at a higher value than the theoretical one. The experimental value of the average momentum of protons is $\bar{p}_p = (0.89 \pm 0.035)$GeV/$c$, while the corresponding theoretical value is equal to 0.8 GeV/c.

As has been shown by calculations, the momenta of particles in two-prong stars are on the average no more than 15 % larger than those in four-prong stars, in agreement with the experimental data of ref. [3]).

Yet while the experimentally observed distributions of stars with number of prongs and with momenta of the particles produced are close to those calculated by the statistical multiple production theory, the angular distributions of the particles produced sharply contradict this theory.

Just as at lower energies, the angular distributions of secondary particles at 6.8 GeV prove to be asymmetrical with respect to the angle $\theta = \frac{1}{2}\pi$ in the system (πp), the experimental values of angular asymmetry of charged π-mesons and protons being equal to

$$A_\pi = \vec{n}_\pi / \overleftarrow{n}_\pi \equiv 1.56 \pm 0.1, \quad A_p \equiv \vec{n}_p / \overleftarrow{n}_p \leqq 0.1 \pm 0.1.$$

(these values are close to *average* values obtained at 5 GeV: $A_\pi = 1.47$, $A_p = 0.23$).

Taking into account the law of conservation of momentum, the ansisotropic angular distributions of the particles produced may be obtained in the statistical Fermi theory; yet it is not known how to explain within the framework of this theory the asymmetry of angular distributions.

3. Account of Peripheral Collisions

Just as in ref. [1]) peripheral ($\pi\pi$)- and (πN)-collisions will be considered to explain the angular distributions of the particles produced.

Fig. 4 represents the values of angular asymmetry of protons A_p calculated for various values of the parameter $\xi = \sigma_p/\sigma_{in}$ (σ_{in} being the total cross section of all inelastic (πN)-interactions). For each value ξ a whole range of values A_p is possible depending on the choice of the coefficients ξ_1 and ξ_2 determining the cross sections of peripheral ($\pi\pi$)- and (πN)-interactions respectively (see ref. [1])). The cross-hatching corresponds to all possible values of the coefficients ξ_1 and ξ_2. For fixed value of ξ the quantity A_p increases with the growth of ξ_1

for an isobar variant and decreases for an non-isobar variant. (At $\xi_1 = 0$ both variants coincide.)

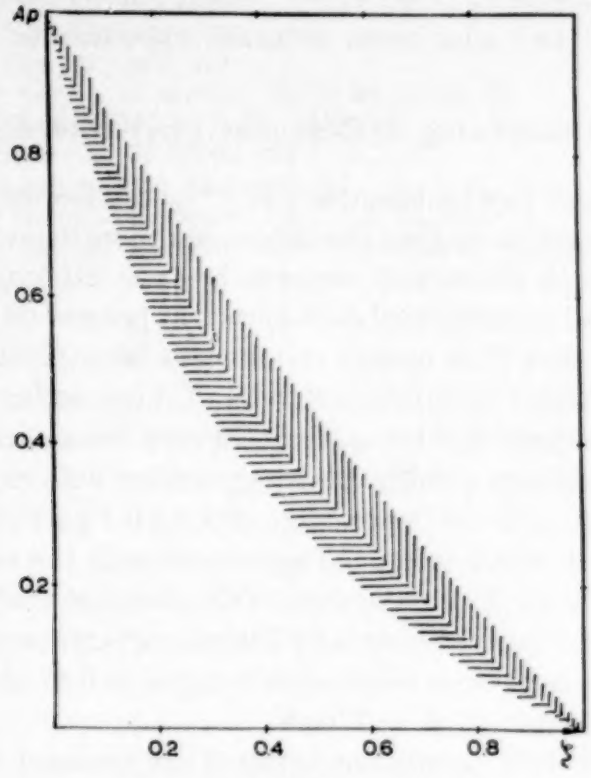

Fig. 4. Angular asymmetry of the protons $A_p = \overrightarrow{n_p}/\overleftarrow{n_p}$ in the centre-of-mass system of the colliding π^--meson and proton. The cross-hatching designates the region of possible values of A_p. Horizontal cross-hatching is for the isobar variant and vertical cross-hatching for the non-isobar one.

From the comparsion with the experimental value of A_p it follows that $\sigma_p > 0.55\ \sigma_{in}$ or $\sigma_p > 0.65\ \sigma_{in}$, depending on whether the isobar variant or the non-isobar one is considered.

It will be noted that the authors [3]) regard the value 0.2 as the extreme upper value of A_p. The true value of A_p does not exceed 0.1, in their opinion †.

The calculation of the angular asymmetry of the π-mesons of A_π is a far more complex task since the amount of this asymmetry is determined by parameters whose exact values are as yet unknown. Calculations have shown that by choosing the values of these parameters, the experimental quantity of A_π can be explained with the same values of the cross section σ_p as for nucleons; the multiplicity of the particles produced and their energy distributions prove to be close to the experimental ones, while the values of the parameters used in the calculations remain within the range of reasonable values (cf. ref. [1])). A far more detailed analysis is needed before drawing more definite conclusions.

† I am indebted to V. V. Glagolev and K. D. Tolstov for numerous discussions of the experimental data of ref. [3]).

A large cross section of peripheral interactions in (πN)-collisions suggests that in (NN)-collisions as well, the cross section σ_p will actually prove higher than the lower estimate $\sigma_p > 0.2\,\sigma_{in}$ [4,7]) which follows from the experimental data of ref. [8]). In this case more accurate experimental data are needed.

4. Concerning a Resonant ($\pi\pi$)-Interaction

A number of papers (see for example refs. [9–12])) discuss the effect of a possible resonant ($\pi\pi$)-interaction on the calculations in the statistical theory. Theoretically, the idea of such interaction seems to be quite attractive and likely. Yet up to $E = 7$ GeV all experimental data known at present on the multiplicity of particles produced and their energy spectra can be explained without taking account of the resonant ($\pi\pi$)-interaction [13]). Taking account of such interactions within the framework of the statistical Fermi theory considerably complicates calculations without yielding better agreement with experiment. Thus, in (π^-p)-collision at $E = 5$ GeV an average of 4.3 ± 0.1 particles [2]) (charged and neutral) is produced, which is in good agreement with the value 4.2 calculated by the statistical theory. Taking account of the resonant ($\pi\pi$)-interaction yields the values 4.7 and 5.1 for the Dyson and Takeda variants respectively (the mass of π-meson isobar in both cases assumed to be equal to 0.47 of the nucleon mass). The situation is similar at $E = 7$ GeV.

Nor is agreement with experiment better if the resonant ($\pi\pi$)-interaction in the case of (NN)-collisions is taken into account.

In ref. [11]) it is supposed that such conclusions arise due to the crudenesss of the statistical theory. But this means precisely that within the accuracy of present-day theory and experiment there is no need to take the resonant ($\pi\pi$)-interaction into account in the analysis of (πN)- and (NN)-collisions. This applies especially to the energy region close to one GeV wherein the statistical theory can only be applied with essential reservations.

Yet taking into account peripheral interactions gives a new angle to the role of the resonant interaction of π-mesons.

In peripheral collisions a somewhat smaller number of particles is produced than in central collisions (cf. table 2 from ref. [1])). This will probably compensate for the increase of multiplicity due to taking account of the resonant ($\pi\pi$)-interaction. It will be possible to obtain the answer after detailed numerical calculations have been completed.

References

1) V. S. Barashenkov, JETP **37** (1959) 1484;
V. S. Barashenkov and V. M. Maltsev, Nuclear Physics **17** (1960) 377
2) G. Maenchen, W. B. Fowler, W. H. Powell and R. W. Wright, Phys. Rev. **108** (1957) 850
3) V. A. Beliakov *et al.*, JETP (to be published)

4) V. S. Barashenkov, V. M. Maltsev and E. K. Mihul, Nuclear Physics **13** (1959) 583
5) V. S. Barashenkov, Nuovo Cimento **14** (1959) 657
6) Van Gan-Chiang *et al.* (to be published)
7) N. P. Bogachev *et al.*, JETP (in print)
8) N. P. Bogachev *et al.*, JETP **37** (1959) 1225
9) E. Eborle, Nuovo Cim. **8** (1958) 610
10) V. S. Barashenkov and V. M. Maltsev, JETP **37** (1959) 884
11) V. I. Ruskin and P. A. Usik, JETP **38** (1960) 929
12) R. Hagendorn, Nuovo Cim. **15** (1960) 246
13) V. S. Barashenkov, Nuovo Cim. **14** (1959) 656;
V. S. Barashenkov, Report at the Second All-Union Conference on Field Theory and Elementary Particles in Uzhgorod, May 1960 (to be published in Fortschritte der Physik)

1.D.4

Nuclear Physics **22** (1961) 78—95; © *North-Holland Publishing Co., Amsterdam*

Not to be reproduced by photoprint or microfilm without written permission from the publisher

VIBRATIONAL STATES OF NUCLEI IN THE RANDOM PHASE APPROXIMATION

D. J. THOULESS †

Institute for Theoretical Physics, University of Copenhagen, Denmark

Received 31 August 1960

Abstract: The properties of those states which can be obtained by exciting a single particle from the ground state of a nucleus are studied by using a perturbation-theory expansion for the Green's function. The formula obtained differs from the one used in a straightforward shell model calculation in some important respects. By comparing this formula with the condition for a solution of the Hartree-Fock equations to give a minimum of the expectation value of the energy, derived in an earlier paper, it is shown that it is always possible to choose an independent particle wave function which makes all collective modes stable in the random phase approximation. A study of the formal properties of solutions of the equation shows that the wave functions should be normalized using an indefinite metric: different eigenfunctions are then orthogonal. The eigenfunctions form a complete set, if there is no degeneracy in the solution of the Hartree-Fock equations, but not if there is a degeneracy. An upper bound for the lowest energy level is established, and the rule for calculating matrix elements of one-particle operators between the ground state and an excited state is given. It is shown to follow from the self-consistent field condition that the energy-weighted sum rules are preserved in this approximation. A discussion of spurious states is given, and it is shown that they separate out and have zero energy. A vector introduced in our earlier discussion of the cranking model is shown to be independent of all eigenvectors in this case.

1. Introduction

The study of collective motion from the point of view of the independent-particle model has considerably increased our understanding of the physics of many-fermion systems. The different methods which have been used to derive the equations of motion of the collective modes seem to be essentially the same, and the approximation which they suggest yields linear equations which are similar to the equations of the random phase approximation used by Bohm and Pines [1]) in their study of the electron gas. This approximation can be obtained by writing the equations of motion for states in which one particle is excited from the ground state, and then linearizing these equations by neglecting terms which are small in the independent-particle approximation. This method has been used most often in connection with extended systems, such as the electron gas, but its usefulness for studying finite systems, such as nuclei, has been pointed out by several authors [2]).

† Permanent address: Department of Mathematical Physics, University of Birmingham.

In this paper, we use the equation of motion for the Green's function, and obtain the random phase approximation from that. The Green's function formalism provides a compact way of writing down the quantities in which we are interested — energies of excited states relative to the ground state, and matrix elements of one-particle operators between the ground state and excited states, — and it leads in a natural way to the random phase approximation. The same answer can be obtained by many other different ways. Our hope, partially borne out by the results, is that, since all quantities are both calculated and observed relative to their values in the ground state, the imperfections of the ground state wave function should not affect our results too strongly.

In a previous paper, which we call (I), it was shown that there is a close connection between the equation for the collective modes in the random phase approximation and the condition for the particular solution of the Hartree-Fock equations which we used in the independent-particle model to be stable [3]). The use of this relation is the principal topic which we discuss here. In the paper of Brown *et al.* (which we refer to as BET), we give a more detailed discussion of the properties of collective states in nuclei from the point of view of the random phase approximation without making any use of the self-consistent field equations [4]). The main reason for this division is that self-consistent calculations have not been made. The wave functions and independent-particle energies used in BET are related to the experimental data, but the interaction between particles which we assume is not one which would lead to these wave functions and energies if it were used in a self-consistent field calculation.

The first conclusion we draw is that it is always possible to find a solution of the Hartree-Fock equations which makes these collective modes stable (ensures that they have real frequencies), since the determinant which actually gives the lowest possible expectation value of the Hamiltonian stabilizes the collective modes in the random phase approximation. As some parameter is altered (physically the only parameters at our disposal are the total numbers of protons and neutrons), one of the collective modes may get a lower and lower frequency, until the frequency becomes imaginary. This indicates that a type of solution of the Hartree-Fock equations, for example a solution which gives a spherical self-consistent field, which was stable in one range of the parameter, is unstable in another range, and some other solution, for example one which gives an ellipsoidal self-consistent field, must be sought. We call, rather loosely, such an occurrence a phase transition. In the neighbourhood of a phase transition, a semi-classical approximation is likely to be valid.

Next, we discuss some of the formal properties of the solutions of the equations. Since the energy levels are given by the eigenvalues of a non-Hermitian matrix, some discussion is necessary. The stability condition assures that the eigenvectors usually form a complete set (with an important exception), and so we can construct a variational principle which enables an upper bound for

the eigenvalues to be established. The rules for calculating matrix elements are given. The most important result we prove is that energy-weighted sum rules are satisfied in this model to a much better approximation than they are in the shell model. This result is true only if the independent-particle model from which we start is a solution of the Hartree-Fock equations. This result is one indication of the superiority of this method of calculating energy levels to the conventional shell-model method, as used by Elliott and Flowers [5]).

Finally, we show that the spurious energy level, a level which just corresponds to oscillation of the centre of mass of the nucleon in the potential well, separates out and has zero energy in our model. This can be regarded as a consequence of the sum rule. In the conventional shell model, this spurious level is mixed in with many other levels, unless the potential well is an oscillator potential [6]).

Lipkin has discussed the importance of the violation of conservation laws by the wave functions used in the independent-particle model [7]). The violation of these conservation laws leads to the spurious states, and so this approximation, by separating off the spurious states, does something to remedy the situation. With a finite number of particles, it is never possible to satisfy momentum conservation in the independent-particle model. Angular momentum is a good quantum number for spherical nuclei, but only one component of angular momentum is conserved in the independent-particle model of deformed nuclei. We shall discuss the spherical case in most of this paper, but the case of axial symmetry is not essentially different. The important restriction we make in this paper is that we do not consider violation of the conservation of the number of particles. It has been shown by Bogoliubov [8]) that the Bardeen, Cooper, and Schrieffer [9]) type of wave functions can be regarded as a generalized independent-particle wave function with an indefinite number of particles. The work of Belyaev [10]) shows that this type of wave functions should be used to describe all nuclei except those with only one particle or one hole outside closed shells. We therefore make this restriction only for the sake of simplicity, not because it is physically justified. The method can be generalized quite easily to allow for this type of wave function, and nothing fundamental is altered — the generalization of methods used for Hartree-Fock wave functions was discussed in (I). The complication is that particle-particle and hole-hole excitations must then be considered at the same time as the particle-hole excitations which we discuss here, and the formulae become more cumbersome. A discussion of collective motion which includes this effect has been given by Baranger [11]).

2. Calculation of the Green's Functions

The Green's functions in which we are interested are those which describe states obtained from the ground state by exciting a single particle. We call these states particle-hole states, since, in the independent-particle model, they

are obtained from the ground state by creating a hole below the Fermi surface and a particle above the Fermi surface. According to the usual conventions, the definition of such a Green's function in its time-dependent form is

$$G(\alpha, \beta; \gamma, \delta; t) = \begin{cases} \langle \Psi_0 | a_\beta^\dagger a_\alpha \exp[i(H-E_0)t] a_\gamma^\dagger a_\delta | \Psi_0 \rangle, & \text{for } t < 0, \\ \langle \Psi_0 | a_\gamma^\dagger a_\delta \exp[-i(H-E_0)t] a_\beta^\dagger a_\alpha | \Psi_0 \rangle, & \text{for } t > 0, \end{cases} \quad (1)$$

where a_α is the operator which annihilates a particle in the level α, $a_\alpha^\dagger$ is the creation operator, H is the true Hamiltonian, $|\Psi_0\rangle$ is the true ground state, and E_0 is the ground state energy. We assume that we can choose a representation such that the independent-particle model is a good first approximation.

To calculate the Green's function we use the method based on perturbation theory used by Landau for the case of the Fermi liquid [12]). The Green's function is obtained in perturbation theory by summing all connected graphs with two external lines; a line representing a particle in the level α leaves the graph at time zero, a line representing β enters the graph at time zero, a line representing γ enters at time t, and a line representing δ leaves at time t. The fermion lines are supposed to represent the true one-particle propagator, which are not, in general, diagonal in the chosen representation; we denote such propagators by the function $S_{\alpha\beta}(t)$. We have to add up the graphs of the type shown in fig. 1.

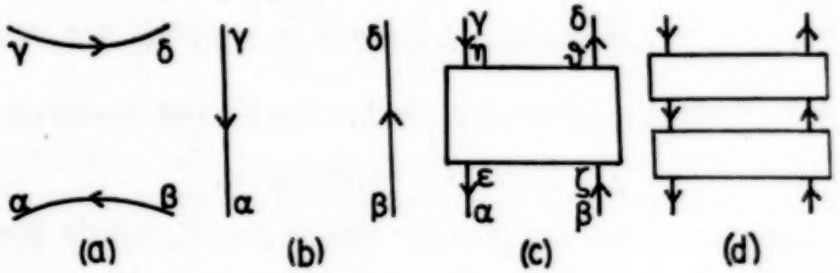

Fig. 1. Graphs which contribute to the Green's function.

The rectangular box denotes an irreducible vertex part, which is defined as part of a graph connected to the rest of the graph by one line entering and one line leaving at both the top and the bottom, which cannot be cut into two separate parts by breaking two fermion lines at the same horizontal level. We denote the contribution of the irreducible vertex part shown in fig. 1(c) by $\Gamma(\varepsilon, \zeta; \eta, \theta; t')$, where t' is the distance from the top to the bottom. Some simple irreducible vertex parts are shown in fig. 2. The summation of graphs like those shown in fig. 1 leads to the integral equation for the Green's function

$$\begin{aligned} &G(\alpha, \beta; \gamma, \delta; t) \\ &\quad = S_{\alpha\beta}(0) S_{\gamma\delta}(0) - S_{\alpha\gamma}(t) S_{\delta\beta}(-t) - \sum_\varepsilon \sum_\zeta \sum_\eta \sum_\theta \int_{-\infty}^{\infty} \int_{-\infty}^{\infty} S_{\alpha\varepsilon}(t') S_{\beta\zeta}(-t') \\ &\quad \times \Gamma(\varepsilon, \zeta; \eta, \theta; t''-t') \{ G(\eta, \theta; \gamma, \delta; t-t'') - S_{\eta\theta}(0) S_{\delta\gamma}(0) \} \mathrm{d}t' \, \mathrm{d}t''. \end{aligned} \quad (2)$$

This equation is exact, and gives the Green's function to all orders in perturbation theory, but it is not very useful, since we know neither the one-particle propagators nor the irreducible vertex parts.

The first assumption we have to make in order to solve this equation is that the quasi-particle approximation is valid. This means that there exists a representation in which the one-particle propagators are approximately diagonal, and in which the propagators have a time-dependence of the form they would have if the particles were non-interacting. That is

$$S_{ii}(t) = \begin{cases} 0, & \text{for } t < 0, \\ -\exp[i(\varepsilon_i - \varepsilon_0)t], & \text{for } t \geqq 0, \end{cases} \tag{3}$$

if i is an occupied state (i runs from 1 to A), and

$$S_{mm}(t) = \begin{cases} \exp[i(\varepsilon_m - \varepsilon_0)t] & \text{for } t < 0, \\ 0, & \text{for } t \geqq 0, \end{cases} \tag{4}$$

if m is an unoccupied state (m runs from A+1 to infinity). Here ε_i and ε_m are the quasi-particle energies and ε_0 is the Fermi energy. If we substitute eqs. (3) and (4) in eq. (2), we can take the Fourier transform of the equation to get

$$\begin{aligned} \mathcal{G}(\alpha, \beta; \gamma, \delta; E) = {} & [(1-n_\alpha)n_\beta - (1-n_\beta)n_\alpha](\varepsilon_\alpha - \varepsilon_\beta - E)^{-1} \\ & \times [\delta_{\alpha\gamma}\delta_{\beta\delta} - \sum_\eta \sum_\theta \Gamma(\alpha, \beta; \eta, \theta; E)\mathcal{G}(\eta, \theta; \gamma, \delta; E)], \end{aligned} \tag{5}$$

where we have written a script $\mathcal{G}$ to denote the Fourier transform of

$$G(\alpha, \beta; \gamma, \delta; t) - S_{\alpha\beta}(0)S_{\delta\gamma}(0),$$

which is, when expanded in terms of the eigenstates $|\Psi_n\rangle$ of the Hamiltonian with eigenvalues E_n,

$$\begin{aligned} \mathcal{G}(\alpha, \beta; \gamma, \delta; E) = {} & \sum_{n \neq 0} \langle \Psi_0 | a_\beta^\dagger a_\alpha | \Psi_n \rangle (E_n - E_0 - E)^{-1} \langle \Psi_n | a_\gamma^\dagger a_\delta | \Psi_0 \rangle \\ & + \sum_{n \neq 0} \langle \Psi_0 | a_\gamma^\dagger a_\delta | \Psi_n \rangle (E_n - E_0 + E)^{-1} \langle \Psi_n | a_\beta^\dagger a_\alpha | \Psi_0 \rangle. \end{aligned} \tag{6}$$

We have written n_α for the function which is unity if α is between one and A and is zero otherwise; n_α is just the unperturbed occupation number of the level α. The Γ which we have written as a function of E is just the Fourier transform of the irreducible vertex part we wrote before.

To first order in perturbation theory, the irreducible vertex part is given by a matrix element of the potential; only graphs of the type shown in figs. 2(a), (b), (c) and (d) contribute. In general, more complicated graphs should be taken into account, such as the one shown in fig. 2(e), and this will certainly be necessary if there is a hard core in the nucleon-nucleon potential. We must therefore understand by the potential some sort of effective potential, such as

has been discussed by Skyrme [13]), but we shall write our approximation to the vertex part just as a single matrix element of the potential, which does not

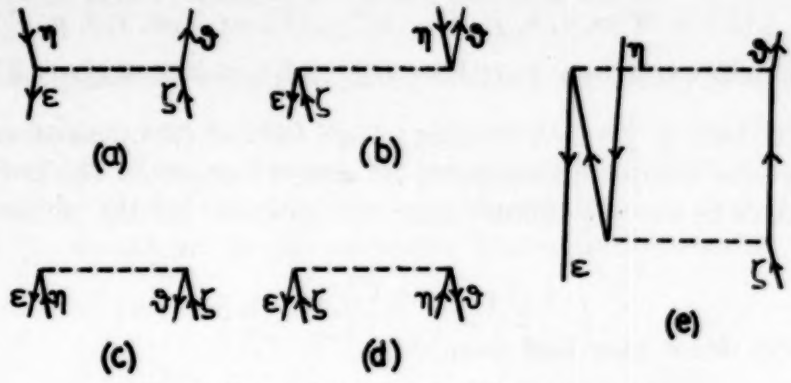

Fig. 2. Some simple irreducible vertex parts.

depend on E. Our approximation is then

$$\Gamma(\varepsilon, \zeta; \eta, \theta; E) = V_{\varepsilon\theta, \zeta\eta} - V_{\varepsilon\theta, \eta\zeta}. \tag{7}$$

To the same approximation, we should take the single-particle levels to be solutions of the Hartree-Fock equations, so that we have

$$T_{\alpha\beta} + \sum_{i=1}^{A} (V_{\alpha i, \beta i} - V_{\alpha i, i\beta}) = \varepsilon_\alpha \delta_{\alpha\beta}, \tag{8}$$

where $T_{\alpha\beta}$ is the matrix element of the kinetic energy.

Eq. (5) only has a non-zero solution if α is an occupied level and β is unoccupied, or vice versa, since the first factor on the right hand side vanishes otherwise. We can consider $\mathcal{G}$ as a matrix (Hermitian by its definition) in the space of particle-hole and hole-particle states. We call the combination α, β which occurs in eq. (5) a particle-hole state if α is an unoccupied level and β is occupied in the independent-particle ground state, and call it a hole-particle state if α is occupied and β is unoccupied. We use the letters i, j, k, l to denote occupied levels, and m, n, p, q to denote unoccupied levels. If we multiply eq. (5) by $(\varepsilon_\alpha - \varepsilon_\beta - E)$, and substitute eq. (7) for Γ, it becomes a matrix equation which we write in block form as

$$\begin{pmatrix} A-EI & B \\ B^* & A^*+EI \end{pmatrix} \begin{pmatrix} G^{(1)}(E) & G^{(2)}(E) \\ G^{(3)}(E) & G^{(4)}(E) \end{pmatrix} = \begin{pmatrix} I & 0 \\ 0 & I \end{pmatrix}, \tag{9}$$

where A is the matrix whose elements are

$$A_{mi, nj} = (\varepsilon_m - \varepsilon_i)\delta_{ij}\delta_{mn} + V_{mj, in} - V_{mj, ni}, \tag{10}$$

B is the matrix whose elements are

$$B_{mi, nj} = V_{mn, ij} - V_{mn, ji}, \tag{11}$$

I is the unit matrix, and the matrixes $G^{(1)}$, $G^{(2)}$, $G^{(3)}$ and $G^{(4)}$ have elements which are equal to matrix elements of the Green's function, defined by

$$\begin{aligned} G^{(1)}_{mi,nj}(E) &= \mathcal{G}(m, i; n, j; E), \quad G^{(2)}_{mi,nj}(E) = \mathcal{G}(m, i; j, n; E), \\ G^{(3)}_{mi,nj}(E) &= \mathcal{G}(i, m; n, j; E), \quad G^{(4)}_{mi,nj}(E) = \mathcal{G}(i, m; j, n; E). \end{aligned} \tag{12}$$

It can be seen that eq. (9) is equivalent to eqs. (5) and (7) by direct comparison. The fact that the complex conjugates B^* and A^* occur on the bottom row of the first matrix in eq. (9) follows from the property of the potential matrix elements

$$V_{\alpha\beta,\gamma\delta} = V^*_{\gamma\delta,\alpha\beta}.$$

It also follows from this and from

$$V_{\alpha\beta,\gamma\delta} = V_{\beta\alpha,\delta\gamma}$$

that A is a Hermitian matrix and B is a symmetric matrix.

It can be seen from eq. (6) that the Green's function has poles at plus and minus the excitation energies of the system. The poles of the matrix defined by the inhomogeneous linear eq. (9) occur where the corresponding homogeneous equation has solutions. Therefore the energies of the excited states, measured from the ground state energy, are given in our approximation by solutions of the equation

$$\begin{pmatrix} A & B \\ B^* & A^* \end{pmatrix} \begin{pmatrix} X_n \\ Y_n \end{pmatrix} = E_n \begin{pmatrix} X_n \\ -Y_n \end{pmatrix}, \tag{13}$$

where X_n and Y_n are column vectors. These energy levels are given by the eigenvalues of the non-Hermitian matrix

$$\begin{pmatrix} A & B \\ -B^* & -A^* \end{pmatrix}.$$

Negative eigenvalues occur at the same magnitudes of E_n as positive eigenvalues since, from the complex conjugate of eq. (13), we have also

$$\begin{pmatrix} A & B \\ B^* & A^* \end{pmatrix} \begin{pmatrix} Y_n^* \\ X_n^* \end{pmatrix} = -E_n^* \begin{pmatrix} Y_n^* \\ -X_n^* \end{pmatrix}. \tag{14}$$

In the shell model calculations of Elliott and Flowers [5]), the energy levels are given simply by the eigenvalues of the matrix A, and so only the graphs shown in figs. 2(a) and (b) are allowed for. When we also allow for the graphs shown in figs. 2(c) and (d), which represent the matrix B, we take into account some of the correlations in the ground state. This is only important if there is a large shift of an energy level from its unperturbed value. The effects of these additional graphs are to lower the energy levels calculated, to reduce matrix elements of operators between the ground state and those levels which are

raised in energy by the interaction, and to increase matrix elements of operators between the ground state and those levels which are lowered in energy by the interaction. This is discussed in more detail in BET.

3. Comparison with the Hartree-Fock Stability Condition

In (I) a condition was derived for the solution of the Hartree-Fock equations chosen as the basis of our representation to be that determinant which minimizes the expectation value of the Hamiltonian. The condition is that eigenvalues of eq. (17) of (I) should all be non-negative. This equation can be written as

$$\begin{pmatrix} A & B \\ B^* & A^* \end{pmatrix} \begin{pmatrix} X \\ X^* \end{pmatrix} = \lambda \begin{pmatrix} X \\ X^* \end{pmatrix}, \tag{15}$$

where A and B are defined by eqs. (10) and (11), and X is a column-vector whose elements are the numbers C_{mi}. We can construct a solution of eq. (15) from any eigenvector of the matrix, since the complex conjugate of the equation

$$\begin{pmatrix} A & B \\ B^* & A^* \end{pmatrix} \begin{pmatrix} X \\ Y \end{pmatrix} = \lambda \begin{pmatrix} X \\ Y \end{pmatrix} \tag{16}$$

is

$$\begin{pmatrix} A & B \\ B^* & A^* \end{pmatrix} \begin{pmatrix} Y^* \\ X^* \end{pmatrix} = \lambda^* \begin{pmatrix} Y^* \\ X^* \end{pmatrix}. \tag{17}$$

Since, as we observed earlier, A is Hermitian and B is symmetric, it follows that this matrix is Hermitian and so λ is real. Therefore the two vectors

$$\begin{pmatrix} X + Y^* \\ X^* + Y \end{pmatrix} \quad \text{and} \quad \begin{pmatrix} iX - iY^* \\ -iX^* + iY \end{pmatrix}$$

are eigenvectors of the form required for eq. (15), and they cannot both be zero.

There must always be at least one independent-particle representation for which this condition is satisfied, since the determinantal wave function which gives the lowest possible expectation value of the Hamiltonian must satisfy the condition. We can therefore always suppose that we have chosen a representation in which the condition is satisfied; if it is not, we must choose another solution of the Hartree-Fock equations as our approximation to the ground state. It can now easily be shown that all the solutions of eq. (13) give real values of the excitation energies. Since a complex eigenvalue represents an unstable collective mode, this means there always exists an approximate ground state wave function from which all collective modes are stable.

We prove this by multiplying eq. (13) on the left by the row-vector $(X_n^\dagger \; Y_n^\dagger)$, where the dagger denotes a Hermitian conjugate. This gives

$$(X_n^\dagger \; Y_n^\dagger) \begin{pmatrix} A & B \\ B^* & A^* \end{pmatrix} \begin{pmatrix} X_n \\ Y_n \end{pmatrix} = E_n (X_n^\dagger X_n - Y_n^\dagger Y_n). \tag{18}$$

The left hand side of this is an expectation value of a Hermitian matrix which has no eigenvalues less than zero, and so it is a real non-negative number. The quantity in brackets on the right hand side is real, and so, if E_n is complex, the quantity in brackets must be zero. Since the expectation value of a Hermitian matrix can only attain its minimum value for an eigenvector, this implies that the vector is an eigenvector with eigenvalue zero. If this is so, eq. (13) shows that E_n must also be zero, so we have shown that E_n cannot be complex.

It also follows that $(X_n^\dagger X_n - Y_n^\dagger Y_n)$ has the same sign as E_n, and can only be zero if E_n is zero.

4. "Phase Transitions"

Suppose that we have a certain system of interacting particles and continuously vary some parameter, such as the strength of the interaction. It may happen that, as the parameter passes through a certain value, the ground state wave function changes suddenly. We could call such an event a first order phase transition, in analogy with thermodynamics. If only the rate of change of the wave function changes suddenly, we would call it a second order phase transition. Physically, the only parameters which vary are the numbers of protons and neutrons, and these take on discrete values. However, a change in the nature of the ground state may be so rapid that it is evidence of such a phase change. This appears to be the case in the region in which nuclei change from spherical shape to spheroidal shape, although it is not possible rigorously to deduce the order of the phase transition from the experimental evidence.

The occurrence of such a phase transition will be of great importance in any theory of nuclear structure which starts from an independent-particle model. For example, it would not be possible to use ordinary perturbation theory to calculate the properties of a spheroidal nucleus starting from an independent-particle model with spherical symmetry. The independent-particle model gives a very simple picture of a first order phase transition. There may be two distinct solutions of the Hartree-Fock equations which give roughly the same energy, so that one is energetically more favourable in one region of values of the parameter, and the other is more favourable in another region. A second order transition may occur if a solution of the Hartree-Fock equations, which gives a minimum for the expectation value of the Hamiltonian for some values of the parameter, gives only a saddle point for other values of the parameter. As in the thermodynamic analogy, a second order phase transition is most likely to occur when there is some change of symmetry.

We now examine in more detail what happens in the transition from the region of spherical nuclei to the region of non-spherical nuclei. If the stable solution of the Hartree-Fock equations has spherical symmetry, the matrices A and B which occur in eq. (13) are invariant under rotation of the system, and

so the solutions of eq. (13) are eigenstates of angular momentum. As the number of particles outside closed shells is increased, the energies of some of these solutions (vibrational modes) will be reduced, as is shown in BET, and may pass through zero, so that the mode becomes unstable. If the spherical solution remains the best solution right up to the point at which the mode becomes unstable, a second order phase transition must occur. If some non-spherical solution has lower energy before the spherical solution becomes unstable against small distortion, a first order phase transition occurs.

In fact it is a mode of even parity, the quadrupole vibration, which is responsible for the phase transition. If we expand the expectation value of the Hamiltonian about the spherical solution, using the coefficients C_{mi} introduced in (I), angular momentum conservation forces the first order term to vanish, but there is no reason for the third order term to vanish. Unless the third order term vanishes, a phase transition must occur before the second order term vanishes, and so the transition must be first order. If an odd-parity mode became unstable, parity conservation would force all odd terms in the expansion to vanish, and a second order phase transition could occur.

5. Formal Properties of the Solutions

5.1. ORTHOGONALITY AND NORMALIZATION

We can take the Hermitian conjugate of eq. (13) to get

$$(X_n^\dagger \; Y_n^\dagger)\begin{pmatrix} A & B \\ B^* & A^* \end{pmatrix} = E_n(X_n^\dagger \; -Y_n^\dagger), \tag{19}$$

since the stability condition ensures that E_n is real. If we have two solutions of eq. (13), with eigenvalues E_m and E_n, we get

$$\begin{aligned}(X_m^\dagger \, Y_m^\dagger)\begin{pmatrix} A & B \\ B^* & A^* \end{pmatrix}\begin{pmatrix} X_n \\ Y_n \end{pmatrix} &= E_m(X_m^\dagger X_n - Y_m^\dagger Y_n) \\ &= E_n(X_m^\dagger X_n - Y_m^\dagger Y_n),\end{aligned} \tag{20}$$

by using eqs. (19) and (13) successively. Thus, if E_m and E_n are different, we have

$$(X_m^\dagger \; -Y_m^\dagger)\begin{pmatrix} X_n \\ Y_n \end{pmatrix} = 0 \tag{21}$$

as the condition on two eigenvectors with different eigenvalues. If we were to introduce an indefinite metric, this could be regarded as the scalar product of the two eigenvectors, so we call vectors which satisfy eq. (21) "orthogonal".

The use of this indefinite metric suggests that we should normalize eigenvectors with non-zero eigenvalue by the relation

$$(X_n^\dagger \; -Y_n^\dagger)\begin{pmatrix} X_n \\ Y_n \end{pmatrix} = \pm 1. \tag{22}$$

Eq. (18) shows that the sign is positive if the eigenvalue is positive and negative if the eigenvalue is negative. Eigenvectors with eigenvalue zero may be orthogonal to themselves, and cannot be normalized in this way.

5.2. COMPLETENESS

If the matrix

$$\begin{pmatrix} A & B \\ B^* & A^* \end{pmatrix}$$

has all its eigenvalues greater than zero, we can construct a proof of the completeness of the set of solutions of eq. (13) along the lines of the proof of the completeness of the eigenvectors of an Hermitian matrix. If one of the eigenvalues of the matrix is zero, the solutions of eq. (13) do not generally form a complete set. For example, if the matrix is a 2×2 matrix there is only one eigenvector, since the equation

$$\begin{pmatrix} 1 & 1 \\ 1 & 1 \end{pmatrix} \begin{pmatrix} x \\ y \end{pmatrix} = E \begin{pmatrix} x \\ -y \end{pmatrix} \tag{23}$$

has only the solution $E = 0$, $x = -y$.

We suppose that A and B are $\nu\times\nu$ matrices, and that we know $2\nu-r$ orthogonal normalized eigenvectors of eq. (13) with non-zero eigenvalue which we call

$$\begin{pmatrix} X_{r+1} \\ Y_{r+1} \end{pmatrix}, \begin{pmatrix} X_{r+2} \\ Y_{r+2} \end{pmatrix}, \ldots, \begin{pmatrix} X_{2\nu} \\ Y_{2\nu} \end{pmatrix}.$$

We can construct a set of r mutually independent vectors

$$\begin{pmatrix} P_1 \\ Q_1 \end{pmatrix}, \begin{pmatrix} P_2 \\ Q_2 \end{pmatrix}, \ldots, \begin{pmatrix} P_r \\ Q_r \end{pmatrix},$$

which are orthogonal to all these known eigenvectors. This set must also be independent of the original set, since a linear combination of the eigenvectors can only be orthogonal to all these eigenvectors if one of the eigenvectors is orthogonal to itself. This cannot occur unless one of the eigenvalues is zero.

Since, from eq. (17) and the orthogonality condition, we have

$$\begin{aligned} (X_n^\dagger\, Y_n^\dagger) \begin{pmatrix} A & B \\ B^* & A^* \end{pmatrix} \begin{pmatrix} P_l \\ Q_l \end{pmatrix} &= E_n (X_n^\dagger - Y_n^\dagger) \begin{pmatrix} P_l \\ Q_l \end{pmatrix}, \\ &= 0, \end{aligned} \tag{24}$$

we can write

$$\begin{pmatrix} A & B \\ B^* & A^* \end{pmatrix} \begin{pmatrix} P_l \\ Q_l \end{pmatrix} = \sum_{m=1}^{r} \alpha_m{}^l \begin{pmatrix} P_m \\ -Q_m \end{pmatrix}. \tag{25}$$

We have used the fact that the r vectors we have constructed form a complete set in the subspace orthogonal to the $2\nu-r$ known eigenvectors. The condition

for a certain linear combination (which must be independent of all the known eigenvectors) to be another eigenvector is

$$\begin{pmatrix} A & B \\ B^* & A^* \end{pmatrix} \sum_i \beta_i \begin{pmatrix} P_i \\ Q_i \end{pmatrix} = E \sum_i \beta_i \begin{pmatrix} P_i \\ -Q_i \end{pmatrix},$$

and so

$$\sum_{i=1}^{r} \sum_{m=1}^{r} \beta_i \alpha_m{}^i = E \sum_{i=1}^{r} \beta_i. \tag{26}$$

This equation must have at least one eigenvalue, so, if none of the eigenvalues is zero, we can repeat this process until the whole space is exhausted. If there is no zero-energy solution of eq. (13), the set of solutions is therefore complete, but our proof breaks down if there are zero-energy solutions, since the eigenvector may then be orthogonal to itself. The set of solutions will generally be one short of completeness for each zero-energy solution. As we show later in this paper, the case in which there is a single zero-energy eigenvalue arises frequently in nuclear physics.

5.3. A VARIATIONAL PRINCIPLE

If there is no zero-energy solution of eq. (13), we can use the completeness proved in the last paragraph to establish an upper bound for the magnitude of the lowest eigenvalue of the equation. We can expand an arbitrary vector as a sum of eigenvectors,

$$\begin{pmatrix} X \\ Y \end{pmatrix} = \sum_n \alpha_n \begin{pmatrix} X_n \\ Y_n \end{pmatrix}, \tag{27}$$

so that we have

$$\begin{aligned} (X^\dagger\ Y^\dagger) \begin{pmatrix} A & B \\ B^* & A^* \end{pmatrix} \begin{pmatrix} X \\ Y \end{pmatrix} &= \sum_n |\alpha_n|^2 E_n (X_n{}^\dagger\ Y_n{}^\dagger) \begin{pmatrix} X_n \\ -Y_n \end{pmatrix} \\ &= \sum_n |\alpha_n|^2 |E_n| \geqq |E_{\min}| \sum_n |\alpha_n|^2, \end{aligned} \tag{28}$$

$$\left| (X^\dagger\ -Y^\dagger) \begin{pmatrix} X \\ Y \end{pmatrix} \right| = |\sum_n (\pm |\alpha_n|^2)| \leqq \sum_n |\alpha_n|^2,$$

where we have used the orthogonality and normalization of the eigenvectors. We therefore have the inequality

$$(X^\dagger\ Y^\dagger) \begin{pmatrix} A & B \\ B^* & A^* \end{pmatrix} \begin{pmatrix} X \\ Y \end{pmatrix} \Big/ \left| (X^\dagger\ -Y^\dagger) \begin{pmatrix} X \\ Y \end{pmatrix} \right| \geqq |E_{\min}|, \tag{29}$$

where $E_{\min}$ is the lowest eigenvalue. This is a variational principle which might be very useful for calculating low-lying eigenvalues of eq. (13).

5.4. EVALUATION OF MATRIX ELEMENTS

The Green's function defined by eq. (6) depends on the matrix element of single-particle operators between the ground state and excited states. The

residues of the Green's function at a pole determine the values of such matrix elements apart from a phase factor. If an operator has the form

$$\mathscr{M} = \sum_{\alpha}\sum_{\beta} M_{\alpha\beta} a_{\alpha}^{\dagger} a_{\beta}, \tag{30}$$

the square of its matrix elements between the ground state and a non-degenerate state Ψ_n with energy E_n (if Ψ_n is degenerate, we will get the sum of squares of the matrix elements to all states of energy E_n) is, from eqs. (6) and (30),

$$|\langle\Psi_0|\mathscr{M}|\Psi_n\rangle|^2 = \lim_{E\to E_n-E_0} (E_n-E_0-E)\sum_{\alpha}\sum_{\beta}\sum_{\gamma}\sum_{\delta} M_{\beta\alpha}\mathscr{G}(\alpha,\beta;\gamma,\delta;E)M_{\gamma\delta}. \tag{31}$$

We can use our approximate eq. (9) to calculate the Green's function. If there is a complete set of solutions of eq. (13), we can use it to solve eq. (9), and we get the solution

$$\begin{pmatrix} G^{(1)}(E) & G^{(2)}(E) \\ G^{(3)}(E) & G^{(4)}(E) \end{pmatrix} = \begin{pmatrix} \pm X_1 & \pm X_2 \dots \pm X_{2\nu} \\ \pm Y_1 & \pm Y_2 \dots \pm Y_{2\nu} \end{pmatrix} \begin{pmatrix} (E_1-E)^{-1}X_1^{\dagger} & (E_1-E)^{-1}Y_1^{\dagger} \\ (E_2-E)^{-1}X_2^{\dagger} & (E_2-E)^{-1}Y_2^{\dagger} \\ \cdot & \cdot \\ \cdot & \cdot \\ \cdot & \cdot \\ (E_{2\nu}-E)^{-1}X_{2\nu}^{\dagger} & (E_{2\nu}-E)^{-1}Y_{2\nu}^{\dagger} \end{pmatrix}, \tag{32}$$

where the signs of the terms in the first matrix on the right hand side of the equation are the signs of the eigenvalues. Substitution of eq. (32) in eq. (9), with use of eqs. (13), (21) and (22), shows that this expression is correct. The residue at $E = E_n$ is just

$$-\begin{pmatrix} X_n \\ Y_n \end{pmatrix} (X_n^{\dagger}\ Y_n^{\dagger}),$$

and so the matrix element is, apart from an arbitrary phase factor,

$$\langle\Psi_0|\mathscr{M}|\Psi_n\rangle = (M_1^{\dagger}\ M_2^{\dagger}) \begin{pmatrix} X_n \\ Y_n \end{pmatrix}, \tag{33}$$

where we have written $M_1^{\dagger}$ for the row vector whose elements are the elements of $\mathscr{M}$ which destroy a particle and a hole, and $M_2^{\dagger}$ for those elements which create a particle and a hole. If $\mathscr{M}$ is Hermitian, then $M_2 = M_1^*$. If the set of solutions is not complete, this relation remains true except for the zero-energy solutions. We can therefore regard an eigenvector of eq. (13) as a representation of the wave function of the excited state.

5.5. SUM RULES

It often happens that the double commutator of the Hamiltonian with some Hermitian operator has a simple form. For example, if the Hamiltonian con-

tains no spin-exchange terms, the double commutator of the Hamiltonian with the electric dipole operator (equal to the sum over all proton coordinates z_i of $ez_i - e\bar{z}$, where $\bar{z}$ is the z-component of the centre of mass) is just $e^2\hbar^2 ZN/MA$, where Z is the number of protons, N is the number of neutrons, A is the mass number, and M is the mass of a nucleon. If the operator is a component of the centre of mass operator, the double commutator is just $\hbar^2/MA$. With more complicated operators, such as quadrupole and octupole operators, the double commutator is not just a number, but is a simple operator. We can use this fact to construct energy-weighted sum rules which have the form

$$2\sum_n |\langle\Psi_0|\mathcal{M}|\Psi_n\rangle|^2(E_n - E_0) = \langle\Psi_0|[\mathcal{M}, [H, \mathcal{M}]]|\Psi_0\rangle. \tag{34}$$

If the double commutator is a number, the right hand side is known exactly. If it is an operator, it may be possible to make a good estimate of the right hand side. The failure of the dipole sum rule has been used by Levinger and Bethe to estimate the amount of charge-exchange force between nucleons [14]). These energy weighted sum rules have been discussed in general by Austern and Sachs [15]).

(32) We now prove an important theorem, which is the following: if we evaluate the left hand side of eq. (34) by using the solutions of eq. (13), together with eq. (33), we get the same result as if we evaluate the right hand side using the self-consistent independent-particle wave function for Ψ_0. In particular, this implies that, if the double commutator is a number, the solutions of eq. (13) satisfy the energy weighted sum rule exactly.

We can use eq. (14) to write the sum on the left hand side of eq. (34) as a sum over both positive and negative energy solutions of eq. (13). We get

$$\begin{aligned} &2\sum_{n=1}^{\nu} |\langle\Psi_0|\mathcal{M}|\Psi_n\rangle|^2(E_n - E_0) \\ &\quad = 2\sum_{n=1}^{\nu} \left| (M^\dagger \; \tilde{M}) \begin{pmatrix} X_n \\ Y_n \end{pmatrix} \right|^2 E_n = \sum_{n=1}^{2\nu} \left| (M^\dagger \; -\tilde{M}) \begin{pmatrix} X_n \\ -Y_n \end{pmatrix} \right|^2 |E_n| \qquad (35) \\ &\quad = \Big\{ \sum_{n=1}^{\nu} - \sum_{n=\nu+1}^{2\nu} \Big\} (M^\dagger \; -\tilde{M}) \begin{pmatrix} A & B \\ B^* & A^* \end{pmatrix} \begin{pmatrix} X_n \\ Y_n \end{pmatrix} (X_n^\dagger \; -Y_n^\dagger) \begin{pmatrix} M \\ -M^* \end{pmatrix}, \end{aligned}$$

where we have numbered the positive energy solutions from 1 to ν, and the negative energy solutions from $\nu+1$ to 2ν. We have written $\tilde{M}$ for the transpose of M. If our set of solutions of eq. (13) is complete, the sum over n just gives the unit matrix, so that we have

$$2\sum_{n=1}^{\nu} |\langle\Psi_0|\mathcal{M}|\Psi_n\rangle|^2(E_n - E_0) = (M^\dagger \; -\tilde{M}) \begin{pmatrix} A & B \\ B^* & A^* \end{pmatrix} \begin{pmatrix} M \\ -M^* \end{pmatrix}. \tag{36}$$

We can evaluate the right hand side of eq. (34) directly, using the solution of the Hartree-Fock equations $|\Phi_0\rangle$ as an approximation to $|\Psi_0\rangle$. The expression

is simplified by the fact that $H|\Phi_0\rangle$ is orthogonal to all one-particle, one-hole states, which is the condition for $|\Phi_0\rangle$ to satisfy the Hartree-Fock equations. Using eq. (10) of (I) for the Hamiltonian, and eq. (13) of (I) for the single-particle energies, we get

$$\begin{aligned}
&\tfrac{1}{2}\langle\Phi_0|[\mathscr{M},[H,\mathscr{M}]]|\Phi_0\rangle \\
&\quad=\sum_m\sum_i[T_{mm}-T_{ii}+\sum_j(V_{mj,mj}-V_{mj,jm}-V_{ij,ij}+V_{ij,ji})-V_{mi,mi}+V_{mi,im}]|M_{mi}|^2 \\
&\quad+\sum_m\sum_i\sum_{j\neq i}[-T_{ji}-\sum_k(V_{jk,ik}-V_{jk,ki})-V_{jm,im}+V_{jm,mi}]M^*_{mi}M_{mj} \\
&\quad+\sum_i\sum_m\sum_{n\neq m}[T_{mn}+\sum_k(V_{mk,nk}-V_{mk,kn})-V_{mi,ni}+V_{mi,in}]M^*_{mi}M_{ni} \\
&\quad+\sum_i\sum_{j\neq i}\sum_m\sum_{n\neq m}[(V_{mj,in}-V_{mj,nj})M^*_{mi}M_{nj}-\tfrac{1}{2}(V_{mn,ij}-V_{mn,ji})M^*_{mi}M^*_{nj} \\
&\quad-\tfrac{1}{2}(V_{ij,mn}-V_{ij,nm})M_{mi}M_{nj}] \qquad (37)\\
&\quad=\sum_i\sum_j\sum_m\sum_n\{[(\varepsilon_m-\varepsilon_i)\delta_{ij}\delta_{mn}+V_{mj,in}-V_{mj,ni}]M^*_{mi}M_{nj} \\
&\quad-\tfrac{1}{2}(V_{mn,ij}-V_{mn,ji})M^*_{mi}M^*_{nj}-\tfrac{1}{2}(V_{ij,mn}-V_{ij,nm})M_{mi}M_{nj}\} \\
&\quad=\tfrac{1}{2}(M^\dagger\ -\tilde{M})\begin{pmatrix}A & B\\ B^* & A^*\end{pmatrix}\begin{pmatrix}M\\ -M^*\end{pmatrix},
\end{aligned}$$

so the proof of this theorem is complete. In eq. (37), we have used the letters i, j and k to denote occupied states and m and n to denote unoccupied states.

It must be emphasized that this is the only result we have obtained which exploits the condition that our trial wave function should be a solution of the Hartree-Fock equations. Our other results have all followed from an inequality which may be satisfied even if the Hartree-Fock equations are not satisfied.

6. Spurious States

As we remarked in the introduction, the use of an independent-particle wave function to approximate the ground state wave function usually involves the neglect of some symmetry. The only exception is when a determinant of plane waves is used as an approximation for the ground state of an infinite system. If some operator, which commutes with the Hamiltonian, (for example, the total momentum) does not have a definite value in the trial ground state, there is necessarily some arbitrariness in our choice of the trial ground state, since we can change the average value of the conjugate variable (in this case the position of the centre of mass) without altering the expectation value of the energy. There is therefore a kind of degeneracy introduced by the neglect of conservation of momentum, since a determinant can be displaced to any point of space without altering its energy. If the self-consistent field is axially symmetric instead of

spherically symmetric, an additional two-fold degeneracy is introduced, since the orientation of the symmetry axis does not affect the energy.

This degeneracy implies that there is no single minimum of the expectation value of the energy, and so eq. (17) of (I) must have eigenvalue zero. This, however, implies that eq. (13) has eigenvalue zero. It is easy to verify that eq. (19) of (I) does give a zero-energy solution by substituting

$$X_{mi} = \int \varphi_m^* (\partial/\partial z)\varphi_i \, d\tau, \quad Y_{mi} = -\int \varphi_i^* (\partial/\partial z)\varphi_m \, d\tau \tag{38}$$

in eq. (13). We have, for example,

$$\begin{aligned}(AX+BY)_{mi} &= (\varepsilon_m-\varepsilon_i)X_{mi}+\sum_j\sum_n (V_{jm,ni}-V_{jm,in})\int \varphi_n^*(\partial\varphi_j/\partial z)d\tau \\ &+\sum_j\sum_n (V_{nm,ji}-V_{nm,ij})\int (\partial\varphi_j^*/\partial z)\varphi_n d\tau \\ &= (\varepsilon_m-\varepsilon_i)X_{mi}+\sum_j (V_{jm,j'i}-V_{jm,ij'}+V_{j'm,ji}-V_{j'm,ij}) \\ &-\sum_j\sum_k [(V_{jm,ki}-V_{jm,ik})\int \varphi_k^*(\partial\varphi_j/\partial z)d\tau+(V_{km,ji}-V_{km,ij})\int (\partial\varphi_j^*/\partial z)\varphi_k d\tau],\end{aligned} \tag{39}$$

where j' is a suffix denoting that the matrix element is taken with respect to the state $\partial\varphi_j/\partial z$. We have used our convention that i, j and k refer to occupied states, while m and n are unoccupied, and have used closure to get this result. The last sum on the right of eq. (39) is identically zero, and translation invariance implies

$$V_{j'm,ji}+V_{jm',ji}+V_{jm,j'i}+V_{jm,ji'} = 0, \tag{40}$$

so that the second sum gives minus the sum of the matrix elements of the Hartree-Fock potential evaluated between $\partial\varphi_m^*/\partial z$ and φ_i, and between φ_m^* and $\partial\varphi_i/\partial z$. This cancels with the potential energy contribution to the first term on the right, which can be evaluated from eq. (13) of (I), and the kinetic energy term just gives a matrix element of the commutator of the kinetic energy operator with $\partial/\partial z$, but this commutator vanishes. The proof that eq. (20) of (I) also provides a zero-energy solution is very similar.

These results follow from the theorem which was proved about energy-weighted sum rules in the last section. If $\mathscr{M}$ is a component either of the linear momentum operator or of the angular momentum operator, the right hand side of eq. (34) vanishes identically. The left hand side must therefore vanish in our approximation, and so the excitation energies of the states generated by these operators acting on the ground state must be zero.

This zero-energy state is the spurious state of the shell-model, which represents simply an oscillation of the centre of mass. In a harmonic oscillator potential this spurious level, which has unit angular momentum and odd parity, is at a definite level, but generally it is mixed in with all the levels [6]). We have

shown that by taking account of interactions in a consistent way we can separate this level out. The spurious level which arises in axially symmetric nuclei has projection of angular momentum along the symmetry axis ± 1 and even parity, and it represents a vibration of the symmetry axis about its assumed direction. A similar result has been obtained by Anderson in the theory of superconductivity, since he found a spurious level at zero energy by using the random phase approximation for a system with an indefinite number of particles [16]).

Although we have discovered five spurious zero-energy states in spheroidal nuclei, and there is a sixth if pairing is taken into account, these all differ from one another, since no two of them have the same projection of angular momentum and parity. Since eq. (13) separates, and its solutions have definite projection of angular momentum parity if the self-consistent field is axially symmetric, we should consider what happens to its solutions when there is a single zero-energy solution.

It is obvious that there cannot be a complete set of solutions in this case, since to every solution with positive energy there corresponds a solution with negative energy. A complete set of solutions would have to consist of an even number of vectors, so the solution corresponding to the zero-energy solution would have to be another zero-energy solution. There could only be this second zero-energy solution if there were an additional degeneracy in the solutions of the Hartree-Fock equations, but there is no reason to expect such an additional degeneracy. There must therefore be vectors which are independent of all the eigenvectors.

If the scalar product of a row-vector $(X^\dagger \; -Y^\dagger)$ with all the eigenvectors with nonzero eigenvalue is zero, so is the scalar product of $(\tilde{Y} \; -\tilde{X})$, because of the relation between positive and negative energy solutions shown in eqs. (13) and (14). We can therefore take the two vectors orthogonal to all these eigenvectors to be

$$\begin{pmatrix} L \\ -L^* \end{pmatrix} \quad \text{and} \quad \begin{pmatrix} \Phi \\ \Phi^* \end{pmatrix}.$$

The first of these we take to be the eigenvector with zero eigenvalue, and the second must be a solution of the equation

$$\begin{pmatrix} A & B \\ B^* & A^* \end{pmatrix} \begin{pmatrix} \Phi \\ \Phi^* \end{pmatrix} = \omega \begin{pmatrix} L \\ L^* \end{pmatrix}, \tag{41}$$

as can be seen by expanding the left hand side in terms of the complete set of vectors

$$\begin{pmatrix} L \\ L^* \end{pmatrix}, \; \begin{pmatrix} \Phi \\ -\Phi^* \end{pmatrix}, \; \begin{pmatrix} X_1 \\ -Y_1 \end{pmatrix}, \; \begin{pmatrix} X_2 \\ -Y_2 \end{pmatrix}, \ldots, \begin{pmatrix} X_{2\nu-2} \\ -Y_{2\nu-2} \end{pmatrix}.$$

Since, for the even-parity (rotational) case, the components of L are just matrix elements of the angular momentum operator J_x, eq. (41) is identical

with eq. (23) of (I). There is therefore a close connection between this additional vector which is independent of all the eigenvectors and the rotational motion of the nucleus. Comparing eq. (41) with eqs. (23) and (24) of (I), we find that the moment of inertia is

$$\mathcal{I} = \omega^{-1}(L^{\dagger}\ \tilde{L})\begin{pmatrix}\Phi\\ \Phi^{*}\end{pmatrix}. \tag{42}$$

It must be emphasized that this rotational motion (or the translational motion) is not described by the approximation to the Green's function used in this paper, but is a symptom of the failure of the theory to allow adequately for conservation laws.

I should like to thank Prof. G. E. Brown and Dr. J. A. Evans for many useful discussions of this subject.

References

1) D. Bohm and D. Pines, Phys. Rev. **92** (1953) 609
2) S. Fallieros and R. A. Ferrell, Phys. Rev. **116** (1959) 660;
Ikeda, Kobayasi, Marumori, Shiozaki and Takagi, Progr. Theor. Phys. **22** (1959) 663
3) D. J. Thouless, Nuclear Physics (to be published)
4) Brown, Evans and Thouless, Nuclear Physics (to be published)
5) J. P. Elliott and B. H. Flowers, Proc. Roy. Soc. A **242** (1957) 57
6) J. P. Elliott and T. H. R. Skyrme, Proc. Roy. Soc. A **232** (1955) 561
7) H. J. Lipkin, Ann. of Phys. **9** (1960) 272
8) N. N. Bogoliubov, Dokl. Akad. Nauk SSSR **119** (1958) 244 (translation: Soviet Phys. Doklady **3** (1958) 292)
9) Bardeen, Cooper and Schrieffer, Phys. Rev. **108** (1957) 1175
10) S. T. Belyaev, Mat. Fys. Medd. Dan. Vid. Selsk. **31**, No. 11 (1959)
11) M. Baranger (to be published)
12) L. D. Landau, JETP **35** (1958) 97 (translation: Soviet Phys. JETP **35** (1959) 70)
13) T. H. R. Skyrme, Nuclear Physics **9** (1959) 615
14) J. S. Levinger and H. A. Bethe, Phys. Rev. **78** (1950) 115
15) R. G. Sachs and N. Austern, Phys. Rev. **81** (1951) 705
16) P. W. Anderson, Phys. Rev. **112** (1958) 1900

2.B

Nuclear Physics **22** (1961) 96—100; © *North-Holland Publishing Co., Amsterdam*

Not to be reproduced by photoprint or microfilm without written permission from the publisher

THE $O^{16}(n, \alpha)C^{13}$ REACTION BY THE THIN CRYSTAL METHOD

N. CINDRO, I. ŠLAUS, P. TOMAŠ and B. EMAN

Institute "Ruđer Bošković", Zagreb, Yugoslavia

Received 6 September 1960

Abstract: The angular distribution of the $O^{16}(n, \alpha)C^{13}$ reaction with 14.4 MeV neutrons has been measured by using a thin crystal, whose thickness was enough to stop alpha particles of a given energy. Thus the use of the telescopic arrangement was avoided. The results show a prounounced backward peaking. A theoretical fit using the "heavy particle stripping" formulae has been attempted.

1. Introduction

The study of the reactions (nucleon, alpha) and (alpha, nucleon) on light elements presents a considerable theoretical interest due to the possibility of occurrence of different mechanisms in the process of reaction. These reactions are of special interest in the study of the process known as the heavy particle stripping [1]). It is also of interest to compare the results of these reactions to other direct reaction theories because of the fact that the alpha particle, though a complex system, could, due to its large binding energy, be considered as a unique projectile.

Recently several authors have measured angular distributions and total cross sections for both types of reactions [2]). However, experimental results for (n, α) and (α, n) reaction are still rather scarce. With the present work we have in mind to contribute to the experimental material on (n, α) reactions and to test a simple method for measuring these reactions.

2. Experimental

14.4 MeV neutrons from the 200 keV Cockcroft-Walton generator of the Institute "Ruđer Bošković" was used for the experiment [3]). A mylar target 3.3 mg/cm² thick was placed at a distance of 8 cm from the tritium target on a gold covered aluminium cylinder. The slope of the cylinder determined the angle of measurement.

The detection of the particles was performed by a thin scintillation crystal whose thickness was just enough to stop alpha particles of a given energy [4]). For this purpose a thin CsI(Tl) crystal evaporated on quartz was used. In this way particles with more energy or less specific ionization lost in total less energy in traversing the crystal while particles with less energy were ruled out

by their smaller light output. The difference in light output for alpha particles, deuterons and protons of the same energy was for most cases of practical interest more than compensated by the less specific ionization of the two latter. In this way the use of a telescopic arrangement was avoided, which greatly facilitated and speeded up the experiment. The accuracy of the measurement, however, seems to lag behind the ones performed with a set of $dE/dx-E$ counters.

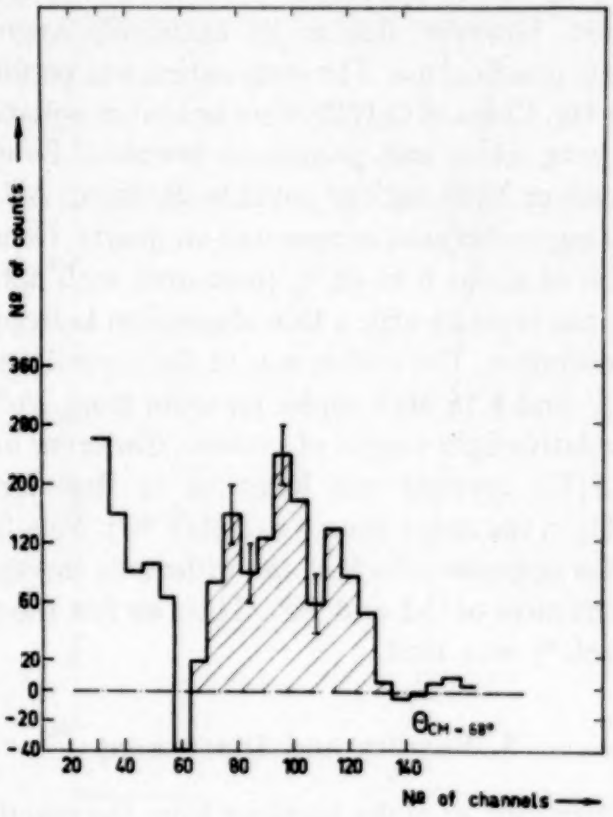

Fig. 1. The spectrum of pulses from particles resulting by neutron bombardment of O^{16} after subtracting the background.

The pulses from an RCA 6342 photomultiplier were fed through a standard equipment to a 256-channel analyzer. A typical spectrum of pulses from particles resulting from neutron bombarding of O^{16} after subtracting the background is shown in fig. 1. The stability of the apparatus was checked before and after each run. The energy resolution of the crystals was from 9 to 12 %, while the total energy resolution of the apparatus amounted to 10 to 17 %. The thickness of CsI(Tl) crystals used was from 15 to 30 mg/cm^2. The monitoring of the neutron beam was performed in two independent ways:

by measuring the number of alpha particles associated to the neutrons in the d+T reaction;

by measuring the neutron flux with an anthracene scintillation counter

placed at a definite distance from the source. A 100-channel Hutchinson type pulse height analyzer was biased in such a way as to cut off always the same part of the neutron spectrum.

The latter system of monitoring gave only relative measurements. In addition, for some measurements a third monitor with a Hornyak type scintillator (NE 451) was used. All the three monitoring systems were usually in agreement within 5 %.

A high vacuum evaporation apparatus [5]) was used to evaporate NaI(Tl) and CsI(Tl). The former, however, due to its extremely hygroscopic character showed to be of little practical use. The evaporation was performed in a vacuum of $2-5\times10^{-5}$ mm/Hg. Chips of CsI(Tl) were heated in a platinum crucible and evaporated on quartz, glass and potassium bromide. Evaporated layers of CsI(Tl) of a thickness up to 50 mg/cm^2 could be obtained. A 7 % resolution was obtained with a 20 mg/cm^2 crystal evaporated on quartz. Generally the crystals showed a resolution of about 9 to 12 % (measured with 5.3 MeV Po^{210} alpha particles). Coating the crystals with a thin aluminium layer apparently did not help to improve resolution. The calibration of the crystal was performed with 5.3 MeV, 6.05 MeV and 8.78 MeV alpha particles from Po^{210} ThC and ThC' respectively. The relative light output of protons, deuterons and alpha particles in evaporated CsI(Tl) crystals was identical to that for monocrystalline CsI(Tl) and NaI(Tl) in the range from 5 to 9 MeV [6,7]). This fact could perhaps be explained by the opposite effect of the difference in vapour pressure and evaporation temperatures of CsI and Tl[5]). Thus we felt the use of calibration curves given by ref. [6]) was lecit.

3. Results and Discussion

The angular distribution of alpha particles from the reaction $O^{16}(n, \alpha)C^{13}$ is shown in fig. 2. The absolute values of differential cross section for this reaction have been measured at the laboratory angles of 30°, 60°, 90°, 120° and 130° with an average angular spread of $\pm10°$. The errors shown in the figure are mainly due to statistics. The absolute values of the differential cross sections have been calculated by measuring the number of associated alpha particles from the d+T reaction and taking into account the centre of mass correction for the cross section of this reaction. However, due to the crudeness of the experimental method, these absolute values should be taken only as indicative. The finite geometry correction, arising from a steeply increasing cross section in the back angle region has been estimated for 90° and found to amount about 4 %. This correction, therefore, has been neglected.

The differential cross sections for the reaction $O^{16}(n, \alpha)C^{13}$ show a pronounced backward rise indicating that an inverse heavy particle stripping process could be responsible for the reaction mechanism. The curve in fig. 2 shows a theoreti-

cal fit based on a heavy particle stripping theory by Owen and Madansky [1,8]) and given by

$$W^2(\theta) \approx G_2^2(K_2)\mathbf{j}_1^2(\mathbf{k}_2 R),$$

where

$$G_2(K_2) = 2(3\pi)^{\frac{1}{2}} \int_0^\infty \mathbf{j}_1(K_2\mathbf{r})\psi(\mathbf{r})\mathbf{r}^2\,\mathrm{d}\mathbf{r},$$

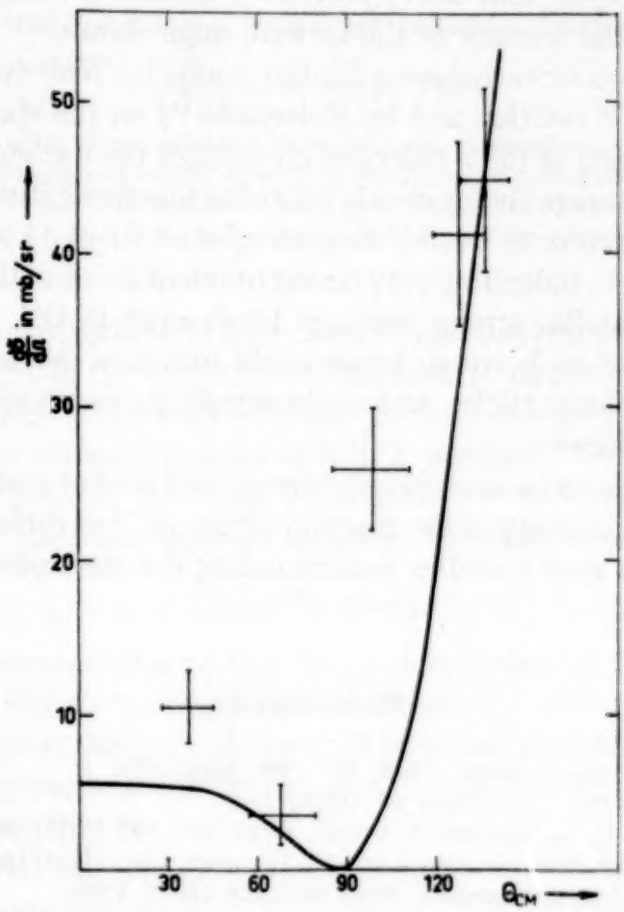

Fig. 2. The angular distribution of alpha particles from the $O^{16}(n, \alpha)C^{13}$ reaction. The curve shows a theoretical fit based on a heavy particle stripping theory.

$\psi(\mathbf{r})$ being the internal wave function of the alpha particle in the heavy nucleus. The square well potential depth of O^{16} taking into account the separation energy of the alpha particle in O^{16}, was calculated to be 47.5 MeV. The parameters were taken as follows:

Radius of the potential of O^{16}	Radius of interaction	Depth of the potential in O^{16}
$R_p = 1.33\,A^{\frac{1}{3}} = 3.4 \times 10^{-13}$ cm	$R = 4.5 \times 10^{-13}$ cm	$V_0 = 47.5$ MeV

Only one value of l, viz. $l = 1$ is allowed by the direct reaction selection rules.

The theoretical curve calculated with the above parameters gives a reasonable good fit to the experimental data above 90°, showing that at these angles of emission an inverse heavy particle stripping process could be predominantly responsible for the mechanism of the reaction. The forward angles region indicates that processes other than the inverse heavy particle stripping contribute to the reaction. A complete analysis of the data, should, therefore, take into account both stripping and heavy particle processes [1]), which was not undertaken in view of the scarcity of the forward angle data.

Our attention has recently been called to results by Whitehead and Foster [9]) on the $O^{16}(p, \alpha)N^{13}$ reaction and by Kobayashi [10]) on the elastic scattering of protons by O^{16}. Both of these reactions go through the nucleus F^{17}, the mirror nucleus of O^{17}, and are probably closely related to the one we study. These authors found striking maxima at bombarding energies of about 11 and 15 MeV with widths $\approx$ 1—2 MeV, indicating very strong resonant levels in the compound F^{17}. It is likely that similar strong resonant levels exist in O^{17}.

The existence of such strong levels could influence markedly the angular distribution of alpha particles, and might invalidate our analysis in terms of a heavy particle process.

These levels seem to be anomalously strong, and are not understood theoretically [11]), so that the study of the reaction $O^{16}(n, \alpha)C^{13}$ at different bombarding energies would be very useful in understanding the mechanism by which this reaction proceeds.

References

1) L. Madansky and G. E. Owen, Phys. Rev. **99** (1955) 1608
2) M. Sakisaka, J. Phys. Soc. Japan **14** (1959) 554;
R. B. Walton, J. D. Clement and F. Borelli, Phys. Rev. **107** (1957) 1065;
I. Kumabe, E. Takekoshi, H. Ogata and V. Tsuneoka, Phys. Rev. **106** (1957) 155;
P. K. Stelson and E. C. Campbell, Phys. Rev. **106** (1957) 1252;
K. Kimura, I. Kumabe, K. Miyake and H. Nugata, J. Phys. Soc. Japan **11** (1956) 1211;
J. Seitz and P. Huber, Helv. Phys. Acta **28** (1955) 227;
A. B. Lillie, Phys. Rev. **87** (1952) 716
3) M. Paić, K. Prelec, P. Tomaš, M. Varćiak and B. Vošicki, Glasnik mat.-fiz. i astr. **12** (1957) 269
4) N. Cindro and N. S. Wall, to be published
5) P. Tomaš, Thesis, University of Zagreb, 1960
6) J. B. Birks, Scintillation counters (Pergamon Press, London, 1954) p. 54
7) R. A. Peck and H. Eubank, Rev. Sci. Instr. **30** (1959) 703
8) G. E. Owen and L. Madansky, Phys. Rev. **105** (1957) 1766
9) A. B. Whitehead and J. S. Foster, Can. J. Phys. **36** (1958) 1276
10) S. Kobayashi, J. Phys. Soc. Japan **15** (1960) 1164
11) G. E. Brown, Proc. Kingston Conf. on Nucl. Structure (1960)

7.B

Nuclear Physics **22** (1961) 101—103; © *North-Holland Publishing Co., Amsterdam*

Not to be reproduced by photoprint or microfilm without written permission from the publisher

"MINIMAL PROPERTY" OF ELECTROMAGNETIC INTERACTION FOR SPIN $\frac{3}{2}$ PARTICLES

A. KOMAR †

Imperial College of Science and Technology, London

Received 29 August 1960

Abstract: The possibility of the extended electromagnetic interaction for spin $\frac{3}{2}$ particles with terms in the Lagrangian depending directly on electromagnetic field tensor $F_{\mu\nu}$ is considered. It is shown that inclusion of such terms leads in all variants to a non-consistent theory, thus making the minimal electromagnetic interaction the only one allowed.

A number of investigations [1]) have been carried out recently on the problem of renormalizability of the vector meson theories. It may be of some interest to see what can be done in this respect for the particles of higher spin. The simplest next choice is the electrodynamics of spin $\frac{3}{2}$ particles.

It is a known fact that the usual formulation of the electromagnetic interaction of spin $\frac{3}{2}$ particles obtained by gauge invariant replacement

$$\partial_\mu \to \partial_\mu - ieA_\mu$$

leads to a nonrenormalizable theory. But it is still possible to introduce direct interaction with the electromagnetic field tensor $F_{\mu\nu}$. One might hope to improve the situation in this way. However, it turns out that this possibility is not realizable. The interaction with the tensor $F_{\mu\nu}$ cannot be introduced consistently into the theory ††.

The set of Fierz-Pauli field equations in the presence of interaction rewritten in spin tensor notations ††† is

$$(\gamma_\mu \partial_\mu + M)\psi_\rho - \tfrac{1}{2}\gamma_\rho \partial_\lambda \psi_\lambda - i\partial_\rho \psi + \tfrac{1}{4} i \gamma_\rho \gamma_\mu \partial_\mu \psi = j_\rho, \tag{1a}$$

$$-i\partial_\lambda \psi_\lambda + 3M\psi - \tfrac{3}{2}\gamma_\lambda \partial_\lambda \psi = j, \tag{1b}$$

where ψ_ρ is a spin-vector and ψ a Dirac spinor; further we have

$$j_\rho = -\left(\frac{\delta \mathscr{L}_{\text{int}}}{\delta \bar{\psi}_\rho} - \tfrac{1}{4}\gamma_\rho \gamma_\lambda \frac{\delta \mathscr{L}_{\text{int}}}{\delta \bar{\psi}_\lambda}\right), \quad j = -\frac{\delta \mathscr{L}_{\text{int}}}{\delta \bar{\psi}}.$$

† On leave of absence from Lebedev Physical Institute, Moscow, USSR.

†† There is brief mention of this fact in the paper by Moldauer and Case (see ref. [2])). No proof is given and their formalism is different from that used in the present note. The author is indebted to S. Kamefuchi for this reference.

††† See for example ref. [3]).

Altogether one has the system of 20 equations for 20 components. As the number of independent physical states is only eight it should be possible to derive 12 subsidiary conditions from this system. In other words one must be able to obtain 12 relations between the components which do not contain time derivatives. Only in this case can one say that interaction is introduced consistently.

The necessary number of combinations without time derivatives can be easily formed from the left-hand sides of the set (1). To this end one should first multiply eq. (1a) by γ_ρ, secondly take derivatives of the eq. (1a) and (1b), thirdly put $\rho = 4$ in eq. (1a) and multiply it by γ_4. Then after some simple manipulations one gets

$$\gamma_\rho \psi_\rho = 0, \tag{2a}$$

$$(M-\gamma_\kappa \partial_\kappa)\gamma_4\psi_4 - \partial_\kappa \psi_\kappa + i\gamma_\kappa \partial_\kappa \psi - \tfrac{3}{2}iM\psi = \gamma_4 j_4 - \tfrac{1}{2}ij, \quad (\kappa = 1, 2, 3), \tag{2b}$$

$$\psi = \frac{i}{3M^2}\,[\partial_\rho j_\rho - \tfrac{1}{2}(\partial_\rho \gamma_\rho + 2M)j]. \tag{2c}$$

In the absence of an interaction the set (2) clearly gives all the necessary subsidiary conditions. For consistency in the general case, the right-hand sides of eqs. (2b) and (2c) should be free of time derivatives. If this is not the case and if $\mathscr{L}_{\text{int}}$ does not contain time derivatives, one can attempt to achieve the desired result by resolving the initial set of eq. (1) in respect to its time derivatives and substituting the corresponding expressions into eq. (2c). This, however, cannot be carried out. In fact, let us rewrite set (1) as following

$$(L^{(\mu)}_{\alpha\beta}\,\partial_\mu + M\delta_{\alpha\beta})\Phi_\beta = I_\alpha, \tag{3}$$

where Φ_β is a 20 component function, $L^{(\mu)}$ are numerical matrices and I_α interaction terms. Resolution of eq. (3) with respect to its time derivatives could be accomplished by multiplying it by L_4^{-1}. But the matrix L_4 is singular and has no inverse. Thus we are bound to ensure non-appearance of time derivatives directly in the right-hand side of (2).

One can easily check that in the case of interaction with electromagnetic potential A_μ alone, when

$$j_\rho = ie(\gamma_\mu A_\mu \psi_\rho - \tfrac{1}{2}\gamma_\rho A_\lambda \psi_\lambda - iA_\rho \psi - \tfrac{1}{4}i\gamma_\rho \gamma_\mu A_\mu \psi),$$
$$j = -ie(iA_\mu \psi_\mu + \tfrac{3}{2}\gamma_\mu A_\mu \psi),$$

our criterion is fulfilled.

Let us now introduce in the Lagrangian all the possible invariant combinations with $F_{\mu\nu}$ (not including terms with field derivatives for the moment)

$$\mathscr{L}'_{\text{int}} = (ig_1\bar{\psi}_\mu \psi_\nu + ig_2\bar{\psi}_\rho \gamma_\mu \gamma_\nu \psi_\rho + g_3\bar{\psi}_\mu \gamma_\nu \psi + ig_4\bar{\psi}\gamma_\mu \gamma_\nu \psi)F_{\mu\nu} + \text{h.c.} \tag{4}$$

With this addition the right-hand side of eq. (2b) is still free of time derivatives

but not eq. (2c). In this case we have

$$\psi = \frac{1}{3M^2}\Big\{e(\gamma_\nu F_{\nu\mu}\psi_\mu - \tfrac{1}{2}i\gamma_\mu\gamma_\nu F_{\mu\nu}\psi)$$
$$+ 2g_1\frac{\partial}{\partial x_\mu}(\psi_\nu F_{\mu\nu}) + 2g_2\gamma_\mu\gamma_\nu\left(\partial_\rho\psi_\rho F_{\mu\nu} + \psi_\rho\frac{\partial F_{\mu\nu}}{\partial x_\rho}\right) - ig_3\gamma_\nu\left(\partial_\mu\psi F_{\mu\nu} + \psi\frac{\partial F_{\mu\nu}}{\partial x_\mu}\right)$$
$$+ (2g_2 - \tfrac{1}{2}(g_1+g_3))\left(2\frac{\partial}{\partial x_\mu}(\psi_\nu F_{\mu\nu}) - \gamma_\mu\gamma_\rho\partial_\rho(\psi_\nu F_{\mu\nu})\right) \qquad (5)$$
$$+ i(\tfrac{1}{4}g_3 - g_4)\left(4\gamma_\nu\frac{\partial}{\partial x_\mu}(F_{\mu\nu}\psi) + \gamma_\mu\gamma_\nu\gamma_\rho\partial_\rho(F_{\mu\nu}\psi)\right)$$
$$+ g_3M\gamma_\nu F_{\mu\nu}\psi_\mu - 2ig_4M\gamma_\mu\gamma_\nu F_{\mu\nu}\psi\Big\}.$$

It turns out that by no choice of arbitrary constants g_1, g_2, g_3, g_4 one can eliminate time derivatives from eq. (5). Thus we cannot obtain the correct number of subsidiary conditions and the theory becomes physically meaningless. Introduction of terms with field derivatives in the Lagrangian makes the situation even worse, as non-removable terms with time derivatives appear also in eq. (2b). Also, introduction of terms non-linear in fields in j_ρ and j does not help. Consequently, we have to deal with the theory where only minimal electromagnetic interaction is allowed. This is very likely to be the general feature of all the theories describing higher spin particles.

The author would like to thank Prof. A. Salam and Dr. S. Kamefuchi for helpful discussions and Prof. R. Peierls for useful comments. He is also grateful to Prof. Salam for the hospitality extended to him during his stay in Imperial College.

References

1) A. Komar and A. Salam, Nuclear Physics **21** (1960) 624; other references can be found there
2) R. A. Moldauer and K. U. Case, Phys. Rev. **102** (1956) 279
3) V. Fainberg, JETP **25** (1953) 644 (in Russian)

2.H:3.B

Nuclear Physics **22** (1961) 104—130; © *North-Holland Publishing Co., Amsterdam*

Not to be reproduced by photoprint or microfilm without written permission from the publisher

INTERNAL CONVERSION ELECTRONS FROM COULOMB EXCITATION OF HEAVY ELEMENTS

D. H. RESTER †, M. S. MOORE ††, F. E. DURHAM † and C. M. CLASS

The Rice University, Houston, Texas ‡

Received 8 August 1960

Abstract: The spectra of internal conversion electrons due to Coulomb excited transitions in Au^{197}, the five abundant isotopes of osmium, $Th^{230, 232}$, and $U^{234, 236, 238}$ have been obtained with a beta-ray spectrometer of the single-segment "orange" type. Some of the experimental problems connected with these measurements are discussed. Reduced transition probabilities have been measured for the first 2^+ excited states of all the even nuclei none of which have been investigated heretofore by means of the conversion electrons. For the even isotopes of osmium, some evidence suggesting enhanced internal conversion is found. The quadrupole moments and deformation parameters derived from the reduced transition probabilities agree well with the values obtained in recent theoretical calculations. Evidence for a weak cascade transition between the well-known states at 548 and 279 keV in Au^{197} has been found, and a level in Os^{189} at 69.7 keV is confirmed which is identified as the $\frac{3}{2}^-$ first excited rotational state. Two weak conversion lines in the osmium spectrum believed to be contributed by Os^{189} are assigned the probable transition energies of 194 and 245 keV.

1. Introduction

In recent years a wealth of nuclear data has been accumulated on low-lying states of many medium and heavy nuclei by means of Coulomb excitation. These data have provided convincing evidence supporting the theory of collective nuclear excitations and, indeed, for the validity of the rotational model for those nuclei possessing large quadrupole deformations [1]).

The major part of the experimental effort has been devoted to determining the energies and reduced transition probabilities of the Coulomb-excited states, chiefly by measuring the γ radiation. Valuable results also have been obtained by measurements utilizing magnetic analysis of either the internal conversion electrons or the inelastically scattered bombarding particles [2, 3, 4, 5]). In the work to be reported here, magnetic analysis of the internal conversion electrons has been employed. The spectrometer used for this purpose is described in the first section below and some discussion is given of the experimental problems which must be dealt with to achieve even a modest degree of accuracy when determining the transition probabilities. The

† Now at Tulane University, New Orleans, Louisiana.

†† Now with Phillips Petroleum Company, Idaho Falls, Idaho.

‡ Supported by the U. S. Atomic Energy Commission.

spectrometer has been used to investigate a number of nuclei which because of special circumstances had not been studied previously by Coulomb excitation, or had been studied less completely than seemed desirable.

Among the relatively few nuclei not previously investigated are the isotopes Th^{230}, U^{234} and U^{236}, which until quite recently were not generally available in separated form. The principal interest in these isotopes currently is attached to the vibrational states accessible by Coulomb excitation which in some cases decay by monopole transitions [6]). However, the first excited rotational states lying at about 50 keV are also of interest since measurements of the reduced transition probabilities $B(E2)$ for these states enables one to derive values for the nuclear deformation parameter for comparsion with theoretical values for nuclei in this mass region [7]). At the time these measurements were undertaken, the few $B(E2)$ values known for even nuclei in this region had been obtained by means of Coulomb excitation with only the γ radiation observed [1]). In order to compare the results of the present conversion electron measurements with the values obtained in this way, the transitions in Th^{232} and U^{238} were also investigated. Recently, Bell, Bjørnholm and Severiens [8]) have determined $B(E2)$ values by measuring the life-times of the first excited states for many members of the actinide series including all those reported on here, using a fast coincidence method. Elbek *et al.* [9]) have also reported results on Th^{232} and U^{238} obtained by magnetic analysis of the inelastically scattered bombarding particles.

Among the heavy nuclei previously studied, measurements by means of the conversion electrons seemed appropriate on the isotopes of osmium, hitherto investigated only by means of the γ ray spectrum [10]). The γ ray spectrum is a composite of partially resolved lines from the five abundant isotopes, which are not available in separated form. Because of the complexity of this spectrum, transitions in the odd isotopes Os^{189} cannot be detected, and the $B(E2)$ values obtained for the even isotopes are subject to uncertainties greater than usual. A complicated γ ray spectrum also is presented by Coulomb excited Au^{197} which contains five transitions. Results from the conversion electron measurements on this much investigated nucleus are included because of the evidence obtained for a previously suspected, but unestablished transition. Some of the other results on gold presented here have appeared earlier in the review article by Alder *et al.* [1]).

2. Experimental Apparatus and Methods

The experiments to be discussed below were carried out with a double-focusing magnetic spectrometer of the single-segment "orange" type [11]) adapted for use in conjunction with the Rice University 5.5 MeV Van de Graaff genera-

tor †. The instrument, shown in fig. 1, was constructed to a scale determined by the source-to-focus distance of 12.5 cm. Under typical operating conditions it has a momentum resolution of 1 % and a transmission of 0.5 %. The spectrometer is mounted on a ruggedly made aluminium table provided with casters, so that it can be moved easily to the beam port of the Van de Graaff accelerator for each experiment. When in the operating position, the spectrometer is located about 2 m from the exit slits of the 90° analyzing magnet of the accelerator. The horizontally directed beam enters the spectrometer at C in fig. 1 after passing through a set of adjustable tantalum slits which restrict the bombarded

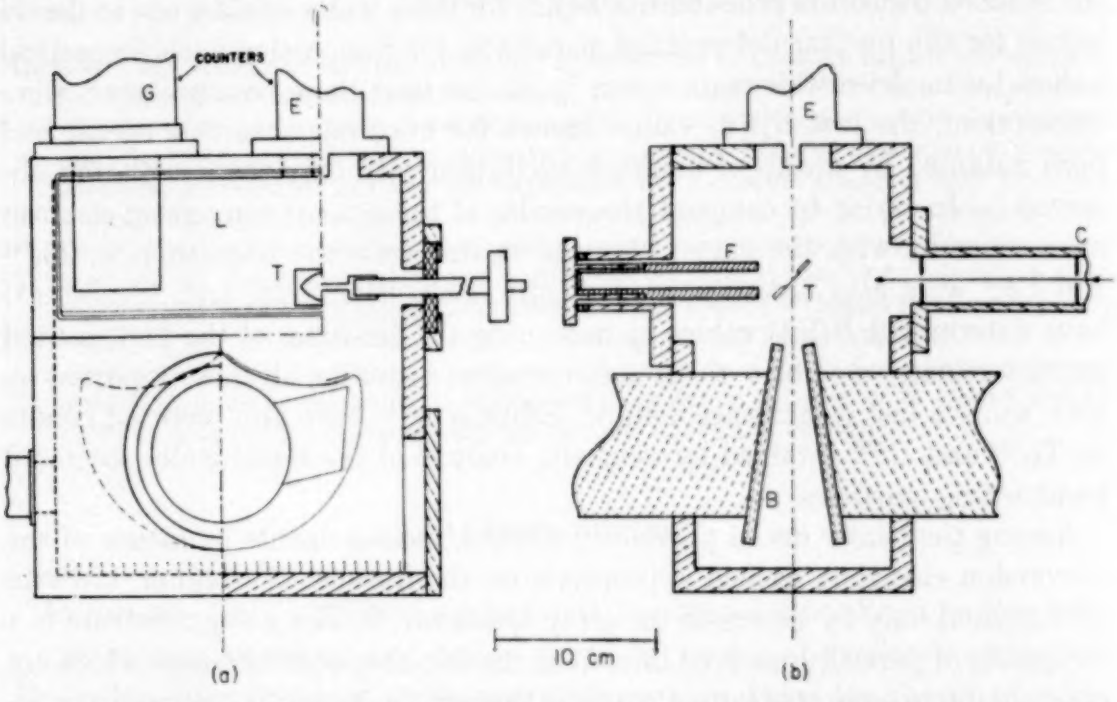

Fig. 1. Sectional view of the magnetic spectrometer. C identifies the beam collimating slits, T the target, F. the Faraday cup, B the wedge shaped magnetic field, E the scintillation counter to measure elastically scattered bombarding particles, and L the region filled with lead to shield the electron counter G from background radiation originating at the target.

area at the target to about 2 mm × 2 mm to insure adequate momentum resolution. Additional fixed slits serve to define the path of the beam and to screen out scattered particles. Electrons from the source enter the wedge-shaped magnetic field B from above and have trajectories in planes transverse to the beam direction. The acceptance angle of the spectrometer in the vertical plane containing the beam is 18°; in the vertical plane perpendicular to the beam direction the acceptance angle is variable but fixed at about 16° for the present work. The bundle of electrons thus defined is brought to focus on a rectangular slit 1.6 mm × 10 mm which serves as the entrance aperture to either of two counters

† Instruments of a design similar to the one described here have been used by the authors of ref. [2, 3, 5]).

G which can be used interchangeably in the spectrometer. A Geiger counter is used to detect low energy electrons from states formed by α particle bombardment, for which background is low. A scintillation counter is used to measure electrons having energies greater than about 100 keV in the presence of high backgrounds such as are usually present when 3 to 5 MeV protons are employed.

2.1. COUNTERS

The scintillation counter consists of an anthracene crystal which can absorb electrons having energies up to about 1 MeV, joined to a magnetically shielded photomultiplier tube by a tapered lucite light pipe 15 cm in length. The output from the counter, after amplification, is sent to a 20-channel pulse height analyzer and a single-channel analyzer, connected in parallel. As the electron energy changes in the course of a run, the gain of the amplifier is adjusted so that the peak of the pulse height distribution stays in the same channel of the 20-channel analyzer. The number of electrons in the distribution is obtained from the single channel analyzer, which is adjusted to integrate the pulses falling in a fixed number of channels centered about the peak. Pulse height distributions are recorded periodically in order to correct the yield for the minor loss of electrons falling outside the integrated channels.

The end window Geiger counter is of conventional design. It is filled with an argon-ethyl alcohol mixture to a pressure of 10 cm. The counter windows are made of vinyl plastic (trade name VYNS) [12]) and average about 200 $\mu g/cm^2$ in thickness, so that electrons having energies as low as about 15 keV can be detected. By keeping the active volume of the counter small (about 2 cm^3) and by carefully shielding with lead inside the spectrometer, response to background is minimized.

2.2. ENERGY CALIBRATION

The energy calibration of the spectrometer is made by relating the known momentum values of the Th(B+C+C″)A, B, F, and I lines [13]), the Cs^{137} K and L lines [14]) and the Bi^{207} K_2 line [15]) † to the potential developed across a standard resistor by the magnet current when the current is set to give the peak of the electron distribution of each line. The energies of the calibration lines range from about 25 keV to 975 keV. Current for the magnet coils is supplied by a regulated source stable to one part in 10^4. To reproduce the field for any given value of the magnet current, the magnet current is cycled before and after each run between empirically determined values of positive and negative current chosen so that the remnant field is essentially zero. Consecutive momentum distributions of the standard lines reproduce to within 0.1 % and energy assignments based on the calibration and recycling procedure outlined may have an error of about 0.5 %.

† The Bi^{207} source, made available through the courtesy of D. E. Alburger and T. W. Bonner, had an activity of 4.5 μc.

2.3. YIELD CALIBRATION

The total electron yield due to conversion in a particular shell is related to the area $P(n)$ of the line at momentum p, if an isotropic angular distribution of the electrons is assumed, by

$$Y(n) = C(p)\,\frac{P(n)}{p}\,D, \tag{1}$$

where the two quantities D, the transmission-dispersion factor, and $C(p)$, the counting loss correction factor, need to be determined empirically. D is related to the spectrometer parameters by

$$D = \frac{\bar{Z}d}{\Delta Z}\,\frac{4\pi}{\mathrm{d}\Omega},$$

where d is the dispersion factor, $\bar{Z}$ is one-half the distance between source and focus, ΔZ is the detector slit width and $\mathrm{d}\Omega$ is the effective solid angle for the entrance aperture used.

By making use of sources of known activities, D was measured at various electron energies, and was found to be substantially constant over the range of energies of interest. In the low energy region D was determined by making use of the conversion electrons from the 67.6 keV state in Ra^{226}, which is populated in the α decay of Th^{230} [16]). The α activity from the Th^{230} source was measured directly by means of a CsI(Tl) crystal scintillation spectrometer with a known solid angle. The α activity was then compared to the yield of the conversion electrons from the same source. The fraction of the α decays which leads to the 67.6 keV state was taken to be 0.262 [16]). At the electron energies of the L_{I+II} and L_{III} lines from this state, 49.2 and 51.8 keV respectively, the Geiger tube window loss was less than 5 %, and it was negligible at the energies of the M and N lines. The sources used in these measurements were less than 30 $\mu g/cm^2$ thick as measured by a method to be discussed below and losses due to scattering are believed to be minor. The value of D determined in this way, together with an independent measurement of the dispersion factor, gave a value for the transmission of 0.5 ± 0.05 %, where the uncertainty stated is that in the measurement of D. Additional determinations of D were made using calibrated Cs^{137} and Bi^{207} sources. With the Cs^{137} source, the corresponding transmission obtained at 625 keV was 0.46 ± 0.05 %. With the Bi^{207} source a measurement of the intensity of the K2 line at 975 keV yielded a value of 0.56 ± 0.1 %. The value adopted for the transmission is 0.50 ± 0.03 %.

The correction factor $C(p)$ occurring in the expression for the yield in the the case of the Geiger counter accounts for the loss of electrons due to scattering and absorption in the counter window. In the case of the scintillation detector, $C(p)$ accounts for the losses due to imperfect integration of the pulse distribution and is readily determined from the display on the 20-channel analyzer.

For the Geiger counter $C(p)$ was determined by measuring the Pm^{147} beta spectrum, which has an end point energy of 227 keV and a Kurie plot known to

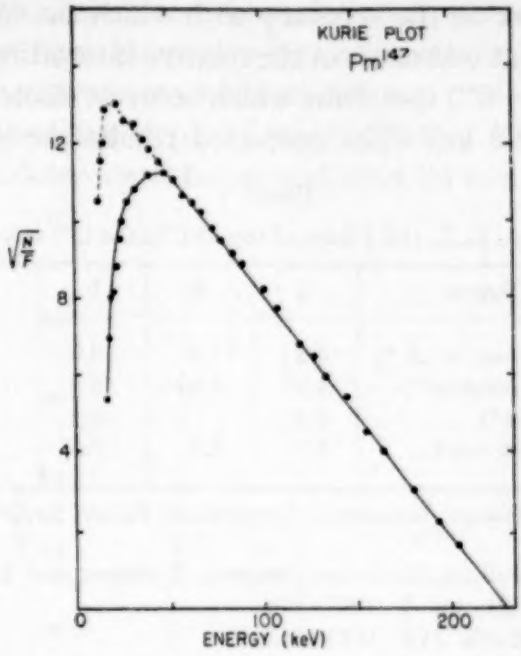

Fig. 2. Kurie plot of the Pm^{147} beta spectrum taken with counter windows of about 30 $\mu g/cm^2$ and 200 $\mu g/cm^2$. The thinner window, impractical for routine use, enabled a check for evidence of source distortion.

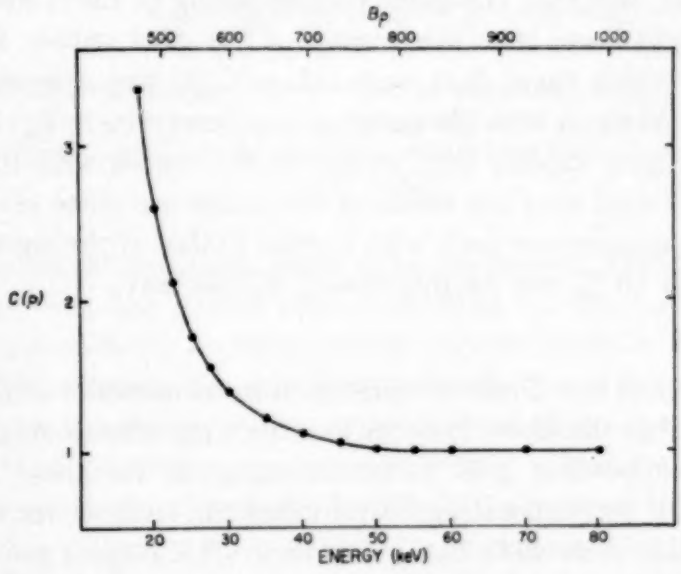

Fig. 3. The correction factor $C(p)$ derived from the Kurie plot of the Pm^{147} spectrum for the approximately 200 $\mu g/cm^2$ thick counter window.

be linear to an energy of 10 keV [17]). Kurie plots of typical spectra from thin sources measured with counter windows of two different thicknesses are shown in fig. 2. Departures of the data points from the straight line extrapolated from

the linear portion of the plot were attributed to the effect of the counter window. The correction curve $C(p)$ determined in this manner for a window of about 200 μg/cm^2 thick, which is typical of those used in this work, is shown in fig. 3. To check further on the accuracy with which the correction curve could be used, a measurement was made of the relative intensities of the A, B, F and I lines of the Th(B+C+C″) spectrum, which occur at electron energies of 24.51, 36.15, 148.1 and 222.2 keV. The corrected results are presented in table 1

TABLE 1

Relative intensities of the A, B, F, and I lines of the Th(B+C+C″) conversion electron spectrum

Source	A	B	F	I
Zhernovoi *et al.* [a])	4.3	1.0	6.0	1.0
Flammersfeld [b])	4.07	0.69	5.5	1.0
Nielsen [c])	4.2		5.5	1.0
Present work	3.7	0.7	6.1	1.0

[a]) Zhernovoi, Krisiuk, Latyshev, Remennyi, Sergeev and Fadev, Soviet Physics JETP **5** (1957) 563;
Vorobeev, Ilin, Kol'Chinskaia, Latyshev, Sergeev, Trofimov and Fadev, Akademiia Nauk. USSR, Physical Series **21**, no. 7 (1957) 956

[b]) A. Flammersfeld, Z. Physik **114** (1939) 227

[c]) O. B. Nielsen, private communication

along with those obtained by other investigators. It is seen that the agreement is reasonably good, but that the value corresponding to the A line intensity is approximately 10 % lower than the average of the other values. For the counter window with which these data were taken, $C(p)$ was approximately 2 in the neighborhood of the A line. However, as can been seen in fig. 3, the correction factor is changing rapidly with energy in this region with the result that the values of $C(p)$ used over the width of the A line are quite sensitive to any small shifts in the momentum scale with respect to that of the correction curve. An uncertainty of 10 % can be introduced in this way.

2.4. TARGETS

The targets used in the Coulomb excitation measurements were in all cases less than 1 mg/cm^2 in thickness in order to reduce the effects of scattering and absorption. Self-supporting gold targets ranging in thickness from 0.3 to 1 mg/cm^2 were made by evaporating the pure metal in vacuum onto a glass plate from which suitable foils were easily removed. The targets for the actinide elements and osmium were prepared on thin ($\approx$ 200 μg/cm^2) carbon backings by slowly evaporating a drop of a salt solution of the material. The thickness of the target material deposited was determined by measuring the yield of protons elastically scattered from the target into a known solid angle. For this purpose a CsI(Tl) crystal scintillation spectrometer labelled E in fig. 1 was provided which viewed the target at 90° with respect to the direction of the beam.

A typical pulse height distribution of the protons elastically scattered from a target of $Th(NO_3)$ is shown in fig. 4. The resolution of the scintillation counter is about 5 % for 3 MeV protons, which provides adequate separation of the elastic groups from the heavy element and the various light elements present for target thicknesses of interest here. Successive measurements on a given target agreed to within 5 %, and measurements made on different portions of the same target showed that in general the deposits were uniform. Whenever possible the target thickness was determined before and after its use in an experiment and

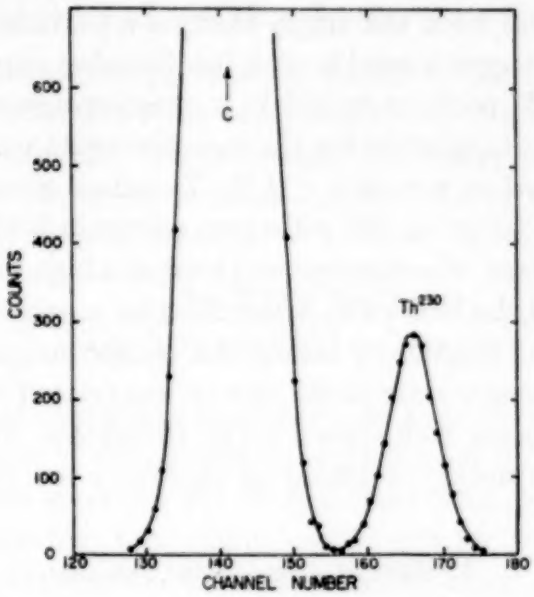

Fig. 4. The pulse height distribution of 3.8 MeV protons elastically scattered from a target containing 30 $\mu g/cm^2$ of thorium in the form of $Th(NO_3)_4$, deposited on a carbon foil. The groups of protons scattered from nitrogen and oxygen are unresolved from the much stronger group scattered from carbon.

in these cases the thickness was found to be unchanged. This method of measuring thickness does not reveal inhomogeneities in the target deposit, since crystals or grains of the material several mg/cm^2 thick in the heavy element have a negligible effect on the pulse height distribution of the protons. However, such granularity can seriously distort the shape of the conversion electron lines, particularly those occurring at energies of 50 keV or less. Indeed, distortions of line shapes were observed with the targets first prepared for measurements in this region. This difficulty was remedied by finding suitable compounds for the target material which was then deposited to thicknesses of less than 50 $\mu g/cm^2$. A more complete discussion of these precautions will be given below in the section devoted to the actinide isotopes.

The targets were held in a frame attached to a brass rod which passed through an insulating nylon bushing in the wall of the vacuum chamber as shown in fig. 1. A sliding seal made it possible to adjust both the lateral and angular

position of the target which was normally inclined at 45° with respect to the direction of the beam. When proton bombardment was used, the beam, after passing through the target, was stopped by a tantalum disc in a lead-lined Faraday cup F insulated from ground by a heavy teflon sleeve. The background produced in the counters by stopping the beam in this manner was negligible. When an α particle beam was used, the beam was collected in a cylindrical carbon cup which enclosed the space behind the target. This arrangement, which was less suitable with proton beams because of increased background, was required in order to avoid errors in current integration due to the stripping of the second electron from the singly-charged α particles on passing through the target foil. The target assembly and the Faraday cup, when in use, were maintained at 300 V positive to aid in supressing secondary electrons.

The beam current integration for the measurements was carried out with a circuit which provided an accuracy of 1 %. To reduce errors in integration due to neutralization of charge on the collectors, particularly during measurements with the α particle beam, the chamber was kept at a high vacuum by a diffusion pump. The energy of the beam was determined by measuring the field strength of the beam analyzing magnet by means of a nuclear magnetic resonance magnetometer. The frequency scale of this device was related to energy by calibration measurements using well-known (p, n) thresholds. The energy spread of the beam under the usual conditions of operation was 0.1 % or less.

3. Results and Discussion

Measurements have been made of conversion lines due to Coulomb excited transitions in 11 different isotopes of the elements gold, osmium, thorium and uranium. The results are summarized in tables 2, 3 and 4, and are discussed in detail in the sections below. Generally, the results for each isotope included the energy, the partial and the total reduced transition probabilities for excitation, and the ratio of the conversion line intensities from the different subshells for each transition observed. The transition energies assigned are based on the electron shell binding energies tabulated by Hill *et al.* [18]). The partial reduced transition probability $\varepsilon(n)B(\mathrm{E2})$ for excitation was calculated from the experimental yield given by eq. (1) by use of the following formulas from the well-known work of Huus *et al.* [2]). For electric quadrupole excitation, the partial cross section is

$$\varepsilon(n)\sigma(\mathrm{E2}) = \left[\frac{69.4}{Z_2}\right]^2 \frac{A_1(E_1-\Delta E')}{(1+A_1/A_2)^2} \frac{B(\mathrm{E2})}{e^2} f_{\mathrm{E2}}(\xi)\ \mathrm{mb}, \qquad (2)$$

where $\Delta E'$, the effective excitation energy, is expressed in MeV and $B(\mathrm{E2})$ in units of $e^2\times 10^{-48}$ cm^4. A_1 is the atomic mass of the incident particle, and E_1 is the incident energy. Z_2 refers to the atomic number of the target nucleus and

A_2 to its atomic mass. The effective excitation energy is expressed in terms of the transition energy ΔE by

$$\Delta E' = (1+A_1/A_2)\Delta E.$$

The function $f_{E2}(\xi)$ is to be found in the work of Alder *et al.* [1]), where ξ is given by

$$\xi = \frac{Z_1 A_1^{\frac{1}{3}}}{(E_{av})^{\frac{1}{2}}} \frac{Z_2 \Delta E'}{12.65},$$

where

$$E_{av} \approx (E_1 - \tfrac{1}{2}\Delta E').$$

The total reduced transition probability $B(E2)$ is derived from the partial reduced transition probability if the decay fraction $\varepsilon(n)$, or fraction of the decays through the conversion line "n", is known. The decay fraction is calculated from the theoretical conversion coefficients $\alpha(n)$, the mixing ratio δ, and the branching fraction β by the formula

$$\varepsilon(n) = \frac{\alpha_{M1}(n)+\delta^2\alpha_{E2}(n)}{1+\sum_\nu \alpha_{M1}(\nu)+\delta^2[1+\sum_\nu \alpha_{E2}(\nu)]}\beta. \qquad (3)$$

The newer theoretical conversion coefficients of Rose [19]) which include corrections for the finite size of the nucleus have been used throughout except that the unscreened values given for the M-shell have been reduced by 50 % †, to take account of screening. Conversion coefficients for the N+O shells have been taken at 20 % of the corrected M-shell values, based on the measurements of Cressman and Wilkinson [20]).

The type of bombarding particle used and the beam energy at which the measurements were carried out depended on the energy of the state to be investigated. For low energy transitions, α particle bombardment provides the most satisfactory experimental conditions, since it is then possible to perform the measurements at the value of the excitation parameter ξ for which the "signal to noise ratio" is optimum [1]), where "noise" here refers to the background of atomic electrons ejected from the target by the bombarding particles. Because the intensity of this "stopping electron" background is proportional to E_δ^{-7}, where E_δ is the energy of the ejected electrons, this contribution to the total background is of minor importance for electron energies above about 100 keV [1]). Consequently, for transition energies greater than this value no effort was made to optimize ξ, and protons of from 4 to 5 MeV were used because of their greater effectiveness for inducing the higher energy transitions.

3.1. OSMIUM

Natural osmium consists of 7 isotopes. Five of these are even, having mass numbers 184 through 192 and occur with abundances of 0.018, 1.59, 13.3, 26.4

† This reduction is based on a recommendation by M. E. Rose, privately communicated.

and 41.0 % respectively. The remaining 2 odd-neutron isotopes, 187 and 189, have abundances of 1.6 and 16.1 %. Because of the toxic properties of osmium compounds the osmium isotopes are among the few not available in separated form.

Targets of $OsCl_3$ on carbon foil backings were prepared as described above.

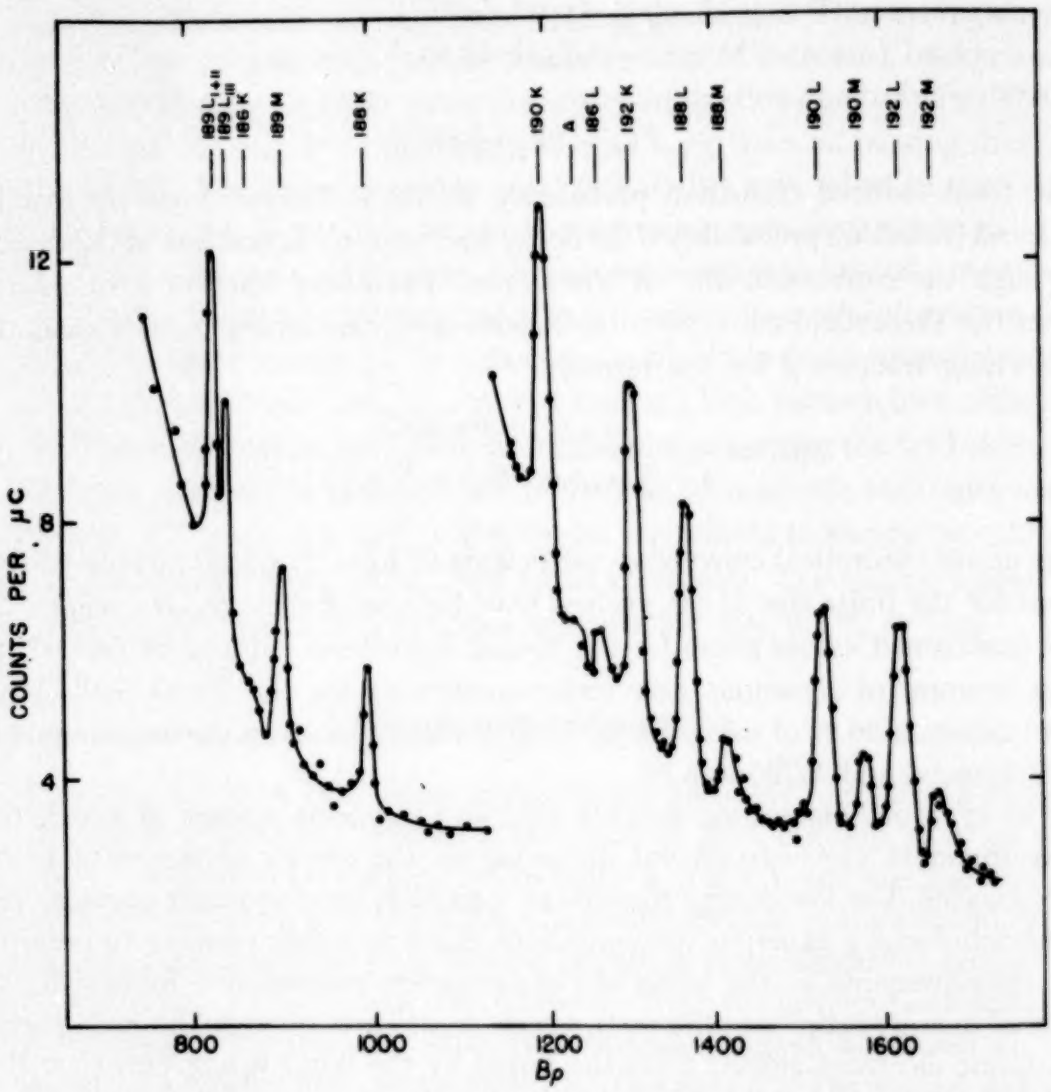

Fig. 5. The spectrum of conversion electrons from Coulomb excited transitions in the osmium isotopes. The portion of the spectrum on the right was obtained with 4.8 MeV protons; that on the left with 3.5 MeV α particles.

A typical conversion electron spectrum is shown in fig. 5, incorporating data from runs with both protons and α particles. Some broadening of the conversion lines beyond instrument resolution may be seen which is attributed to the thickness ($\approx$ 300 $\mu g/cm^2$) of the target. The background apparent in the data taken with proton bombardment originates almost entirely from γ radiation, whereas the background in the data taken with α particle bombardment is con-

tributed principally by the stopping electrons. A survey of the spectrum in the region above that shown and extending to an electron energy of 300 keV ($B\rho = 2100\,\mathrm{G \cdot cm}$) revealed no additional transitions. The regions of $B\rho = 850$—900 and $B\rho = 1200$—$1250\ \mathrm{G \cdot cm}$ are shown in detail in fig. 6 in order to display the structure which emerges under more favorable bombarding conditions.

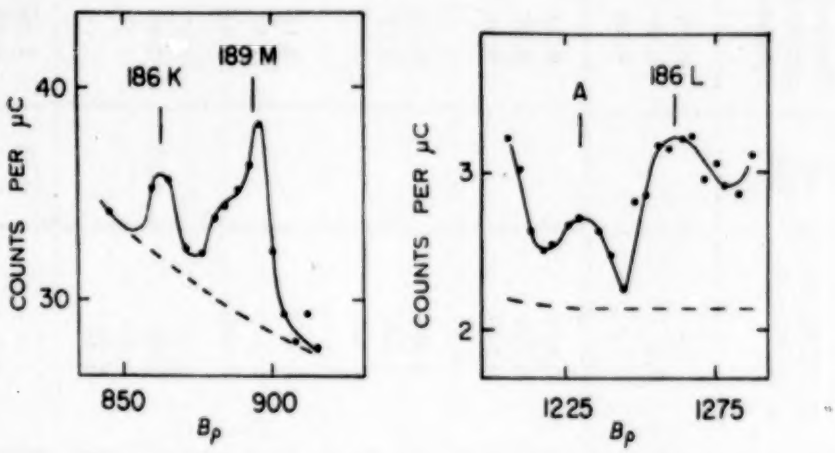

Fig. 6. Detail of portions of the conversion electron spectrum for the osmium isotopes. The spectrum on the left was obtained with 4.5 MeV α particles to improve the relative intensity of the Os^{186} K line. The spectrum on the right was obtained with 3.0 MeV protons. The reduced background at this energy causes the line marked A in fig. 5 to become distinct.

The identification of most of the electron peaks shown in fig. 5 was aided by information available from beta decay studies of the neighbouring isobars. The lines labeled 192K, 192L and 192M are assigned as the K, L and M lines of the transition from the first excited state of Os^{192}, the most abundant isotope. The transition energy derived from these lines is 206.0 keV as compared with the reported value of 205.75 keV [21]). The lines labeled 190K, 190L, and 190M are due to transitions from the first excited state of Os^{190} for which an energy of 187.3 keV is assigned. An energy reported for this state is 187 keV [22]). Transitions from the first excited state of Os^{188}, which has a reported energy 154.87 keV [23]), can be associated with the lines marked 188K, 188L, and 188M which correspond to a transition energy of 155.3 keV. Weak electron lines corresponding to K and L shell conversion for a 136.3 keV transition also are seen. This transition is assigned to Os^{186} for which the first excited state is reported to be 137.7 keV [24, 25]). In addition to these transitions there are 5 electron lines which cannot be associated with any known transitions in the even isotopes. It is reasonable to identify these lines with transitions in the isotopes Os^{187} and Os^{189}, the latter isotope being favored because of its 16 % abundance. On this basis, 3 of the lines in fig. 5 marked 189 L_{I+II}, 189 L_{III} and 189 M can be accounted for by a 69.7 keV transition in Os^{189}. The fourth weak line at 120.3 keV labeled A in figs. 5 and 6, has no related lines and, there-

TABLE 2

Summary of experimental results

Isotope	Target compound	Typical target thickness (mg/cm²)	Projectile and energy (MeV)	Transition energy (keV)	Electron subshell (n)	$B_{ex}(E2)\varepsilon(n)$ ($e^2 10^{-48}$ cm⁴)	$\frac{E2}{M1}$	Theoretical conversion coefficient	Total $B(E2)_{ex}$ ($e^2 10^{-48}$ cm⁴)
Os^{186}	$OsCl_3$	0.208	4.8p 3.5α	136.3	K L M+N	— 1.2 —		0.43 0.64 0.25	4.3 ±1.1
Os^{188}	$OsCl_3$	0.208	4.8p 3.5α	155.3	K L M+N	0.690 0.780 0.210		0.32 0.37 0.14	3.7 ±0.5
Os^{190}	$OsCl_3$	0.208	4.8p	187.3	K L M+N	0.494 0.402 0.120		0.20 0.17 0.06	3.38±0.4
Os^{192}	$OsCl_3$	0.208	4.8p	206.0	K L M+N	0.337 0.246 0.088		0.15 0.11 0.04	2.92±0.4
Os^{189}	$OsCl_3$	0.196	3.5α	69.7	L_{I+II} L_{III} M+N	0.56 0.24 0.22	0.18	2.95 1.27	1.2 ±0.2
Au^{197}	Au	0.90	3.8p 4.8p	191 268 269 279 548	K L K L K L M+N K	 0.064 0.011 0.004 0.0066	0.53 0.98 0.16 	1.29 0.30 0.23 0.054 0.34 0.051 0.017 0.016	 0.076 0.30 0.40

					L	0.011		0.031	0.30
					M+N	0.004		0.017	
				548	K	0.0066		0.016	0.40
					L+M	0.0018		0.0056 [a])	
Th^{230}	$Th(NO_3)_4$	0.030	2.2α	53.4	L_{I+II}	4.4			11.1 ±1.7 [a])
					L_{III}	4.0			
Th^{232}	$Th(NO_3)_4$	0.010	2.2α	50.1	L_{I+II}	4.4			11.5 ±1.7
					L_{III}	4.4			
					M	1.9			
					N+O	0.8			
U^{234}	UO_2Cl_2	0.018	2.2α	43.5	L_{I+II}	4.9			11.4 ±1.7
					L_{III}	3.7			
					M	1.9			
					N+O	0.9			
U^{236}	UO_2Cl_2	0.036	2.2α	44.9	L_{I+II}	5.1			13.1 ±2.0
					L_{III}	4.7			
					M	2.2			
					N+O	1.1			
U^{238}	$UO_2(NO_3)_2$	0.019	2.2α	44.7	L_{I+II}	5.7			13.2 ±2.0
					L_{III}	4.6			
					M	2.2			
					N+O	0.7			

[a]) Assumes (M+N)/L = 0.3.

fore, is not assigned a transition energy for the present. This line together with a partially resolved satellite of the 190 L line will be discussed further below.

Partial B(E2)-values derived for all conversion lines are listed in table 2. Also included are the total theoretical conversion coefficients interpolated for the appropriate energies from the tables of Rose [19]), and the total B(E2)-values. A 6 % correction has been made to the yield of the K-shell conversion electrons to account for the non-isotropic angular distribution of these electrons. Formulas for computing the corresponding correction for L- and M-shell electrons are unavailable. No corrections have been made for the minor effects associated with the cascade transitions from the weakly populated second Coulomb excited states which have been observed in the most abundant even isotopes [10]). The errors of the B(E2)-values include uncertainties in the transmission-dispersion factor D, in the target thickness and in the current integration of 6 %, 5 % and 1 % respectively. In addition, errors in determining the areas of the conversion lines $P(n)$ occur which depend on the relative intensities of the lines with respect to their backgrounds and on the decomposition of the lines when incompletely resolved. The resulting uncertainty in $P(n)$ for any single measurement did not usually exceed 10 %, and in most cases data on the same line were obtained several times with different targets. The B(E2)-values quoted are averages of the different determinations and are believed to have a probable error of about 12 %, except in the case of Os^{186}. The low abundance of this isotope with subsequent low intensity results in a relative error about twice that of the other cases.

The B(E2)-values derived from the measurements are listed in table 3, and for comparison other reported values are included which were obtained by Coulomb excitation in all cases except that of Os^{186}. The decrease of the osmium B(E2)-values with increasing mass is in agreement with the systematic trend displayed by the even nuclei in this region, but is to be noted that the values derived from the conversion electron measurements are higher in most cases than those obtained from the γ ray measurements. If the comparison is made between the present results and those of Stelson and McGowan [10]) as is done in fig. 7. it is apparent that the straight lines fairly representing both groups of data are parallel and shifted with respect to the extrapolation of the straight line through the data points of Elbek [9]) given for the neighboring even nuclei. This systematic displacement although barely outside the range of error for any single isotope is believed to be significant and can be construed as evidence for enhanced internal conversion in these isotopes. Such an interpretation is both suggested and supported by the work of McGowan and Stelson [26]) who have found an excess of K-shell electron conversion of 40 % or more in both the tungsten and osmium isotopes. To be sure, their result on osmium was somewhat uncertain because the contribution to K-shell conversion from the odd-mass isotopes was unknown. However, the present measurements show

that the contribution from these isotopes is negligible. Furthermore, a recent re-investigation of this effect in the tungsten isotopes by these authors with improved experimental conditions has confirmed the results of their earlier work [27]).

TABLE 3

The measured transition probabilities and derived quantities

Nucleide	$B(E2)_{ex}$ ($e^2 \times 10^{-48}$ cm^4)	Other reported values of $B(E2)_{ex}$	Quadrupole moment $Q_0(10^{-24}$ cm$^2)$	Deformation parameter δ
Os^{186}	4.3 ±1.1	4.36 [a] 3.3 [b]	6.6	0.208
Os^{188}	3.7 ±0.5	2.8 [b] 2.8 [c] 3.46 [d]	6.1	0.191
Os^{189}	1.2 ±0.2		4.8	0.158
Os^{190}	3.38 ±0.4	2.55 [c] 2.46 [d]	5.8	0.183
Os^{192}	2.92 ±0.4	2.05 [c] 2.1 [d]	5.4	0.170
Au^{197}(268 keV)	0.076±0.008	0.082 [e] 0.066 [f]		
Au^{197}(279 keV)	0.30 ±0.04	0.32 [e] 0.30 [f]		
Au^{197}(548 keV)	0.40 ±0.05	0.45 [e] 0.42 [f]		
Th^{230}	11.1 ±1.7	7.70±0.63 [g]	10.5	0.242
Th^{232}	11.5 ±1.7	8.50±0.37 [g] 9.7 ±0.5 [h]	10.8	0.245
U^{234}	11.4 ±1.7	9.5 ±0.72 [g]	10.7	0.238
U^{236}	13.1 ±2.0	10.70±0.92 [g]	11.5	0.252
U^{238}	13.2 ±2.0	11.05±0.98 [g] 12.6 ±0.6 [h]	11.5	0.251

[a]) E. E. Berlovich, Soviet Physics JETP **6** (1958) 1176
[b]) A. W. Sunyar, Phys. Rev. **98** (1955) 653
[c]) F. K. McGowan and P. H. Stelson, Phys. Rev. **109** (1958) 901
[d]) Barloutaud, Lehmann and Leveque, Compt. rend. **245** (1957) 523
[e]) P. H. Stelson and F. K. McGowan, Phys. Rev. **99** (1955) 112
[f]) B. Elbek and C. K. Bockelmann, Phys. Rev. **105** (1957) 657
[g]) Bell, Bjørnholm and Severiens, Mat. Fys. Medd. Dan. Vid. Selsk., to be published
[h]) Skurnik, Elbek and Olesen, private communication

An effort was made on the basis of this information to bring the two groups of data on the $B(E2)$ values into agreement by an alteration of the total conversion coefficient α_T. It was found that an increase of approximately 30% in α_T brought about satisfactory agreement as shown in fig. 7 and, moreover, caused the resulting values to lie along the extrapolation of the straight line fitting the data on hafnium and tungsten [9]) which do not depend on conversion

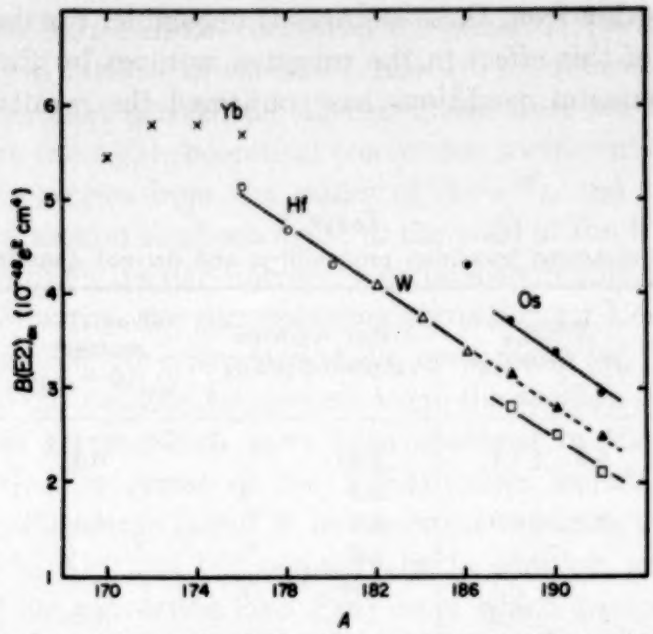

Fig. 7. B(E2) values for osmium and neighboring even isotopes. The results of Elbek *et al.* [9]) for Yb, Hf and W are shown by ×, ○ and △ respectively, values for osmium due to Stelson and McGowan [10]) by □, and the present results by ●. Values resulting from an approximately 30 % increase in α_T are shown by ▲.

TABLE 4

A comparison of the measured and theoretical conversion line intensity ratios for E2 transitions

Isotope	Transition energy (keV)	K/L			L_{I+II}/L_{III}		$\frac{M+N}{L}$
		Present measurement	Theory	Other measurements	Present measurement	Theory	Present measurement
Os^{186}	136.3		0.67	0.68±0.03 [a])			
Os^{188}	155.3	0.89±0.2	0.865	0.70±0.05 [b])			0.27 ±0.05
				0.79±0.15 [c])			
				0.92±0.05 [a])			
Os^{190}	187.3	1.23±0.2	1.18				0.30 ±0.06
Os^{192}	206.0	1.37±0.2	1.36	1.83±0.04 [d])			
				1.37 [e])			0.37 ±0.05
Au^{197}	548	3.7 ±0.4 [f](	2.9 [f])				
Ra^{226}	67.7				1.3±0.2	1.14	0.32 ±0.04
Th^{230}	53.4				1.1±0.15	1.14	
Th^{232}	50.1				1.0±0.15	1.12	0.306±0.04
U^{234}	43.5				1.3±0.15	1.14	0.326±0.04
U^{236}	44.9				1.1±0.15	1.15	0.337±0.04
U^{238}	44.7				1.2±0.15	1.14	0.282±0.04

[a]) K. Nielsen and O. Nielsen, Nuclear Physics **5** (1958) 319

[b]) V. R. Potnis, Phys. Rev. **104** (1956) 722

[c]) See ref. [24])

[d]) V. M. Kelman, R. Ya. Metskhvarishvili, V. A. Romanov and V. V. Tuchkevich, Nuclear Physics **4** (1957) 240

[e]) See ref. [21])

[f]) Both the experimental and theoretical ratios are for K/(L+M) in this case. The theoretical ratio is obtained by assuming the M shell contribution is 30 % that of the L shell.

coefficients. Furthermore, the B(E2) values obtained by Huus *et al.* [2]) for $W^{184,186}$ by means of conversion electrons are also brought into agreement with the results of Elbek for these isotopes by the same adjustment of α_T. An increase of α_T by this amount, if contributed only by the K-shell should show up in anomalous K/L ratios; but as may be seen in table 4, the ratios agree with the theoretical values within experimental error. Thus, if there is in-

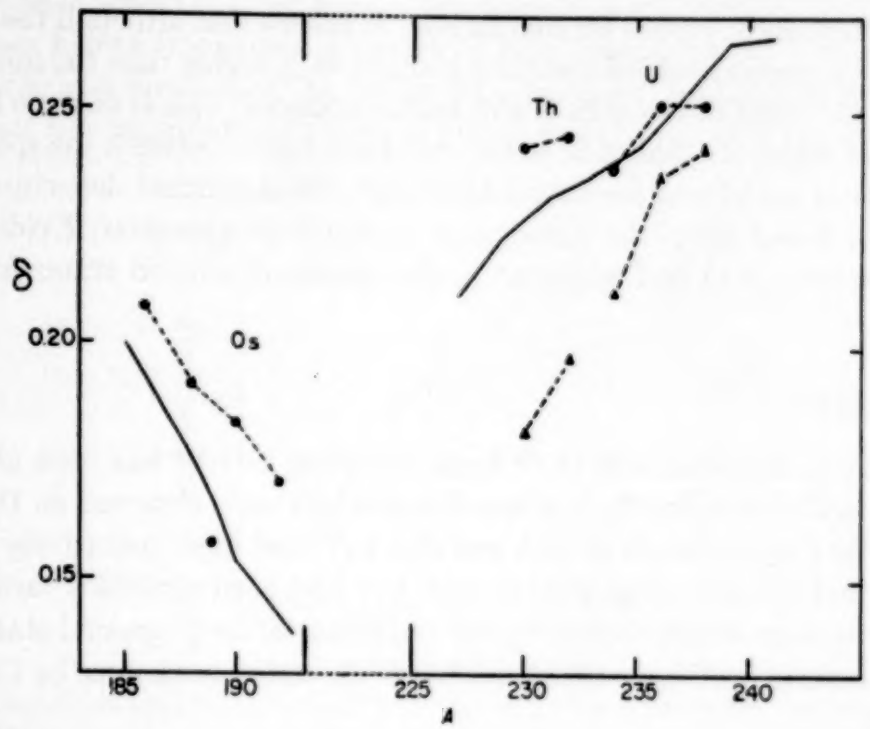

Fig. 8. The experimentally determined deformation parameters for the osmium and actinide isotopes investigated. The theoretical values are represented by the solid line [7]), ▲ indicates the results of Bell *et al.* [8]), and ● the present work.

deed any enhancement of electron conversion, the L-shell must share in the effect.

An additional feature of interest in the results of these measurements is the comparison of the B(E2) values found for these states with the predictions of theory for rotational states in this region of nuclear mass. For rotational states of even nuclei the reduced transition probability is related to the intrinsic quadrupole moment Q_0 of the nucleus by the expression

$$B(\mathrm{E2};\, 0^+ \rightarrow 2^+) = \frac{5e^2}{16\pi} Q_0^2. \qquad (4)$$

If the nuclear charge distribution is assumed to have the same shape as the nuclear potential, it is also possible to express the intrinsic quadrupole moment in terms of the deformation parameter δ, which characterizes the eccentricity

of the nuclear potential. Q_0 is given in terms of δ to second order by †

$$Q_0 = \tfrac{4}{5}\delta Z R_0^2(1+\tfrac{1}{2}\delta), \quad R_0 = 1.2A^{\frac{1}{3}} \times 10^{-13} \text{ cm}. \tag{5}$$

Consequently, the quantity can δ be determined experimentally by a measurement of the E2 transition probability, and a comparision can be made to the theoretical estimate of δ. The values of Q_0 and δ obtained from the present measurements are listed in table 3, and those for δ are plotted in fig. 8 together with the theoretical values for comparison. It is seen that although the magnitude of the experimental deformations is about 10 % higher than the theoretical estimate, the trend of the data is still well reproduced. This is of some interest since the isotopes of osmium lie in the transition region between the spheroidal and spherical nuclei and one might have expected significant departures from predictions based upon the assumption of rotational character. Evidence for such departures is in fact apparent in the spectra of excited states for these nuclei [25]).

3.2. OSMIUM-189

A report on transitions in Os^{189} from the decay of Ir^{189} has been given by Diamond and Hollander [25]). Numerous transitions were observed on the basis of which they assign levels at 30.8 and 69.5 keV, and more tentatively at 219, 255, 276 and 314 keV. The level at 30.8 keV had been identified earlier as a $\frac{9}{2}^-$ isomeric state which decays by M3 radiation to the $\frac{3}{2}^-$ ground state [22, 28]). No transitions in Os^{189} have been reported in the earlier work done by Coulomb excitation.

The 69.5 keV transition observed in the Ir^{189} decay corresponds well with the 69.7 keV transition found in this work with α particle bombardment. The intensity of this transition as a function of bombarding energy is shown in fig. 9. The trend of the data is well fitted by the excitation function calculated for an excitation energy of 69.7 keV indicating both a state at this energy and negligible population of the state from any higher lying levels at least for the bombarding conditions used here. For comparison, the curve calculated for an excitation energy of 136 keV is shown also. The observed $(L_I+L_{II})/L_{III}$ conversion intensity ratio of 2.2 leads to a value of $\delta^2 = 0.18$, where δ is the mixing ratio, its square giving the ratio of the number of E2 γ quanta to the number of M1 quanta emitted in the transition. By use of this mixing ratio, a total B(E2)-value of 1.2 $e^2 \times 10^{-48}$ cm^4 is obtained for the excitation. Since Os^{189} is the only stable odd-neutron nucleus in this region with spin $\frac{3}{2}^-$, a level scheme cannot be inferred from systematics. However, the value of B(E2) for the exci-

† Various expressions are found in the papers of the Copenhagen group relating Q_0 to the deformation parameters δ or β. The expression given here has been used by the authors of ref. [7]) to compare the experimental data with their theoretical values for δ versus A.

tation of the 69.7 keV state is large enough to imply that this state is a member of the ground state "rotational" band. Tentatively then, the 69.7 keV state is assigned a spin of $\frac{5}{2}^-$. The intrinsic nuclear quadrupole moment determined from the above $B(E2)$ value is $Q_0 = 4.8 \times 10^{-24}$ cm^2. This value fits well with the trend of the data for other odd-mass nuclei in this region, and corresponds to a spectroscopic $Q = 0.97$ as compared to a reported value [28]) of 0.6.

As mentioned above, a transition energy cannot be assigned to the 120.2 keV electron peak since the other lines of this transition are obscured by the strong lines from known transitions. However, a rough measurement of the intensity of this line as a function of the proton (or α particle) bombarding energy indicates that it originates from a state at higher energy than does the neighboring

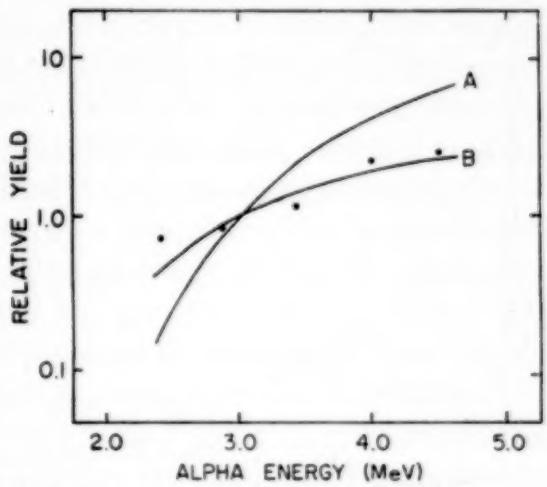

Fig. 9. The relative yield of the 69.7 keV transition in Os^{189} as a function of bombarding energy. Curve A shows the trend expected for the yield if the transition originated from a state at 136 keV, curve B from a state at 69.7 keV.

L line from the 136.3 keV transition in Os^{186}, although by not more than a factor of two. The simplest assumption consequently is to identify this peak with the K line of a ground state transition from a state at 194.1 keV and on this basis, $B(E2) \approx 0.3\ e^2 \times 10^{-48}$ cm^4 is obtained. Unfortunately, no transition of this energy was observed in the measurements of Diamond and Hollander, nor can such a transition be fitted into their tentative level scheme. On the other hand, a weak line was seen in the electron spectrum at 171.4 keV which is possibly the K-line of the 245 keV E2 transition seen by these authors. This line is unresolved on the low energy side of the Os^{190} L-line in fig. 5, but was partially resolved when re-run with a 70 μg/cm^2 thick target and has an intensity about 10 % that of its strong neighbor. If the transition energy is indeed properly assigned, then the L line should have been just barely detectable, but no convincing evidence for it was found. In the proposed level scheme, the 245 keV transition occurs between levels at 314.5 and 69.5 keV, although levels of 275.8 and 30.8 keV also provide this energy difference. No other transitions associated

with these levels were detected, including transitions from the 30.8 keV isomeric state.

3.3. GOLD-197

The level scheme for gold is well-known both from beta decay studies and from many investigations using Coulomb excitation [1]). With the latter method the inelastically scattered protons, γ radiation, and the internal conversion electrons all have been measured and there is a reasonable degree of consistency among the results.

The spectrum of conversion electrons obtained in the present work with protons at a bombarding energy of 3.8 MeV is shown in fig. 10. Lines are identi-

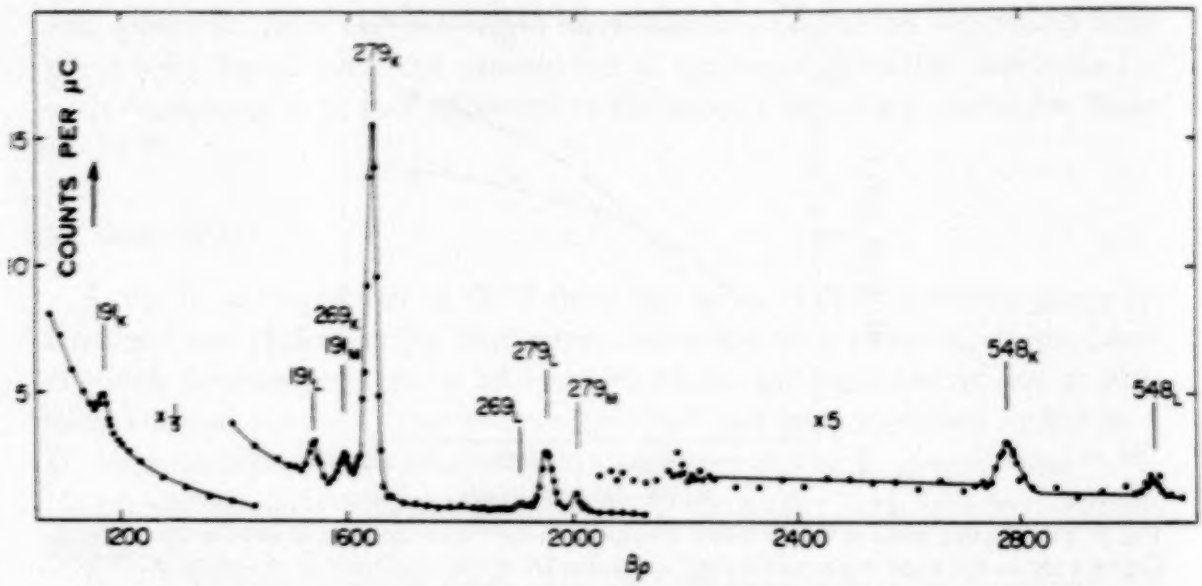

Fig. 10. The spectrum of conversion electrons due to transitions in Coulomb excited Au^{197} obtained with 3.8 MeV protons.

fied in the figure corresponding to conversion in the K, L and M shells for transitions having energies of 191, 269, 279 and 548 keV. Only the assignment of the 269 transition in the decay scheme requires discussion, since the 191 keV transition is known to occur between states at 268 keV and 77 keV and the 279 keV and 548 keV transitions are known to occur between states at these energies and the ground state. Evidence for the 269 keV transition is quite clear, both K and L conversion lines being apparent. The K line of the 269 keV transition does, however, coincide with the M line from the 191 keV transition. The contribution of the M line accounts for about 30 % of the total intensity of the line if $(M+N)/L = 0.3$ is assumed for the 191 keV transition. The resulting K/L ratio for the 269 keV transition is roughly 4, which corresponds to a value of $\delta^2 = 1$. The 269 keV transition is taken to be the cascade from the 548 keV level to the 279 keV level. No contribution is expected from the 268 keV state since beta decay studies show that this state de-excites entirely by cascading

through the 77 keV level. Furthermore, the intensity of the 269 keV transition is consistent with the value calculated on the basis of a 4% branching intensity from the 548 keV level which has been determined by coincidence measurements [1]).

The results obtained from these measurements are presented in tables 2 and 3 along with other reported values of $B(E2)$ for comparison. The agreement between present values and previously reported values of $B(E2)$ is generally good.

3.4. THE NUCLEI $Th^{230, 232}$ AND $U^{234, 236, 238}$

In addition to the "stable" actinide isotopes Th^{232} and U^{238}, there are several other nucleides in this series having half-lives long enough to render them essentially stable for most purposes. Among the even members of this class of isotopes are three hitherto unstudied by Coulomb excitation; Th^{230}, U^{234} and U^{236}, having half-lives of 8.0×10^4, 2.48×10^5 and 2.39×10^7 years respectively[16]). Milligram quantities of these materials, enriched to about 90 % in the desired isotopes, were obtained through the Atomic Energy Commission † and, together with Th^{232} and U^{238}, were investigated by means of their conversion electron spectra. The states of interest were the first 2^+ states, which lie in every case at about 50 keV above the ground state.

There are special problems in observing the low-energy conversion electrons from these transitions following Coulomb excitation. On the one hand, there is intense background of stopping electrons even when low-energy α particles are used. There is also a strong attenuation of the electron yield due to scattering losses in the Geiger counter window, especially for L shell electrons, which fall below 30 keV. Moreover, it is necessary that thin targets be used in order to avoid scattering and absorption of electrons in the target itself.

The targets finally used in these measurements were in every case less than 50 $\mu g/cm^2$ thick, and were prepared from the natural or the enriched materials which were available originally in the form of oxides. While it was possible to make targets from the oxides which had an average thickness of less than 50 $\mu g/cm^2$, the adverse effect of granularity was apparent in the electron spectra. In an effort to circumvent this difficulty the ThO_2 was converted to $Th(NO_3)_4$ and the U_3O_8 was converted to UO_2Cl_2. Both these compounds gave apparently homogeneous targets, and in addition these compounds were found to undergo decomposition under bombardment, further decreasing the effective thickness for electron scattering. An indication of the homogeneity of targets prepared in this way is provided by a comparison of the shapes of the L lines due to the 67.7 keV transition in Ra^{226} following the α decay of Th^{230} and the A and B lines of the thorium active deposit, which is necessarily thin and uniform.

† These materials were obtained by loan from the U. S. Atomic Energy Commission with the assistance of Drs. G. L. Rogosa and D. C. Davis, Jr.

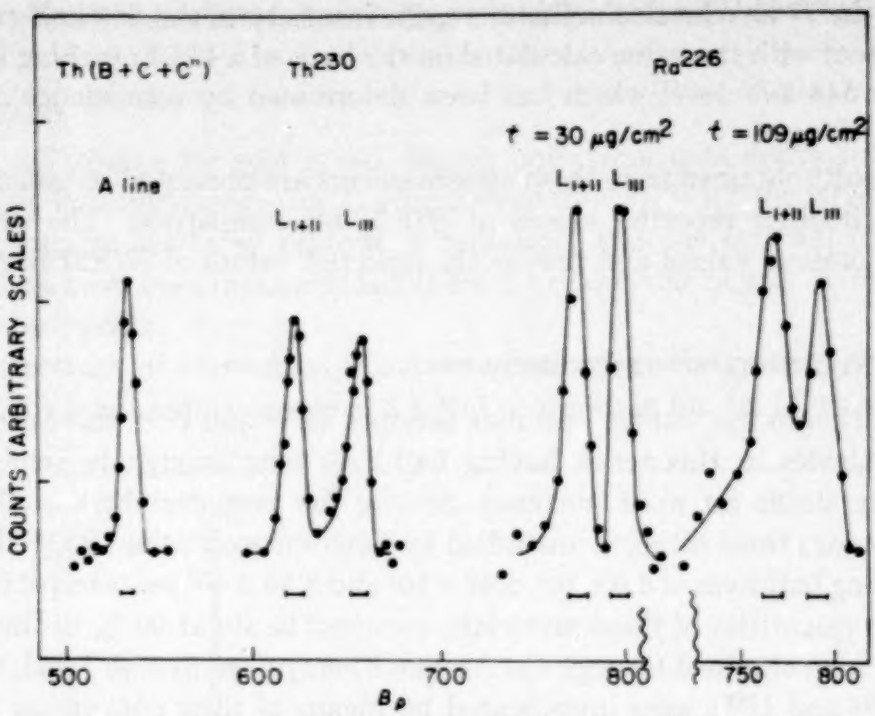

Fig. 11. Comparison of conversion line shapes from Th(B+C+C'') Coulomb excited Th^{230} and Ra^{226}. The electron energies range from about 25 to 50 keV. The target used for the Th^{230} measurement was 30 $\mu g/cm^2$ thick and served as the source for the Ra^{226}. The distortion of the line shapes resulting from a thicker source is shown on the right.

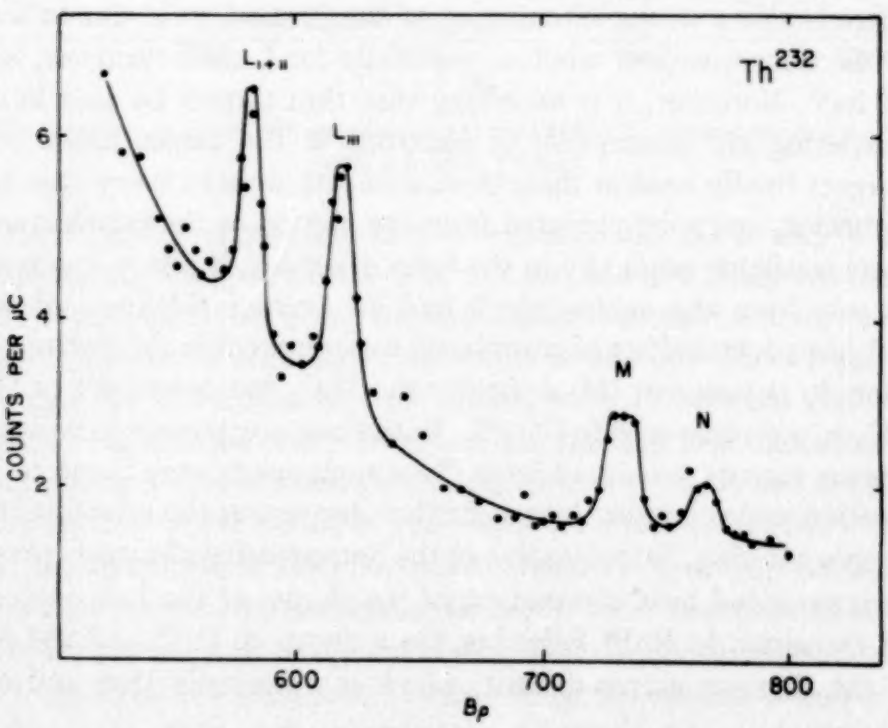

Fig. 12. The spectrum of conversion electrons due to the 50.1 keV transition of Coulomb excited Th^{232} obtained with 2.2 MeV α particles. The target thickness was 10 $\mu g/cm^2$.

This comparison is made in fig. 11 for two Th^{230} targets, 30 $\mu g/cm^2$ and 109 $\mu g/cm^2$ thick respectively. The deterioration of the line shape due to the thicker source is apparent, whereas the thinner source gives line shapes which compare favorably with those from Th(B+C+C''). Also shown, are the L lines from the 53.4 keV Coulomb excited transition in Th^{230} measured with the thinner target which served as a reference in terms of which the homogeneity of the targets

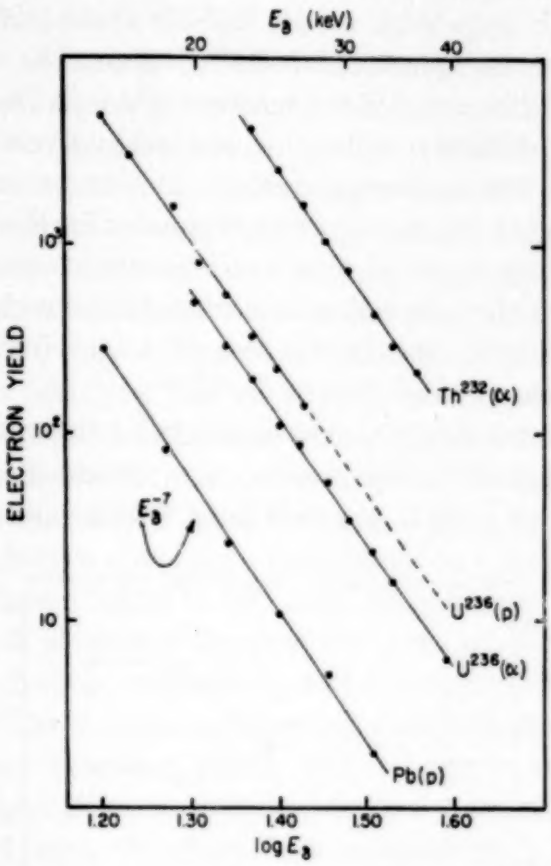

Fig. 13. The logarithm of the stopping electron yield versus the logarithm of the stopping electron energy for various targets having typical thicknesses. The lines through the points give the energy dependence expected from the semi-empirical formula (ref. [1])), but the yield scale is relative. (p) and (α) indicate data taken with proton and α particle bombardment respectively.

prepared for the other isotopes could be estimated. A complete spectrum, representative of those obtained for the low energy transitions, is shown for Th^{232} in fig. 12.

Additional evidence as to the homogeneity of the targets was supplied by the spectra of the stopping electrons, which is expected to display an E_β^{-7} energy dependence for sufficiently thin, homogeneous targets [1]). This dependence was confirmed over the relevant energy interval for the stopping electrons ejected under proton bombardment from a thin evaporated lead target, 46 $\mu g/cm^2$ thick, as well as for the stopping electrons from the targets employed for these measurements, as can be seen in fig. 13.

The spectra of stopping electrons also provided a useful internal check on the thicknesses of the targets as measured by means of the elastically scattered protons. This check was accomplished by comparing the stopping electron yields from the various targets with that measured with the reference Th^{230} target. The thickness of this target was measured carefully by the elastic proton method both before and after taking the electron spectrum, and in addition by determining the yield of the α particles from the radioactive decay which together with knowledge of the half-life leads to an accurate and independent value for the quantity of Th^{230} present. The three measurements agree to within 5%. For some of the targets the normalization of their continuum yields to that of Th^{230} revealed the need for small corrections to the thicknesses obtained by the scattering method, but never exceeding 10 %.

The energies found in this series of measurements for the first 2^+ states agree within error with those reported from radioactivity studies [28]). It was only in the case of Th^{230} that the conversion lines from the α-daughter interfered with those from Coulomb excitation. In this case the L lines from the 67.6 keV state in Ra^{226} obscured the M and N lines in Th^{230}.

The partial and total B(E2)-values obtained for the various transitions are given in tables 2 and 3. Total B(E2)-values were obtained simply by adding the partial B(E2)-values for the L, M and N lines. This is valid because the conver-

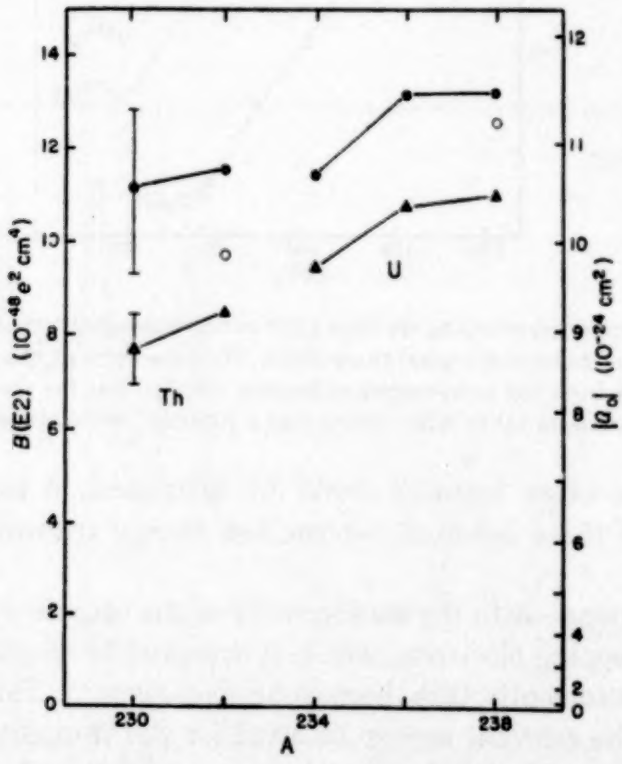

Fig. 14. The reduced transition probabilieties and intrinsic quadrupole moments obtained for the actinide isotopes. For comparison, values obtained by Bell *et al.* [8]) and Elbek *et al.* [9]) are shown by ▲ and ⊙ respectively. Typical errors are indicated.

sion coefficients for all the transitions are greater than 100. The error assigned to the total $B(E2)$-values is about 15% and arises in the same manner as described above except that the uncertainty in the window loss correction factor $C(p)$ of eq. (1) is also taken into account. The average M+N+ . . . to L conversion line intensity ratio obtained from the 6 measurements is 0.31 ± 0.02, which is in agreement with the other reported experimental values of this ratio [29]). The experimental L_{I+II}/L_{III} ratios agree satisfactorily with the theoretical values as may be seen in table 4.

The $B(E2)$-values are seen to be about the same magnitude for all five states, as would be expected from the similarity of their excitation energies. These values are plotted in fig. 14 along with other recently reported values for comparison. It should be noted that again the present $B(E2)$-values are systematically higher by amounts ranging from 20 % to 50% than those obtained from lifetime measurements, which are very strongly dependent on the theoretical conversion coefficients at these transition energies. On the other hand, the present values for U^{238} and Th^{232} agree much better with those of Elbek *et al.*[9]) obtained by inelastic scattering. In view of the large experimental errors quoted for all results, the marginal differences among them should not be taken too seriously and especially so since the present measurements are uncorrected for the angular distribution of the L shell electrons, which may be important. Yet, it is interesting to observe that here a reduction rather than an enhancement of the conversion coefficient might be indicated. Some evidence for such an occurrence in the K shell of several isotopes has been reported recently [30]).

The intrinsic quadrupole moments Q_0 and the deformation parameters δ for each of the thorium and uranium isotopes have been calculated from the $B(E2)$ values in the manner described above, and the results are listed in table 4. In fig. 8, a comparison is made of the values of δ from the present work and that of Bell *et al.* [8]) with the theoretical deformation [7]). It is seen that the observed nuclear distortion in this region of mass also is well represented by the theoretical estimate.

The authors would like to thank Drs. J. P. Schiffer, R. H. Davis and F. W. Prosser Jr., for much valuable assistance in the early stages of this work and Dr. Hans Severeins for several helpful discussions.

References

1) Alder, Bohr, Huus, Mottelson and Winther, Rev. Mod. Phys. **28** (1956) 432
2) Huus, Bjerregaard and Elbek, Mat. Fys. Medd. Dan. Vid. Selsk. **30**, No. 17 (1956)
3) E. M. Bernstein and H. W. Lewis, Phys. Rev. **100** (1955) 1345
4) See e.g. M. C. Olesen and B. Elbek, Nuclear Physics **15** (1960) 134
5) E. M. Bernstein and R. Graetzer. Phys. Rev. **119** (1960) 1321
6) Durham, Rester and Class, Phys. Rev. Letters **5** (1960) 202, and Proc. Intern. Conf. on Nuclear Structure (Kingston), ed. by D. A. Bromley and E. W. Vogt (North-Holland Publishing Co., Amsterdam 1960) p. 594

7) B. R. Mottelson and S. G. Nilsson, Mat. Fys. Skr. Dan. Vid. Selsk. **1**, No. 8 (1959)
8) Bell, Bjørnholm and Severiens, Mat. Fys. Medd. Dan. Vid. Selsk. **32**, No. 12 (1960)
9) Skurnik, Elbek and Olesen, private communication
10) Barloutaud, Lehmann and Leveque, Compt. rend. **245** (1957) 523;
F. K. McGowan and P. H. Stelson, Phys. Rev. **109** (1958) 901
11) Kofoed-Hansen, Lindhard and Nielsen, Mat. Fys. Medd. Dan. Vid. Selsk. **25**, No. 16 (1950)
12) B. D. Pate and L. Yaffe, Can. J. Chem. **33** (1955) 15
13) Beta and gamma-spectroscopy, edited by K. Siegbahn (North-Holland Publishing Co., Amsterdam, 1955)
14) Muller, Hoyt, Klein and DuMond, Phys. Rev. **88** (1952) 775
15) D. E. Alburger and A. W. Sunyar, Phys. Rev. **99** (1955) 695
16) I. Perlman and J. D. Rasmussen, in Encyclopedia of Physics, Vol. 42 (Springer-Verlag, Berlin, 1957)
17) R. D. Lane and D. J. Zaffarano, Phys. Rev. **94** (1954) 960
18) Hill, Church and Mihelich, Rev. Sci. Inst. **23** (1952) 523
19) M. E. Rose, Internal conversion coefficients (North-Holland Publishing Co., Amsterdam, 1958)
20) P. J. Cressman and R. G. Wilkinson, Phys. Rev. **109** (1958) 872
21) Baggerly, Marmier, Boehm and DuMond, Phys. Rev. **100** (1955) 1364
22) Scharff-Goldhaber, Alburger, Harbottle and McKeown, Phys. Rev. **111** (1959) 913
23) N. Ryde and B. Andersson, Proc. Phys. Soc. **68**B (1955) 1117
24) Johns, McMullen, Williams and Nablo, Can. J. Phys. **34** (1956) 69
25) R. M. Diamond and J. M. Hollander, Nuclear Physics **8** (1958) 143
26) F. K. McGowan and P. H. Stelson, Phys. Rev. **107** (1957) 1674
27) F. K. McGowan, private communication
28) Strominger, Hollander and Seaborg, Revs. Mod. Phys. **30** (1958) 585
29) Rasmussen, Slätis and Passell, Phys. Rev. **99** (1955) 42
30) S. Hultberg, private communication

4.E:3.A

Nuclear Physics **22** (1961) 131—137; © *North-Holland Publishing Co., Amsterdam*

Not to be reproduced by photoprint or microfilm without written permission from the publisher

HIGHER-ORDER EFFECTS IN AN ALLOWED POSITON DECAY IN Co^{56}

B. G. PETTERSSON, J. H. HAMILTON † and J. E. THUN

Institute of Physics, University of Uppsala, Uppsala, Sweden

Received 29 August 1960

Abstract: The allowed positon decay of Co^{56} to the second excited state of Fe^{56} has the unusually large log *ft* value of 8.7. A study of the directional correlation of this positon group with the two cascade gamma rays of energy 0.85- and 1.24-MeV which depopulate this level has been measured as a function of beta energy from 0.7 to 1.2 MeV to yield new information about the decay to this level. A magnetic spectrometer was used as the beta analyzer. An anisotropic correlation was measured, $A_{max} = (2.5—3.3)$ % near 1.2 MeV. This is only the third case where any correlation has been observed in an allowed beta decay and it is much larger than the other two. An explanation may be found in higher order terms predicted by the Gell-Mann theory or in terms of cross terms between allowed and second forbidden matrix elements Unfortunately, better theoretical calculations are needed, especially for large *ft* decays, before theory and experiment can be compared favourably.

1. Introduction

The normal theory of beta decay predicts an isotropic beta-gamma directional correlation for allowed beta decay. Gell-Mann has proposed a theory of beta decay which involves an additional term from the meson cloud of the nucleons [1]). This would lead to a term in the beta-gamma directional correlation which is best observed at high beta energy. Such a measurement has been reported by Boehm, Soergel and Stech [2]) in the high-energy beta decay of F^{20}. The anisotropy was small, $A = (0.94 \pm 0.28)$ %, where A is defined in eq. (1). This is near the value of ≈ 0.45 % predicted by the Gell-Mann theory and is the first anisotropy reported in allowed beta-gamma directional correlations.

Also it has been suggested [3, 4]) and studied theoretically [4]) how cross terms between allowed and second forbidden matrix elements or other small effects may give rise to an anisotropic beta-gamma directional correlation in allowed beta decays. This, too, is most pronounced at high beta energy. However, this effect may become more important when the normal allowed matrix elements are reduced. Such cases should be allowed beta decays with large *ft* values, indicative of a reduction in the magnitude of the allowed matrix elements.

While this work was in progress, Steffen [5]), guided by high *ft* values, searched for such higher-order effects in the beta-gamma directional correlations of the

† National Science Foundation postdoctoral fellow on leave from Vanderbilt University, Nashville, Tennessee.

allowed beta decays in Na^{24}, Sc^{46}, Co^{60} and Na^{22} which have log *ft* values from 6.1 to 7.4. Only in Na^{22}(log *ft* = 7.4) was any anisotropy observed and this was quite small, $A = -(0.27 \pm 0.04)$ %. Steffen suggested that the Na^{22} results may be interpreted in terms of the cross terms as given by Morita [4]) although good agreement is lacking.

The decays of Co^{56} and Mn^{56} to levels in Fe^{56}, have been studied recently with scintillation spectrometers [6]). The positon and negaton capture groups of Co^{56} are all reported to be allowed although all have log *ft* values (6.1—8.7) which are greater than those of normal allowed transitions [6]). The main positon group from the 4^+ ground state of Co^{56} to the 4^+ second excited state of Fe^{56} (fig. 1)

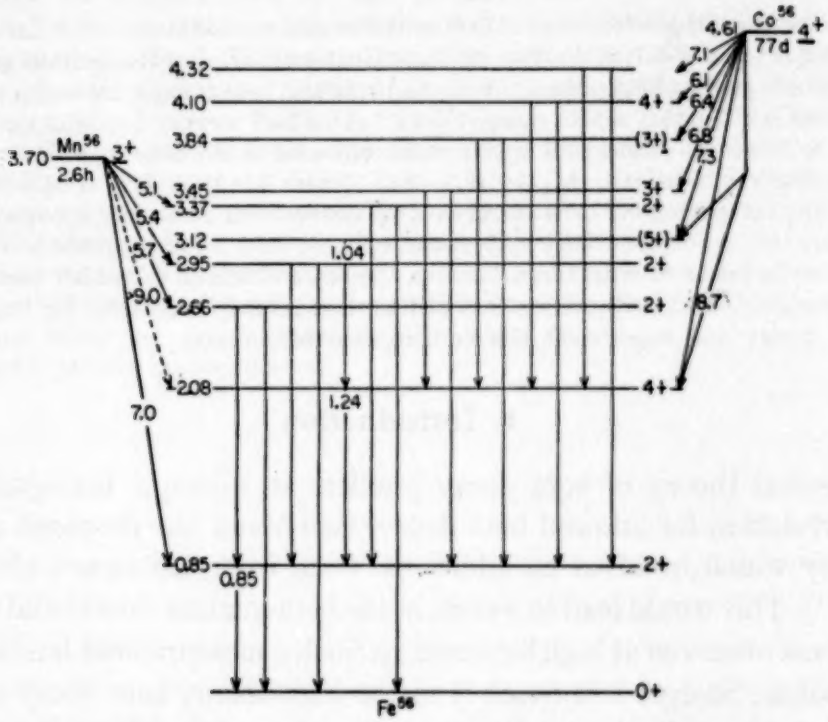

Fig. 1. Decay schemes for Mn^{56} and Co^{56} as taken from ref. [6]). Energies are in MeV. The numbers accompanying the beta branches indicate the measured log *ft* values.

has the unusual log *ft* value of 8.7 (the others in the Co^{56} decay range from 6.1—7.3). This suggests peculiar properties for decay to this level in Fe^{56}. This is supported by an upper limit of 9.0 for the log *ft* for the allowed beta decay of Mn^{56} to this same level. Other groups in Mn^{56} have normal allowed log *ft* values. A careful study of observables such as beta-gamma directional correlation, shape of the beta spectrum, and others should be useful in further analysis of the decays to this 4^+ level in Fe^{56}. The directional correlation of the allowed, 1.5-MeV positon group from the Co^{56} ground state to the second excited state of Fe^{56} with the gamma rays which de-excite this level was measured and an anisotropy observed.

2. Experimental Procedures

The Co^{56} for these studies was produced by an $Fe^{56}(p, n)Co^{56}$ reaction in the cyclotron at Oak Ridge National Laboratory. The iron was dissolved in 6*N* HCl and the iron extracted with ether. The cobalt was purified further by an ion exchange column (Dowex 1 resin). The source was made by electroplating onto a 3.9-mg/cm² palladium foil. The source thickness was well below 100 μg/cm².

The directional correlation of the 1.5-MeV, allowed positon group with the 0.85- and 1.24-MeV gamma rays which depopulate the second excited state (see fig. 1) was measured as a function of beta energy 0.7 to 1.2 MeV. A magnetic lens spectrometer adapted for correlation studies was used [7]). Further details are given elsewhere [8]). The beta spectrometer was set at a momentum resolution of 9 % for the analysis of the positons. The gamma rays were detected in a 6.4 cm diameter × 5.1 cm thick NaI(Tl) crystal which was coupled to a DuMond 6363 photomultiplier tube. A fast-slow coincidence analyzer was used where $2\tau_0 = 4 \times 10^{-8}$ sec for the fast circuit; $2\tau_0$ was measured to be constant to within 2 % throughout the entire measuring period.

The gamma analyzer was set to accept all pulses which corresponded to photons with energy greater than 750 keV (see fig. 2). Thus, the photopeaks and

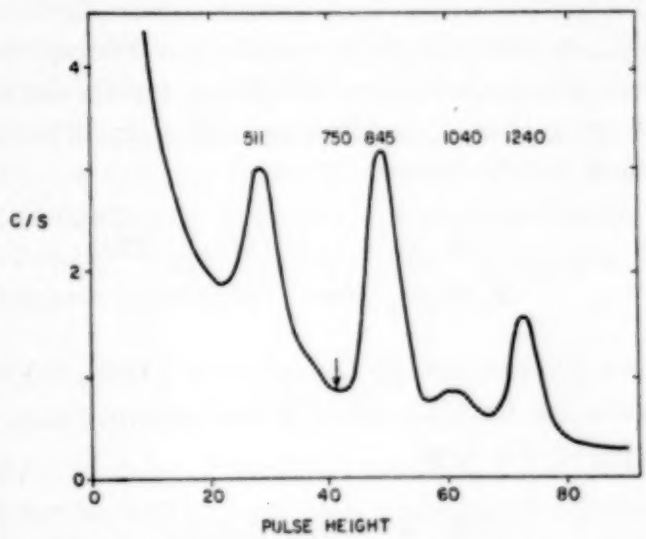

Fig. 2. Co^{56} gamma singles spectrum in the energy range of interest as measured with the gamma detector of the beta-gamma spectrometer. The vertical scale is counts per second; the numbers are relative.

part of the Compton distributions of the 0.85-, 1.04- and 1.24-MeV gammas were accepted. Acceptance of this broad energy region in the gamma spectrum was necessary to obtain good coincidence counting rates. The correlation is not hurt by this; however, one must consider the correlation of the beta rays with the two cascading gamma rays. This complication is considered in the analysis Only the 1.04 MeV gamma appears to be strong enough to possibly effect the

true correlation and its intensity was $\lesssim 5\,\%$ of the intensity of the other two gamma rays accepted. However, the 1.04 MeV gamma ray is not in coincidence with beta rays of the energy accepted. This is also true for all the other higher energy gamma rays. Therefore the measured correlation is that of the beta rays of the accepted energy with the two cascade gamma rays which depopulate this second excited state undistorted by other gamma rays.

The gamma detector was rotated every 1000 sec between 90°, 180° and 270°. The centering at the source was determined with an accuracy of 0.1 % and checked each day. The difference between the gamma single rates at the different angles was less than 0.6 %. The positon single and coincidence counting rates were measured at each setting, and the single gamma rates every few hours at each angle. Both the positon and gamma-ray single rates decayed with the reported half-life of 77 days. The true/accidental ratio was greater than 20 for every measurement. Approximately 80000 coincidences were recorded for each beta energy at 180° and (90°+270°).

The anisotropy was calculated from

$$A = \left[\frac{N_c(180)}{N_\gamma(180)N_\beta(180)} \Big/ \frac{\langle N_c(90)\rangle_{av}}{\langle N_\gamma(90)\rangle_{av}\langle N_\beta(90)\rangle_{av}}\right] - 1, \tag{1}$$

where N_c, N_γ, N_β, are the coincidence counts, gamma-ray single counts and beta-ray single counts respectively and $\langle N(90)\rangle_{av}$ means the average of $N(90)$ and $N(270)$. This corrects for small differences in the single rates. The reliability of this was checked by the ratio

$$F = \frac{N_c(90)}{N_\gamma(90)N_\beta(90)} \frac{N_\gamma(270)N_\beta(270)}{N_c(270)}, \tag{2}$$

which should be one. Experimentally this ratio was 1.003 ± 0.005.

A above was corrected for solid angles in the following way. The correlation was assumed to be of the form

$$N(\theta) = 1 + A_2 P_2(\cos\theta); \tag{3}$$

then

$$A_2 = \frac{2A}{3+A}, \tag{4}$$

and

$$A_2(\text{corrected}) = \frac{A_2}{A_\beta A_\gamma}. \tag{5}$$

The correction factors were $A_\beta = 0.92$ and $A_\gamma = 0.96$.

3. Results

The results are given in table 1. The errors are stastistical ones.

TABLE 1

Measured beta-gamma directional correlation coefficient A_2 as a function of beta energy

Beta energy (keV)	A_2(corr ted) in %
700	0.9±0.3
1000	1.1±0.6
1100	2.2±0.5
1200	1.2±0.4

These results are quite large for an allowed decay. Only in the F^{20} and Na^{22} decays, have anisotropic beta-gamma directional correlations been reported [2, 5]) in allowed beta decay and these are both small, $A \lesssim 1$ %. This new result in Co^{56} has $A_{max} = (2.5—3.3)$ % (an order of magnitude greater than the Na^{22} result).

The equipment has been carefully checked for possible instrumental distortions which might give anisotropic directional correlations but none were found. The beta-gamma directional correlation in Co^{60} which is known to be isotropic [5]), has been measured to have $A = 0 \pm 0.002$. Additional checks indicate no instrumenal distortions of the result. Anisotropic beta-gamma directional correlations with A_{max} from -2.3 % to $+38$ % have been measured in the once forbidden beta decays in Ag^{111}, Pa^{233} and Rb^{86} in the last one and a half years with this equipment [8]), as well as several conversion electron-gamma directional correlations. These experiments all support the reliability of the equipment to measure true correlations.

4. Analysis

The spins and the parities of the levels involved in this beta-gamma-gamma cascade are well established and the beta transition is allowed on the basis of spins and parities [6, 9]). Kienle and Segel have discussed in terms of the shell model how the transitions from Co^{56} to Fe^{56} are l-forbidden and how the transitions to the first excited state of Fe^{56} from Mn^{56} are also l-forbidden but transitions to the upper levels are not [6]). This l-forbiddenness could retard all these decays and give them anomalous ft values. Then all these decays should have similar larger than normal ft values. Indeed according to Kienle and Segel, five of the six Co^{56} decays and this Mn^{56} decay have log ft values between 6.1 and 7.3. Three other decays in Mn^{56} which should not be l-forbidden have log ft values between 5.1 and 5.7 as may be expected for normal allowed transitions. However, decays from Mn^{56} and Co^{56} to the 4^+, second excited

state in Fe^{56} have much higher log *ft* values (> 9.0 and 8.7 respectively) than the other *l*-forbidden transitions. The anomalous behaviour of these two decays is difficult to understand.

The large beta-gamma directional correlation reported here supports the anomalous behaviour of decays to this level. The normal Gell-Mann term and the normal Morita cross terms are much too small to account for these results. To correct the Gell-Mann predictions for the large *ft* value is difficult as Steffen pointed out [5]). Rough calculations indicate that if the normal Gell-Mann and Morita terms are corrected for this anomalous *ft* value, the theoretical anisotropy can be made in both cases higher than the experimental one. Unfortunately, because of a sign ambiguity in the matrix elements, the measured sign of the anisotropy does not help distinguish between the formulations of Morita and Gell-Mann.

Before better comparisons between theory and experiment can be made better theoretical calculations of higher order effects in beta-gamma correlations are needed. It is hoped that these results which offer a good case for comparison will stir further theoretical considerations of this problem.

In view of the anomalies in *ft* value and beta-gamma directional correlation, a more careful study of the positon spectrum is being made now to see if it deviates from the allowed shape [10]). The Fermi-Kurie plot has been reported previously to be allowed [11]) with some question about a possible weak second group with $E_{max} \approx 900$ keV, the highest energy a second group could have in the present level scheme. Even if this weak second group exists it should not affect our data at even 700 keV because of its weak intensity near its end point. The $\beta^+ - \gamma$ coincidence measurements do not indicate such a group [6, 9]). New studies to date do not indicate a group with an energy of ≈ 900 keV [10]).

The authors wish to thank Dr. R. E. Segel for calling our attention to this problem. We also wish to thank Professor R. M. Steffen for helpful discussions.

We are indebted to Professor Kai Siegbahn for the use of the laboratory. One of us (J. H. H.) wishes to thank Professor Siegbahn and others at the Institute for their kind hospitality. One of us (J. H. H.) gratefully acknowledges a National Science Postdoctoral Fellowship which made these studies possible for him.

References

1) M. Gell-Mann, Phys. Rev. **111** (1958) 362
2) F. Boehm, V. Soergel and B. Stech, Phys. Rev. Letters **1** (1958) 77
3) T. Kotani and M. Ross, Phys. Rev. **113** (1959) 622
4) M. Morita, Phys. Rev. **113** (1959) 1584
5) R. M. Steffen, Phys. Rev. Letters **3** (1959) 277
6) P. Kienle and R. E. Segel, Phys. Rev. **114** (1959) 1554
7) T. R. Gerholm and B. G. Pettersson, Nuclear Instruments **4** (1959) 107

8) J. H. Hamilton, B. G. Pettersson and J. M. Hollander, Arkiv Fysik **18** (1960) 273
J. H. Hamilton, J. M. Hollander, B. G. Pettersson and B. N. Subba Rao (to be published);
J. H. Hamilton, B. G. Pettersson and J. M. Hollander, Bull. Am. Phys. Soc. **4** (1959) 426
9) A. N. Diddens, W. J. Huiskamp, J. C. Severiens, A. R. Miedema and M. J. Steenland, Nuclear Physics **5** (1958) 58
10) J. H. Hamilton, L. M. Langer and D. R. Smith (to be published)
11) M. Sakai, J. L. Dick, W. S. Anderson and J. D. Kurbatov, Phys. Rev. **95** (1954) 101;
K. P. Howard, T. A. Pond and P. S. Jastram, private communication to Nuclear level schemes, $A = 40$—$A = 92$, compiled by K. Way, R. W. King, C. L. McGinnis and R. van Lieshout, Atomic Energy Commission Report TID-5300 (U.S. Government Printing Office, Washington, D. C., 1955);
C. S. Cook and F. M. Tomnovec, Phys. Rev. **104** (1956) 1407;
P. S. Jastram, private communication;
J. D. Kurbativ, private communication

2.E

Nuclear Physics **22** (1961) 138—144; © *North-Holland Publishing Co., Amsterdam*

Not to be reproduced by photoprint or microfilm without written permission from the publisher

THE ELASTIC SCATTERING OF 19.5 MeV DEUTERONS BY KRYPTON

P. E. HODGSON,
Clarendon Laboratory, Oxford
J. AGUILAR, A. GARCÍA,
Department of Physics, University of Valencia
and
J. B. A. ENGLAND,
Department of Physics, University of Birmingham

Received 19 September 1960

Abstract: Experimental elastic differential cross-sections for the scattering of 19.5 MeV deuterons by krypton in the range 13° to 90° in the centre of mass system have been measured using a nuclear emulsion plate camera. The results are compared with calculations based on the optical model of the interaction.

1. Introduction

In a previous paper, by England, McKeague and Hodgson [1]), experimental results on the elastic scattering of 19.5 and 19.0 MeV deuterons from krypton and xenon were reported. An attempt was made to fit these results with a simple optical model. The experimental results did not cover a large enough angular range to justify a detailed optical model analysis and the best fit parameters obtained for these results were therefore of a preliminary nature.

In the present work the elastic angular distribution of 19.5 MeV deuterons scattered by krypton has been extended to 90° in the centre of mass system and a detailed optical model analysis of the distribution has been made.

2. Experimental Method

The use of a gas scattering nuclear emulsion camera, with an external beam from the Nuffield Cyclotron of the University of Birmingham, has been described in detail by England *et al.* [1]) and by Gibson, Prowse and Rotblat [2]). The plates were examined for deuterons elastically scattered by krypton over the angular range 13° to 89° in the centre of mass system.

Up to 70° the elastically scattered particles were distinguished by their range in emulsion, but above this angle geometric considerations made it impossible to measure the full range and therefore all tracks whose range was greater than 700 μm were ascribed to elastically scattered deuterons, although most of them

escaped through the glass of the plates. At high angles inelastic processes give rise to appreciable numbers of tracks which were possibly included in these measurements. This must be taken into consideration when comparing the best fit optical model curve with the experimental measurements in the angular range 80° to 90° in the centre of mass system. At smaller angles, inelastic processes do not contribute appreciably to the cross-sections. This was verified by scanning some angles between 60° and 70° by two methods; firstly with identification of the elastically scattered particles by their range in emulsion and secondly with a count of the total number of tracks over the given 700 μm range. The cross-sections obtained by these two methods were equal within the limits of the statistical errors on the numbers of tracks observed.

3. Experimental Results

The experimental elastic differential cross-sections for deuterons of 19.5 MeV scattered by krypton are shown in fig. 1. The results show diffraction maxima

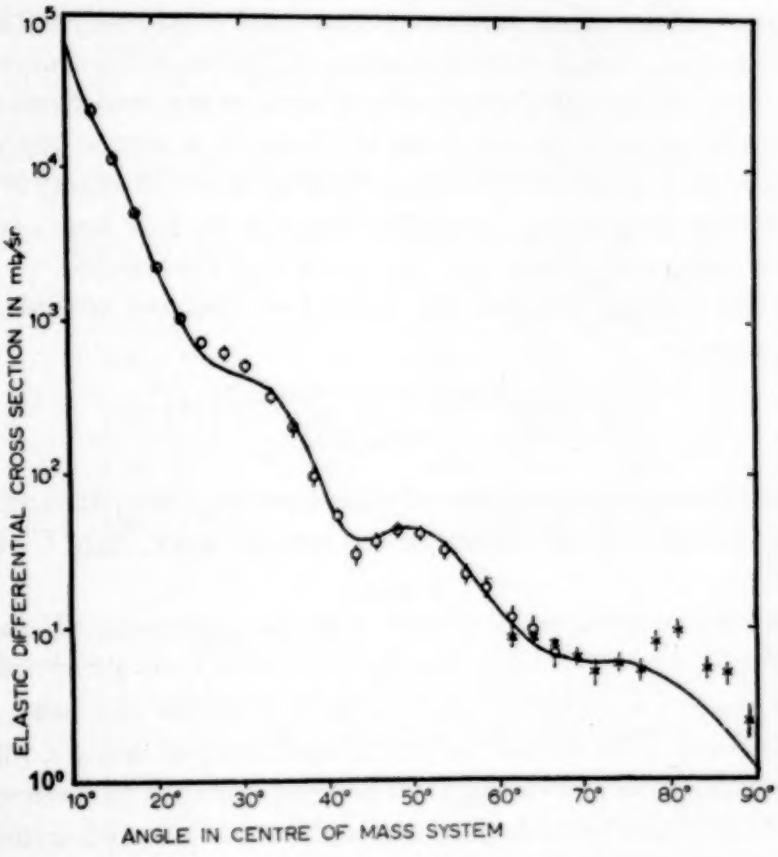

Fig. 1. Elastic scattering of 19.5 MeV deuterons from krypton. The observed cross-sections for the centre of mass system are plotted as a function of centre of mass angle. The experimental results are compared with calculations based on the optical model using parameters of value $U = -35$ MeV, $W = -9.5$ MeV, $r_0 = 1.60 \times 10^{-13}$ cm and $a = 0.52 \times 10^{-13}$ cm.
○ experimental (England), ✕ experimental (Aguilar and García) and ——— theoretical (Hodgson).

and minima which are similar to those obtained by other workers at similar energies, Greenlees and Lowe [3]) at 19.6 MeV, Yntema [4, 5]) at 21.6 MeV, Fischer and Fischer [6]) at 21 MeV and Freemantle, Gibson, Prowse and Rotblat [7]) at 19 MeV.

4. Optical Model Analysis

The angular distribution was calculated using an optical model potential with both refracting and absorbing parts: $V(r) = Uf(r)+iWf(r)$, where the radial variation has the Saxon-Woods form $f(r) = (1+\exp((r-R)/a))^{-1}$ with a nuclear radius $R = r_0 A^{\frac{1}{3}}$ and a parameter a determining the diffuseness of the nuclear surface. The same radial variation was used for the refracting and absorbing parts of the potential and no account was taken of the deuteron spin. Details of the method of calculation are given by Buck, Maddison and Hodgson [8]). This method also provides a value for the reaction cross-section for the interaction.

In the previous work [1]) the differential cross-sections corresponding to several trial sets of the parameters were compared graphically with the experimental distribution. Some empirical rules on the way the cross-sections are affected by each of the parameters in turn were found, and these enabled the parameters to be varied to give the best fit. However, a precise analysis requires goodness of fit to be precisely defined so that the best set or sets of parameters can be unambiguously found. It is also desirable to find how accurately the experimental data determines the parameters of the model.

To make this analysis possible, the best fit was defined as that which minimises the quantity

$$\Delta = \sum \left(\frac{(\mathrm{d}\sigma/\mathrm{d}\Omega)_{\mathrm{Th}} - (\mathrm{d}\sigma/\mathrm{d}\Omega)_{\mathrm{Exp}}}{\delta(\mathrm{d}\sigma/\mathrm{d}\Omega)_{\mathrm{Exp}}} \right)^2,$$

the summation being extended over all experimental points. This Δ is a function of all the parameters of the model; in the present work, only U, W, a and r_0 were varied.

The procedure adopted was to begin with the parameters $U = -35$ MeV, $W = -15$ MeV, $a = 0.6\times10^{-13}$ cm, $r_0 = 1.6\times10^{-13}$ cm previously found to give a good fit, and to calculate Δ for a mesh of values of U and W, keeping a and r_0 constant. This defines a bowl-shaped surface with a minimum for $U \approx -32.5$ MeV, $W \approx -13$ MeV. Then keeping U and W to these values Δ was calculated for a mesh of a and r_0, giving another surface with a minimum at $a \approx 0.56\times10^{-13}$ cm, $r_0 \approx 1.58\times10^{-13}$ cm. With these values another Δ surface was constructed for U and W and so on. The process was repeated until the final minimum was found. The surfaces for the successive iterations are shown in tables 1—6. In no case was there any suggestion of other minima, though conceivably these could exist in other regions of parameter space. The final

value of $\Delta = 132$ corresponds to a very low probability that the theoretical curve is consistent with the 31 experimental points. However, if the contributions $\delta\Delta$ of the individual experimental points to Δ are examined, it is found that a few of them are abnormally large: the largest is 39.9, the next three largest total 34.6, and the next four 27.6, leaving a Δ of only 29.9 for the remaining 23 points. This corresponds to a probability of about 0.2, indicating consistency between the experimental and theoretical distributions. It is possible that some of the eight experimental points with large $\delta\Delta$ are in error, but as three of them are around 27° and four around 82°, it is more likely that a significant discrepancy is indicated.

TABLE 1

Δ as a function of U and W for $r_0 = 1.6$, $a = 0.6$. U and W are in MeV and r_0 and a are in 10^{-13} cm

W \ U	−30	−32.5	−35	−37.5	−40
−11		276	291		482
−13	297	274	293		420
−15	285	277			

TABLE 2

Δ as a function of r_0 and a for $U = -32.5$, $W = -13$. U and W are in MeV and r_0 and a are in 10^{-13} cm

r_0 \ a	0.54	0.56	0.58	0.60	0.62
1.56	225	215	228		
1.58	213	212	231	266	
1.60		218	242	274	329
1.62				300	

TABLE 3

Δ as a function of U and W for $r_0 = 1.58$, $a = 0.56$. U and W are in MeV and r_0 and a are in 10^{-13} cm

W \ U	−30	−32.5	−35	−37.5	−40
−8		294	197		
−10			167		306
−12	266		181		
−13		212			
−14	251		204		

TABLE 4

Δ as a function of r_0 and a for $U = -35$, $W = -10$. U and W are in MeV and r_0 and a are in 10^{-13} cm

r_0 \ a	0.50	0.52	0.54	0.56	0.58
1.56			172		207
1.58		150		167	
1.60	157	136	145		229
1.62		153	170		

TABLE 5

Δ and σ_R as a function of U and W for $r_0 = 1.6$, $a = 0.52$. U and W are in MeV, r_0 and a are in 10^{-13} cm and σ_R is in mb.

W \ U	−34	−35	−36	−34	−35	−36
−8.5		142			1781	
−9	147	133	151	1779	1784	1788
−9.5		132			1786	
−10	146	136	149	1783	1788	1793
−10.5	152	143		1784	1789	
−11	161	153		1785	1790	

TABLE 6

Δ and σ_R as a function of r_0 and a for $U = -35$, $W = -9.5$. U and W are in MeV, r_0 and a are in 10^{-13} cm and σ_R is in mb.

r_0 \ a	0.51	0.52	0.53	0.51	0.52	0.53
1.58		153			1743	
1.60	138	132	134	1770	1786	1802
1.62		146			1829	

The large $\delta\Delta$ for the four points around 82° may, however, be due to the contribution of inelastic reactions to the measured cross-sections.

This method is not the most efficient way of finding the minimum value of Δ, and more powerful methods are at present being investigated. However, it is worthwhile working through it once to show in detail how the goodness of fit depends on the four parameters chosen. The convergen[illegible]f the method might have been more rapid if use had been made of the insensitivity of the distribution

to those variations of U and r_0 that keep Ur_0^2 constant. Investigation showed, however, that the distribution is not completely insensitive to these changes, so this was not done. The variation of Δ with U in two regions of parameter space when Ur_0^2 is kept constant is shown in table 7.

TABLE 7

Variation of Δ with U, keeping Ur_0^2 constant, in two regions of parameter space. In the first the other parameters are $W = -9.5$, $a = 0.52$, and in the second $W = -13$, $a = 0.56$. U and W are in MeV and r_0 and a are in 10^{-13} cm

U	r_0	Δ	σ_R	U	r_0	Δ	σ_R
−32	1.673	174	1930	−33.339	1.56	202	1761
−35	1.6	132	1786	−32.5	1.58	212	1799
−38	1.536	205	1665	−31.693	1.60	227	1838

The calculated reaction cross-section σ_R is also given in tables 5 and 6 in the region of best fit. As was found previously, this is sensitive to r_0 and a. It will be an important test of the present analysis to measure the reaction cross-section and compare it with the calculated values. The accuracy to which the parameters of the model are determined may be estimated from tables 5 and 6 to be about ± 1 MeV for the potentials and $\pm 0.02 \times 10^{-13}$ cm for r_0 and a. These values can only be considered provisional while Δ remains high and the reaction cross-section is not known.

There is some evidence that the radial variation of the potential is not the same for the real and imaginary parts, so it is useful to see if different r_0 and a for them improves the fit in the present case. The results of a preliminary investigation of this are given in table 8, and show no significant improvement.

TABLE 8

Variation of radial form factors for refracting and absorbing potentials, keeping $U = -35$ MeV., $W = -9.5$ MeV.

U		W		Δ	σ_R
r_0	a	r_0	a		
1.6	0.51	1.6	0.53	139	1777
1.6	0.53	1.6	0.51	137	1795
1.58	0.52	1.62	0.52	168	1752
1.62	0.52	1.58	0.52	156	1824

The spin-orbit forces have not been taken into account in this analysis. It is possible that their inclusion would improve the agreement between theory and experiment.

We would like to express our thanks to Professor G. E. Brown, Professor W. E. Burcham, F. R. S., and Professor D. H. Wilkinson, F. R. S., for valuable discussions, to Dr. L. Fox, Director of the Oxford University Computing Laboratory, for permitting us to use the Mercury computer, to Dr. B. Buck and Mr. R. N. Maddison for their work on the computer programme, to Mrs. D. E. Anderson, Miss M. Crozier and Miss A. Iscar for the microscope work, to Miss N. Reynolds, Miss S. Tilley and the staff of the Computing Laboratory for their assistance, and to the D.S.I.R. for its support.

References

1) J. B. A. England, R. McKeague and P. E. Hodgson, Nuclear Physics **16** (1960) 52
2) W. M. Gibson, D. J. Prowse and J. Rotblat, Proc. Roy. Soc. **243** (1957) 237
3) G. W. Greenlees and J. Lowe, Proc. Phys. Soc. **76** (1960) 149
4) J. L. Yntema, Phys. Rev. **113** (1959) 261
5) J. L. Yntema, Phys. Rev. **114** (1959) 820
6) G. E. Fischer and V. K. Fischer, Phys. Rev. **114** (1959) 533
7) R. G. Freemantle, W. M. Gibson, D. J. Prowse and J. Rotblat, Phys. Rev. **92** (1953) 1268
8) B. Buck, R. N. Maddison and P. E. Hodgson, Phil. Mag. (1960) (in print)

3.A

Nuclear Physics **22** (1961) 145—156; © *North-Holland Publishing Co., Amsterdam*

Not to be reproduced by photoprint or microfilm without written permission from the publisher

THE GYROMAGNETIC RATIO OF THE 80 keV ROTATIONAL STATE OF ERBIUM 166

E. BODENSTEDT, H. J. KÖRNER, C. GÜNTHER and J. RADELOFF

II. Institut für Experimentalphysik der Universität Hamburg

Received 8 August 1960

Abstract: The angular correlation of the (1380 keV) – (80 keV) gamma-gamma cascade in the decay of 27 h Holmium 166 has been measured in an external magnetic field of 13 550 G. The observed rotation yields for the nuclear g-factor of the 80 keV 2+ rotational state

$$g_R = +0.260 \pm 0.034.$$

A paramagnetic correction factor of $\beta = 8.36$ ($B_{eff} = \beta\, B_{ext}$) has been applied in the calculation of this value.

There is a strong attenuation of the (1380 keV) – (80 keV) angular correlation by internal fields. The attenuation factors for a liquid source of $HoCl_3$ in aqueous solution were determined as

$$G_2 = 0.80 \pm 0.08, \quad G_4 = 0.56 \pm 0.04.$$

A measurement of the (1380 keV) – (80 keV) angular correlation for different delays showed agreement with a time dependent attenuation

$$A_k(t) = A_k(0)\, e^{-\lambda_k t},$$

where the λ_k are

$$\lambda_2 = 0.09 \times 10^9\ \mathrm{sec}^{-1}, \quad \lambda_4 = 0.30 \times 10^9\ \mathrm{sec}^{-1}.$$

The ratio of λ_4/λ_2 suggests that the attenuation is caused mainly by magnetic interaction between the 4f electron shell and the magnetic moment of the nucleus. The spin relaxation time for the 4f electron shell was calculated as

$$\tau_J = (3.4 \pm 0.9) \times 10^{-13}\ \mathrm{sec}.$$

1. Introduction

The magnetic moments of the rotational states of even-even nuclei provide a sensitive test of the theory of the nuclear rotational motion. The experimental determination by the method of perturbing angular correlations or angular distributions by external magnetic fields is very difficult in most cases, since the interesting strongly deformed nuclei are mainly the rare earth elements and the transuranic elements which show strong paramagnetism of the electron shells. In the case of the rare earth elements the increase of the effective magnetic field at the position of the nucleus recently has been calculated with an accuracy of 5 % [1–4]; but it is uncertain how fast the final electronic configuration is reached after the β-decay of the mother isotope or after the Coulomb excitation process. A rather reliable correction for the paramagnetism can be made, however, for those cases of radioactive sources where the mother element

and the daughter element have approximately the same paramagnetic field. One of the most advantageous cases is Holmium 166 which decays by β^--transitions into excited states of the even-even nucleus Erbium 166. Therefore, this nucleus has been chosen for this investigation.

2. The Angular Correlation of the 0^+—2^+—0^+ Cascade of Erbium 166

The decay scheme of 27 h Holmium 166 is shown in fig. 1. The main fraction of the β^--transitions leads to the 80 keV-rotational state and the ground state of

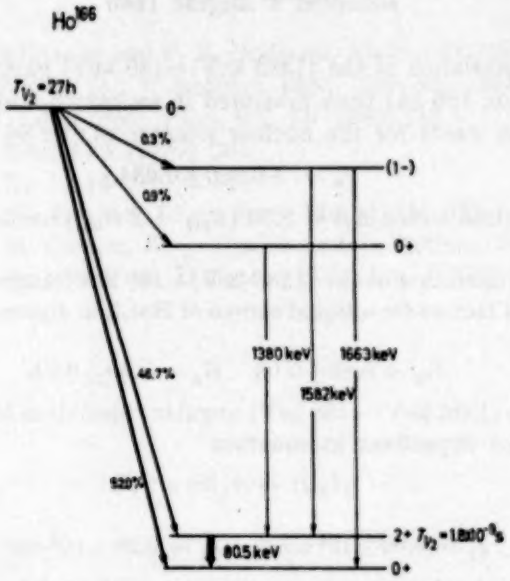

Fig. 1. Decay scheme of 27 h Holmium 166.

Erbium 166. Only a fraction of a percent populates the 1663 keV and the 1460 keV levels from which the 1582 keV—80 keV cascade and the 1380 keV—80 keV cascade go to the ground state.

Evidence for the rotational character of the 80 keV level follows from the characteristic spin sequence and the excitation energy ratios of the 0^+, 2^+, 4^+, 6^+ band which was found in the decay of the $>$ 30y Holmium 166 isomeric state [5]). Another argument is the half life of 1.8×10^{-9} sec of the 80 keV level. This is by a factor of about 100 shorter than the expectation for a single particle transition.

We have repeated the half life measurement by the method of delayed coincidences between the 1380 keV and the 80 keV gamma lines and obtained the result of fig. 2. The least square fit yields

$$T_{\frac{1}{2}} = (1.98\pm0.21)\times10^{-9}\ \text{sec}$$

in agreement with the results of earlier measurements [6–9]).

The angular correlation of the (1380 keV)—(80 keV) cascade has been measured by J. S. Fraser and J. D. C. Milton [10]) and by I. Marklund *et al.* [11]).

In both investigations a strong attenuation of this angular correlation by internal fields was found. J. S. Fraser and J. D. C. Milton used a source of molten $Ho(NO_3)_3$ and found

$$A_2 = +0.127 \pm 0.004, \quad A_4 = +0.56 \pm 0.02.$$

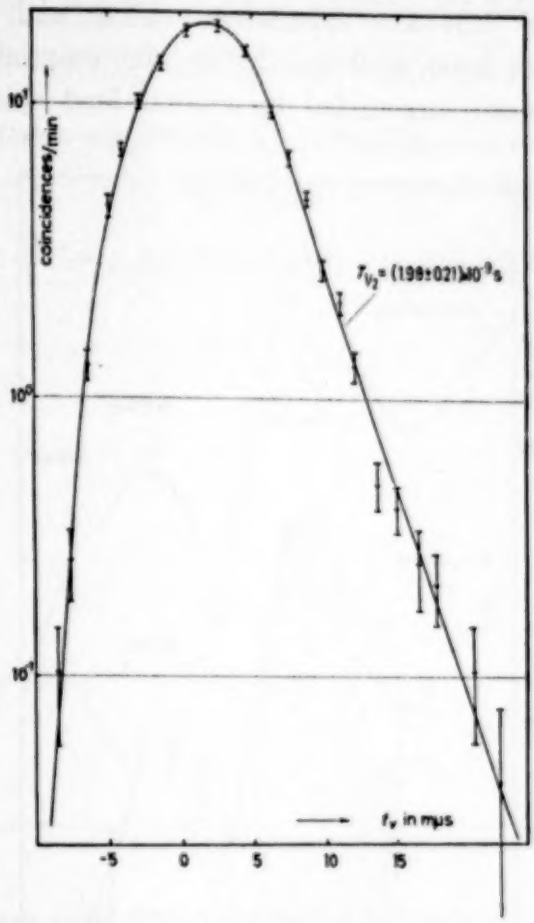

Fig. 2. Measurement of the half life of the 80 keV level by the method of delayed coincidences between the 1380 keV and the 80 keV gamma rays.

By a comparison with the theoretical values for a 0^+, 2^+, 0^+ cascade they derived for the integral attenuation factors

$$G_2 = 0.38 \pm 0.01 \quad \text{and} \quad G_4 = 0.49 \pm 0.02.$$

I. Marklund *et al.* found for a liquid source of $HoCl_3$ in aqueous solution

$$A_2 = +0.225 \pm 0.010, \quad A_4 = +0.79 \pm 0.03,$$

which corresponds to attenuation factors of

$$G_2 = 0.63 \pm 0.03 \quad \text{and} \quad G_4 = 0.69 \pm 0.03.$$

The authors pointed out, that $G_4 > G_2$ as predicted by A. Abragam and R. V. Pound [12]) for attenuations by time dependent electric interactions.

For the determination of the nuclear g-factor by angular correlation measure-

ments a precise knowledge of the attenuation by internal fields and its time dependence is necessary. Therefore, a reinvestigation of the perturbation of the (1380 keV)—(80 keV) angular correlation has been performed.

The 27 h Holmium 166 activity has been produced by neutron irradiation of Ho_2O_3 in the Saclay pile. The source was prepared as an unsaturated solution of $HoCl_3$ in water. A "fast-slow"-coincidence circuit with a resolving time of $2\tau = 8 \times 10^{-9}$ sec has been used for the angular correlation measurements. The NaI-detectors were surrounded by conical lead shields. In addition a

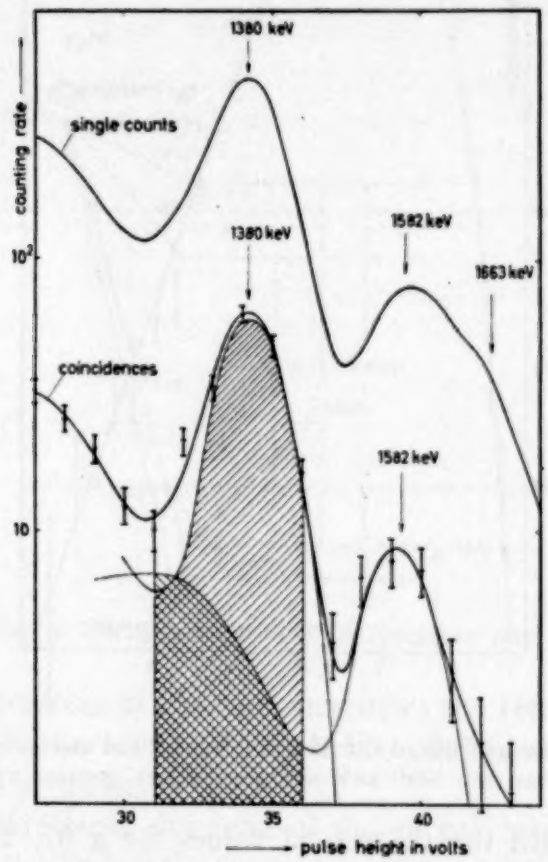

Fig. 3. Coincidence spectrum with the 80 keV gamma line. The setting of the single channel analyser accepting the 1380 keV gamma ray for the measurement of the (1380 keV) — (80 keV) angular correlation is drawn in. The double shaded area indicates the contribution from the 1582 keV gamma line.

2g/cm² lead absorber in front of the high energy detector has been used to reduce 180° back scattering effects. The setting of the single channel analyser on the 80 keV photopeak prevents an unreasonable admixture from the K X-ray peak. The channel for the 1380 keV line contains, however, 13.1 % admixture of the 1582 keV radiation as obtained from an analysis of the coincidence spectrum (fig. 3).

The result of the present angular correlation measurement is shown in fig. 4.

The coefficients, corrected for the solid angles of the detectors are

$$A_2 = +0.209 \pm 0.020 \quad \text{and} \quad A_4 = +0.584 \pm 0.033.$$

For a correction of the 1582 keV admixture the angular correlation of the (1582 keV)−(80 keV) cascade must be known. We found

$$W(\theta) = 1 - (0.29 \pm 0.06) P_2(\cos\theta) + (0.19 \pm 0.12) P_4(\cos\theta),$$

in agreement with the measurement by I. Marklund *et al.* [11]). The final result for the (1380 keV)−(80 keV) angular correlation of the liquid source is now

$$W(\theta) = 1 + (0.285 \pm 0.030) P_2(\cos\theta) + (0.642 \pm 0.045) P_4(\cos\theta)$$

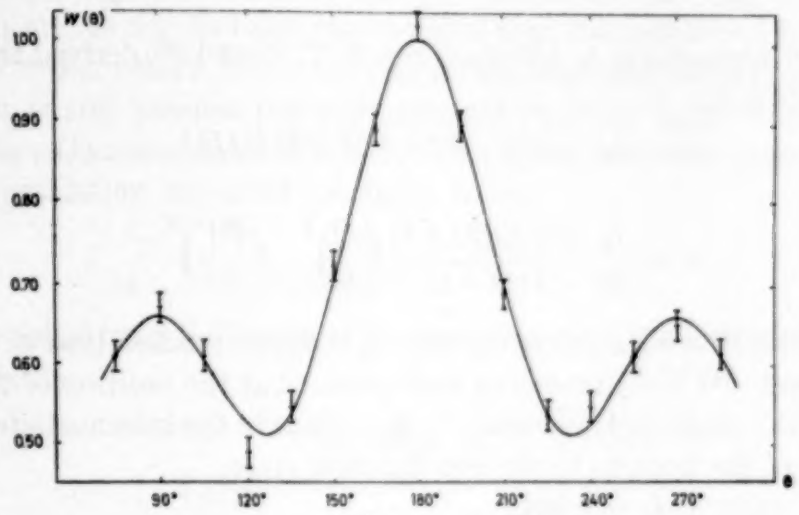

Fig. 4. Angular correlation of the (1380 keV)−(80 keV) cascade. The curve shows the result of the least squares fit to the experimental points. The corrections for the contribution of the (1582 keV)−(80 keV) angular correlation and for the solid angles of the detectors (3.8 cm × 2.5 cm NaI crystals have been used at a distance of 70 mm) have not yet been applied.

The comparison with the theoretical angular correlation for a 0^+, 2^+, 0^+ cascade,

$$W(\theta) = 1 + 0.3571 P_2(\cos\theta) + 1.1428 P_4(\cos\theta),$$

gives for the integral attenuation coefficients

$$G_2 = 0.80 \pm 0.08 \quad \text{and} \quad G_4 = 0.56 \pm 0.04.$$

There is some discrepancy compared to the results of I. Marklund *et al.* [11]) since the attenuation factor G_4 is smaller than G_2. The ratio $G_4/G_2 < 1$ as determined by our measurement is not compatible with the prediction of A. Abragam and R. V. Pound [12]) for a time dependent electric interaction.

3. Attenuation by Internal Fields

Under the assumption that time dependent attenuations of the angular correlation coefficients in liquid sources follow the exponential law

$$A_k(t) = A_k(0)\mathrm{e}^{-\lambda_k t}, \tag{1}$$

one gets for the integral attenuation coefficients (assuming $2\tau \gg T_{\frac{1}{2}}$)

$$G_k = \frac{\lambda}{\lambda+\lambda_k}. \tag{2}$$

From our values for G_2 and G_4 we get

$$\lambda_2 = 0.09\times 10^9\,\mathrm{sec}^{-1}, \quad \lambda_4 = 0.30\times 10^9\,\mathrm{sec}^{-1} \quad \text{and} \quad \frac{\lambda_4}{\lambda_2} = 3.3\pm 1.3.$$

For electric interactions A. Abragam and R. V. Pound [12]) derived the following expression for λ_k:

$$\lambda_k = a\big(1-(2I+1)W(I2kI/II)\big), \tag{3}$$

where

$$a = \frac{\tau_e}{40}\,\frac{(I+1)(2I+3)}{I(2I-1)}\left(\frac{eQ}{\hbar}\right)^2\left\langle\left(\frac{\partial^2 V}{\partial z^2}\right)^2\right\rangle_{\mathrm{av.}}, \tag{4}$$

the quantities W are Racah-coefficients, τ_e is the correlation time of the electric field gradient, $\partial^2 V/\partial z^2$ the electric field gradient at the position of the nucleus, Q the electric quadrupole moment of the nucleus in the intermediate state, and I the spin of the nucleus in the intermediate state.

For the ratio λ_4/λ_2 one gets

$$\frac{\lambda_4}{\lambda_2} = \frac{1-(2I+1)W(I24I/II)}{1-(2I+1)W(I22I/II)} \tag{5}$$

and especially for the spin of the intermediate state $I = 2$

$$\frac{\lambda_4}{\lambda_2} = 0.59.$$

This value is in disagreement with our result. We therefore conclude that the perturbation is not due to pure electric interaction. For time dependent magnetic interactions the theory of A. Abragam and R. V. Pound [12]) gives

$$\lambda_k = a'\big(1-(2I+1)W(I1kI/II)\big), \tag{6}$$

where

$$a' = \tfrac{2}{3}\tau_J\omega_J{}^2 I(I+1)J(J+1), \quad \omega_J{}^2 = \frac{g^2 B_{\mathrm{inst}}^2 \mu k^2}{\hbar^2 J(J+1)}, \tag{7}$$

τ_J is the spin relaxation time of the 4f electron shell, J the total angular

momentum of the electronic shell, B_{inst} the instantaneous magnetic field at the position of the nucleus resulting from the 4f electron shell, g the nuclear g-factor of the intermediate state, and μ_k the nuclear magneton. For the ratio λ_4/λ_2 one gets

$$\frac{\lambda_4}{\lambda_2}=\frac{1-(2I+1)W(I14I/II)}{1-(2I+1)W(I12I/II)} \quad \text{or} \quad \frac{\lambda_4}{\lambda_2}=3.34 \quad \text{for} \quad I=2. \tag{8}$$

The agreement of this value with our measurement suggests that the perturbation is caused mainly by magnetic dipole interaction †. To confirm this result we have measured the exponential dependence of the time dependent attenuation by a delay experiment.

A measurement of the differential angular correlation for different delays was rather difficult because it was impossible to make the resolving time of a fast coincidence circuit for NaI-detectors smaller than the half life of 1.8×10^{-9} sec of the intermediate state. If the resolving time is large compared to $T_{\frac{1}{2}}$ the delay experiment is still possible but the measured function $A_k(t)$ is smeared out.

Assuming a Gaussian shape of the efficiency of the fast coincidence which is a good approximation for small resolving times,

$$\varepsilon(t)=\mathrm{e}^{-\pi\left(\frac{t-t_\mathrm{v}}{2\tau}\right)^2} \tag{9}$$

(t_v = time delay from the centre of the prompt curve), one gets for the measured coefficients

$$A'_k(t_\mathrm{v})=\frac{\int_0^\infty \mathrm{e}^{-\lambda t}A_k(t)\mathrm{e}^{-\pi\left(\frac{t-t_\mathrm{v}}{2\tau}\right)^2}\,\mathrm{d}t}{\int_0^\infty \mathrm{e}^{-\lambda t}\mathrm{e}^{-\pi\left(\frac{t-t_\mathrm{v}}{2\tau}\right)^2}\,\mathrm{d}t}. \tag{10}$$

Especially for exponential time dependence

$$A_k(t)=A_k(0)\mathrm{e}^{-\lambda_k t},$$

the integrals can be reduced to Gaussian error integrals and one gets the expression

$$A'_k(t_\mathrm{v})=A_k(0)\mathrm{e}^{\left[\frac{\lambda\lambda_k\tau^2 2}{\pi}+\frac{\lambda_k^2\tau^2}{\pi}-\lambda_k t_\mathrm{v}\right]}\frac{1-\Phi\left(\frac{\lambda+\lambda_k}{\sqrt{\pi}}\tau-\frac{t_\mathrm{v}\sqrt{\pi}}{2\tau}\right)}{1-\Phi\left(\frac{\lambda\tau}{\sqrt{\pi}}-\frac{t_\mathrm{v}\sqrt{\pi}}{2\tau}\right)}. \tag{11}$$

We have measured the coefficients $A'_k(t_\mathrm{v})$ for five different delays t_v. The results are shown in figs. 5a and 5b. The experimental values for A'_k are plotted as a function of the mean delay $\bar{t}$ of the coincidences accepted.

† *Note added in proof*: The existence of appreciable magnetic attenuation in the rear earth region was first shown experimentally by M. Deutsch *et al.* [17]) in the case of gadolinium. Magnetic attenuation was also found for Er^{166} and Dy^{160} by W. Kundig [18]).

The mean delay $\bar{t}$ can be calculated from the delay t_v by

$$\bar{t} = \frac{\int_0^\infty t e^{-\lambda t} e^{-\pi\left(\frac{t-t_v}{2\tau}\right)^2} dt}{\int_0^\infty e^{-\lambda t} e^{-\pi\left(\frac{t-t_v}{\tau}\right)^2} dt}. \tag{12}$$

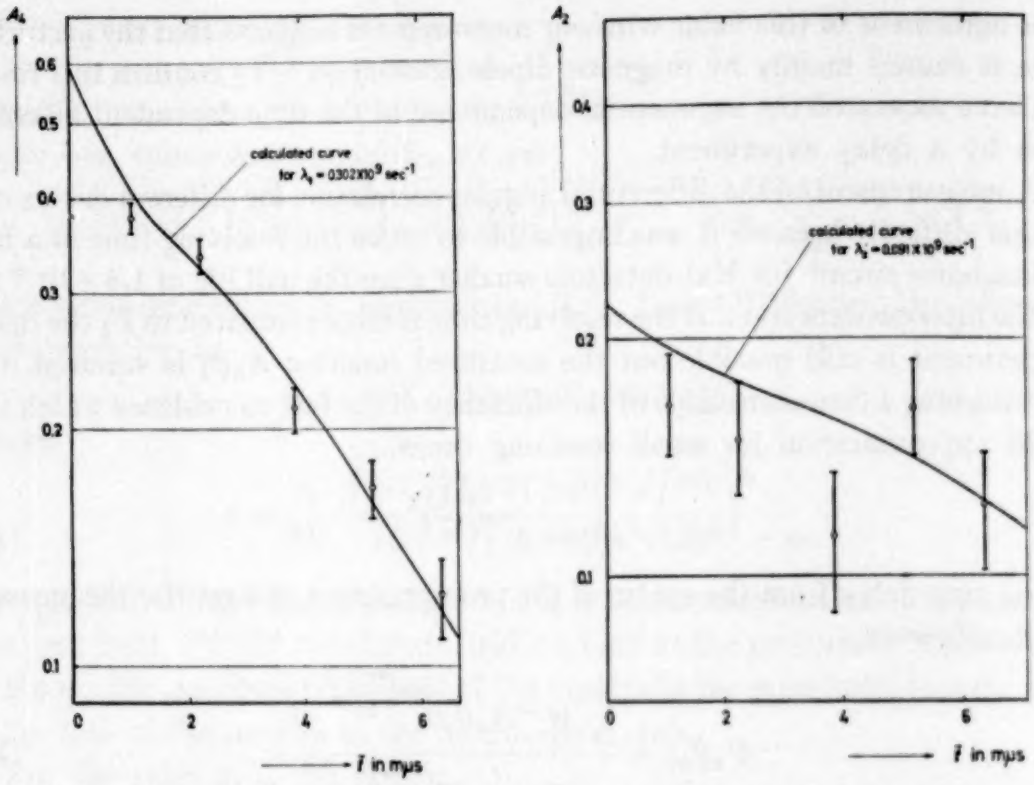

Fig. 5. Measurement of the 1380 keV−80 keV angular correlation at different delays. $\bar{t}$ = mean delay of the coincidences accepted.

The numerical values for $\bar{t}$ for the five different delays t_v used in our experiment are given in the following table:

t_v (in 10^{-9} sec)	−4.73	+2.99	+6.88	+8.94	+10.44
$\bar{t}$ (in 10^{-9} sec)	1.06	2.24	3.84	5.17	6.36

The measurement shows that a strong time dependent attenuation of $A_4(t)$ exists whereas the attenuation of $A_2(t)$ is rather small.
We have evaluated the function $A'_k(t_v)$, which one expects from the experimental values of G_2 and G_4 for pure exponential attenuation, using formulas (2) and (11). Figs. 5a and 5b show that the resulting curves are in good agreement with the experimental points, thus confirming the assumption of a pure exponential time dependent attenuation.

4. Rotation in an External Magnetic Field and the g-Factor of the 80 keV-Level

The experimental set up for the observation of gamma-gamma angular correlations in an external magnetic field has been described earlier [13]). The measurement was done in a field of 13550 G perpendicular to the plane of the two counters. The results for field direction up and down and the measurement without magnetic field are plotted in fig. 6.

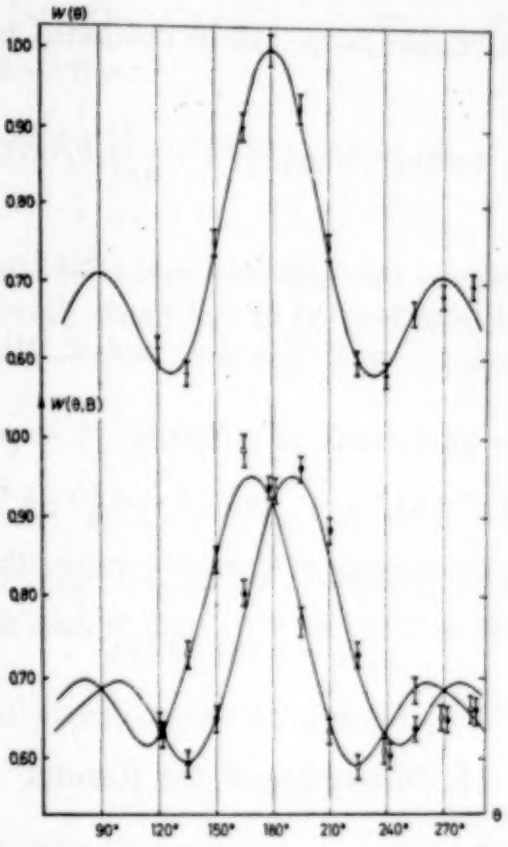

Fig. 6. Measurement of the nuclear g-factor of the 80 keV level. The upper curve shows the angular correlation of the (1380 keV) – (80 keV) cascade measured in the magnet without magnetic field. The lower two curves are the result of the measurement at a magnetic field of 13550 G.
⊤ = experimental points for field direction up.
⊥ = experimental points for field direction down.

The calculation of the g-factor of the intermediate state is rather complicated because the different attenuations for A_2 and A_4 must be taken into account. If time dependent attenuations

$$A_k(t) = A_k(0)\mathrm{e}^{-\lambda_k t}$$

are present, the angular correlation in a magnetic field B_{eff} is given by

$$W(\theta, B_{\mathrm{eff}}) = 1 + \sum_{k=2,4} \int_0^\infty \mathrm{e}^{-(\lambda+\lambda_k)t} A_k(0) P_k(\cos[\theta - \omega_L t])\mathrm{d}t. \qquad (13)$$

Using this formula and the value 1.82×10^{-9} sec for the half life of the intermediate state [7]) we determined the Larmor frequency ω_L by a least square fit as

$$\omega_L = +(0.140\pm0.007)10^9\,\mathrm{sec}^{-1}.$$

For the nuclear g-factor one gets

$$g_R = \frac{\omega_L\hbar}{\mu_k B_{eff}} = \frac{\omega_L\hbar}{\mu_k B_{ext}\beta} = \frac{(2.18\pm0.12)}{\beta}. \tag{14}$$

The paramagnetic correction factor can be calculated from the approximate formula [3])

$$\beta = 1+2\mu_B^2\langle r^{-3}\rangle g_J J(J+1)\frac{1}{3kT}\langle J\|N\|J\rangle,$$

where

μ_B is the Bohr magneton, r the radius of the 4f orbit ($\langle r^{-3}\rangle$ can be calculated from the approximate formula given by B. Bleaney [11])), $\langle J\|N\|J\rangle$ the reduced matrix element, tabulated by R. J. Elliott and K. W. H. Stevens [15]), and g_J the Landé-factor.

The evaluation for Ho^{+++} and Er^{+++} gives

$$\beta = 8.61\pm5\,\% \quad \text{and} \quad \beta = 8.10\pm5\,\%$$

respectively. Taking the average of these two values the final result for the g_R-value is

$$g_R = +0.260\pm0.034.$$

5. Discussion of the Results

The existence of a strong attenuation of the angular correlation of the 0^+, 2^+, 0^+ cascade by magnetic interactions can be understood from the fact, that the instantaneous internal magnetic fields of Ho^{+++} and Er^{+++} are extremely large. From the theory of paramagnetism one gets for the absolute value of the instantaneous magnetic field at the position of the nucleus for the $^{+++}$ions of the rare earth elements † the expression

$$B_{Inst.} = 2J\mu_B\langle r^{-3}\rangle\langle J\|N\|J\rangle. \tag{16}$$

The evaluation gives for Ho^{+++} and Er^{+++} 9.10×10^6 and 9.35×10^6 G respectively, which are the largest values of all for rare earth $^{+++}$ions.

Since we know the interacting internal field and the magnetic moment of the $2+$ level, it is possible to calculate the spin relaxation time τ_J of the 4f electron

† This formula cannot be applied in the cases Pm^{+++}, Sm^{+++} and Gd^{+++}, as shown by J. Kanamori and K. Sugimoto [2]).

shell from the explicit expression for a' in eq. (7). Assuming that contributions by electric interaction are negligible, one gets

$$\tau_J = \tfrac{3}{2} \frac{a' \hbar^2}{\omega_J^2 I(I+1) g^2 B_{\text{inst}}^2 \mu_k^2}. \tag{17}$$

When the values $B_{\text{inst}} = 9.2 \times 10^6$ G and $g = 0.260$ and

$$a' = \frac{\lambda_4}{1-(2I+1)W(I14I/II)} = \frac{\lambda_2}{1-(2I+1)W(I12I/II)}$$
$$= 0.18 \times 10^9 \text{ sec}^{-1}$$

are inserted, the result for the relaxation time τ_J is

$$\tau_J = (3.4 \pm 0.9) \times 10^{-13} \text{ sec.}$$

It is interesting to note that a very short spin relaxation time for the 4f electron shell of erbium has been found also in paramagnetic resonance experiments with a single crystal of erbium ethyl sulphate [16]). The results are

$$\tau_J = (0.95 \pm 0.05) \times 10^{-9} \text{ sec, at } 13^\circ \text{ K}$$

and

$$\tau_J = 1 \times 10^{-10} \text{ sec} \quad \text{at } 20^\circ \text{ K.}$$

From the observed strong temperature dependence of τ_J one must expect a relaxation time much smaller than 10^{-11} sec for $T = 300^\circ$ in agreement with our observation.

Our result for the nuclear rotational g-factor,

$$g_R = +0.260 \pm 0.034,$$

deviates substantially from the prediction of the hydrodynamic model of rotational motion,

$$g_R = Z/A = 0.41.$$

The authors are indebted to Prof. W. Jentschke for stimulating discussions of the experimental results and to W. Kündig for sending us his results [18]) before publication. The financial support given by the Bundesministerium für Atomkernenergie und Wasserwirtschaft is gratefully acknowledged.

References

1) G. Goldring and R. P. Scharenberg, Phys. Rev. **110** (1958) 701
2) J. Kanamori and K. Sugimoto, J. Phys. Soc. Japan **13** (1958) 754
3) G. Manning and J. D. Rogers, Nuclear Physics **15** (1960) 166
4) G. Süssmann and W. Donner, private communication

5) P. Boskma and H. de Waard, Nuclear Physics **12** (1959) 533
6) F. K. McGowan Phys. Rev. **80** (1950) 923
7) R. Graham, J. Wolfson and M. A. Clark, Nucl. Data Sheets (1959)
8) E. E. Berlowich, Izvest. Akad. Nauk S.S.S.R. Ser. Fiz. **20** (1959) 1438
9) M. Birk, G. Goldring and Y. Wolfson, Phys. Rev. **116** (1959) 730
10) J. S. Fraser and J. D. C. Milton, Phys. Rev. **98** (1955) 1173
11) I. Marklund, B. van Nooigen and Z. Grabowski, Nuclear Physics **15** (1960) 555
12) A. Abragam and R. V. Pound, Phys. Rev. **92** (1953) 943
13) E. Bodenstedt, E. Matthias and H. J. Körner, Z. f. Physik **153** (1958) 423
14) B. Bleaney, Proc. Phys. Soc. A **68** (1955) 937
15) R. J. Elliott and K. W. H. Stevens, Proc. Roy. Soc. A **218** (1953) 553
16) B. Bleaney and H. E. D. Scovil, Proc. Phys. Soc. A **64** (1951) 204
17) M. Deutsch *et al.*, MIT Lab. Nucl. Science, SSR Progress Report, Nov. 1 (1959) p. 101
18) W. Kündig, Helv. Phys. Acta (to be published)

1.D.1 *Nuclear Physics* **22** (1961) 157—163; © *North-Holland Publishing Co., Amsterdam*
Not to be reproduced by photoprint or microfilm without written permission from the publisher

SPURIOUS STATES ARISING FROM THE CENTRE-OF-MASS MOTION OF A NUCLEUS

ELIZABETH BARANGER and CHONG WAN LEE
University of Pittsburgh, Pittsburgh, Pennsylvania †

Received 21 July 1960

Abstract: A simple method is given for generating the spurious states which arise from the incorrect treatment of the centre-of-mass motion by nuclear shell model calculations. It is not necessary to know the spurious states in order to find their weight in a particular shell model state. It is also shown which *jj* configurations have no spurious states. Some examples are given.

1. Introduction

In nuclear shell model calculations, the failure to separate out the centre-of-mass motion from the internal motions can lead to the appearance of spurious states. As was first shown by Elliott and Skyrme [1]), if one takes a harmonic oscillator potential as the effective central potential, these spurious states can be calculated explicitly. In this paper, we will derive a simple method for the generation of these states and give some examples. We will also show which *jj* configurations have no spurious states.

The shell model Hamiltonian which we are considering is

$$H_{\mathrm{SM}} = \sum_{i=1}^{A} \frac{(\mathbf{p}_i)^2}{2m} + \tfrac{1}{2}m\omega^2 \sum_{i=1}^{A} (\mathbf{r}_i)^2, \tag{1}$$

where A is the number of nucleons, $\mathbf{r}_i$ and $\mathbf{p}_i$ are the coordinates and momenta of the individual nucleons. One body and two body potential terms are added to this Hamiltonian and usually treated by perturbation theory. A set of properly antisymmetrized eigenfunctions of H_{SM} is the usual shell model wavefunctions, $\psi_{\nu\gamma}(r_1 \ldots r_A, \xi_1 \ldots \xi_A)$, with energy eigenvalue E_ν. Here ξ_i are the spin and isobaric spin coordinates of the ith particle and γ represents all other quantum numbers necessary to specify the state.

Because the central potential is taken to be a harmonic oscillator, H_{SM} can be separated as follows:

$$H_{\mathrm{SM}} = H_R + H' = \frac{(\mathbf{P})^2}{2Am} + \tfrac{1}{2}Am\omega^2(\mathbf{R})^2 + H', \tag{2}$$

† Work done at Sarah Mellon Scaife Radiation Laboratory and assisted by the joint program of the Office of Naval Research and the U. S. Atomic Energy Commission.

where $\mathbf{R} = \sum_{i=1}^{A} \mathbf{r}_i/A$ is the coordinate of the centre of mass, $\mathbf{P} = \sum_{i=1}^{A} \mathbf{p}_i$ is its conjugate momentum and H' is a Hamiltonian involving only internal coordinates and their conjugate momenta. Thus a set of properly antisymmetrized eigenfunctions of H_{SM} is $\psi_{m\beta}(R)\varphi_{n\alpha}(\rho_1 \ldots \rho_{A-1}, \xi_1 \ldots \xi_A)$ with energy eigenvalue $E_m + E_n$. Here $\psi_{m\beta}(R)$ is an eigenfunction of H_R. The function $\varphi_{n\alpha}(\rho_1 \ldots \rho_{A-1}, \xi_1 \ldots \xi_A)$, where $\rho_1 \ldots \rho_{A-1}$ are the $A-1$ internal coordinates, is an eigenfunction of H' and is antisymmetric in the interchange of any two nucleons.

The problem of nuclear spectroscopy is the study of the set of internal states of the system. If we restrict ourselves to those solutions of the shell model Hamiltonian with the centre of mass in the ground state, i.e. to those wavefunctions of the form $\psi_{00}(R)\varphi_{n\alpha}(\rho_i \xi_i)$, we will be studying these internal states. All states with the centre of mass in an excited state, which are redundant, are called spurious and must be eliminated.

Since an energy level E_ν is usually very degenerate, the usual shell model wavefunctions, $\psi_{\nu\gamma}(r_i \xi_i)$, are not necessarily eigenstates of H_R. The problem is to find what linear combinations of these states are the spurious states. Sometimes one is satisfied in only computing the weight of spurious states in a given shell model state. Previous investigators [1, 2, 3]) have constructed the matrix of H_R using the states $\psi_{\nu\gamma}(r_i \xi_i)$ as bases and diagonalized it. The spurious states are those with eigenvalue $> \frac{3}{2}\hbar\omega$. Unna and Talmi [5]) found the percentage weight of spurious states in some shell model states with energy $1\hbar\omega$ above the ground state by only computing the expectation value of H_R. We feel that the procedure given below is simpler for the following reasons. First, the matrix elements involved in this method are matrix elements of one body operators instead of the two body operators which occur in H_R. Second, the diagonalization of a matrix is not necessary, although due to the degeneracy of the eigenvalues this is not very difficult [2, 3]). Third, the weight of spurious states in a given shell model state can be found without calculation of the spurious states, and in particular for states of higher excitation than $1\hbar\omega$ above the ground state.

2. Generation of the Spurious States

It is well known that all of the wavefunctions with the lowest energy allowed by the Pauli principle must be eigenstates of H_R with eigenvalue $\frac{3}{2}\hbar\omega$ [1, 2]). If we operate on these ground states with the raising operator of the centre-of-mass coordinate, we will generate those spurious states with energy $1\hbar\omega$ above the ground state energy. This operator $A^+{}_k{}^{(1)}$ is defined by

$$\begin{aligned} A^+{}_k{}^{(1)} &= \frac{1}{(2Am\hbar\omega)^{\frac{1}{2}}} \left(P_k{}^{(1)} + iAm\omega R_k{}^{(1)}\right) \\ &= \frac{1}{\sqrt{A}} \sum_{i=1}^{A} a^+{}_k{}^{(1)}(i), \end{aligned} \tag{3}$$

where $P_0^{(1)} = P_z$, $P_{\pm 1}^{(1)} = \mp 1/\sqrt{2}(P_x \pm iP_y)$ and similarly for $R_k^{(1)}$, and

$$a^+{}_k^{(1)}(i) = \frac{1}{(2m\hbar\omega)^{\frac{1}{2}}}(p_{i,k}^{(1)} + im\omega r_{i,k}^{(1)}).$$

It is obviously a tensor of rank one, and has the property that

$$A^+{}_k^{(1)}\psi_{00}(R) = \psi_{1,\,l=1,\,m=k}(R).$$

A set of spurious states with angular momentum J', M' and isobaric spin T, M_T are

$$\phi_{1J'M'TM_T\tau}(r_i\xi_i) = \sum_{M,k,i} \frac{1}{\sqrt{A}} C(J1J'; MkM') a^+{}_k^{(1)}(i)\psi_{0JMTM_T\beta}(r_i\xi_i), \quad (4)$$

where $C(J1J'; MkM')$ is the usual Clebsch-Gordan coefficient, the subscripts 0 and 1 on the wavefunctions designate the energy above the ground state, and β and τ represent the other quantum numbers necessary to complete the specification of the states. By choosing all possible values of $JMTM_T\beta$ we generate all the spurious states with energy $1\hbar\omega$ above the ground state. We can expand the spurious states in terms of the shell model states $\psi_{1J'M'TM_T\tau'}(r_i\xi_i)$. The expansion coefficients are

$$\begin{aligned}\langle\psi_{1J'M'TM_T\tau'}|\phi_{1J'M'TM_T\tau}\rangle &= \sum_{M,k,i} \frac{1}{\sqrt{A}} C(J1J'; MkM')\langle\psi_{1JM'TM_T\tau'}|a^+{}_k^{(1)}(i)|\psi_{0JMTM_T\beta}\rangle \quad (5)\\ &= \sum_i \frac{1}{\sqrt{A}}(2J'+1)^{-\frac{1}{2}}\langle\psi_{1J'T\tau'}||a^{+(1)}(i)||\psi_{0JT\beta}\rangle,\end{aligned}$$

where the double bar signifies a reduced matrix element. These reduced matrix elements can be calculated using the usual methods of Racah [4]) and the single particle reduced matrix elements given in Gartenhaus and Schwartz [3]). The spurious states must turn out normalized and must be orthogonal to each other, which provides a check on the calculation.

If it is desired to use an LS representation, the following set of spurious states with orbital angular momentum L', M'_L, spin angular momentum S, M_S and isobaric spin T, M_T is more convenient:

$$\phi_{1L'M'_LSM_STM_T\tau}(r_i\xi_i) = \sum_{M_L,k,i} \frac{1}{\sqrt{A}} C(L1L'; M_LkM'_L) a^+{}_k^{(1)}(i)\psi_{0LM_LSM_STM_T\beta}(r_i\xi_i). \quad (6)$$

Spurious states with energy $2\hbar\omega$ above the ground state are either states with the same internal wave functions as the ground states and with the centre of mass in the second excited state, or with the same internal wavefunctions as

the non-spurious states with energy $1\hbar\omega$ above the ground state and with the centre of mass in the first excited state. The latter, we treat as above. For the former, we construct the tensor operator of rank j

$$B^{+}{}_{k}^{(j)} = \frac{1}{\sqrt{2}} \sum_{m,n} C(11j; mnk) A^{+}{}_{m}^{(1)} A^{+}{}_{n}^{(1)},$$

where j can obviously be only 0 or 2. It has the property that

$$B^{+}{}_{k}^{(j)} \psi_{00}(R) = \psi_{2,\, t-j,\, m-k}(R)$$

and is used, just as we used $A^{+}{}_{k}^{(1)}$, to generate these spurious states.

The weight of spurious states w in a particular shell model state $\psi_{1J'M'TM_T\tau'}(r_i\xi_i)$, can be obtained by squaring the coefficients given in (5) and summing over all values of J, β. It is obviously not necessary to generate the spurious states in order to compute this quantity. To calculate w for a shell model state, $\psi_{2J'M'TM_T\tau'}(r_i\xi_i)$, with excitation energy $2\hbar\omega$, it is necessary to sum the contributions from both types of spurious states discussed above. The result can be put in the following form:

$$\begin{aligned} w = & \sum_{J_1,\tau} |\langle \psi_{2J'M'TM_T\tau'} | \sum_{M_1,m} C(J_1 1 J'; M_1 m M') A^{+}{}_{m}^{(1)} | \psi_{1J_1M_1TM_T\tau} \rangle|^2 \\ & - \sum_{J,j,\beta} |\langle \psi_{2J'M'TM_T\tau'} | \sum_{M,k} C(Jj J'; MkM') B^{+}{}_{k}^{(j)} | \psi_{0JMTM_T\beta} \rangle|^2. \end{aligned} \tag{7}$$

The first sum runs over *all* states with excitation energy $1\hbar\omega$, so that it is not necessary to generate the spurious states with energy $1\hbar\omega$ in order to calculate w.

3. Selection Rules

There are some shell model states with certain values of J, T or belonging to certain configurations which have the centre of mass in its ground state. It is very useful to be able to say immediately when one is given a state whether it has this property or not. Such a state has the property that if one applies to it the lowering operator $A_{k}^{(1)}$, which is the Hermitian conjugate of $A^{+}{}_{k}^{(1)}$, the result is zero. Thus the state $\psi_{\nu JMTM_T\gamma}(r_i\xi_i)$ is a state with its centre of mass in the ground state, if all of the folowing matrix elements vanish:

$$\langle \psi_{\nu-1J'M'T'M_T\beta} | \sum_{i=1}^{A} a_{k}^{(1)}(i) | \psi_{\nu JMTM_T\gamma} \rangle. \tag{8}$$

Here J', T', β can take all the values allowed by the Pauli principle for the configurations with energy $1\hbar\omega$ less than the original state.

If $\psi_{\nu JMTM_T}(r_i\xi_i)$ is to be non-spurious, obviously T must differ from T' or $\mathbf{J}$ differ from $\mathbf{J'}+\mathbf{1}$. For instance, the $(p_{\frac{1}{2}}{}^{-1}s_{\frac{1}{2}})$ states in O^{16} with $T=1$, $J=1$ or 0

or with $T = 0$, $J = 0$ are such states, since J' and T' are uniquely zero. If we use an LS representation, S must differ from S', $\mathbf{L}$ from $\mathbf{L}'+\mathbf{1}$. Several authors have discussed examples of these rules [1, 2, 5]).

The operator $a_k^{(1)}(i)$ demotes one particle to a lower oscillator shell. Thus the matrix elements (8) will vanish if there is only one unfilled harmonic oscillator shell in the configuration γ, and if this unfilled shell is the lowest allowed by the Pauli principle. This is just restating the theorem that the ground state configuration has no spurious states.

If the state we are considering belongs to a jj configuration such that it is necessary in order to satisfy the Pauli principle to change the j of an individual nucleon by more than one when it is demoted to the lower oscillator shell, then the matrix elements (8) all vanish. Thus configurations with the highest j of the lower oscillator shell filled and only the highest j of the higher oscillator shell with particles in it have no spurious states. Some examples of this rule are the configurations $(1s)^4(1p_{\frac{3}{2}})^8(1p_{\frac{1}{2}})^n d_{\frac{5}{2}}$ discussed by Unna and Talmi [5]), who showed by very similar arguments to the above that these configurations are free of spurious states. It is just configurations of this kind which are expected to lie lowest in heavy nuclei due to the strong one body spin orbit force. Thus for many calculations concerning low excitations, the spurious state problem does not arise.

4. Examples

The spurious state with energy $1\hbar\omega$ above the ground state for closed shell nuclei has been given by Gartenhaus and Schwartz [3]) and can be easily verified using eq. (6).

A further example is given in table 1. Here we have listed the spurious states with energy $1\hbar\omega$ above the ground state for $A = 17$ using a jj representation. The ground state configurations for a nucleus with $A = 17$ are a closed shell plus a $d_{\frac{5}{2}}$, $d_{\frac{3}{2}}$ or $s_{\frac{1}{2}}$ particle. Thus we get three spurious states (rows 1—3) with $J' = \frac{7}{2}, \frac{5}{2}, \frac{3}{2}$, $T = \frac{1}{2}$ with the same internal wavefunction as the $d_{\frac{5}{2}}$ state, three

TABLE 1

The spurious states with energy $1\hbar\omega$ above the ground state for $A = 17$, using jj states as a basis. All the numbers must be multiplied by $1/\sqrt{17 \times 45}$.

J'	ρ	$f_{\frac{7}{2}}$	$f_{\frac{5}{2}}$	$p_{\frac{3}{2}}$	$p_{\frac{1}{2}}$	$(p_{\frac{3}{2}}^{-1} d_{\frac{5}{2}})_{1,0\rho}$	$(p_{\frac{3}{2}}^{-1} d_{\frac{3}{2}})_{1,0\rho}$	$(p_{\frac{3}{2}}^{-1} s_{\frac{1}{2}})_{1,0\rho}$	$(p_{\frac{1}{2}}^{-1} d_{\frac{3}{2}})_{1,0\rho}$	$(p_{\frac{1}{2}}^{-1} s_{\frac{1}{2}})_{1,0\rho}$
$\frac{7}{2}$	$d_{\frac{5}{2}}$	$\sqrt{135}$				$-\sqrt{270}$	$-\sqrt{40}$	$\sqrt{80}$	$\sqrt{200}$	$\sqrt{40}$
$\frac{5}{2}$	$d_{\frac{5}{2}}$		$\sqrt{9}$			$\sqrt{396}$	$\sqrt{40}$	$-\sqrt{80}$	$-\sqrt{200}$	$-\sqrt{40}$
$\frac{3}{2}$	$d_{\frac{5}{2}}$			$\sqrt{54}$		$-\sqrt{351}$	$-\sqrt{40}$	$\sqrt{80}$	$\sqrt{200}$	$\sqrt{40}$
$\frac{5}{2}$	$d_{\frac{5}{2}}$		$\sqrt{126}$			$\sqrt{360}$	$\sqrt{34}$	$\sqrt{80}$	$-\sqrt{125}$	$\sqrt{40}$
$\frac{3}{2}$	$d_{\frac{5}{2}}$			$-\sqrt{6}$		$-\sqrt{360}$	$-\sqrt{29}$	$-\sqrt{80}$	$\sqrt{250}$	$-\sqrt{40}$
$\frac{1}{2}$	$d_{\frac{5}{2}}$				$\sqrt{60}$	$\sqrt{360}$	$\sqrt{50}$	$\sqrt{80}$	$-\sqrt{175}$	$\sqrt{40}$
$\frac{3}{2}$	$s_{\frac{1}{2}}$			$\sqrt{75}$		$\sqrt{360}$	$-\sqrt{40}$	$\sqrt{70}$	$\sqrt{200}$	$\sqrt{20}$
$\frac{1}{2}$	$s_{\frac{1}{2}}$				$\sqrt{75}$	$-\sqrt{360}$	$\sqrt{40}$	$-\sqrt{40}$	$-\sqrt{200}$	$-\sqrt{50}$

states (rows 4—6) with $J' = \frac{5}{2}, \frac{3}{2}, \frac{1}{2}$ and $T = \frac{1}{2}$ with the same internal wavefunction as the $d_{\frac{5}{2}}$ state, and two states (rows 7—8) with $J' = \frac{3}{2}, \frac{1}{2}$ and $T = \frac{1}{2}$ and the same internal wavefunction as the $s_{\frac{1}{2}}$ state. The columns are labelled by the *jj* states which are involved. The first four are configurations of a closed shell plus a particle in the orbit listed. The next five represent core excited states, where the core is coupled to $J = 1, T = 0$, and the last particle, in a state ρ, which is listed in column 2, is then coupled on to give J' and the result antisymmetrized. When ρ occurs also in the core configuration the state can be related to a more usual set of states as follows:

$$[(\rho_1^{-1}\rho)_{1,0}\rho]_{J',\frac{1}{2}} = \frac{1}{\sqrt{\mathcal{N}}} \sum_{J'',T''}{}' U(\tfrac{1}{2}\tfrac{1}{2}\tfrac{1}{2}\tfrac{1}{2}; 0T'')U(\rho_1 \rho J'\rho; 1J'') \times [\rho_1^{-1}(\rho^2)_{J'',T''}]_{J',\frac{1}{2}} \tag{9}$$

where $\mathcal{N}$ is an easily computed normalizing constant and the prime on the summation means that the sum is taken only over $J''+T'' =$ odd. Here $U(abcd; ef) = [(2e+1)(2f+1)]^{\frac{1}{2}} W(abcd; ef)$, where $W(abcd; ef)$ is the usual Racah coefficient.

When ρ does not occur in the core configuration, the coefficients in table 1 are seen to be independent of ρ, except for a sign, and in fact are just proportional to the coefficients obtained in expanding the spurious state for $A = 16$ in a *jj* representation.

The weight of spurious states in each of the states with one particle outside a closed shell can be seen from table 1 to be $\frac{3}{17} = N/A$, where $(N+\frac{3}{2})\hbar\omega$ is the energy of a particle in the last shell. This theorem is true for corresponding configurations in $A = 5$ or $A = 41$.

The generation of spurious states with excitation energy $2\hbar\omega$ is tedious because there are so many of them, but the weight of spurious states w in any particular shell model state can be easily calculated. As an example, consider the state for $A = 18$ with two $f_{\frac{7}{2}}$ particles outside the O^{16} closed shell coupled to $J = 0$, $T = 1$. Such a state is of interest because a recent experiment has shown that the O^{18} ground state contains a fairly large percentage of it [6]). Using eq. (7), one can show that

$$w = \frac{2N}{A} - \frac{N^2}{A^2}(1+U(1\rho_2\rho_2 1; \rho_1\rho_1)),$$

where, for the case above, $N = 3$, $\rho_1 = \frac{7}{2}$, $\rho_2 = \frac{5}{2}$ and the result is 0.30. For the state in $A = 42$ with two $g_{\frac{9}{2}}$ particles outside the Ca^{40} closed shell coupled to $J = 0$, $T = 1$, the same formula can be used with $N = 4$, $\rho_1 = \frac{9}{2}$, $\rho_2 = \frac{7}{2}$ and the result is 0.18.

We would like to thank J. B. French for pointing out the centre of mass problem to us and S. Meshkov for many useful discussions.

References

1) J. P. Elliott and T. H. R. Skyrme, Proc. Roy. Soc. A **232** (1955) 561
2) E. C. Halbert and J. B. French, Phys. Rev. **105** (1957) 1565;
E. C. Halbert, Thesis, University of Rochester (1956)
3) S. Gartenhaus and C. Schwartz, Phys. Rev. **108** (1957) 482
4) G. Racah, Phys. Rev. **63** (1943) 367
5) I. Unna and I. Talmi, Phys. Rev. **112** (1958) 452
6) J. C. Armstrong, K. S. Quisenberry and S. Meshkov, Bull. Am. Phys. Soc. **5** (1960) 247

8.B

Nuclear Physics **22** (1961) 164—167; © *North-Holland Publishing Co., Amsterdam*

Not to be reproduced by photoprint or microfilm without written permission from the publisher

A CONTRIBUTION TO THE ANOMALOUS MAGNETIC MOMENTS OF THE BARYONS

T. T. CROW and W. G. HOLLADAY

Department of Physics and Astronomy, Vanderbilt University Nashville, Tennessee

Received 8 September 1960

Abstract: A method of calculation and results are presented for the fourth order one-pion, one-kaon contribution to the magnetic moments of the baryons. Static, charge-independent interactions of spin $\frac{1}{2}$ baryons with pseudoscalar kaons are assumed. For this calculation a renormalization program is formulated similar to that of Chew but in which the baryon mass differences are taken into account. Generally speaking, the contributions calculated here are comparable to second order kaon contributions. Therefore, it would appear that more accurate and elaborate computations of these moments should incorporate combined effects of the pion and kaon fields.

1. Introduction

That the anomalous magnetic moments of baryons could provide important information concerning the various theoretical proposals for the interactions of baryons with mesons has been discussed previously [1]). A static cutoff perturbation theory has been used to calculate the contributions of 2nd and 4th order pion processes [1, 2]) and 2nd order kaon processes [1]) to the anomalous moments. In the next section we discuss a renormalization program in which baryon mass differences are taken into account. This program is then used to calculate 4th order moment contributions in which one pion and one kaon participate. We present results for the moments which include the 2nd and 4th order pion, 2nd order kaon, and 4th order pion kaon cross terms evaluated for various choices of the coupling constants. In these calculations we have neglected the contributions due to baryon currents. It is reasonable to expect that this introduces greater error in the case of heavy mesons; nevertheless, we feel our results can still indicate certain interesting characteristics of these moments.

2. Fourth Order Anomalous Moments

We assume all baryons have spin $\frac{1}{2}$ and all mesons have spin zero. All hyperons are assumed to have the same parity and kaons are assumed to be pseudoscalar with respect to the hyperons. We assume the Gell-Mann Nishijima [3]) isobaric spin assignments. The static version of the Hamiltonian density we use is one used by others previously (e.g. see ref. [1])). The Hamiltonian densities for the

interactions of charged boson fields with the electromagnetic field are

$$\mathscr{H}_{\pi,\gamma} = -ie[\pi^+\nabla\pi^- - \pi^-\nabla\pi^+]\cdot\mathbf{A},$$
$$\mathscr{H}_{K,\gamma} = -ie[K^+\nabla\bar{K}^+ - \bar{K}^+\nabla K^+]\cdot\mathbf{A}.$$

We neglect effects of source currents [4]).

We have repeated the 2nd and 4th order calculations of Friedman [2]) and Holladay [1]) and agree with their results †). To find the 4th order pion kaon cross terms, we use a renormalization procedure similar to Chew's [5]). To 2nd order the modified renormalized propagator for a baryon with physical mass M_1 is

$$S'_r(p_0-M_1) = \frac{1}{p_0-M_1} + \sum_j \left(\frac{g'_j}{M_1+M_j}\right)^2 V_j V_j^* \frac{1}{(p_0-M_j-w_j)(M_1-M_j-w_j)^2},$$

where p_0 is $-i$ times the fourth component of the momentum four vector for the baryon of mass M_1, M_j is the physical mass of the baryon in the intermediate state, g_j is the appropriate renormalized coupling constant, the V's are the vertex operators, and w_j is $(k^2+m^2)^{\frac{1}{2}}$, the quantity m being the mass of the meson in the intermediate state. The sum over j means sum over all momenta of all pion and kaon processes allowed by the interaction Hamiltonian. Our result reduces to the special cases treated by Chew [6]) and Lee [7]).

The modified renormalized vertex operator is given by $V_j L_r$, where L_r is

$$L_r(p_0-M_4, p_0+k_0-M_1) = 1+C\sum_{j_1,j_2}\left(\frac{g_{j_1}}{M_3+M_4}\right)\left(\frac{g_{j_2}}{M_1+M_2}\right)V_{j_1}V_{j_2}^*$$
$$\times\left[\frac{1}{(p_0-M_3-w_j)(p_0-M_2+k_0-w_j)} - \frac{1}{(M_4-M_3-w_j)(M_1-M_2-w_j)}\right].$$

The Feynman diagram for such a process is given in fig. 1. Again p_0 is $-i$ times

Fig. 1. Sample diagram for vertex modification.

† Eq. 2 of ref. [1]) should read $(\omega_k-\Delta)^2$ in the denominator. Moments given in ref. [1]) are based on the correct expression.

the fourth component of the momentum four vector for M_4. The summation over j_1 and j_2 means sum over all momenta of all allowed processes, both pion and kaon, which conserve charge and strangeness. For each modification of the type shown in fig. 1, the baryon M_1 which enters the diagram must be the same, and the baryon M_4 which leaves the diagram must be the same. The quantity w_j is the energy of the "modifying" meson. The emission or absorption of the meson represented by V_j must be able to go in each case. C is the numerical factor due to commutation rules when V_j is moved through V_{j1}. For the pion-nucleon case, our result reduced to Chew's [6]).

We obtain 4th order terms from 1) renormalized propagators, 2) renormalized vertex operators, and 3) irreducible diagrams.

The integrals for the pion-kaon cross terms are of two forms:

$$\iint \frac{\mathrm{d}k\mathrm{d}l\; l^4 k^4 v^2(l) v^2(k)}{w_l{}^3 (w'_k)^2 (w'_k + w_l - \Delta)} \left[\frac{1}{w'_k} + \frac{1}{w'_k + w_l - \Delta}\right], \tag{1}$$

$$\iint \frac{\mathrm{d}k\mathrm{d}l\; l^4 k^4 v^2(l) v^2(k)}{w'_l (\Delta - w'_l)^2 w_k{}^2 (w_k + w'_l - \Delta)} \left[\frac{1}{w_k} + \frac{1}{w_k + w'_l - \Delta}\right], \tag{2}$$

where (1) results from kaon-photon interactions and (2) results from pion-photon interactions. In these expressions $w_k{}^2 = k^2 + m_\pi{}^2$ and $(w'_l)^2 = l^2 + m_K{}^2$, and Δ is the appropriate baryon mass difference. For example, in nucleon calculations $\Delta = M_n - M_\Sigma$. In all 4th order calculations, the Λ—Σ mass difference is neglected and all integrals are evaluated numerically. In the evaluation of these integrals a uniform cutoff based on the rest mass of the emitting baryon is used; namely $k_{max} = 4.5\, M_B/6.7$ — this is in the neighborhood of the ratio used by Chew for pion-nucleon phenomena.

3. Results and Conclusions

For purposes of comparison table 1 shows the various individual contributions to the baryon anomalous moments in nuclear magnetons with all coupling constants $(g^2/4\pi)$ chosen to be 14. It is observed that the fourth order pion-kaon contributions are in most cases by no means negligible in comparison to the second order kaon results. Thus, we feel justified in concluding that in more elaborate computations of these moments, combined effects of the pion and kaon field must be considered.

Table 2 presents the total contributions for the different baryons for various choices of the coupling constants. The second row serves to indicate what these moments might be, if kaon couplings are really smaller than those for the pion or if kaon contributions are appreciably reduced by recoil corrections as is expected to be the case. Rows 3 and 4 are simply included for the sake of comparison, as very little is known about these coupling constants. The sign of these constants

slightly changes the calculated moments but not in a definitive and discriminating way.

TABLE 1

Contributions to the anomalous moments of the baryons in nuclear magnetons from pion and kaon currents for all coupling constants $g^2/4\pi = 14$. $\mathcal{M}_{2\pi}$ and $\mathcal{M}_{4\pi}$ are the second and fourth order pion contributions, $\mathcal{M}_{2K}$ the second order kaon contributions and $\mathcal{M}_{4K}$ the fourth order pion-kaon results

	$\mathcal{M}_{2\pi}$	$\mathcal{M}_{4\pi}$	$\mathcal{M}_{2K}$	$\mathcal{M}_{4K}$
P	1.51	0.57	0.27	0.22
N	−1.51	−0.57	0.25	−0.02
Λ^0	0	0	−0.28	−0.29
Σ^0	0	0	−0.41	−0.29
Σ^+	1.55	0.47	0.36	0.94
Σ^-	−1.55	−0.47	−1.18	−1.53
Ξ^0	1.27	0.43	−0.76	0.28
Ξ^-	−1.27	−0.43	−0.81	−1.27

TABLE 2

Anomalous magnetic moments of baryons for coupling constants given below

	P	N	Λ^0	Σ^0	Σ^+	Σ^-	Ξ^0	Ξ^-
1	2.57	−1.85	−0.57	−0.70	3.32	−4.73	1.22	−3.78
2	2.13	−2.05	−0.06	−0.07	2.15	−2.29	1.65	−1.91
3	2.13	−2.06	−0.07	−0.08	0.97	−1.13	−0.01	−0.20
4	2.39	−1.95	−0.04	−0.70	0.12	−1.52	−0.76	−0.81

	$g^2_{N\pi}/4\pi$	$g^2_{\Lambda\pi}/4\pi$	$g^2_{\Sigma\pi}/4\pi$	$g^2_{\Xi\pi}/4\pi$	$g^2_K/4\pi$
1	14	14	14	14	14
2	14	14	14	14	1.4
3	14	7	7	1	1.4
4	14	0	0	0	14

References

1) W. G. Holladay, Phys. Rev. **115** (1959) 1331
2) M. H. Friedman, Phys. Rev. **97** (1955) 1123
3) M. Gell-Mann, Phys. Rev. **92** (1953) 833;
   K. Nishijima, Progr. Theor. Phys. (Japan) **10** (1953) 581
4) R. H. Capps and W. G. Holladay Phys. Rev. **99** (1955) 931
5) G. F. Chew, Phys. Rev. **94** (1954) 1748
6) G. F. Chew, Phys. Rev. **94** (1954) 1755
7) T. D. Lee, Phys. Rev. **95** (1954)1329

8.B

Nuclear Physics **22** (1961) 168—176; © *North-Holland Publishing Co., Amsterdam*

Not to be reproduced by photoprint or microfilm without written permission from the publisher

ISOSPIN FOR $N+\bar{N} \to K+\bar{K}+k\pi$ AND SIMILAR REACTIONS

H. PILKUHN †

Institute for Theoretical Physics, University of Stockholm

Received 31 August 1960

Abstract: For antiproton annihilation into a $K\bar{K}$ pair and k pions, multiple pion production in nucleon-nucleon and pion-nucleon collisions, the transition rates into states with given charge configurations of the outgoing particles are expressed in terms of isospin amplitudes. For the pions' states, representations of the permutation group are employed. Interference terms are discussed, and explicit expressions are given for k up to 5.

1. Introduction

Let us consider the following reactions:

$$N+\bar{N} \to K+\bar{K}+k\pi, \tag{1}$$

$$N+\pi \to N+k\pi, \tag{2}$$

$$N+N \to N+N+k\pi. \tag{3}$$

Specifying the charges of the incoming and outgoing particles, each reaction may be divided into a series of reactions, each having its own transition rate. For instance, the rate of $p\bar{p}$ annihilation into K^+, $\bar{K}^0$, one π^- and two π^0 will be denoted by $R_0(+0, -00)$. In this paper we will express the various rates for the reactions in terms of isospin amplitudes.

For the states of the pions, we will employ representations of the permutation group. These have been recently discussed by Pais [1]), in connection with the reaction $N+\bar{N} \to k\pi$. All the $I_\pi = 0$ and most of the $I_\pi = 1$ coefficients of table 1 have been given before [1, 2, 8])††. For our reactions, even $I_\pi = 2$ will occur, and so we had to use a more general method than that given in ref. [1]). This method is presented in sect. 3. Sect. 4 deals with a more subtle orthogonalization problem. In sect. 5, the possibility of predictions for the various reactions is discussed.

Since the formalism for reaction (3) is contained as a special case in the formalism for (1), reaction (3) will not be mentioned until the end of sect. 5.

† Work performed under U. S. Air Force contract nr. AF 61(052)—47.

†† The authors of ref. [8]) give even $I_\pi = 2$ coefficients, but neglect the interference problem.

2. General Formalism

For reactions (1), we may express the initial charge state in terms of the outgoing particles' charge states. For antiproton annihilation on proton, we have

$$(p\bar{p}) = C_0(K\bar{K}, cl\alpha\beta)x(K)y(\bar{K})z(cl\alpha\beta). \tag{4a}$$

Here $x(K)$ and $y(\bar{K})$ denote the charge states of the K and $\bar{K}$, respectively, and $z(cl\alpha\beta)$ denotes the charge states of the pions, characterized by charge configuration c(= (−00) in the introduction's example), symmetry under permutations of the pions (= labeled Young tableau) $l\alpha$, and possible additional quantum numbers β. Summation over all arguments is understood. Of course only those c are admitted for which $Q_\pi = Q - Q_K$ (Q_π = the pions' charge, Q = total charge, Q_K = charge of the $K\bar{K}$ pair = $I_3(K)+I_3(\bar{K})$).

For antiproton annihilation on neutron we write

$$(n\bar{p}) = C_-(K\bar{K}, cl\alpha\beta)x(K)y(\bar{K})z(cl\alpha\beta). \tag{4b}$$

Then the transition rate into a charge configuration $(K\bar{K}, c)$ will be

$$R_0(K\bar{K}, c) = \sum_{l\alpha\beta} |C_0(K\bar{K}, cl\alpha\beta)|^2, \quad R_-(K\bar{K}, c) = \sum_{l\alpha\beta} |C_-(K\bar{K}, cl\alpha\beta)|^2. \tag{5}$$

On the other hand, we may write

$$(p\bar{p}) = \tfrac{1}{2}\sqrt{2}(00)+\tfrac{1}{2}\sqrt{2}(10), \quad (n\bar{p}) = (1-1), \tag{6}$$

where (IQ) denotes a $N\bar{N}$ state with isospin I and $I_3 = Q$. These states may be expanded in terms of eigenstates of I, Q, I_K, I_π and pion tableau $l\alpha$:

$$(00) = A(0, 0l\alpha)w(00, 0, 01\alpha)+A(1, 1l\alpha)w(00, 1, 1l\alpha), \tag{7a}$$

$$(1Q) = B(0, 1l\alpha)w(1Q, 0, 1l\alpha)+B(1, 0l\alpha)w(1Q, 1, 0l\alpha)+B(1, 1l\alpha)w(1Q, 1, 1l\alpha) + B(1, 2l\alpha)w(1Q, 1, 2l\alpha). \tag{7b}$$

The notation is $w(IQ, I_K, I_\pi, l\alpha)$, $A(I_K, I_\pi l\alpha)$, $B(I_K, I_\pi l\alpha)$. The A and B are our isospin amplitudes. Since for $k < 6$ all isospin states of the pions are completely distinguished by labeled tableau, we really have as many amplitudes as isospin states. The dependence of A and B on l will allow the occurrence of intermediate particles, provided that isospin is conserved in the decay of these particles.

Now we establish the connection between (6) and (4) in two steps:

$$w(IQ, I_K, I_\pi l\alpha) = \sum_{I_3(K), I_3(\bar{K})} x(K)y(\bar{K})u(I_\pi Q_\pi l\alpha)f(IQ, I_K, I_3(K), I_3(\bar{K}), I_\pi). \tag{8}$$

Here the $K\bar{K}$ part of the w state is already labeled by the charges of the kaons,

but the pion part u will still contain several charge configurations:

$$u(I_\pi Q_\pi l\alpha) = \sum_{c,\beta} d(I_\pi \alpha, c\beta) z(cl\alpha\beta). \tag{9}$$

Here, α denotes the unlabeled tableau. For the proof that the d coefficients do not depend on l, see ref. [1]).

Now from (4), (6), (7), (8), (9) we will be able to express the C amplitudes in terms of the A and B amplitudes, if we know the coefficients f and d. The f are simple products of vector-addition coefficients:

$$f(IQ, I_K, I_3(K), I_3(\bar{K}), I_\pi) = (I_\pi Q_\pi, I_K Q_K | IQ)(\tfrac{1}{2}, I_3(K), \tfrac{1}{2}, I_3(\bar{K}) | I_K Q_K). \tag{10}$$

That is a complicated notation for simple numbers, so we calculate them first and then give the C amplitudes in terms of the A and B amplitudes, with only the d coefficients undetermined. This is done in table 1. For compactness, the

TABLE 1

The amplitudes C in terms of A and B

		$d(2)$	$d(1)$	$d(0)$
$N+\bar{N} \to K+\bar{K}+k\pi$	$\sqrt{2}C_0(K^+K^-)$	$-\sqrt{\frac{1}{5}}\ B(1,2)$	$-\sqrt{\frac{1}{6}}A(1,1)+\sqrt{\frac{1}{2}}B(0,1)$	$\sqrt{\frac{1}{2}}A(0,0)+\sqrt{\frac{1}{2}}B(1,0)$
	$\sqrt{2}C_0(K^0K^0)$	$-\sqrt{\frac{1}{5}}\ B(1,2)$	$-\sqrt{\frac{1}{6}}A(1,1)-\sqrt{\frac{1}{2}}B(0,1)$	$-\sqrt{\frac{1}{2}}A(0,0)+\sqrt{\frac{1}{2}}B(1,0)$
	$\sqrt{2}C_0(K^-K^0)$	$\sqrt{\frac{3}{10}}B(1,2)$	$\sqrt{\frac{1}{3}}A(1,1)+\sqrt{\frac{1}{2}}B(1,1)$	0
	$\sqrt{2}C_0(K^+K^0)$	$\sqrt{\frac{3}{10}}B(1,2)$	$\sqrt{\frac{1}{3}}A(1,1)-\sqrt{\frac{1}{2}}B(1,1)$	0
	$C_-(K^+K^-)$	$-\sqrt{\frac{3}{20}}B(1,2)$	$\sqrt{\frac{1}{2}}B(0,1)-\frac{1}{2}B(1,1)$	0
	$C_-(K^0K^0)$	$-\sqrt{\frac{3}{20}}B(1,2)$	$-\sqrt{\frac{1}{2}}B(0,1)-\frac{1}{2}B(1,1)$	0
	$C_-(K^-K^0)$	$\sqrt{\frac{1}{10}}B(1,2)$	$\sqrt{\frac{1}{2}}B(1,1)$	$B(1,0)$
	$C_-(K^+K^0)$	$\sqrt{\frac{3}{5}}\ B(1,2)$	0	0
		$d(2)$	$d(1)$	$d(0)$
$N+\pi \to N+k\pi$	$C_+(+)$	$-\sqrt{\frac{2}{15}}B(2)$	$\frac{1}{3}\sqrt{2}(-A(1)+B(1))$	$\sqrt{\frac{2}{3}}A(0)$
	$C_+(0)$	$\sqrt{\frac{1}{5}}\ B(2)$	$\frac{2}{3}A(1)+\frac{1}{3}B(1)$	0
	$C_{++}(+)$	$-\sqrt{\frac{1}{5}}\ B(2)$	$B(1)$	0
	$C_{++}(0)$	$\sqrt{\frac{4}{5}}\ B(2)$	0	0

arguments $cl\alpha\beta$ have been omitted. For instance, the third row of table 1 reads, with all indices on,

$$\sqrt{2}C_0(K^-K^0, cl\alpha\beta) = \sqrt{\tfrac{3}{10}}B(1, 2l\alpha)d(2\alpha, c\beta) + (\sqrt{\tfrac{1}{3}}A(1, 1l\alpha) + \sqrt{\tfrac{1}{2}}B(1, 1l\alpha))d(1\alpha, c\beta).$$

The amplitudes for reaction (2) may be obtained in the same way. To (4) corresponds

$$(\pi^+ n) = C_+(N, cl\alpha\beta)x(N)z(cl\alpha\beta), \quad (\pi^+ p) = C_{++}(N, cl\alpha\beta)x(N)z(cl\alpha\beta). \tag{11}$$

To (6) corresponds

$$(\pi^+ n) = \sqrt{\tfrac{2}{3}}(\tfrac{1}{2}, \tfrac{1}{2})+\sqrt{\tfrac{1}{3}}(\tfrac{3}{2}, \tfrac{1}{2}), \quad (\pi^+ p) = (\tfrac{6}{2}, \tfrac{3}{2}), \tag{12}$$

and to (7) corresponds

$$\begin{aligned}(\tfrac{1}{2}, \tfrac{1}{2}) &= A(0, l\alpha)w(\tfrac{1}{2}, \tfrac{1}{2}, 0l\alpha)+A(1l\alpha)w(\tfrac{1}{2}, \tfrac{1}{2}, 1l\alpha),\\ (\tfrac{3}{2}, I_3) &= B(1l\alpha)w(\tfrac{3}{2}, I_3, 1l\alpha)+B(2l\alpha)w(\tfrac{3}{2}, I_3, 2l\alpha).\end{aligned} \tag{13}$$

The notation is $A(I_\pi l\alpha)$, $B(I_\pi l\alpha)$ and $w(I, I_3, I_\pi l\alpha)$. Since the isospin of one nucleon is always $\frac{1}{2}$, we could drop that index. In the second part of table 1 the C_+ and C_{++} are expressed in terms of the A and B, the coefficients d being the same, of course.

3. Calculation of the *d*-Coefficients

In this and the following chapter we only consider the pions' states, so let us drop the index π.

The problem is to solve eq. (9). The states u may be constructed by means of fractional parentage coefficients [3]), and the d may be calculated from them. But since the d only depend on unlabeled tableau, we really need not orthogonalize states with the same α but different l, and the symmetrization of the z may be done by the nonorthogonal Young symmetrizers corresponding to the first labeled tableau (cf. Pais, page 578. Note, however, that we have to normalize z, since we are not working with ratios).

The orthogonalization of z with equal $cl\alpha$ but different β will be discussed in the next chapter. The normalization of u then implies

$$\sum_{c,\beta} d^2(I\alpha, c\beta) = 1. \tag{14}$$

Now the d will be determined by

$$\mathbf{I}^2 u(IQl\alpha) = I(I+1)u(IQl\alpha). \tag{15}$$

$\mathbf{I}^2$ is the total isospin operator (of the pions)

$$\mathbf{I}^2 = (\sum_{i=1}^{k} \mathbf{I}_i)^2 = 2k+2\sum_{i<j}^{k} Q_i Q_j + I_{+-}. \tag{16}$$

Q_i denotes the charge of the ith pion, and I_{+-} is the only part of $\mathbf{I}^2$ which contains nondiagonal elements,

$$I_{+-} = \sum_{i<j}^{k} (I_{i+} I_{j-} + I_{i-} I_{j+}). \tag{17}$$

Table 2

Squares of the coefficients d

	I_π	(00)	(+−)	(−0)	(−−)
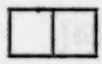	0	$-\frac{1}{3}$	$+\frac{2}{3}$	0	0
	2	$+\frac{2}{3}$	$+\frac{1}{3}$	1	1
	1	0	1	1	0

	I_π	(000)	(+−0)	(−00)	(+−−)	(−−0)
	1	$\frac{3}{5}$	$\frac{2}{5}$	$\frac{1}{5}$	$\frac{4}{5}$	0
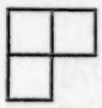	1	0	1	$-\frac{1}{2}$	$+\frac{1}{2}$	0
	2	0	1	$-\frac{1}{2}$	$-\frac{1}{2}$	1
	0	0	1	0	0	0

	I_π	(0000)	(+−00)	(++−−)	(−000)	(+−−0)s	(+−−0)a	(−−00)	(+−−−)
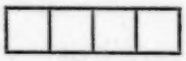	0	$+\frac{3}{15}$	$-\frac{4}{15}$	$+\frac{8}{15}$	0	0	0	0	0
	2	$-\frac{12}{21}$	$+\frac{1}{21}$	$+\frac{8}{21}$	$\frac{3}{7}$	$\frac{4}{7}$	0	$\frac{1}{7}$	$\frac{6}{7}$
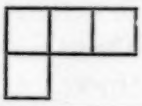	1	0	$\frac{1}{5}$	$\frac{4}{5}$	$+\frac{2}{5}$	$+\frac{2}{5}$	$-\frac{1}{5}$	0	0
	2	0	1	0	$+\frac{1}{3}$	0	$+\frac{2}{3}$	$\frac{1}{3}$	$\frac{2}{3}$
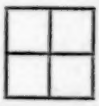	0	0	$-\frac{1}{3}$	$+\frac{1}{3}$	0	0	0	0	0
	2	0	$+\frac{1}{3}$	$+\frac{2}{3}$	0	1	0	1	0
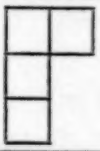	1	0	1	0	0	0	1	0	0

	I_π	$\binom{00}{000}$	$\binom{+-}{000}$	$\binom{++}{--0}$	(−0000)	$\binom{+-}{-00}$s	$\binom{+-}{-00}$a	(++−−−)	$\binom{--}{000}$	$\binom{+-}{--0}$
	1	$\frac{15}{35}$	$\frac{12}{35}$	$\frac{8}{35}$	$\frac{3}{35}$	$\frac{8}{35}$	0	$\frac{24}{35}$	0	0
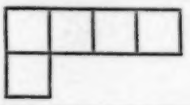	1	0	$\frac{1}{5}$	$\frac{4}{5}$	$+\frac{6}{20}$	$-\frac{1}{20}$	$-\frac{5}{20}$	$+\frac{8}{20}$	0	0
	2	0	$\frac{3}{7}$	$\frac{4}{7}$	$+\frac{30}{84}$	$+\frac{5}{84}$	$-\frac{9}{84}$	$-\frac{40}{84}$	$\frac{5}{21}$	$\frac{16}{21}$
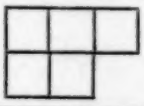	1	0	$\frac{4}{5}$	$\frac{1}{5}$	0	$+\frac{2}{5}$	$-\frac{1}{5}$	$+\frac{2}{5}$	0	0
	2	0	0	1	0	0	$-\frac{2}{3}$	$-\frac{1}{3}$	$\frac{2}{3}$	$\frac{1}{3}$
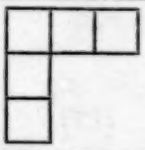	0	0	$-\frac{1}{3}$	$+\frac{2}{3}$	0	0	0	0	0	0
	2	0	$+\frac{2}{3}$	$+\frac{1}{3}$	0	0	1	0	0	1
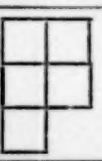	1	0	0	1	0	1	0	0	0	0

I_{i+} and I_{i-} are the plus and minus components of the isospin operator of the ith pion. Their matrix elements are all $= 0$ or $\sqrt{2}$.

Whether or not an $u(IQl\alpha)$ with given I can be constructed from the $z(cl\alpha\beta)$ depends upon α. If it cannot be constructed, the system of eq. (15) has the only solution $d(I\alpha, c\beta) = 0$ (all c and β). If it can be constructed, the equations will be linearly dependent. This provides a check for the calculation.

It should be remarked, that already for $k=6$ there exists one tableau, namely

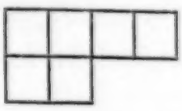

which contains $I = 2$ twice. Then (15) will not suffice to determine the d, and additional quantum numbers must be introduced.

For k up to 5, the *squares* of the d are given in table 2. For most α, β, only one of the isospins 0, 1, 2, will be contained in the z, but for some α, β, $I = 0$ and $I = 2$ may be both contained, or $I = 1$ and $I = 2$ may be both contained (see next sect.). In these cases, d with different isospins will contribute to some of the amplitudes C according to table 1 and thus will give rise to "interferences" between amplitudes of different I_π in (4). For these cases, the *signs* of the d-coefficients are important, and are given in table 2 in front of d^2. They are only determined up to a common sign, and that has been chosen such that it does not contradict the sign convention for vector-addition coefficients [4]). Still, some arbitrariness remains.

4. Orthogonalization of the $z(cl\alpha\beta)$ for equal $cl\alpha$

In ref. [1]), the additional quantum number β was taken to be a "charge tableau". To orthogonalize according to charge tableau, we have to use the Young-Yamanuchi representation. For $k < 6$, however, there may be at most two z with equal $cl\alpha$, and we need not employ the general formalism.

Consider first the pion states with $Q = 0$. The states $u(I0l\alpha)$ are eigenstates of the charge conjugation operator, so let us take those combinations of the two z states which are symmetric and antisymmetric, respectively, under charge conjugation. We denote them by $z(cl\alpha)$s and $z(cl\alpha)$a. Clearly, they are orthogonal. Moreover, one can see by vector-addition considerations, that $u(I0l\alpha)$ has the eigenvalue $(-)^{I+k}$ under charge conjugation. So for k even, $u(00l\alpha)$ and $u(20l\alpha)$ will only have components in $z(cl\alpha)$s, and for k odd, they will only have components in $z(cl\alpha)$a. The opposite is true for $u(10l\alpha)$. Consequently, $u(20l\alpha)$ and $u(10l\alpha)$ have no z in common. Keeping this in mind, we have dropped the distinction s and a for the zero charge states of table 2. Since those u which do have some z in common are marked by the signs of the corresponding d-coefficients, no confusion will arise.

For $Q=-1$, there may be two states $z(+--0l\alpha)$ and two states $z(+--00l\alpha)$. They may be distinguished by their symmetry under the transformations $\pi^+\leftrightarrow\pi^0$, and $\pi^-\leftrightarrow\pi^0$, respectively. Thus, $(+--0)$s denotes the state which is symmetric under $\pi^+\leftrightarrow\pi^0$. Clearly, it is orthogonal to $(+--0)$a.

The d coefficients for $Q=+1$ are obtained from the $Q=-1$ coefficients by charge conjugation. This implies a change of sign for $k+I$ odd. This is of importance for the rates $R_0(\bar{\mathrm{K}}\mathrm{K}^0c)$ and $R_0(\mathrm{K}^+\bar{\mathrm{K}}^0c_{\text{ charge conj.}})$. The interference term I_7 of (22) has the same coefficient for both rates, but opposite signs.

5. Discussion

Before going into details let us state a theorem given by Watson [5]):

$$2(\langle N_0\rangle_{\mathrm{p\bar{p}}}+\langle N_0\rangle_{\mathrm{n\bar{p}}})=\langle N_{\mathrm{ch}}\rangle_{\mathrm{p\bar{p}}}+\langle N_{\mathrm{ch}}\rangle_{\mathrm{n\bar{p}}}. \tag{18}$$

Here, $\langle N_0\rangle_{\mathrm{p\bar{p}}}$ means the average number of π^0 created in $\mathrm{p\bar{p}}$-annihilation, $\langle N_{\mathrm{ch}}\rangle_{\mathrm{p\bar{p}}}$ means the average number of charged pions created in $\mathrm{p\bar{p}}$-annihilation, etc.

The theorem follows from the conservation of the system's "isotropy in isospace," and it is easy to prove that it holds not only for each pion number k seperately, but also for each number of additional particles. For instance, for $\bar{\mathrm{p}}\mathrm{N}\to 2\pi$:

$$R(00)=\tfrac{1}{2}R(+-)-\tfrac{1}{4}R(-0), \tag{19}$$

and for $\bar{\mathrm{p}}\mathrm{N}\to\mathrm{K}+\bar{\mathrm{K}}+\pi$:

$$\begin{aligned}2[R(0\bar{0},0)+R(+-,0)+R(-0,0)]\\ =R(+-,-)+R(0\bar{0},-)+R(+\bar{0},-)+R(-0,+)\end{aligned} \tag{20}$$

(it should be pointed out, however, that for the case of protonium, the above "absolute" rates depend not only on the number of "stars", but also on the lifetime of protonium).

Let us now see what results our formalism may give. Consider first antiproton annihilation into pions only. There, $I=I_\pi=0$ or 1. Now we have seen that $u(1Ql\alpha)$ and $u(00l\alpha)$ have no z state in common, and so the transition rates do not contain any interference terms:

$$\begin{aligned}R_0(c)&=\sum_{l,\alpha,\beta}\tfrac{1}{2}[|A(l\alpha)|^2d^2(0\alpha c\beta)+|B(l\alpha)|^2d^2(1\alpha c\beta)],\\ R_-(c)&=\sum_{l,\alpha,\beta}|B(l\alpha)|^2d^2(1\alpha c\beta).\end{aligned} \tag{21}$$

So the only things that can be determined from the R_0, R_- are $\sum_l|A(l\alpha)|^2$ and $\sum_l|B(l\alpha)|^2$. Call these the "parameters" for the reaction. For $k=2, 3, 4, 5, 6$

there are 2. 3, 4, 5, 7 parameters respectively. On the other hand, the numbers of transition rates are 3, 4, 5, 6, 7 respectively. This shows that for no k there will be more than one relation between the rates. But since, by Watson's theorem, we have already one relation for each k, our general formalism will be of no use unless some "dynamical" assumptions on the amplitudes are added. For instance, there may be a resonance in one of the amplitudes, and then we can tell to what extent the different rates participate in the resonance.

We can make the following four remarks:

(1) For reaction (1), we have 2, 3, 6, 13, 30 isospin amplitudes, and 3, 7, 11, 15, 19 transition rates, for $k = 0, 1, 2, 3, 4$ respectively. So here the formalism will indeed give some relations in addition to those following from Watson's theorem. These will now involve the interference terms:

$$\left.\begin{aligned} &I_1(\alpha) = \sum_l \operatorname{Re} A(0, 0l\alpha)B(1, 0l\alpha), \qquad I_3(\alpha) = \sum_l \operatorname{Re} A(1, 1l\alpha)B(1, 1l\alpha), \\ &I_2(\alpha) = \sum_l \operatorname{Re} A(1, 1l\alpha)B(0, 1l\alpha), \qquad I_4(\alpha) = \sum_l \operatorname{Re} B(0, 1l\alpha)B(1, 1l\alpha), \\ &\text{and for some } \alpha \\ &I_5(\alpha) = \sum_l \operatorname{Re} A(0, 0l\alpha)B(1, 2l\alpha), \qquad I_6(\alpha) = \sum_l \operatorname{Re} B(1, 0l\alpha)B(1, 2l\alpha), \\ &\text{and for some other } \alpha \\ &I_7(\alpha) = \sum_l \operatorname{Re} A(1, 1l\alpha)B(1, 2l\alpha), \qquad I_9(\alpha) = \sum_l \operatorname{Re} B(1, 1l\alpha)B(1, 2l\alpha). \\ &I_8(\alpha) = \sum_l \operatorname{Re} B(0, 1l\alpha)B(1,2\,l\alpha), \end{aligned}\right\} \tag{22}$$

So far, no assumptions have been made on the space states of our systems, and all the formulas will be valid for differential cross-sections. On the other hand, a resonance may occur in one partial wave. For the rest of this remark, we will take the $p\bar{p}$-state to be an eigenstate of charge conjugation, and the $\bar{p}n$ state to be an eigenstate of G-parity [6]). For these states, the isospin of the $K\bar{K}$ pair will determine the space parity of the $K\bar{K}$ pair. Actually, for one value of that parity,
$A(1, 1l\alpha) = B(0, 1l\alpha) = 0$, and for the opposite value, $A(0, 0l\alpha) = B(1, 0l\alpha) = B(1, 1l\alpha) = B(1, 2l\alpha) = 0$. Consequently, $I_3 = I_4 = I_7 = I_8 = 0$ in (22), and $R_0(+\bar{0}, c) = R_0(-0, c_{\text{charge conj.}})$; $R_-(+-, c) = R_-(\bar{0}\bar{0}, c)$.

(2) For reaction (2), everything runs in complete analogy. There will be four different types of interference terms. Here, too, a theorem like Watson's may be formulated. Again, it will not give all the relations which result from the above formalism.

(3) Transition rates for (3) are obtained from the rates for (1) by substituting

$$p \to n, \quad K^+ \to p, \quad K^0 \to n, \quad K^- \to n, \quad \bar{K}^0 \to p, \quad Q \to Q+1. \tag{23}$$

Since then both the K^+K^- and the $K^0\bar{K}^0$ rates contribute to the pn rate, they have to be added. This addition will cause the Interference terms I_1, I_2, I_4, I_5 and I_8 to cancel. It has been pointed out, however [7]), that the $I = \frac{3}{2}$ resonance in the elastic part of (2) makes another coupling scheme for (3) more appropriate: One nucleon is coupled to the pions first to give $I_{\pi N} = \frac{1}{2}$ and $\frac{3}{2}$, and then the second nucleon is coupled on to give $I = 0$ and 1. Of course, a strong $K\pi$ resonance may give a similar argument in favour of that kind of coupling even for reaction (1).

(4) Finally we remark that for reaction (2), the transformation of the incoming pion into a $\bar{\Sigma}$ of the same charge, and the outgoing nucleon into a kaon of the same charge, will give the transition rates for $\bar{\Sigma}+N \to K+k\pi$.

The author thanks Professor O. Klein for the hospitality extended to him at the Institute for Theoretical Physics, University of Stockholm. Thanks are also due to Professor A. G. Ekspong, for a stimulating discussion.

References

1) A. Pais, Annals of Physics **9** (1960) 548; see there also for further references
2) A. I. Nikishov, JETP **3** (1957) 976
3) H. Jahn and H. van Wieringen, Proc. Roy. Soc. A **209** (1951) 502
4) See for instance: A. R. Edmonds, Angular momentum in quantum mechanics (Princeton University Press, 1957)
5) K. M. Watson, Phys. Rev. **85** (1952) 852
6) T. D. Lee and C. N. Yang, Nuovo Cim. **3** (1956) 749;
Charles Goebel, Phys. Rev. **103** (1956) 258
(Note: In table I of Goebels article, the column "like" should be taken)
7) L. I. Lapidus, JETP **4** (1957) 740
8) S. Z. Belenkij, V. M. Maksimenko, A. I. Nikishov and I. L. Rozental, Uspekhi fiz. Nauk **62** (1957) 1 (German translation in Fortschritte der Physik **6** (1958) 524)

NORTH-HOLLAND BOOKS

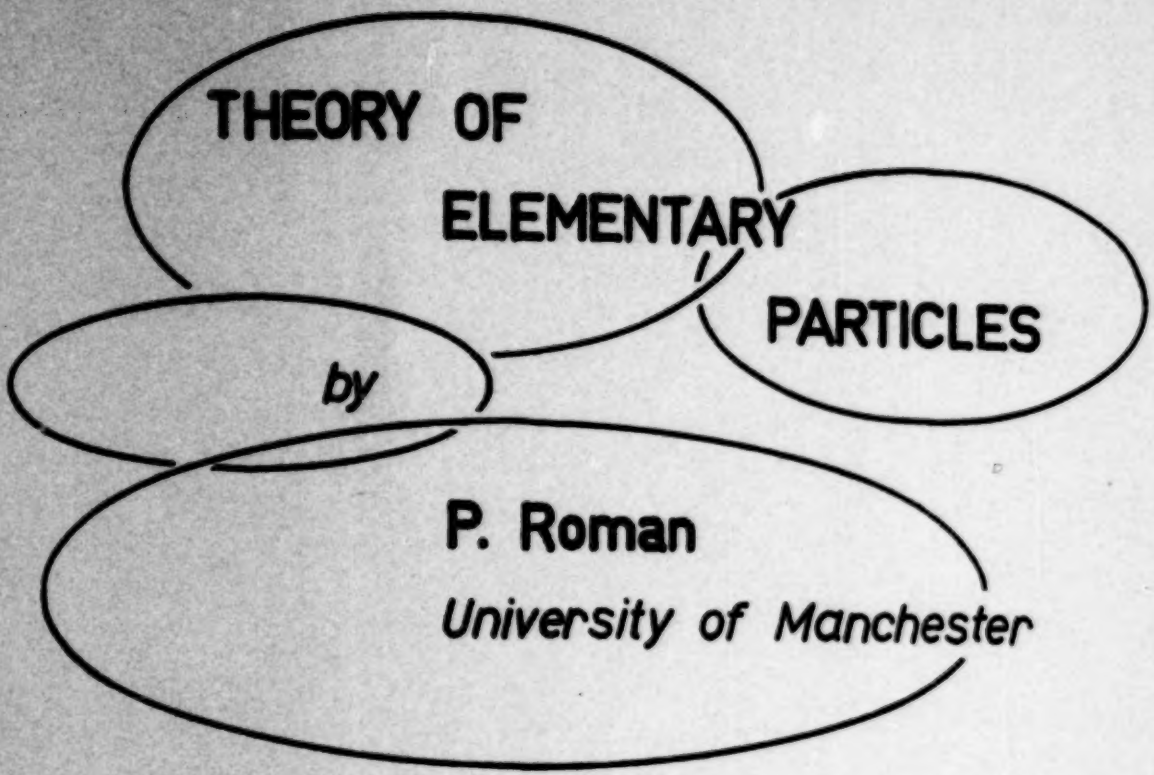

"This is the first detailed and up-to-date textbook specially devoted to the theory of the fundamental constituents of matter and their interactions. One can therefore safely predict that this book, by its substantial and well-balanced contents, and its outstanding didactic qualities, will long remain unchallenged as an introduction into the domain of fundamental research from which we expect decisive new insight into the properties of matter."

Nuclear Physics

Ask your bookseller or

6×9" 587 pp. 32 figs. Guilders 50.00 (100s.)

NORTH-HOLLAND PUBLISHING COMPANY

P.O. Box 103 - AMSTERDAM

Distributor for U.S.A.: Interscience Publishers, Inc. - New York

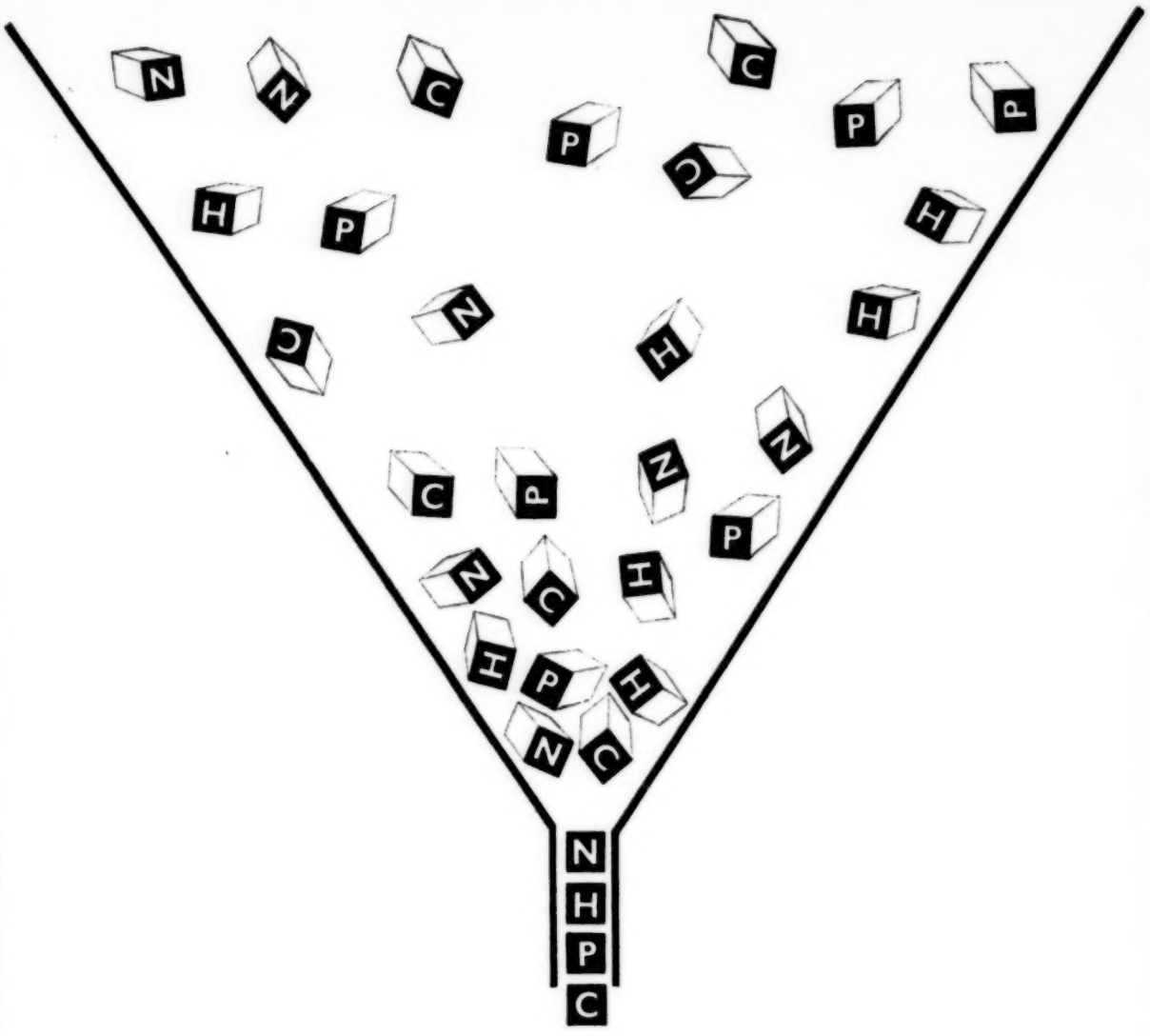

NEW BOOKS

J. L. SYNGE:
Relativity: The general theory

H. G. VAN BUEREN:
Imperfections in crystals

H. JONES:
The theory of Brillouin zones and electronic states in crystals

H. KALLMANN BIJL (Editor):
Space research (Proceedings Nice conference, 1960)

Send your order to your bookseller or directly to:

NORTH-HOLLAND PUBLISHING COMPANY - AMSTERDAM

Sole Agency in the U.S.A.: Interscience Publishers Inc. – New York